REPORT NO. FRA/ORD-80/22-1 PB

PB81-179020

STATISTICAL REPRESENTATIONS OF TRACK GEOMETRY

VOLUME I—TEXT

MARCH 1980

Document is available to the U.S. public through
The National Technical Information Service,
Springfield, Virginia 22161

U.S. DEPARTMENT OF TRANSPORTATION
FEDERAL RAILROAD ADMINISTRATION
Office of Research and Development
Washington, D.C. 20590

NOTICE

This document is disseminated under the sponsorship of the Department of Transportation in the interest of information exchange. The United States Government assumes no liability for its contents or use thereof.

The contents of this report reflect the views of ENSCO, Inc., which is responsible for the facts and the accuracy of the data presented herein. The contents do not necessarily reflect the official views or policy of the Department of Transportion. This report does not constitute a standard, specification, or regulation.

The United States Government does not endorse products or manufacturers. Trade or manufacturers' names appear herein only because they are considered essential to the object of this document.

Technical Report Documentation Page

1. Report No.	2. Government Accession No.	3. Recipient's Catalog No.
FRA/ORD-80/22.1		

4. Title and Subtitle	5. Report Date
STATISTICAL REPRESENTATIONS OF TRACK GEOMETRY Volume I -- Main Text	March 1980
	6. Performing Organization Code
7. Author(s) John C. Corbin	8. Performing Organization Report No. DOT-TSC-FRA-80-4,I
9. Performing Organization Name and Address ENSCO, INC.* Transportation and Instrumentation Sciences Division 5408A Port Royal Road Springfield VA 22151	10. Work Unit No. (TRAIS) RR019/R0323
	11. Contract or Grant No. DOT-TSC-1211-1
12. Sponsoring Agency Name and Address U.S. Department of Transportation Federal Railroad Administration Office of Research and Development Office of Rail Safety Research Washington DC 20590	13. Type of Report and Period Covered Final Report May 1976 to April 1978
	14. Sponsoring Agency Code

15. Supplementary Notes

*Under contract to: U.S. Department of Transportation
Research and Special Programs Administration
Transportation Systems Center
Cambridge MA 02142

16. Abstract

Mathematical representations of railroad track geometry variations are derived from time series analyses of track measurements. Since the majority of track is free of anomalies (turnouts, crossings, bridges, etc.), representation of anomaly-free track is first considered. Anomalies are then represented by using a combination of processes used to describe joints or welds in the anomaly-free track.

In practice, anomaly-free track is constructed by joining many rails of the same length together so that periodic behavior is expected. Results indicate that the geometry of such track structures is completely represented by a periodically modulated random process whose first, second, and higher order statistics are a function of position along the rail relative to a joint or weld.

This process is the synthesis of two simpler processes. The first is a stationary random process completely described by its power spectral density (PSD), which is modeled as a smooth function described by a roughness parameter and a set of corner frequencies (wavelengths). This process gives a complete representation of a homogeneous track structure free of joints or welds. The second process, which represents the joints or welds, involves a shape function, a decay rate away from the peak, and a correlation between joint amplitudes. The sequence of shape amplitudes is also a stationary random process having a non-zero mean. The mean amplitude and the decay rate of the shape function can be estimated from track geometry PSD's.

Roughness parameters, corner frequencies, mean shape amplitudes and decay rates of the processes are related to track classes as defined by FRA Track Safety Standards, and to the measurements prescribed by those standards.

Volume II -- Appendixes has 202 pages.

17. Key Words	18. Distribution Statement
Track Geometry, Track Irregularities, Track Inspection Cars, Simulation Models, Railhead Profile, Statistical Analyses, Statistical Models	DOCUMENT IS AVAILABLE TO THE PUBLIC THROUGH THE NATIONAL TECHNICAL INFORMATION SERVICE, SPRINGFIELD, VIRGINIA 22161

19. Security Classif. (of this report)	20. Security Classif. (of this page)	21. No. of Pages	22. Price
Unclassified	Unclassified	208	

Form DOT F 1700.7 (8-72) Reproduction of completed page authorized

PREFACE

The Federal Railroad Administration (FRA) is sponsoring research, development, and demonstration programs to provide improved safety, performance, speed, reliability, and maintainability of rail transportation systems at reduced life-cycle costs. The Transportation Systems Center (TSC) is assisting FRA by investigating the relationships among track geometry variations, wheel/rail forces, and derailment tendencies. To accomplish this goal, it is necessary to have a reliable description of these variations as a function of distance along the track. This description should envelop the universe of track irregularities as implied by current construction and maintenance practices, and by the physical factors that determine track degradation.

Since there are an infinite number of possible track geometry variations that can occur in track structures, the only way that the universe of track in use in the United States can be characterized is through the statistics of the population. The study described in this report derives some basic random processes that can be used to generate the full range of track geometry variations actually observed in track structures and the statistics of the parameters which define these processes. The values of these parameters for a given section of track reflect the quality of the track and are expected to correlate with rail car dynamic performance as defined by derailment tendency, wheel/rail forces, ride vibration and other measures of dynamic performance.

In this effort studies were conducted on existing measured track geometry to estabish statistical descriptions of track geometry variations and descriptions of the parameters associated with these statistical descriptions. The parameters are functions of the track classes defined by current FRA Track safety standards.

The author wishes to thank Dr. Herbert Weinstock, the TSC Technical Monitor, Dr. Russel Brantman of TSC, Messrs. William B. O'Sullivan and Jerry Sullivan of FRA and Mr. Chip Hale of Thomas K. Dyer Associates for their comments which have contributed greatly to the quality of this study. Appreciation is also extended to ENSCO co-workers, Messrs. Richard Sutermeister and Edward Cunney who assisted with computer programming, data collection, and analysis of results.

METRIC CONVERSION FACTORS

Approximate Conversions to Metric Measures

Symbol	When You Know	Multiply by	To Find	Symbol
		LENGTH		
in	inches	*2.5	centimeters	cm
ft	feet	30	centimeters	cm
yd	yards	0.9	meters	m
mi	miles	1.6	kilometers	km
		AREA		
in^2	square inches	6.5	square centimeters	cm^2
ft^2	square feet	0.09	square meters	m^2
yd^2	square yards	0.8	square meters	m^2
mi^2	square miles	2.6	square kilometers	km^2
	acres	0.4	hectares	ha
		MASS (weight)		
oz	ounces	28	grams	g
lb	pounds	0.45	kilograms	kg
	short tons (2000 lb)	0.9	tonnes	t
		VOLUME		
tsp	teaspoons	5	milliliters	ml
Tbsp	tablespoons	15	milliliters	ml
fl oz	fluid ounces	30	milliliters	ml
c	cups	0.24	liters	l
pt	pints	0.47	liters	l
qt	quarts	0.95	liters	l
gal	gallons	3.8	liters	l
ft^3	cubic feet	0.03	cubic meters	m^3
yd^3	cubic yards	0.76	cubic meters	m^3
		TEMPERATURE (exact)		
°F	Fahrenheit temperature	5/9 (after subtracting 32)	Celsius temperature	°C

*1 in = 2.54 (exactly). For other exact conversions and more detailed tables, see NBS Misc. Publ. 286, Units of Weights and Measures, Price $2.25, SD Catalog No. C13.10:286

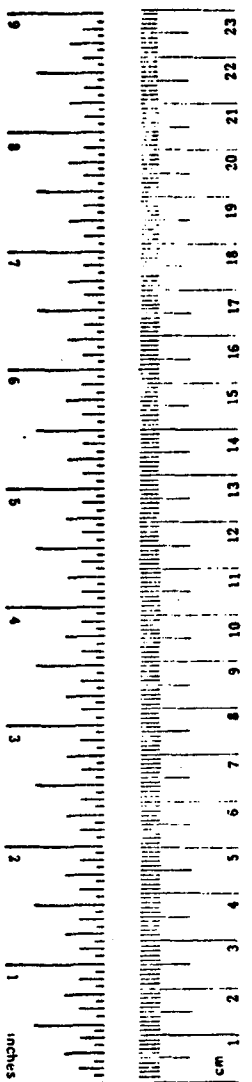

Approximate Conversions from Metric Measures

Symbol	When You Know	Multiply by	To Find	Symbol
		LENGTH		
mm	millimeters	0.04	inches	in
cm	centimeters	0.4	inches	in
m	meters	3.3	feet	ft
m	meters	1.1	yards	yd
km	kilometers	0.6	miles	mi
		AREA		
cm^2	square centimeters	0.16	square inches	in^2
m^2	square meters	1.2	square yards	yd^2
km^2	square kilometers	0.4	square miles	mi^2
ha	hectares (10,000 m^2)	2.5	acres	
		MASS (weight)		
g	grams	0.035	ounces	oz
kg	kilograms	2.2	pounds	lb
t	tonnes (1000 kg)	1.1	short tons	
		VOLUME		
ml	milliliters	0.03	fluid ounces	fl oz
l	liters	2.1	pints	pt
l	liters	1.06	quarts	qt
l	liters	0.26	gallons	gal
m^3	cubic meters	35	cubic feet	ft^3
m^3	cubic meters	1.3	cubic yards	yd^3
		TEMPERATURE (exact)		
°C	Celsius temperature	9/5 (then add 32)	Fahrenheit temperature	°F

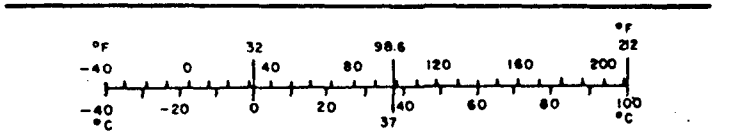

TABLE FOR METRIC CONVERSION OF SPATIAL FREQUENCY

Given:	To find: cy/ft — Multiply by:	To find: cy/m — Multiply by:
cy/ft	1.00	3.28
cy/in	12.0	39.4
rad/ft	0.159	4.85×10^{-2}
rad/in	1.91	4.04×10^{-3}
cy/m	0.305	1.00
cy/cm	30.5	1.00×10^{2}
rad/m	4.85×10^{-2}	0.159
rad/cm	4.85	15.9

TABLE FOR METRIC CONVERSION OF PSD LEVELS

Given:	To find: $in^2/cy/ft$ — Multiply by:	To find: $cm^2/cy/m$ — Multiply by:
$ft^2/cy/ft$	144.	2.83×10^2
$in^2/cy/ft$	1.00	1.97
$in^2/cy/in$	8.33×10^{-2}	0.164
$ft^2/rad/ft$	9.05×10^2	1.78×10^3
$in^2/rad/ft$	6.28	12.4
$in^2/rad/in$	0.524	1.03
$m^2/cy/m$	5.09×10^3	1.00×10^4
$cm^2/cy/m$	0.509	1.00
$cm^2/cy/cm$	5.09×10^{-3}	1.00×10^{-2}
$m^2/rad/m$	3.20×10^4	6.28×10^4
$cm^2/rad/m$	3.20	6.28
$cm^2/rad/cm$	3.20×10^{-2}	6.28×10^{-2}

TABLE OF CONTENTS

TABLE OF CONTENTS (Cont'd)

TABLE OF CONTENTS (Cont'd)

LIST OF ILLUSTRATIONS

LIST OF ILLUSTRATIONS (Cont'd)

LIST OF ILLUSTRATIONS (Cont'd)

LIST OF ILLUSTRATIONS (Cont'd)

LIST OF ILLUSTRATIONS (Cont'd)

LIST OF TABLES

LIST OF TABLES (Cont'd)

1. SUMMARY

1.1 BACKGROUND

A particular section of railroad track is represented by a set of graphs, called space curves, that define the vertical (profile and crosslevel) and lateral (alignment and gage) rail deviations as functions of distance along the track. These records are adequate to define the peak values and rates of geometric variations and vehicle responses to steady state and time varying changes in that geometry. However, no two lengths of track have identical geometry, and the evaluation of vehicle performance requires relating track geometry to vehicle responses for the totality of track in the United States. Such a treatment requires the study of a great number of geometry records and an expensive data processing effort.

Careful examination of geometry space curve graphs reveals that a large class of arbitrary wave shapes (spikes, jump discontinuities) do not occur in actual track. Further study reveals that there are regularly occurring patterns in the data, and that these are superimposed on a background of apparently random behavior. If the zone is long enough, the peak values of geometry variation will be associated with one or more excursions that are notably large. Such observations indicate that the bulk of the geometry and the vehicular responses to that geometry may be represented by some form of analytical process.

Accordingly this report describes studies of existing track geometry data to derive analytical representations of track geometry variations. The results of these studies describe the amplitude versus distance characteristics of track geometry variation in a manner that permits analytical predictions of vehicle response.

Most track segments are constructed in a uniform manner and many of these are maintained to provide the same performance levels. These segments produce families of graphs that exhibit the same features observed in the individual segments of track cited above. In order to observe these features, however, it is necessary to separate them as described below.

- Peak excursions of geometry are often associated with physical features whose presence is obvious when subsequent field verifications are performed. These anomalous features such as turnouts, crossings, bridges, and broken rails, require special analytical treatment.

- The vast majority of track lies between these anomalies. It is constructed by welding or bolting together many short pieces of rail, all having the same length. Field verifications reveal that the regularly occurring patterns found in geometry traces are caused by joints and welds.

1.2 METHODOLOGY

Time series analysis techniques were applied to track geometry data to obtain an analytical representation of the irregularities produced in current track structures. *For anomaly-free variations of profile and crosslevel, these analyses indicate that a periodically modulated random process is the single, all-inclusive representation of these variations.* This process is characterized by means, covariance functions and higher order statistical moments whose values vary cyclically with position in each rail length. For corresponding positions in each rail length, these moments are stationary.

The periodically modulated random process includes two subset processes that have been used historically to represent track geometry behavior:

- A periodic deterministic process, which is obtained by letting the mean be a function of position in the rail length, and by letting all higher order moments vanish.
- A stationary random process, which is obtained by letting all moments be constant (stationary) throughout the rail length.

Prior analyses, however, did not include analytical descriptions of random variations in the amplitudes of joints. It is this phenomenon that necessitates the more complete statistical description afforded by the periodically modulate random process.

1.2.1 CAPABILITIES AND LIMITATIONS OF THE PSD

The power spectral density (PSD) is a useful tool for estimating some properties of the periodically modulated random process. Application of the PSD to data that includes many rail lengths produces graphs that exhibit a relatively smooth continuum punctuated by sharp, harmonically spaced spikes. The continuum is an estimator of the covariance function (auto-correlation) of the parent random process, which averages over many rail lengths and over all positions within the rail length, transformed into the frequency domain. The pronounced peaks are estimators of the component magnitudes obtained in a harmonic analysis of the cyclically varying mean.

For a linear vehicle responding to the geometry deviations, the PSD's and cross-PSD's of all geometry inputs are sufficient to define the PSD's and cross-PSD's of all vehicle responses. All of the PSD's can be processed to yield mean square values of rail deviations, rail slopes, rail curvatures, accelerations, relative displacements between vehicle components, stresses and strains. Because they come from the PSD, these mean square values are averaged over many rail lengths, and they do not single out responses at specific locations within the averaging window.

The PSD is, however, a limited analysis tool for several reasons. Without detailed knowledge of the parent probability distributions governing each input and each response mode, mean square values cannot predict peak values. Another deficiency of the PSD concerns its averaging property. Identical PSD's result from a wide variety of time histories.

For example, the PSD calculated from a time history consisting of a series of large random amplitude pulses spaced at discrete intervals and that calculated from a time history composed of small amplitude pulses occuring continuously (at overlapping intervals) will be identical. The two processes will also produce identical mean square values; however, other characteristics of the two processes, for example, peak amplitudes, are quite different. Therefore, track geometry PSD's do not imply unique vehicle response PSD's for nonlinear vehicles such as rail car trucks which are highly nonlinear.

The PSD also destroys phase information so that the periodic deterministic wave shape cannot be reliably reconstructed by using just the magnitudes of the peaks. To determine wave shapes an auxiliary assumption is needed, for example, even symmetry at joints.

Thus, when applied to the periodically modulated random process, the PSD ignores the possibility that the covariance function varies cyclically over a rail length. It lumps together all covariances in a rail length average, averages this result over many rail lengths and transforms this answer into a frequency domain. *Therefore, the PSD cannot distinguish between a periodically modulated random process and a stationary random process where the former has a rail length averaged covariance equal to the stationary covariance of the latter.*

A related problem concerns time histories of track geometry in which an occasional anomaly is processed. A particular anomaly has a fixed structure that is deterministic in nature. Its geometry will not be produced by any reasonably structured random process. The effect of including the anomalous event in PSD evaluation is to elevate the continuum slightly. No details of the anomaly structure or wave shape are forthcoming from the PSD.

1.2.2 CIRCUMVENTING THE LIMITATIONS OF PSD PROCESSING

The PSD is a well understood, readily available, and relatively inexpensive computer processing tool. For these reasons, there is considerable impetus to use it in many applications of time series analysis. The PSD, however, has limitations, such as those discussed above, that severely restrict its applicability to track goemetry. In this report an improved means of characterizing track is developed to overcome the limitations of the PSD approach.

To this end, it was determined that the periodically modulated random process, ascribed to anomaly-free profile and crosslevel geometry, is the synthesis of two simpler processes: a stationary random variation, and a joint shape function occurring periodically and having random amplitudes. In track geometry PSD's it is found that the stationary random process produces the smooth continuum and that a non-zero mean in the joint amplitudes causes the spectral peaks.

Random variations of the joint amplitudes also produce a continuum contribution to the PSD. In the few examples studied, this component was found to be uniformly below the continuum generated by the stationary random process. It was concluded that the continuum is a more reliable characterizer of the continuous process than it is for the randomness concentrated at joints.

1.2.3 THE PSD AND PROCESS MODELING

The PSD supplies too many data values in a form which does not define the component processes. Nor is it particularly useful for the comparative evaluation and classification of the track deviations, and of the vehicle responses to these deviations. What is needed is a process model for the two simplified processes identified in the previous section. Then the model can be applied to develop a short parameter list that describes all salient features of the rail deviations.

The stationary random deviations represent the cumulative history of forces that have shaped the track structure during its lifetime. This force-induced waviness begins with rail manufacture, cooling, and straightening. Terrain variations and survey errors add to this. Various deformations are induced by lining and surfacing operations, tamping, train operations, and the environment.

Each new deformation of geometry can be modeled using linear differo-integral operators functioning on a combination of white noise and previous deformation conditions, all of which are ultimately derived from white noise sources.[1] By virtue of the equivalency properties of linear systems, the individual operators and noise sources can be combined. *Therefore, the stationary random process is given by a single equivalent linear differo-integral operator representing the composite of all force histories and functioning on a single white noise source.*

The linear differo-integral operator completely specifies both the random process and the analytical form of the PSD. For reasonably simple operators, the analytical PSD will exhibit distinct frequency (inverse wavelength) bands where the

[1]R. Cousty and G. Tro, "A Theoretical Study of the Development of Progressive Permanent Deformation in Longitudinal Profile of Railway Track under the Influence of Repeated Rolling Loads," *Revue Generale des Chemins de Fer* 91, p. 205-216, March 1972.

asymptotic behavior is an *even* power of frequency. Examination of the continuum of geometry PSD's indicates that they are good estimators of the stationary random component, and that they can be used to determine the specific form of the linear operator.

Analysis of profile geometry PSD's was performed over the frequency range of 10^{-3}cy/ft to 0.2 cy/ft. For these frequencies the following even power law approximation to empirical PSD's could be fitted universally to the continuum with a residual of less than 10%:

$$\hat{S}_1(\phi) \sim \begin{cases} \dfrac{A_1\phi_{13}^2}{\phi^4}, & 10^{-3}\text{cy/ft} < \phi \leq \phi_{13}; \\ \dfrac{A_1}{\phi^2}, & \phi_{13} \leq \phi \leq \phi_{14}; \text{ and} \\ \dfrac{A_1\phi_{14}}{\phi^4}, & \phi_{14} \leq \phi \leq 0.2 \text{ cy/ft}. \end{cases}$$

where

ϕ = spatial frequency;

$\hat{S}_1(\phi)$ = discontinuous analytical PSD;

A_1 = profile roughness for ϕ^{-2} range; and

ϕ_{13}, ϕ_{14} = break frequencies.

Since this PSD model does not translate directly into a simple differo-integral operator, a smooth functional fit was sought. This is given by:

$$S_1(\phi) = \frac{A_1\phi_{14}^2(\phi^2 + \phi_{13}^2)}{\phi^4(\phi^2 + \phi_{14}^2)}$$

Both $\hat{S}_1(\phi)$ and $S_1(\phi)$ are shown in Figure 1 along with raw profile PSD data.

For track that is in regular commercial service, ϕ_{13} and ϕ_{14} are both constant with values of 6.3×10^{-3} cy/ft and 4.0×10^{-2} cy/ft, respectively. *Therefore, over the range of wavelengths most critical to vehicle dynamics, the continuum portion of the profile PSD is adequately specified by the single remaining constant,* A_1.

If rail were to be rolled in lengths that are long compared to the longest wavelength of interest, say 2000 ft, the infrequent joints would be classified as anomalies and the stationary random process would be the sole describer of anomaly-free track. However, the predominant North American practice is to roll rail in the shorter, more manageable lengths of 39 ft. Then it is bolted or welded into the longer strings to form the track. Both bolted and welded joints are the sites of structural weakness and accelerated degradation of geometry. Additionally, the inability to straighten vertical deflections at the end of the rail segments is incorporated into the profile geometry of the weld.[2]

The profile space curve at the joint is adequately represented by a cusp shape of the form:

$$y(x) = Ce^{-k|x|}$$

where

x = distance along the rail
$y(x)$ = rail profile
C = joint cusp amplitude
k = decay rate, assumed constant on a particular section of track.

[2]K. W. Schoenenberg, "Rail Research--Problem Definition," Report No. R-120, AAR Research Center, Chicago IL, March 1973.

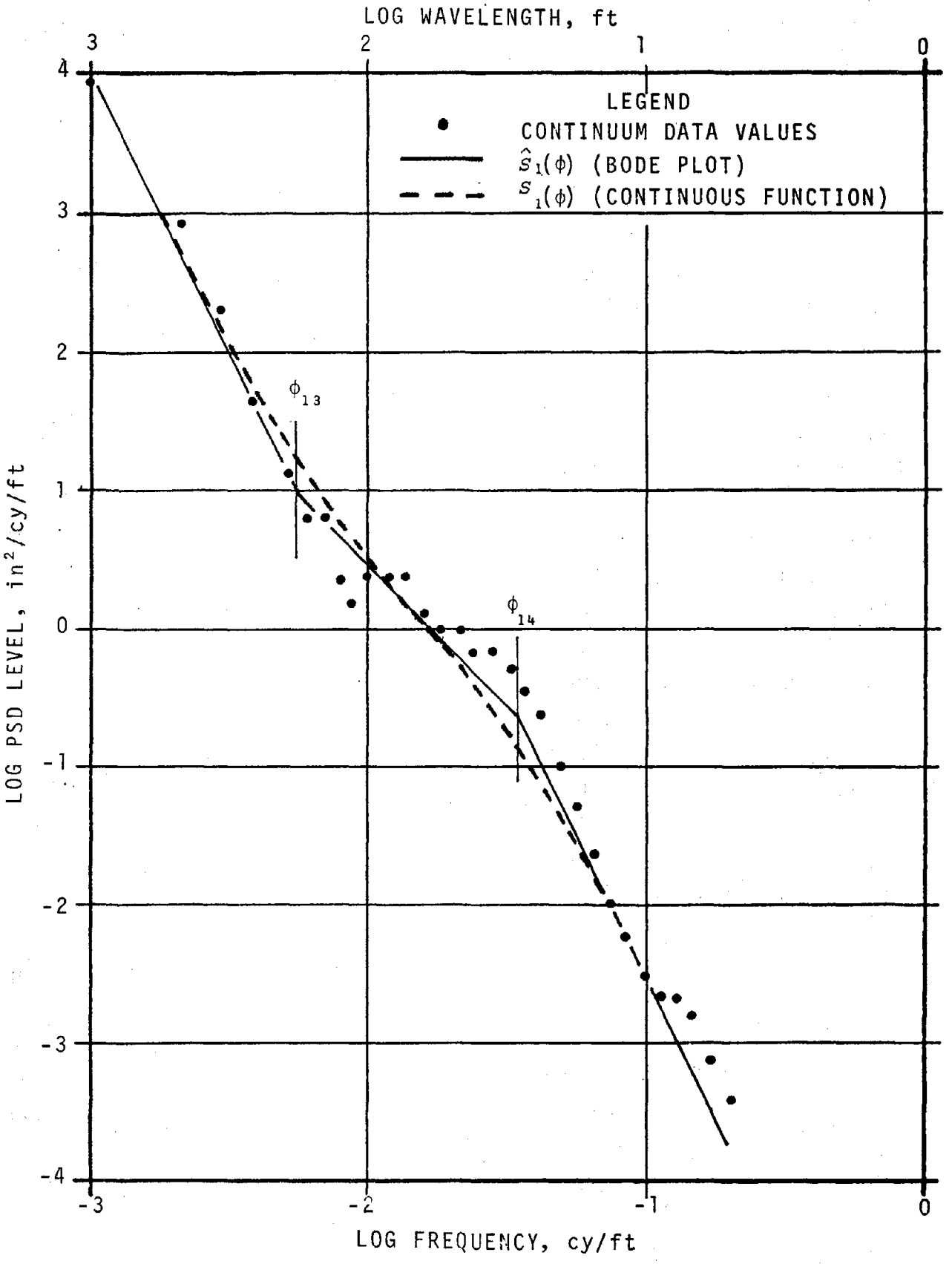

FIGURE 1. COMPARISON OF TYPICAL PROFILE CONTINUUM VALUES, BODE PLOT FIT, AND CONTINUOUS FUNCTION FIT

Thus, the shape of an individual joint is defined by its amplitude and its decay rate. On the basis of very limited analysis the c values are found to be represented by a stationary random process governed by Γ-distribution with a non-zero mean, $\bar{c}$.

The spectral peaks can be used to evaluate $\bar{c}$ and k. The PSD provides no information on the distribution of c. The PSD provides unreliable information on the correlation properties of the c values since the continuum due to random variations of c is masked by the stationary random continuum.

1.3 RESULTS

1.3.1 PRINCIPAL FINDINGS

A data base was established consisting of recent track geometry data collected on 29 sections of track broadly distributed throughout the United States. These zones reflect the various types of operating conditions and maintenance philosophies of different railroad properties. Typically, the zones vary in length from one to ten miles, three miles being the average.

Empirical PSD's and cross-PSD's were generated for the track profile, crosslevel, alignment and gage data. On the basis of these, analytical models of the continuum portion of the PSD's were developed for all of the geometry measurements. These models are given in Tables 1 and 2. Analysis of cross-PSD and coherence function data revealed that there is no correlation in the stationary random component between any pair of: mean profile, crosslevel, mean alignment and gage.

The PSD's generated above were tagged by the track speed classification as identified in the current FRA Track Safety Standards.[3] By fitting the models to the continuum, a list of parameters

[3]Title 49, Code of Federal Regulations, Part 213.

TABLE 1. MODELS FOR PSD CONTINUUM: SURFACE GEOMETRY VARIABLES

For wavelength coverage from 10 to 1000 ft, omit the term in [ ].
To extend wavelength coverage to 0.2 ft, include the term in [ ].

ϕ = spatial frequency (cy/ft)

λ = wavelength (ft) = ϕ^{-1}

$S_n(\phi)$ = PSD (in^2/cy/ft)

n = a geometry variable designator:

n = 1 → Left rail profile
2 → Right rail profile
3 → Mean profile
4 → Crosslevel

ϕ_{nm} = mth corner frequency of nth track geometry PSD

$\lambda_{nm} = \phi_{nm}^{-1}$

PROFILE (n = 1,2,3)

$$S_n(\phi) = \frac{A_n \phi_{n4}^2 (\phi^2 + \phi_{n3}^2)}{\phi^4 (\phi^2 + \phi_{n4}^2)} \left[\frac{\phi_{n6}^2 (\phi^2 + \phi_{n5}^2)}{\phi_{n5}^2 (\phi^2 + \phi_{n6}^2)}\right]$$

with:

$\lambda_{n3} \cong 140$ ft $\qquad \lambda_{n4} \cong 25$ ft

$\lambda_{n5} \cong 5 - 10$ ft $\qquad \lambda_{n6} \cong 1.0$ ft

CROSSLEVEL (n = 4)

$$S_4(\phi) = \frac{A_4 \phi_{44}^2 (\phi^2 + \phi_{42}^2)}{(\phi^2 + \phi_{41}^2)(\phi^2 + \phi_{43}^2)(\phi^2 + \phi_{44}^2)} \left[\frac{\phi_{46}^2 (\phi^2 + \phi_{45}^2)}{\phi_{45}^2 (\phi^2 + \phi_{46}^2)}\right]$$

with:

$\lambda_{41} \cong 200 - 1000$ ft $\qquad \lambda_{42} \cong 40 - 200$ ft

$\lambda_{43} \cong 25 - 50$ ft $\qquad \lambda_{44} \cong 18$ ft.

$\lambda_{45} \cong 5 - 10$ ft $\qquad \lambda_{46} \cong 1.0$ ft

$\hat{\lambda}_{43} = \lambda_{43}$ (effective combination of λ_{41}, λ_{42}, λ_{43})

$\hat{\lambda}_{43} = 140$ ft (Use with $\lambda_{41} = \lambda_{42} = \infty$)

TABLE 2. MODELS FOR PSD CONTINUUM: LINE GEOMETRY VARIABLES

For wavelength coverage from 10 to 1000 ft, omit the term in [ ].
To extend wavelength coverage to 1.0 ft, include the term in [ ].

ϕ = spatial frequency (cy/ft)

λ = wavelength (ft) = ϕ^{-1}

$S_n(\phi)$ = PSD (in^2/cy/ft)

n = a geometry variable designator:

n = 5 → Left rail alignment
6 → Right rail alignment
7 → Mean alignment
8 → Gage

ϕ_{nm} = mth corner frequency of nth track geometry PSD.

$\lambda_{nm} = \phi_{nm}^{-1}$

ALIGNMENT (n = 5,6,7)

$$S_n(\phi) = \frac{A_n \phi_{n4}^2 (\phi^2 + \phi_{n3}^2)}{\phi^4 (\phi^2 + \phi_{n4}^2)} \left[\frac{\phi^2 + \phi_{n5}^2}{\phi_{n5}^2} \right]$$

with:

$\lambda_{n3} \cong 100$ ft

$\lambda_{n4} \cong 18$ ft

$\lambda_{n5} = 5 - 10$ ft

GAGE (n = 8)

$$S_8(\phi) = \frac{A_8 \phi_{84}^2 (\phi^2 + \phi_{82}^2)}{(\phi^2 + \phi_{81}^2)(\phi^2 + \phi_{83}^2)(\phi^2 + \phi_{84}^2)} \left[\frac{\phi^2 + \phi_{85}^2}{\phi_{85}^2} \right]$$

with:

$\lambda_{81} \cong 200 - 1000$ ft

$\lambda_{83} \cong 25 - 50$ ft

$\hat{\lambda}_{83} \cong 40 - 200$ ft

$\lambda_{84} \cong 14$ ft

$\lambda_{85} \cong 5 - 10$ ft

$\hat{\lambda}_{83} = \lambda$ (effective combination of λ_{81}, λ_{82} and λ_{83})

$\hat{\lambda}_{83} = 120$ ft (Use with $\lambda_{81} = \lambda_{82} = \infty$)

was obtained for the geometry of each section of track. To determine how the parameters so developed were related to one another, or to track class, a regression analysis of the parameters versus track class was performed. It was found that parameters related to the roughness of the track were strongly related to the speed classification of the track. Parameters related to corner frequency rates were invariant or only weakly dependent on the speed classification of the track. The results presented in Table 3 and in the Bode plots of Figure 2 are those obtained from this regression analysis. The reader is cautioned that these tabulated values are means of the regressions, and that scatter of data values about mean regression lines is on the order of ±1 track class.

Using the PSD models and the associated parameters derived above, standard deviations (σ) of the stationary random component were generated for the track measures cited in the FRA Track Safety Standards. This included gage, crosslevel, 31 foot warp*, and 62-foot mid-chord offsets of both profile and alignment. Comparing these results with threshold in the Track Safety Standards reveals that:

- In the lower classes of track (1 to 4) gage requires as little as a 3- or 4-σ event to exceed an exception level.
- Other geometry measurements for classes 1 to 4 require 5-σ or even higher multiples of σ to produce an exception.

To better understand the implications of this result, the correlation properties of gage, crosslevel, and 62-foot mid-chords of alignment and profile were computed, assuming a stationary random input described by the model PSD's. The results are shown in Figure 3. A correlation distance, x_0,

*The standard deviation for 62-foot warp is close to 1.41 times the standard deviation of crosslevel.

TABLE 3. SUMMARY OF SPECTRUM MODELS AND IMPACT ON TRACK MEASURES AS A FUNCTION OF TRACK CLASS AS DEFINED IN CURRENT TRACK SAFETY STANDARDS

Track Class by Geometry				"8"	"7"	6	5	4	3	2	1
Continuum: Units: A_n: in^2-cy/ft, ϕ_{mn}: cy/ft; All σ's (standard errors) in inches		Profile	$A_3 \times 10^{-4}$	0.06	0.18	0.45	0.79	1.4	2.5	4.5	7.9
			$\phi_{33} \times 10^{-3}$	11.2	8.9	7.1	7.1	7.1	7.1	7.1	7.1
			$\phi_{34} \times 10^{-2}$	(†)	4.0	4.0	4.0	4.0	4.0	4.0	4.0
			$\phi_{35} \times 10^{-1}$	(†)	0.71	1.2	1.4	1.6	1.8	2.1	2.4
			σ, 62' MCO	0.07	0.10	0.15	0.20	0.26	0.35	0.47	0.62
		Crosslevel	$A_4 \times 10^{-4}$	0.12	0.20	0.34	0.50	0.74	1.1	1.6	2.3
			$\phi_{43} \times 10^{-3}$	7.1	7.1	7.1	7.1	7.1	7.1	7.1	7.1
			$\phi_{44} \times 10^{-2}$	(†)	4.0	4.0	4.0	4.0	4.0	4.0	4.0
			$\phi_{45} \times 10^{-1}$	(†)	0.84	1.0	1.1	1.1	1.2	1.2	1.3
			σ, X-lev	0.05	0.07	0.09	0.11	0.13	0.16	0.20	0.23
			σ, 31'Warp	0.06	0.08	0.11	0.13	0.16	0.19	0.23	0.28
		Alignment	$A_7 \times 10^{-4}$	0.06	0.13	0.28	0.50	0.89	1.6	2.8	5.0
			$\phi_{73} \times 10^{-3}$	15.8	12.6	10.0	10.0	10.0	10.0	10.0	10.0
			$\phi_{74} \times 10^{-2}$	(†)	5.6	5.6	5.6	5.6	5.6	5.6	5.6
			$\phi_{75} \times 10^{-1}$	(†)	0.71	0.97	1.8	1.3	1.5	1.7	2.0
			σ, 62' MCO	0.09	0.11	0.13	0.18	0.24	0.32	0.42	0.57
		Gage	$A_8 \times 10^{-4}$	0.20	0.22	0.28	0.50	0.89	1.6	2.8	5.0
			$\phi_{83} \times 10^{-3}$	8.9.	8.9	8.9	8.9	8.9	8.9	8.9	8.9
			$\phi_{84} \times 10^{-2}$	(†)	(†)	7.1	7.1	7.1	7.1	7.1	7.1
			$\phi_{85} \times 10^{-1}$	(†)	(†)	0.87	1.00	1.15	1.30	1.5	1.8
			σ, Gage	0.04	0.06	0.07	0.09	0.13	0.17	0.22	0.30
Periodic Deterministic Process (Individual Rail)		Profile	Joint Ampl. $\bar{c}$ (in)	0.06	0.08	0.11	0.14	0.19	0.25	0.33	0.45
			Decay Rate, k (ft^{-1})	0.42	0.33	0.25	0.20	0.15	0.14	0.13	0.13
		Alignment	Joint Ampl. $\bar{c}$ (in)	0.04	0.06	0.08	0.11	0.15	0.20	0.27	0.35
			Decay Rate, k (ft^{-1})	*	*	0.57	0.46	0.35	0.20	0.15	0.12

* = Reliable estimators not currently available.

† = Degenerate pair of corner frequencies.

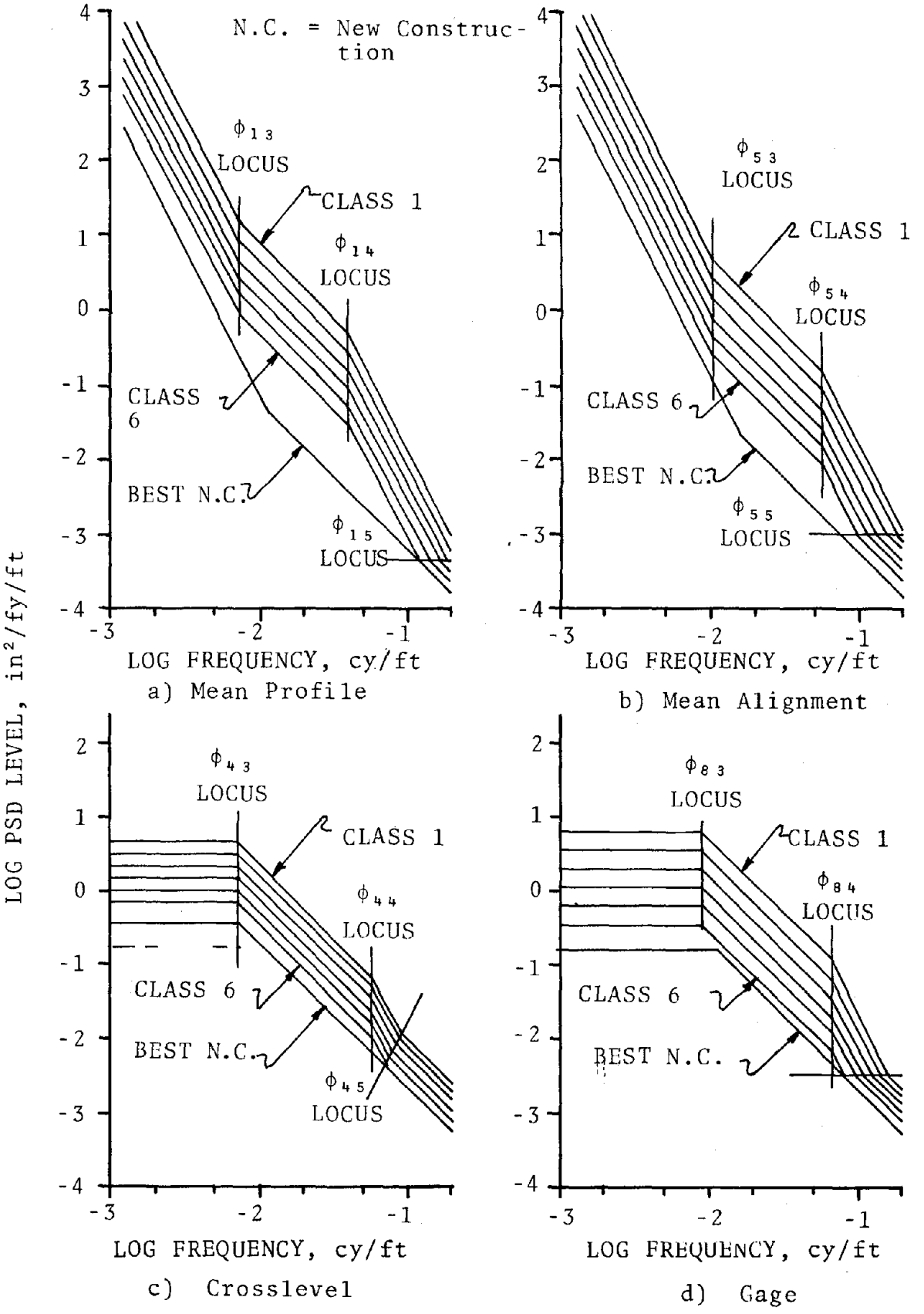

FIGURE 2. SPECTRAL MODELS AS A FUNCTION OF TRACK CLASS AS DEFINED IN CURRENT TRACK SAFETY STANDARDS

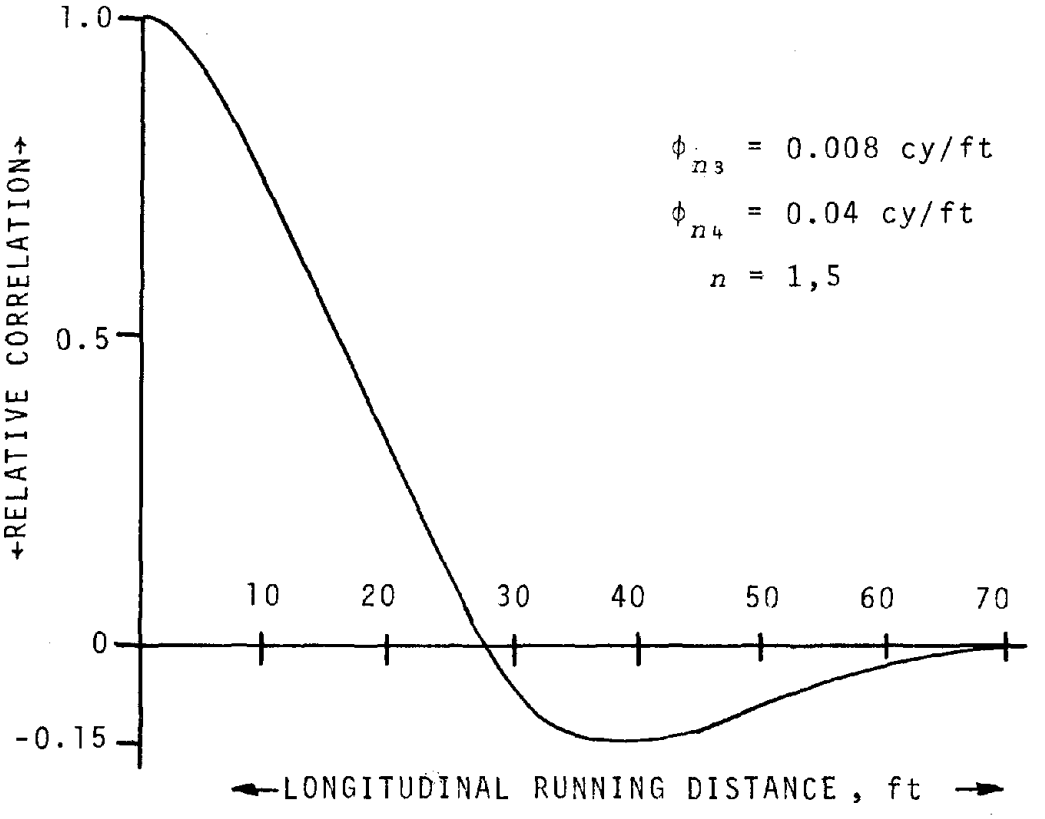

a) 62 FOOT MID-CHORD ON MODEL SPECTRUM, $A_n(\phi)$

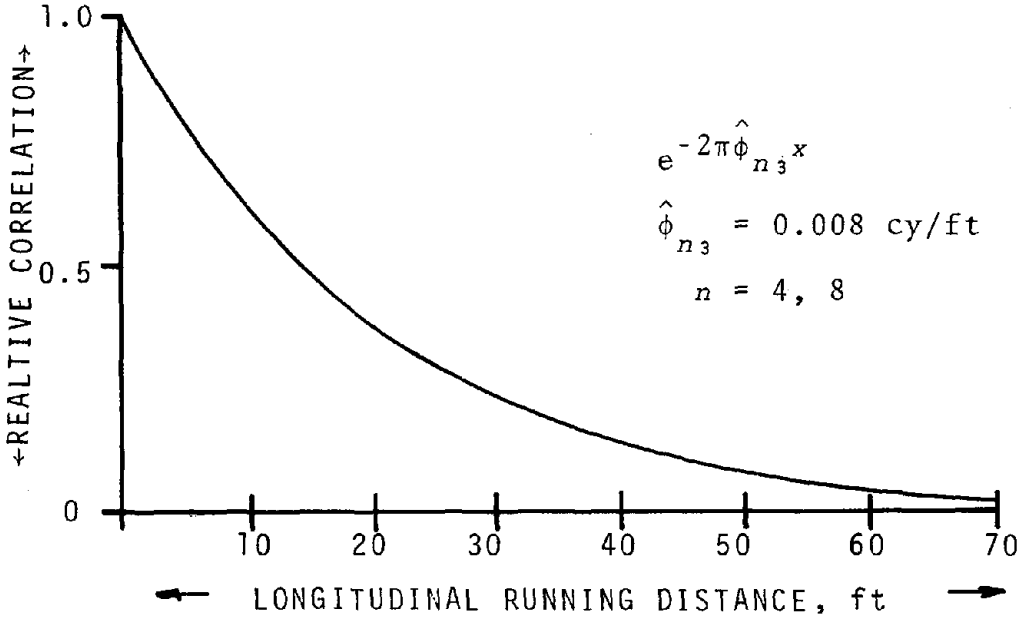

b) CROSSLEVEL AND GAGE ON MODEL SPECTRUM, $A_n(\phi)$

FIGURE 3. CORRELATION PROPERTIES OF CURRENT TRACK GEOMETRY MEASUREMENTS

describes how far along the track one must travel to obtain an independent measurement of geometry. This distance is given by:

$$x_0 = \left[\frac{\int_0^\infty x^2 |R(x)| dx}{\int_0^\infty |R(x)| dx} \right]^{\frac{1}{2}} ;$$

where $R(x)$ is the correlation function.

Values of x_0 are on the order to 20 feet for the above track measures. The above measures of track geometry respond predominantly to long wavelength deviations in the space curve. By virtue of the central limit theorem of statistics, the longer wavelength components of the space curve produced by the stationary random component are normally distributed random variables. Using this distribution, and the 20 foot distance between indenpendent measurements a $+5\sigma$ level is exceeded once every 6,600 miles per geometry variable. A $+4$-σ exception is exceeded once every 60 miles. A $+3$-σ value occurs once every 1.4 miles. *Therefore, for class 4 through 1, the stationary random process acting by itself is unlikely to produce exceptions to the safety standards for geometry variations other than gage.*

The curve fitting procedure was applied to the spectral line components of the empirical PSD's. The mean amplitude, $\bar{c}$, and the decay rate, k, were thus evaluated. A regression against track class produced the results summarized in the bottom part of Table 3. There are significant variations of both $\bar{c}$ and k as a function of track class with both the amplitude and the duration (k^{-1}) growing with degradation. Also, the scatter in $\bar{c}$ about the regression lines increases significantly for the lower classes of track.

Preliminary analysis indicates that joint amplitudes are distributed according to a Γ-distribution. This process is more likely to produce an exception in crosslevel. Also, crosslevel is more likely to produce an exception than is profile. The

crosslevel exception requires a low joint of amplitude $6\text{-}\bar{c}$ in classes 1-4.* The probability that a single low joint will exceed a level of $6\text{-}\bar{c}$ is on the order of 10^{-7}. With each joint acting independently and spaced on the average of 19.5 ft, a $6\text{-}\bar{c}$ joint will happen once every 38,000 miles.

In actual anomaly-free track, the randomly distributed joints are superimposed on the stationary random process. If the random joint process ($6\bar{c}$ = exception level) is combined with the stationary random process (5σ = exception level), then the combined process produces a crosslevel exception once every 60 miles. The history of crosslevel data collection reveals that, on the average, there is one crosslevel exception to the posted operating class every 2 miles. *Therefore, it is concluded that the periodically modulated random process ascribed to anomaly-free track cannot account for the observed frequency of geometry exceptions.*

1.3.2 FINDINGS BY TASK

1.3.2.1 System Noise Floors

The definition of track geometry characteristics and the evaluation of the process parameters is limited by the noise floors, dynamic range, calibration accuracy, and response characteristics of the measurement systems. In the geometry measurement systems currently used, the noise floor represents the most persistent problem. Careful design of the new inertial systems has helped to eliminate most of the other problems.

Noise floors are separated into long and short wavelength classifications. In the long wavelength limit, all profile and alignment systems examined produce a noise spectrum given by

$$\lim_{\phi \to 0} \; S_n(\phi) = \frac{\alpha}{\phi^4} \;,$$

*Warp requires only a $3\text{-}\bar{c}$ event to produce an exception. However, warp involves *pairs* of joints on opposite rails and the associated probability is more complex than the Γ-distribution that applies to individual joints.

where α is a constant and $S_n(\phi)$ is the noise spectrum. Since profile and alignment deviations have this form for their long wavelength spectrum it is important to learn that the signal to noise ratio is greater than unity in this limit. Generally, crosslevel and gage do not experience long wavelength noise problems.

In the short wavelength limit, system performance is invariably limited by the error in measuring rail displacements. In profile and crosslevel, displacement uncertainty is introduced by wheel roughness and wheel taper which are not accounted for in the measurement process. Alignment and gage are dependent on gage sensors that are free to vibrate relative to one another, and which exhibit occasional noise spikes. Short wavelength noise floors are of the form ,

$$\lim_{\phi \to \infty} S_n(\phi) = \beta,$$

where β is a constant.

Values of α and β for the various systems currently in use are given in Table 4. They reveal that greater precautions, relative to operating speed and shortest valid wavelength, are needed for T-2 and T-3 than are required for either the TSD or T-6.

1.3.2.2 Analytical Representations of Geometry Statistics

Analytical models of the continuum portion of geometry PSD's were determined. These are given in Tables 1 and 2. These PSD's are associated with the stationary random component of geometry. As far as typical geometry measures (space curves, midchord offsets) are concerned the stationary random process is a normally distributed random variable represented by the density function, $p_1(y)$:

TABLE 4. COMPARATIVE NOISE FLOORS FOR FRA GEOMETRY MEASUREMENT SYSTEMS

Vehicle →	TSD	T-2	T-3	T-6
α : in^2-$(cy/ft)^3$ $\times 10^{-10}$				
Profile	0.04	32.0*§	8.0*	2.0*
Alignment	0.08	N/A	N/A	2.0
Curvature	N/A	0.25†	0.25†	0.25†
β : $in^2/cy/ft$ $\times 10^{-4}$				
Profile	<<1.0	~2.0	~2.0	~2.0
Alignment	<<1.0	N/A	N/A	4.0
Crosslevel	<<1.0	~3.2	~3.2	~3.2
Gage	<<1.0	~16.0¶	~16.0¶	~6.4

* At 30 mph. Noise floor varies as $(speed)^{-3}$.
† At 30 mph. Noise floor varies as $(speed)^{-1}$.
§ High noise level is the result of constant wavelength analog processing.
¶ High noise floor due to gage sensor vibration.

$$p_1(y) = \frac{1}{\sqrt{2\pi}\,\sigma} e^{-\frac{1}{2}(y/\sigma)^2},$$

where y is a geometry variable, and σ is its standard deviation.

It was further determined that there is no cross correlation between any pair of: mean profile, crosslevel, mean alignment, and gage. Therefore, the corresponding cross PSD's vanish.

The periodic occurrence of joints produces the periodically modulated random process. Joints produce a distinctive cusp shape when observed in geometry space curves. To this end three cusp joint models were examined. It was found that differences between the models were buried in the stationary random fluctuations. Therefore, the exponential joint was used for its analytical simplicity. This is given by:

$$y(x) = Ce^{-k|x|},$$

where the amplitudes are independent, random variables represented by the density function, $p_2(C)$:

$$p_2(C) = \begin{cases} 0, & -\infty < C < 0; \\ \left(\frac{4}{\bar{C}}\right)^4 \frac{C^3 e^{-4C/\bar{C}}}{6}, & 0 \le C < \infty \end{cases}$$

where $\bar{C}$ is the mean of C.

The distribution has a non-zero mean and this produces the line component found in empirical PSD's. This analytical model produces line components in the PSD whose peak values are bounded by the envelope function, $S_e(\phi)$, given by

$$S_e(\phi) = \frac{8}{B}\left[\frac{\bar{C}}{Lk}\right]^2 \left[\frac{1}{k^2 + (2\pi\phi)^2}\right]^2,$$

where L is the rail length in feet, and B is the bandwidth in cycles/ft of the PSD processor.

The stationary random process and the periodic joint process occur simultaneously. The density function for this combined process is given by

$$p_3(y) = Ke^{-\frac{1}{2}(y/\sigma)^2}\left\{(1+\ell^2) + \frac{\sqrt{\pi}}{2}(3\ell + 2\ell^3)[1 + \mathrm{erf}(\ell)]\, e^{\ell^2}\right\},$$

where:

$$K = \frac{1}{3\sigma\sqrt{2\pi}}\left(\frac{4\sigma}{\overline{c}}\right)^4; \quad \ell = \frac{1}{\sqrt{2}}\left(\frac{y}{\sigma} - \frac{4\sigma}{\overline{c}}\right).$$

The densities $p_1(y)$, $p_2(y)$ and $p_3(y)$ are graphed in Figure 4.

1.3.2.3 Formulation of Hypotheses

It was concluded that a necessary and sufficient representation of anomaly-free track geometry is provided by a periodically modulated random process. This process includes, as subsets, two processes that have been traditionally associated with track geometry and which are manifest by distinctive PSD signatures:

- A continuous stationary random process that accounts for random behavior uniformly distributed throughout the rail length, and
- A periodic deterministic process that accounts for uniform dips at periodically spaced joints.

Further, it is concluded that the stationary random component can be represented by PSD's of the form given in Tables 1 and 2.

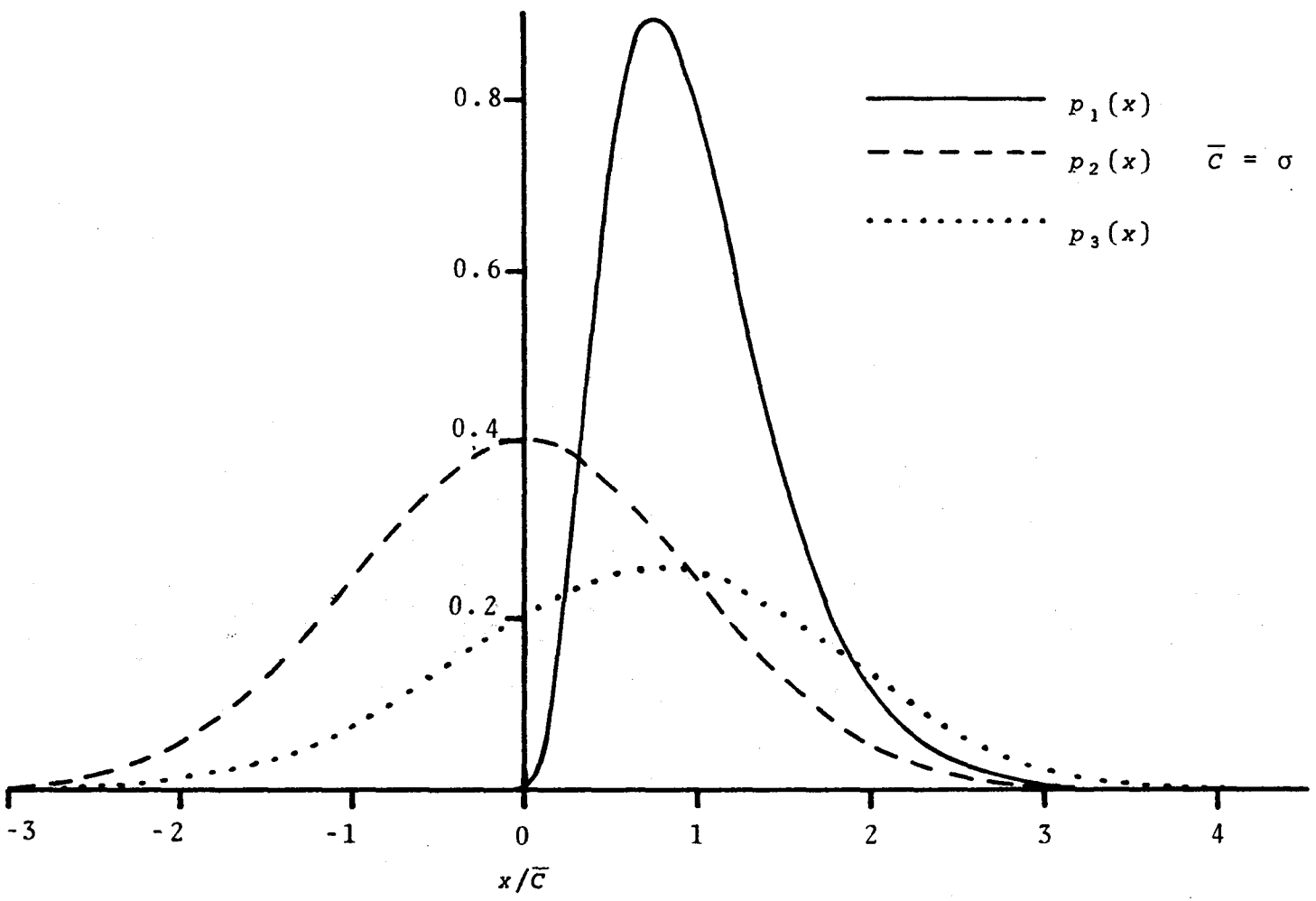

FIGURE 4. COMPARISON OF PROBABILITY DENSITIES $p_1(x)$, $p_2(x)$, and $p_3(x)$

1.3.2.4 Processing of Empirical PSD's

Empirical PSD's were processed from geometry data representing the full range of track classes as defined in the Track Safety Standards.[3] Twenty-nine zones of track representing a total of 150 miles of track data were so processed. From these, the various parameters such as the roughness constant, A_n, corner frequencies, ϕ_{nm}, mean joint amplitude, $\bar{c}$, and decay rate, k, were estimated. Each of these was plotted as a function of track class, giving data values that clustered about a smooth curve.

The results are tabulated in Table 3. Observed scatter in the curve fits is on the order of +60%, -40% worst case.

1.3.2.5 Characterization of Anomalies

Characterization of anomalies was performed on profile and crosslevel geometry using a newly developed space curve output that is free of phase distortion. Anomalies were identified by type as listed in Table 5. Examination of anomalies reveals that:

- On 95% of the track studied anomalies define the peak geometry values.
- Their frequency of occurrence combined with their characteristic signatures are such that they will not be produced by a simply formulated statistical process.
- They have both fixed and random components.
- They are modelable by a combination of joint-like cusp shapes and depression shapes such as shown in Figure 5.

TABLE 5. LIST OF TRACK ANOMALIES

- JOINT-RELATED ANOMALIES:
  - Splice Bar Joints in Continuous Welded Rail;
  - Spliced or Welded Rail Sections with Shorter than Normal Length;
  - Field Welds in Shop Welded Rail.
  - Soft Joints due to Loose Bolts or Soft Ballast Under the Joint;
  - Change in Type of Rail, e.g., Bolted to Continuous and Vice Versa;
  - Insulated Joints.
- ROADBED AND SUBGRADE ANOMALIES:
  - Fill-Cut Transitions;
  - Transitions to Bridge Structures;
  - Washouts and Soft Spots;
  - Soft and Unstable Subgrades.
- TRACK ASSEMBLIES:
  - Turnouts, Especially Points and Frogs.
  - Crossing Frogs.
- MAINTENANCE-INDUCED ANOMALIES:
  - Areas of Spot Maintenance;
  - Areas of Low Maintenance, e.g., Grade Crossings;
  - Areas of Intensive Maintenance due to Rapid Degradation Rate;
  - Change from One Track Class to Another.
- FAULTY TIES:
  - Individual Rotten Ties;
  - Broken or Missing Ties.

A. CUSPS

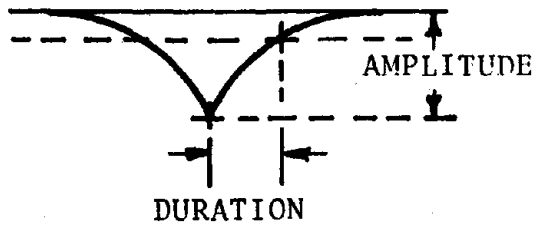

B. DEPRESSIONS

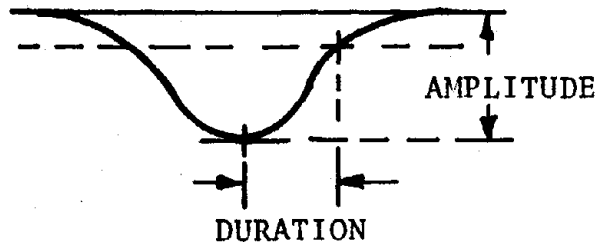

FIGURE 5. DEFINITION OF ANOMALY COMPONENTS AND COMPONENT PARAMETERS

- Both cusp and depression shapes are characterized by an amplitude and a duration.
- For a given type of anomaly, the amplitude will be a random variable.

Additional randomness is uniformly distributed throughout such extended anomalies as turnouts and interlockings. The level of this uniform randomness is on the order of twice the levels associated with the stationary random process in the anomaly-free surroundings.

1.3.2.6 Characterization Using Field Measurement Procedures

The relationships between the analytical models and readily performed field measurements were established and the following conclusions were reached:

- Profile and alignment of anomaly-free track sections are best characterized by using mid-chord offsets with a chord length of $\frac{1}{2}L$.
- Measurements of profile, crosslevel, alignment, and gage should be collected at intervals of $\frac{1}{4}L$ starting at a joint.
- The mean values of joint-centered chords, quarter-point chords and mid-rail chords should be computed independently and then combined to yield $\bar{c}$ and k.
- The stationary random component appears as a normally distributed random variable characterized by its standard deviation, σ.
- The standard deviation of the distribution of all measurements is directly related to the PSD roughness amplitude and at least one corner frequency.

Field data is collected without loading the track. Unless this data is corrected for the effects of load, parameters derived from field data may differ significantly from the same parameters computed from geometry car data.

1.3.2.7 Vertical Track Static Compliance Characteristics

Vertical track static compliance data was collected and processed by ENSCO, Inc. under a separate contract to the Federal Railroad Administration (FRA). Analysis of this data revealed the following characteristics for anomaly-free track[4]:

---

[4]G. Gunn, "Test Results Report, Track Stiffness Evaluation Program," Report No. FRA-ORD-77-45, December 1977.

- The nominal, or average vertical compliance of the track surveyed was 3.5 μin/lb.
- There were slow, long wavelength variations in compliance about the nominal compliance that vary from 2.0 to 6.0 μin/lb with the more compliant track resting on an embankment (fill) or a swampy area, and less compliant track resting in a cut.
- There were sinusoidal variations of 39 ft wavelength whose peak-to-peak variations are 0.8 μin/lb on stretches of track in which welds are not staggered.
- There were sinusoidal variations of 19.5 ft wavelength whose peak-to-peak variations are 0.4 μin/lb on stretches of track where welds are staggered.

Compliance anomalies cannot be properly characterized by this measurement technique without performing a detailed analysis of the compliance measurement system as related to the specific anomalous track structure.[5]

1.4 CONCLUSIONS

The principal conclusions resulting from this research are summarized as follows.

- The PSD continuum gives a good indication of the stationary random component.
- The pronounced peaks in the PSD give the duration (increase decay rate) and the mean amplitude of a cusp joint shape.
- The specific analytical form of the cusp shape is not critical. Differences in analytical form are obscured by the stationary random process.
- The PSD continuum is modeled by even power laws and break frequencies that do not change significantly for different track classes.

[5]G. Hayes, P. Joshi, and J. Sullivan, "Track Stiffness Measurement System Evaluation Program," Final Report, FRA/ORD-79/30, May 1979.

- The stationary random process is well represented by a single roughness parameter that is strongly related to track class.

- Within a track class, different mixtures of the stationary random component and the joint-related component can exist.

- Both mean joint amplitude and joint duration increase with track degradation. There is considerable evidence that additional parameters that describe the randomness of joint amplitudes will play a role here.

- The periodically modulated random process is not adequately defined by PSD or other homogeneous statistical processing techniques that ignore the larger deviations at and around joints and welds.

- The periodically modulated random process as currently modeled is capable of producing by itself, one exception to the FRA track safety standards every 66 miles. This is less than 3% of the observed rate of exceptions.

- The bulk of exceptions are associated with anomalies.

1.5 RECOMMENDED AREAS FOR FURTHER STUDY

In this effort significant progress was made not only in demonstrating the feasibility of statistically characterizing track geometry, but also in the characterization process itself. However, a full characterization of track geometry requires certain data collection and processing techniques that exceed the state-of-the-art in several key areas as described below. It is recommended that the concepts developed in this project be expanded in the four areas described below.

First, an operational inertial alignment system was not developed until the end of this study. Alignment data used here was drawn from two sources:

- The now-abandoned capacitive alignment system whose performance is limited to wavelengths between 10 ft and 100 ft. Alignment data collected is available from a wide range of track classes and territory.

- The Track Survey Device (TSD) whose output is limited by cost ($200-1000/mi) and effective speed (1 mi/hr) of data collection. Available data is also highly localized, all of it being collected in the Pueblo, Colorado area.

Therefore, the existing data is restricted with respect to bandwidth or area. Nonetheless, some provisional models for alignment PSD's are advanced. Universality of these models is questionable since they do not take into account known alignment periodicities that are observed in track used by unit trains or dynamically troublesome locomotives.

The recently developed inertial alignment system on the FRA Survey Car, T-6, allows examination of alignment geometry in a manner that is not contaminated by the frequency response of a mid-chord offset. Alignment anomalies can also be examined by using the inertial alignment system in conjunction with a zero phase shift space curve processor. (Such a processor was successfully applied to inertial profile data during this effort to characterize profile anomalies.)

Second, homogeneous processing techniques such as autocorrelations, PSD's, and histogrammetry, cannot distinguish between the stationary random process and the periodically modulated random process. In order to recover the periodic features from track geometry data, the data must first be classified according to its position in each length of rail. During the period of this project, automated methods of performing this classification existed in concept only. Data that was analyzed for the periodically modulated random process required considerable

manual interpretation, therefore, such analysis was only able to cover a very restricted subset of this process as found in U.S. practice.

Third, in order to develop field-implementable methodologies that would account for all processes in anomaly-free track, a very simplistic model of the periodically modulated random process was adopted. It was assumed that the random amplitude of the joint/weld cusp was independent from one rail to the next. The fact that the presence of a low joint on one rail results in a depression on the opposite rail was ignored. Since joint-to-joint correlation and rail-to-rail correlation are common in field data, it is quite important that the statistical model take these observables into account. Further, proposed field-implementable techniques must be modified to reflect this more informed point of view.

Fourth, it is important to recognize that traditional alignment and gage measurements of track geometry are concerned with the location of the rail head at a point 5/8" down from the rolling surface. This geometry does not properly describe the dynamic input to the vehicle or track structure in terms of the lateral position of the wheel except in the case of flanging. Dynamic behavior is concerned with the location of the wheel/rail contact patch, which itself depends on the existing state of wear of the rail head. Consequently, an analysis procedure is needed which will enable rail head wear and the contact patch to be characterized.

2. TECHNICAL APPROACH

2.1 CLASSIFICATION OF PROCESSES

By identifying time with longitudinal distance, conventional methods for analyzing time series signals can be applied to the analysis of track geometry data. Such data can be sorted into two major categories (deterministic and random) and can be classified further as is illustrated in Figures 6 and 7.[6] All of the signal types shown and described in Figures 6 and 7 are found in track geometry data, often in combination.

Each signal type dictates the procedure which should be applied to its analysis. For example, most Stationary Random Processes (SRP) are well defined by their probability distributions and by the covariance between events separated by time, τ, also called the correlation function. In the case where the SRP is a normally distributed random variable, the correlation function, or equivalently, the PSD, completely describes the process. Therefore, the applicable analytical techniques for the SRP are histograms and PSD's.

The categories of signals illustrated in Figures 6 and 7 are rarely present individually in track geometry. They combine additively, and in order to determine whether a particular variation in the geometry belongs to a specific signal category or to some combination of categories, it is necessary to examine the data in conjunction with field observations or physical knowledge of the track structure.

At the same time, the analytical technique must take into account the most complex process present. For example, anomaly-free track is the synthesis of three component processes identified in this signal classification process:

---

[6] J. S. Bendat and A. G. Piersol, *Random Data: Analysis and Measurement Procedures*, Wiley, New York, 1971, p. 2-14.

A. CLASSIFICATION DIAGRAM

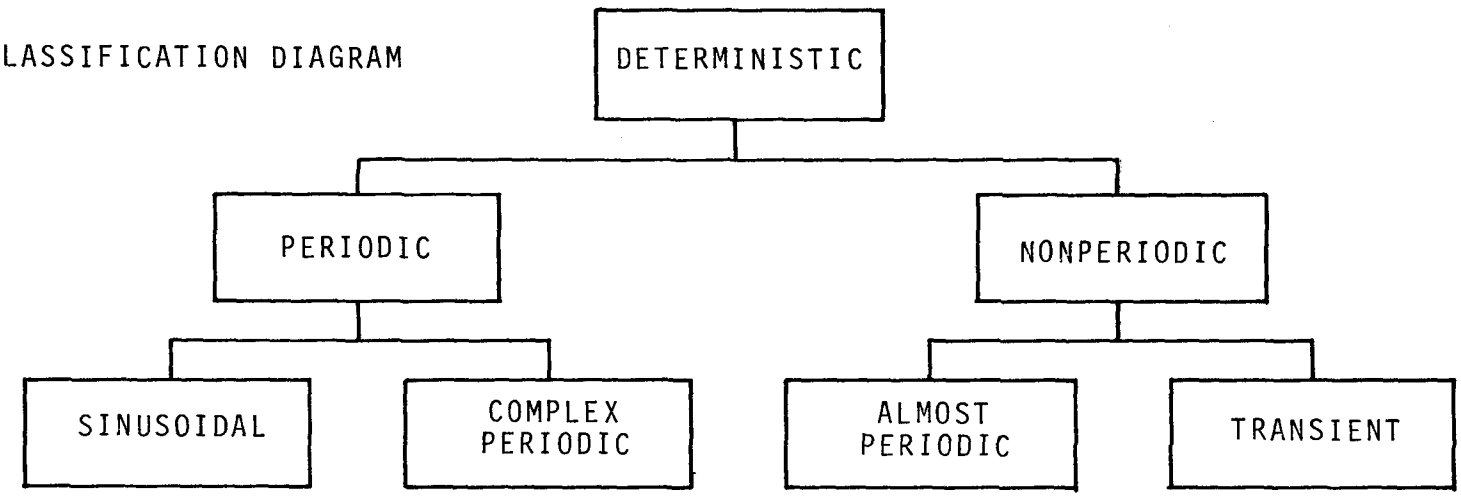

B. ILLUSTRATIVE EXAMPLES

C. EXAMPLES IN RAILWAY TRACK

- CORRUGATIONS (~1 FOOT WAVE-LENGTH)
- NON-ZERO MEAN OF JOINTS AMPLITUDES
- PLASTIC DEFORMATION OF BALLAST/ ENBANKMENT (BALLAST MEMORY)
- FIXED OR MEAN COMPONENT OF ANOMALIES

FIGURE 6. CLASSIFICATION OF DETERMINISTIC SIGNALS

A. CLASSIFICATION DIAGRAM

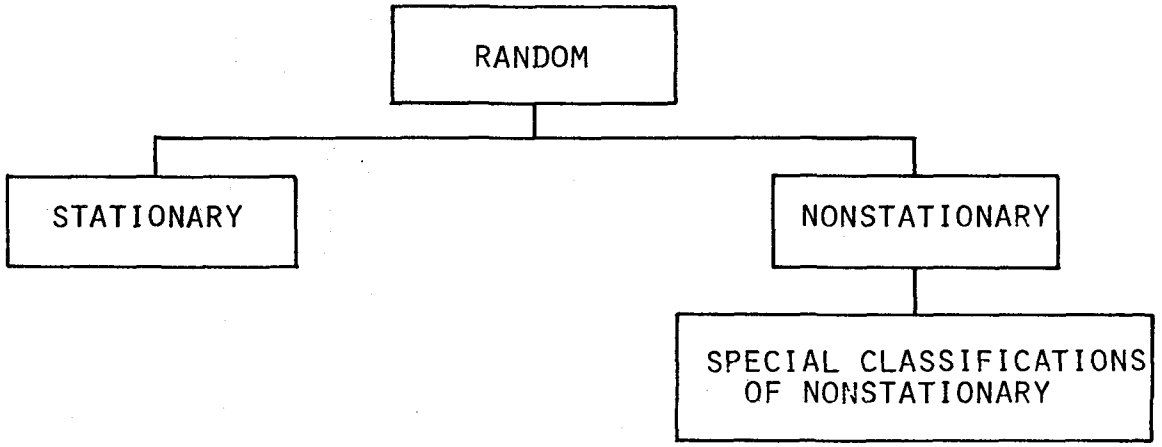

B. ILLUSTRATIVE EXAMPLES

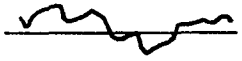

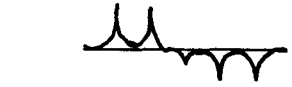

C. EXAMPLES IN RAILWAY TRACK

- RANDOM WAVINESS

- RANDOM FLUCTUATIONS OF JOINTS AMPLITUDES ACTING ON JOINT SHAPE
- RANDOM COMPONENT OF ANOMALIES
- SPOT MAINTENANCE

FIGURE 7. CLASSIFICATION OF RANDOM SIGNALS

- Random irregularities accumulated during the course of rail manufacture, survey, lining, surfacing, embankment support variations, degradation, and maintenance are embodied in the SRP.

- Random variations in the amplitude(s) of one or more shape functions associated with joints or welds which occur periodically are manifest under a "special classification of non-stationarity".

- A non-zero mean in the randomly varying amplitude(s) associated with joints or welds, producing the Periodic Deterministic Process (PDP).

These last two processes are the result of the practice of rolling rails in relatively short but constant lengths (mostly 39 ft, but anywhere from 33 ft to 80 ft in practice) and then bolting or welding them into the longer sections found in track.

The all-inclusive process for anomaly-free track is the Periodically Modulated Random Process (PMRP), one in which the mean, the covariance, and higher order statistics are periodic functions of position in the rail length. That the PMRP is indeed the all-inclusive process can be demonstrated from the following special cases of the PMRP.

- If all moments are made to be constant, i.e., independent of position along the rail, this defines the SRP, and

- If the mean is allowed to remain periodic, and if all higher order moments vanish, a PDP results.

Periodic variations in the covariance and higher order moments of the PMRP require further elaboration. For now, it is asserted

that these variations can be linked to random variations in the amplitude of joint shape functions. However, it is thought that the rolling of the rail and the factory straightening of rail produces other locations in the rail length that exhibit relatively large random variations.

2.2 THE STATIONARY RANDOM PROCESS (SRP)

The SRP describes the geometric irregularities that cannot be linked to such physical causes as joints, welds and anomalies. It is the only process present if the track is constructed in the following manner:

- The rail is manufactured in long lengths in much the same way that wire is drawn.
- Aligning and surfacing operations are such that they transform an existing SRP into a new SRP.
- Subsequent degradation of the track is such that the existing SRP transforms into a new SRP.

Because of dimensional constraints of existing cooling beds, most U.S. rail is rolled in 39 foot lengths. Even Continuous Welded Rail (CWR) consists of these 39-foot lengths welded into strings of 700 feet or longer. As a result, additional signal components contaminate the SRP. Nonetheless in the statistical representation of track irregularities, it is adequate to consider the SRP as derived from these sources:

- Rail manufacturing,
- Laying the track,
- Support properties of the embankment,

- Subsequent degradation of the track
- Maintenance of the track.

2.2.1 CONTINUOUS TREATMENT OF SRP GENERATION

As indicated previously, the SRP is described by its probability distribution and its PSD. Hence, a given SRP can be produced from a white noise source operated on by a linear filter that is designed to give the desired PSD. A procedure is described below for designing a filter to yield a PSD similar to the PSD of the track measurement. The response characteristics of this filter are prescribed by,

$$|H(\phi)| = [S(\phi)]^{\frac{1}{2}}$$

where $H(\phi)$ is the filter frequency response, generally a complex function of ϕ.

It was also indicated that the SRP in railway track was produced by physical processes acting on the track, the composite of which could be represented by linear differo-integral operators functioning on a white noise source, The generalized form for such an operator is given by:

$$\prod_{n=1}^{N} \left(\frac{d}{dx} + 2\pi a_n \right) y(x) = H_0 \prod_{m=1}^{M} \left(\frac{d}{dx} + 2\pi b_m \right) w(x)$$

where:

$w(x)$ = white noise function,
H_0 = an overall scaling constant,
a_n, b_m = process constants, and
$y(x)$ = resulting SRP.

The process constants may be complex, in which case, they occur in conjugate pairs for real $w(x)$ and $y(x)$. Under Fourier transformation to the frequency domain, symbolized by F_ϕ, the differential elements of the equation give:

$$F_\phi\left\{\frac{d}{dx}\right\} = 2\pi i\phi F_\phi,$$

$$F_\phi\{y(x)\} = Y(\phi), \text{ and}$$

$$F_\phi\{w(x)\} = W(\phi) = 1,$$

so that,

$$Y(\phi) = (2\pi)^{N-M} H_0 \prod_{n,m=1}^{N,M} \frac{i\phi + a_n}{i\phi + b_m} \equiv H(\phi).$$

The resultant PSD is given by:

$$S(\phi) = (2\pi)^{2(N-M)} H_0^2 \prod_{n,m=1}^{N,M} \frac{(\phi - ia_n)(\phi + ia_n^*)}{(\phi - ib_m)(\phi + ib_m^*)},$$

$$= (2\pi)^{2(N-M)} H_0^2 \prod_{n,m=1}^{N,M} \frac{\phi^2 + 2\mathrm{Im}\{a_n\}\phi + |a_n|^2}{\phi^2 + 2\mathrm{Im}\{b_m\}\phi + |a_m|^2}$$

The quantitaites, $|a_n|$ and $|b_m|$ define corner frequencies. The asymptotic behavior of the PSD between and beyond these corners is an *even integer* power law. At a corner, $|a_n|$, the change in power law is +2, and at a corner, $|b_m|$, a change of -2 is observed.

The SRP is also describable in terms of a convolution with the white noise process. Let $k_a(x)$ represent the response of the left hand differential operator to an impulse input. Then,

$$y(x) = H_0 \prod_{m=1}^{M} \left(\frac{d}{dx} + 2\pi b_m \right) \int_{-\infty}^{\infty} k_a(\xi)\ w(x - \xi)\, d\xi.$$

where ξ is an integration variable. The right hand differtial operator can be moved inside of the integral and the resultant integrated by parts to yield,

$$y(x) = \int_{-\infty}^{\infty} k(\xi)\ w(x - \xi)\, d\xi = \int_{-\infty}^{\infty} k(x - \xi)\ w(\xi)\, d\xi.$$

where,

$$k(x) = H_0 \prod_{m=1}^{M} \left(\frac{d}{dx} + 2\pi b_m \right) k_a(x).$$

This result says that a SRP variable, $y(x)$, is the weighted sum (integral) of all white noise values. The weighting is dependent only on the difference in position (time) between where the white noise value is generated and where the current geometry variable is to be measured. $k(\xi)$ is called the process kernel.

It was indicated that the geometry SRP is caused by a history of forces applied to the rail. Hence, the process kernel should be of a causal form, $k_c(x)$ which has the property:

$$k_c(x) = \begin{cases} 0, & x < 0; \text{ and} \\ k(x), & x > 0. \end{cases}$$

The geometry variable is now given by,

$$y(x) = \int_{0}^{\infty} k_c(\xi) w(x - \xi)\, d\xi = \int_{-\infty}^{x} k(x - \xi)\ w(\xi)\, d\xi.$$

Hence, a causal SRP is the weighted sum of only past values of random generators. The necessary and sufficient conditions for a causal process is that:

$\mathrm{Re}\{a_n\} > 0$ for all $n = 1,2\ldots,N$.

This is not a severe constraint since virtually any form of PSD can be modeled using a sufficient number of a_n satisfying the causality condition together with a sufficient number of b_m.

2.2.2 DISCRETE TREATMENT OF SRP GENERATION

The final positioning of the rail consists of fastening it to periodically spaced ties. The data that is used to characterize geometry is sampled at distinct evenly spaced intervals. Therefore, it is reasonable to expect that discrete differo-integral operators and discrete process kernels would be more appropriate to understanding and analyzing of track data.

Let $y_n = y(nX)$ be a sequence of discrete geometry measurements, and $w_n = w(nX)$, be a sequence of discrete random white noise values where x is the sample interval. Then the process kernel convolution becomes a sum,

$$y_n = \sum_{m=1}^{\infty} \eta_n w_{n-m} = \sum_{m=-\infty}^{n} \eta_{n-m} w_m$$

where the η_m define a causal discrete process kernel. In some situations, it is sufficient to equate the discrete process kernel with sampled values of the continuous kernel, that is,

$$\eta_m = k(nX).$$

However, some continuous process kernels do not admit to such treatment.

As written, y_n, is generated as the infinite weighted sum of all past values of w_m. This is the definition of a discrete, or digital filter. Digital filters that are designed to behave like continuous causal filters can generally be implemented in the form of a finite recursive sum[7]:

$$y_n = \sum_{m=1}^{M} h_m w_{n-m} - \sum_{m=1}^{N} g_m y_{n-m}$$

where h_m and g_m are filter coefficients. In this form, a current value of y_n is given as the weighted sum of a few white noise values, and the weighted sum of a few previous values of y_n. This equation should be compared to the differo-integer operator equation at the beginning of Paragraph 2.2.1. Indeed, the digital equivalent of the continuous operator will have the same values of N and M.

2.2.3 RANDOM WALKS

A random walk is an evolutionary process by which a new position is determined from previous positions and a random variable. The random variable may be the flip of a coin, the output of a random number generator, or sampled values of filtered Gaussian noise. Because of its step-by-step way of evolving, a random walk is explicitly a discrete function of time. By this definition, it is a special form of digital filter represented by

$$y_n = - \sum_{m=1}^{N} g_m y_{n-m} + h_0 w_n.$$

---

[7] L. R. Rabiner and B. Gold, *Theory and Application of Digital Signal Processing*, Prentice-Hall, Englewood Cliffs NJ, 1975, p. 205-292.

The simplest random walk, designated as Type 1, consists of an attempt to place steps about a straight line reference as shown in Figure 8. In placing these steps, offsets are generated that are directly proportional to the white noise source. This is analogous to the process of gaging a second rail relative to a first, or of lining a rail relative to precise survey markers. Some error creeps into the rail positioning and these deviations are given by

$$y_n = h_0 w_n .$$

If the white noise has unit standard error, h_0 becomes the standard error of the steps. The PSD of the w_n is given by

$$S_w(\phi) = \frac{1}{\phi_0} = 2x, \quad 0 < \phi < \phi_0$$

where ϕ_0 is the folding frequency and x is the step length. The PSD of the y_n is

$$S_y(\phi) = h_0^2 S_w(\phi) = 2h_0^2 x, \quad 0 < \phi < \phi_0$$

A Type 2 random walk is illustrated in Figure 9. Here no local reference line is provided. Instead, a sequence of random directions, θ_n, are generated. This is the type of walk generated on a plane while approaching a very distant fixed reference such as a point on the horizon. In laying rail, it is the kind of error experienced when extrapolating the rail position beyond or interpolating between infrequently occuring survey markers. For this walk,

$$\theta_n = h_0 w_n ,$$

- AN ATTEMPT IS MADE TO PLACE EACH STEP ON A GIVEN REFERENCE LINE.
- THE RANDOM WALK LOOKS LIKE:

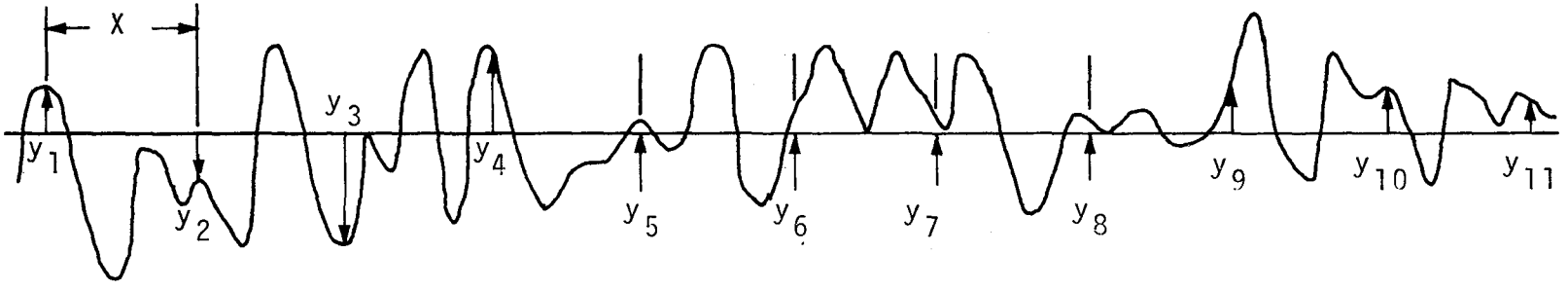

- THE RANDOM WALK IS CHARACTERIZED BY
  - -- THE OFFSET OF STEP, y_n, IS A RANDOM VARIABLE.
  - -- EACH NEW STEP IS INDEPENDENT OF ALL OTHERS.
  - -- THE PSD OF STEP OFFSETS FROM REFERENCE LINE IS A CONSTANT.

FIGURE 8. RANDOM WALK TYPE 1

- AN ATTEMPT IS MADE TO ADJUST THE DIRECTION OF EACH STEP TO A GIVEN REFERENCE DIRECTION.

- THE RANDOM WALK LOOKS LIKE:

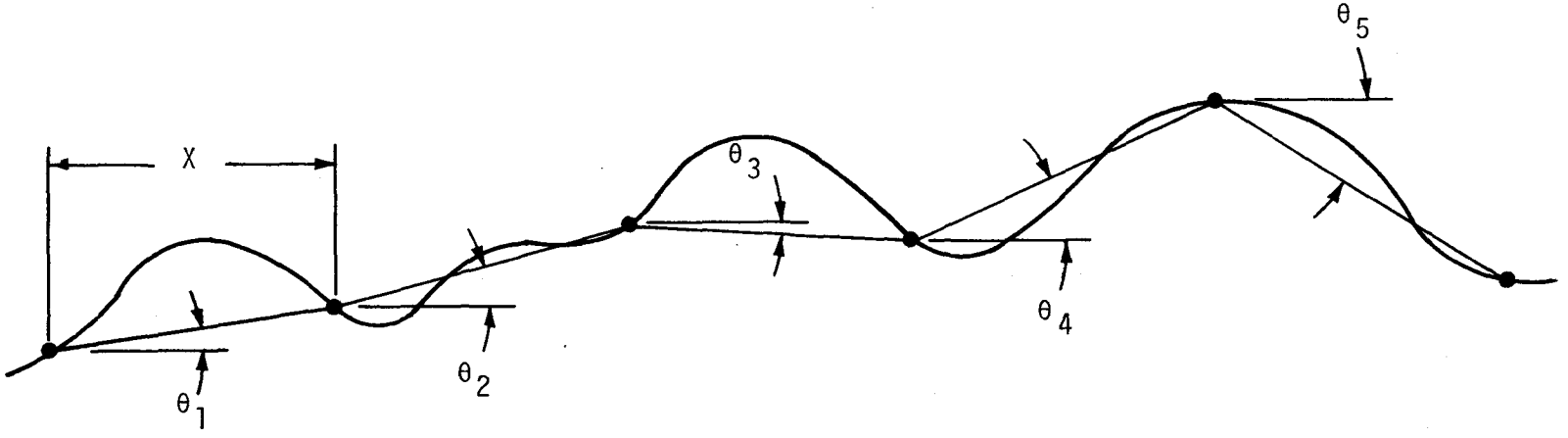

- THE RANDOM WALK IS CHARACTERIZED BY:
  - -- THE ANGLE OF THE STEP RELATIVE TO REFERENCE DIRECTION IS RANDOM.
  - -- EACH ANGLE IS INDEPENDENT OF ALL OTHERS.
  - -- THE PSD OF THE ANGLES IS A CONSTANT.

FIGURE 9. RANDOM WALK TYPE 2

with,

$$\theta_n = (y_n - y_{n-1})/X.$$

Between the equations, θ_n is eliminated and the geometry variable is now given by,

$$y_n = Xh_0 w_n + y_{n+1} .$$

The PSD of the y_n is given by:

$$S_y(\phi) = \frac{h_0^2 X^2}{4 \sin^2(\pi X \phi)} S_w(\phi),$$

$$= \frac{h_0^2 X^3}{2 \sin^2(\pi X \phi)}, \quad 0 < \phi < \phi_0 .$$

For $\phi << \phi_0$ (away from folding) the asymptotic behavior is

$$S_y(\phi) = \frac{h_0^2 X}{2\pi^2 \phi^2} \propto \phi^{-2}.$$

The Type 3 random walk is illustrated in Figure 10. In this model, the only reference for placing a new step is the direction established by two previous steps. This is analogous to walking on a featureless plane without any external landmarks. In laying rail, it is this kind of randomness that is imposed by the terrain. Each new step is defined by a sequence of random angle changes, ψ_n, that are given by,

$$\psi_n = h_0 w_n ,$$

- AN ATTEMPT IS MADE TO CONTINUE IN THE SAME DIRECTION AS WAS TAKEN IN THE PREVIOUS STEP.

- THE RANDOM WALK LOOKS LIKE:

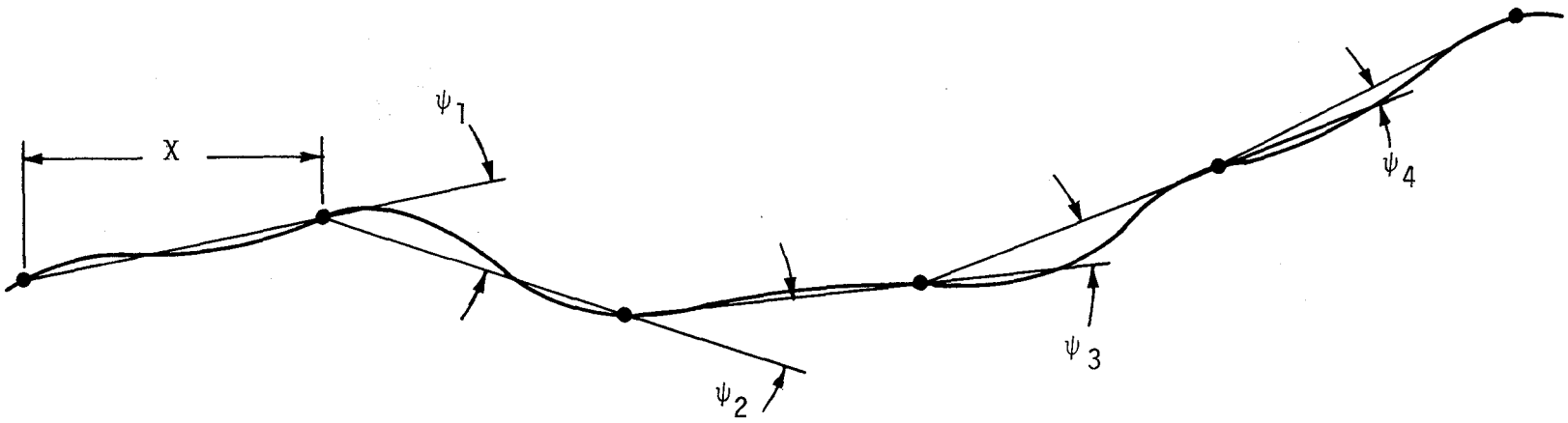

- THE RANDOM WALK IS CHARACTERIZED BY:
  - -- ANGLE OF THE STEP RELATIVE TO PREVIOUS STEP IS RANDOM.
  - -- EACH ANGLE IS INDEPENDENT OF ALL OTHERS.
  - -- PSD OF THE ANGLES IS A CONSTANT.

FIGURE 10. RANDOM WALK TYPE 3

and are related to slopes and space curve by

$$\psi_n = (\phi_n - \phi_{n-1}),$$

$$= (y_n - 2y_{n-1} + y_{n-2})X,$$

respectively. By eliminating ψ_n between these equations, the space curve is given by

$$y_n = Xh_0 w_n + 2y_{n-1} - y_{n-2} .$$

The PSD of the y_n is given by

$$S_y(\phi) = \frac{h_0^2 X^2}{16 \sin^4(\pi X \phi)} S_w(\phi)$$

$$= \frac{h_0^2 X^3}{8 \sin^4(\pi X \phi)}, \quad 0 < \phi < \phi_0 .$$

For $\phi << \phi_0$, the asymptotic behavior is

$$S_y(\phi) = \frac{h_0^2}{8\pi^4 X \phi^4} \propto \phi^{-4} .$$

In an analogous fashion, it is possible to define random walks of even higher orders. For example, a Type 4 random walk is produced from random variations in curvature rate. Its PSD has the asymptotic form

$$S_y(\phi) \sim \phi^{-6} .$$

So far, the Type 4 random walk has been attributed only to mean alignment in spirals, where it appears at wavelengths of 100 to 500 feet. Higher order random walks have not been observed in track geometry.

To summarize, it is seen that random walks of types 2, 3, and 4 produce PSD's whose asymptotic low frequency behavior is represented by negative even power laws. For continuous differo-integral operators, PSD's having these power laws are produced by one or more integrations of white noise. Thus, it is concluded that the discrete random walks found in track geometry are readily related to continuous operators.

The characteristics, PSD's, and asympotic power laws for Types 1, 2 and 3 random walks are summarized in Table 6.

2.2.4 PHYSICAL INTERPRETATION OF COMPOSITE SRP

Track geometry PSD's are often presented as PSD-level versus frequency in a log-log form. As a result, a power law relationship for a continuum appears as a straight line slope. Review of PSD's from railroads in many parts of the world indicates a consistent pattern of distinct frequency bands wherein the PSD is well modeled by an even-powered straight line segment. Power laws 0, -2, -4 and -6 are observed corresponding to Type 1, 2, 3 or 4 random walks, respectively. The ordering of these frequency bands and their power laws is also consistent. PSD models reflecting these observations are illustrated via the Bode plots in Figure 11.

The individual segments of PSD's represented in Figure 11 can be linked to manufacture, installation, and subsequent degradation of the rail. As an example, consider rail profile. Over the range of wavelengths for which data is available, several distinct regions are identifiable. These are summarized in Table 7 and their physical causes are discussed as follows, starting at the short wavelength end of the spectrum.

TABLE 6. SUMMARY OF RANDOM WALK MODELS

Random Walk Type	1	2	3
Random Variable	Offset=Space Curve $Y_n = h_0 w_n$	Direction $\theta_n = h_0 w_n$	Angle Change $\psi_n = h_0 w_n$
Relationship to Space Curve	$y_n \equiv y_n$	$\theta_n = (y_n - y_{n-1}) X$	$\psi_n = \theta_n - \theta_{n-1}$
Random Walk Filter	$y_n = h_0 w_n$	$y_n = X h_0 w_n + y_{n-1}$	$y_n = X h_0 w_n + 2y_{n-1} - y_{n-2}$
PSD, $0 < \phi < \phi_0$ $S_y(\phi)$	$2h_0^2 X$	$\frac{h_0^2 X^3}{2 \sin^2(\pi X \phi)}$	$\frac{h_0^3 X^3}{8 \sin^4(\pi X \phi)}$
Asymptotic PSD, $\phi << \phi_0$	$2h_0^2 X$	$\frac{h_0^2 X}{2\pi^2 \phi^2}$	$\frac{h_0^2}{8\pi^4 X \phi^4}$
Power Law	n = 0	n = -2	n = -4

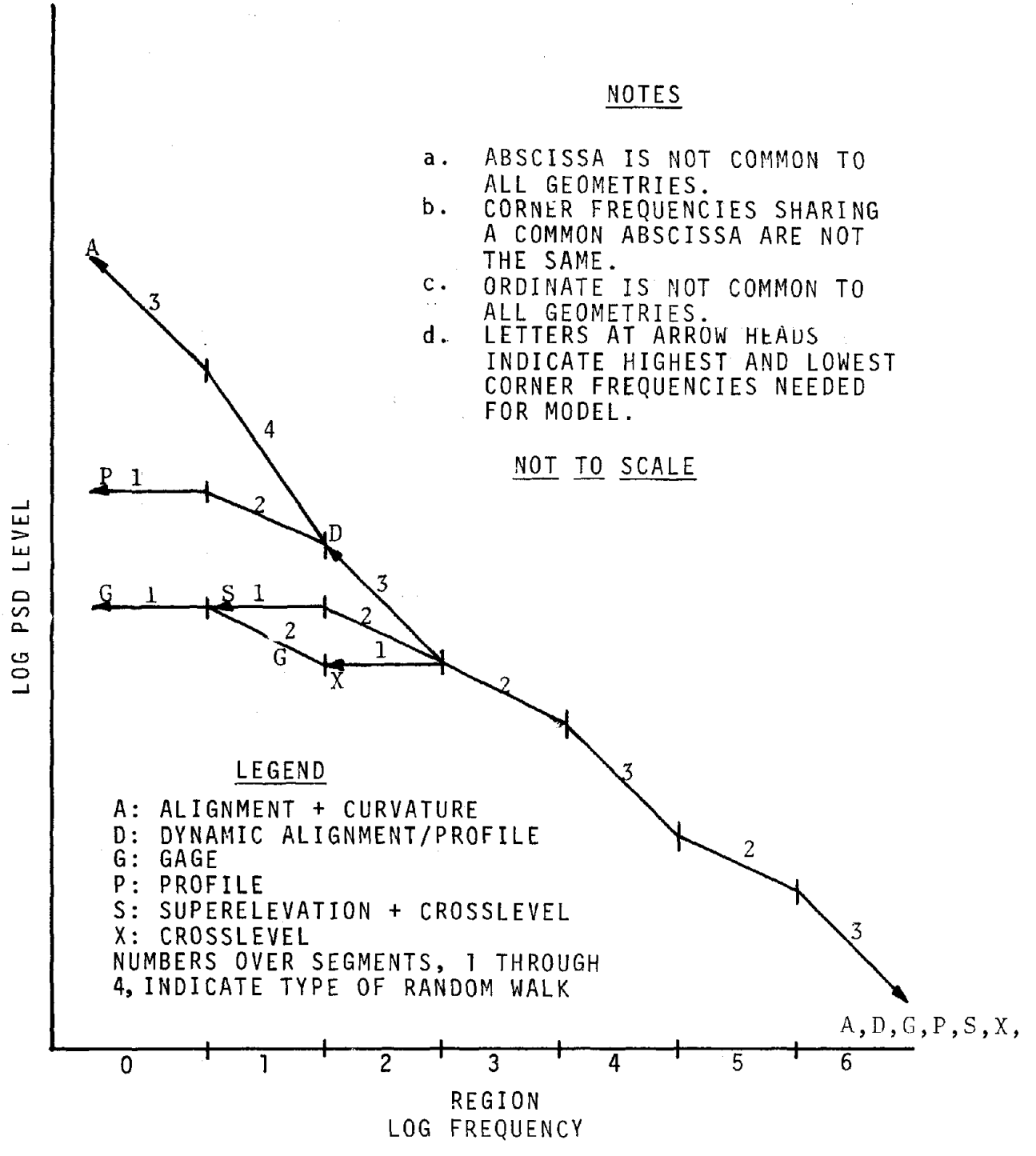

FIGURE 11. PSD REGIONS SHOWING FREQUENCY AND POWER LAW ORDERING OF RANDOM WALKS

TABLE 7. REGIONS OF RAIL PROFILE PSD's

Region	Spectral Behavior	Random Walk Type	Wavelength Range
6	$S(\phi) \sim \phi^{-4}$	3	1 ft $\lesssim \lambda \lesssim$ 2 in
5	$S(\phi) \sim \phi^{-2}$	2	5 ft $\lesssim \lambda \lesssim$ 1 ft
4	$S(\phi) \sim \phi^{-4}$	3	25 ft $\lesssim \lambda \lesssim$ 5 ft
3	$S(\phi) \sim \phi^{-2}$	2	125 ft $\lesssim \lambda \lesssim$ 25 ft
2	$S(\phi) \sim \phi^{-4}$	3	2 mi $\lesssim \lambda \lesssim$ 125 ft

- Region 6, wavelengths from 2 inches to 1 foot:

  The spectrum rises at a λ^4 rate in this band. This is due to roughness in the rollers which induces an unreferenced Type 3 random walk.

- Region 5, wavelengths from 1 foot to 5 feet:

  Grinding operations which are slope-controlled are used by railroads to effect smoothing of the surface geometry so that a Type 2 random walk controls these wavelengths

- Region 4, wavelengths from 5 feet to 25 feet, and Region 3, wavelengths from 25 feet to 125 feet:

  This is the degradation range of wavelengths described by Cousty and Tro.[1] In the very best new contruction, the λ^2, Type 2 random walk (trend established in region 5) is observed to continue through these regions.

- Region 2, wavelengths greater than 125 feet:

  The unreferenced random walk of terrain takes over and establishes a λ^4 trend.

Additionally, very long wavelength regions can be defined, but they have very little impact on the vehicle dynamics or setting of safety standards. In any case, the behavior at these wavelengths ceases to be statistical in nature.

2.2.5 SIMPLE VERSUS MORE DETAILED SPECTRAL MODELS

Returning to the differo-integral operator of Paragraph 2.2.1, and incorporating the results summarized in Table 7, it is seen that the simplest operator that will produce the desired asymptotic fit is one in which $N = 4$ and $M = 2$.

The constants, a_n and b_m are rigorously real having values:

$a_1 = a_2 = 0$

$b_1 = \phi_{13}$ = transition frequency between Regions 2 and 3.

$a_3 = \phi_{14}$ = transition frequency between Regions 3 and 4.

$b_2 = \phi_{15}$ = transition frequency between Regions 4 and 5.

$a_4 = \phi_{16}$ = transition frequency between Regions 5 and 6.

For the range of wavelengths that are validly resolved by current routine geometry surveys, regions 5 and 6 of Table 7 can be ignored so that $N = 3$ and $M = 1$. The PSD of individual rail profile is given by,

$$S_1(\phi) = \frac{A_1 \phi_{14}^2 (\phi^2 + \phi_{13}^2)}{\phi^4 (\phi^2 + \phi_{14}^2)},$$

where, A_1 = profile roughness constant = $H_0^2 / (2\pi)^4 \phi_{14}^2$.

The dashed line of Figure 12 shows a least squares fit of this function to the empirical continuum data of Figure 1. It is achieved using the following corner frequencies:

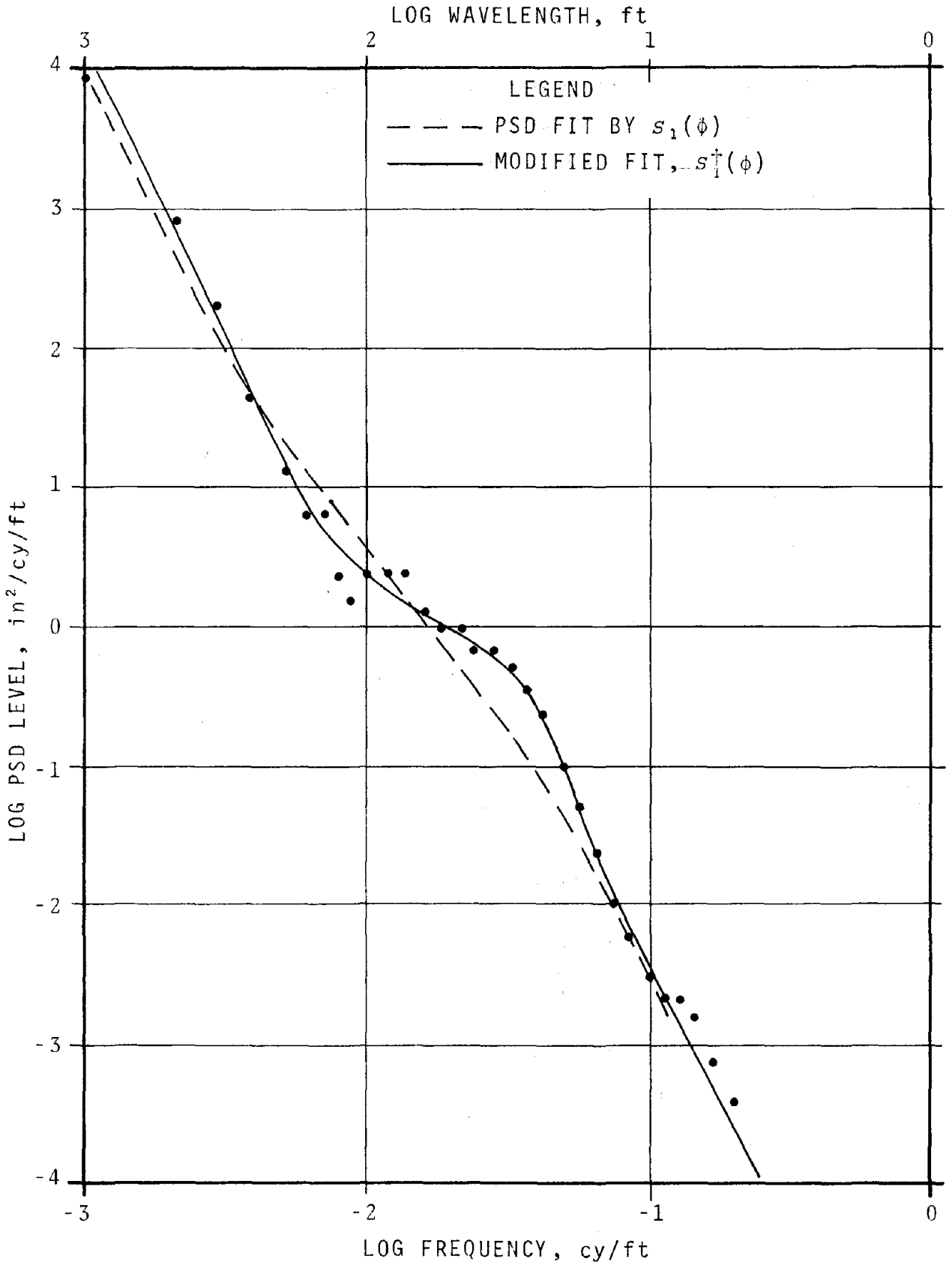

FIGURE 12. COMPARISON OF RAW DATA, $s_1(\phi)$ FIT AND $s_1^\dagger(\phi)$ FIT

$$\phi_{13} = 0.006 \text{ cy/ft},$$

$$\phi_{14} = 0.031 \text{ cy/ft} .$$

Examining this fit reveals that the spectral model cuts the corners too smoothly. It is known that complex a_n and b_m can be made to produce resonance peaks or anti-resonance nulls or minima at the corner frequencies. However, the differo-integral operator is rigorously real so that complex zeros or poles must occur in conjugate pairs.

Using this knowledge, the simplest operator that incorporates the complex transitions at or near $\phi_{13} - \phi_{14}$ requires that $N = 2$ and $M = 4$, and $b_1 = b_2 = 0$.

The associated PSD is

$$S_1^{\dagger}(\phi) = \frac{H_0[\phi^4 + 2(2\text{Re}^2\{a_1\} - |a_1|^2)\phi^2 + |a_1|^4]}{(2\pi\phi)^4 [\phi^4 + 2(2\text{Re}^2\{b_3\} - |b_3|^2)\phi^2 + |b_3|^4]} .$$

The process constants for the least squares fit are

$$|a_1| = |a_2| = 0.011 \text{ cy/ft},$$

$$|b_3| = |b_4| = 0.025 \text{ cy/ft},$$

$$\text{Re}\{a_1\} = \text{Re}\{a_2\} = 0.007 \text{ cy/ft},$$

$$\text{Re}\{b_3\} = \text{Re}\{a_4\} = 0.014 \text{ cy/ft}.$$

Figure 12 shows the improved fit that results from this treatment. In spite of the reduced residuals afforded by this expanded model, it was not adopted for several reasons:

- Frequency parameters are proliferated - four are needed where two sufficed before.
- PSD parameters are estimators of a statistical process. Increasing their number also increases their uncertainty levels.
- The additional parameters are not amenable to the manual analysis of PSD's that is currently used.
- Corner frequencies must be separated into two classes (simple and complex-conjugate pairs) in advance.
- Least squares fitting procedures are likely to encounter difficulties with the increased numbers of parameters, some of them complex.
- The ultimate development of joint identification procedures and the removal of joint-related processes from the data stream will produce a bare SRP which may need a different continuum model.

Eventually the question of more detailed spectral models will need to be addressed. The complex corner frequencies produce PSD's that are much more in line with the analytical results of Cousty and Tro[1]. It is thought that track subject to unit train operations or to the dynamics of a particular locomotive type will exhibit even more pronounced resonances and anti-resonances than were found here.

2.2.6 IMPACT OF SRP ON TRACK MEASUREMENTS

Track measurements that are currently specified in the FRA Track Safety Standards operate on the space curve geometry in the same manner that a linear filter processes a time series. Therefore, if only the SRP is present in the geometry, the track measurement is a random variable that is adquately described by its variance.

Profile and alignment measurements are often specified in terms of an MCO of half-length, s. An MCO measuring a SRP produces a fluctuating random variable having zero mean and correlation function, $\Lambda(x,s)$. The expression for $\Lambda(x,s)$ is given in Appendix A as:

$$\Lambda(x,s) = \tfrac{1}{4}U(x - 2s) - U(x - s) + \tfrac{3}{2}U(x) - U(x + s) + \tfrac{1}{4}U(x + 2s),$$

where $U(x)$ is a function of the process PSD. The simple model for profile and alignment from the previous paragraph,

$$S_n(\phi) = \frac{A_n \phi_{n_4}^2 (\phi^2 + \phi_{n_3}^2)}{\phi^4 (\phi^2 + \phi_{n_4}^2)},$$

gives,

$$U(x) = A\pi^2 \frac{S}{u}\left[\frac{1}{6}\rho|v|^3 - (1 - \rho)\left(|v| + e^{-|v|}\right)\right],$$

where,

$A \to A_n$ = Roughness constant, $n = 1,2,5,6$,
$u \to u_n = 2\pi s \phi_{n_4}$,
$v \to v_n = 2\pi s \phi_{n_4}$, $\rho \to \rho_n = (\phi_{n_3}/\phi_{n_4})^2$.

The correlation properties of a 62-foot MCO were computed for the condition that $\phi_{n_3} = 0.008$ cy/ft and $\phi_{n_4} = 0.04$ cy/ft. The results, normalized to $\Lambda(0,s) = 1$, are shown in Figure 3.

The variance of a MCO is given by $\Lambda(0,s)$:

$$\Lambda_n(0,s) = \pi^2 A_n s Q(\rho,u) ,$$

where

$$Q(\rho,u) = \frac{1}{3}\rho u^2 + (1-\rho)\left[1 - \frac{1}{u}\left(\frac{3}{2} - 2e^{-u} + \frac{1}{2}e^{-2u}\right)\right].$$

Crosslevel and gage deviations from a local mean that influence current measures of track geometry can be modeled by the spectrum:

$$S_n(\phi) = \frac{A_n(\phi^2 + \phi_{n2}^2)}{(\phi^2 + \phi_{n1}^2)(\phi^2 + \phi_{n3}^2)} ,$$

where,

A_n = roughness constant, $n = 4,8$,
ϕ_{n1} = corner frequency, region 0-1,
ϕ_{n2} = corner frequency, region 1-2, and
ϕ_{n3} = corner frequency, region 2-3.

The variance of crosslevel and gage, Ξ, is given by:

$$\Xi_n = \frac{\pi A_n(\phi_{n3}\phi_{n4} + \phi_{n2}^2)}{2\phi_{n3}\phi_{n1}(\phi_{n3} + \phi_{n1})} .$$

In some cases separate values of ϕ_{n1} and ϕ_{n2} cannot be identified in the spectra. In this situation, $\phi_{n1} = \phi_{n2}$ is used, and the expression for crosslevel and gage variance becomes,

$$\Xi_n = \frac{\pi A_n}{2\phi_{n3}} .$$

For purposes of establishing the invariance of spectral parameters it is convenient to define an effective corner frequency, $\hat{\phi}_{n3}$ that summarizes the combined impact of the three corner frequencies, ϕ_{n1}, ϕ_{n2} and ϕ_{n3}. One approach is to make $\hat{\phi}_{n3}$ specify the variance by a relationship similar to that when $\phi_{n1} = \phi_{n2}$, i.e.:

$$\Xi_n = \frac{\pi A_n}{2\hat{\phi}_{n3}} \quad .$$

To do this, $\hat{\phi}_{n3}$ is given by,

$$\hat{\phi}_{n3} = \frac{\phi_{n3}\phi_{n1}(\phi_{n3} + \phi_{n1})}{\phi_{n3}\phi_{n1} + \phi_{n2}^2} \quad .$$

Warp, or twist, is the difference in crosslevel measured at two locations, separated by longitudinal distance, s. Using the simplified crosslevel model spectrum cited above, the variance of warp is given by:

$$\Theta_4(s) = \frac{\pi A_4}{\phi_{43}^2 - \phi_{41}^2}\left[\frac{\phi_{42}^2 - \phi_{41}^2}{\phi_{41}}\left(1 - e^{-2\pi\phi_{41}s}\right) + \frac{\phi_{43}^2 - \phi_{42}^2}{\phi_{43}}\left(1 - e^{-2\pi\phi_{43}s}\right)\right] .$$

The degenerate case of $\phi_{41} = \phi_{42}$ gives:

$$\Theta_4(s) = \frac{\pi A_4}{\phi_{43}}\left(1 - e^{-2\pi\phi_{43}s}\right).$$

2.3 RANDOM VARIATIONS OF THE JOINT SHAPE AMPLITUDE

Physical observation of track geometry and stiffness measurements indicate that joints and welds are locations in the track where conditions differ significantly in character from

those found between the joints and welds. Profile geometry data collected at joints and welds shows a definite cusp shape.

On bolted rail and on some CWR fabricated from relay bolted rail, the cusp is downward. Its duration is on the order of 2 to 10 feet long and its amplitude can vary from 0 to 3 or more inches. Both duration and amplitude increase with degradation, which results from the structural weakness of the joint and is accelerated by loosening and wear of the joint bars.

On CWR fabricated from new rail, the cusp is usually upward and much shorter, 2 to 4 feet long, and its amplitude may be as great as 0.3 inches. It is caused by the rolling-cooling process during which the rail bends upward. Even though the rail is straightened after this process, straightening does not totally remove the curvature from the ends and a cusp occurs at the location of the weld in the CWR strings[2]. CWR joint degradation consists of the development of a depression around the upward cusp, rather than in the cusp itself.

Joints occur with such regularity that they cannot be regarded as anomalies. At the same time, their presence implies a non-stationary process in the geometry data. The adequacy of analytical techniques that are geared to stationary processes, for example, PSD's and histograms, must be examined.

2.3.1 CONTRIBUTION OF JOINTS TO MEASURED PSD's

A process model of the form:

$$y(x) = \sum_{n=-\infty}^{\infty} C_n e^{-k|x-nL|},$$

is first assumed. In this model:

$y(x)$ = rail profile or alignment as a function of x,

x = longitudinal distance along the rail,

C_n = amplitude of the n^{th} joint depression,

n = counting index,

k = decay rate for the joint depression typically 0.15 ft^{-1},

L = rail length.

It is shown in Appendix B that the associated PSD is given by:

$$S(\phi) = R(\phi)W(\phi),$$

where,

$W(\phi)$ = squared spectrum of a single joint cusp,

$$= \frac{8}{Lk^2}\left[1 + (2\pi\phi/k)^2\right]^{-2},$$

= spectrum of joint-joint correlations,

$$R(\phi) = r(0) + 2\sum_{m=1}^{\infty} r(m)\cos(2\pi mL\phi),$$

$r(0)$ = variance of joint depths about mean,

$$= \langle (C_n - \bar{C})^2 \rangle,$$

$\bar{C}$ = mean of joint depths,

$$= \langle C_n \rangle, \text{ and}$$

$r(m)$ = covariance between joint depths separated by m rail lengths,

$$= \langle (C_n - \bar{C})(C_{n+m} - \bar{C}) \rangle.$$

A case worthy of further study is where the $r(n)$ decay exponentially:

$$r(n) = r(0)\gamma^{|n|} \quad , \quad -\infty < n < \infty .$$

Here, γ is a parameter whose characteristics are:

$\gamma = 0$:	No correlation between joints.
$0 < \gamma < 1$:	Positive correlation.
$\lim_{\gamma \to 1}$:	Periodic deterministic process, period L.
$-1 < \gamma < 0$:	Negative correlation (anti-correlation).
$\lim_{\gamma \to -1}$:	Periodic deterministic process oppositely lined joints, length $2L$, odd harmonics only.

$R(\phi)$ now assumes the analytical form:

$$R(\phi) = \frac{(1 - \gamma^2)}{1 - 2\gamma \cos(2\pi\phi L) + \gamma^2} .$$

By varying γ, it is possible to visualize how $S(\phi)$ makes the transition from highly correlated to highly anti-correlated extremes. This is illustrated in the log-log plot of Figure 13 for the case where $k = 2\pi/L$. This figure displays some surprising results:

- Despite the rigorous periodic placement of joints the completely uncorrelated case ($\gamma=0$) produces a smooth continuum that is given by:

$$S(\phi) = r(0)W(\phi).$$

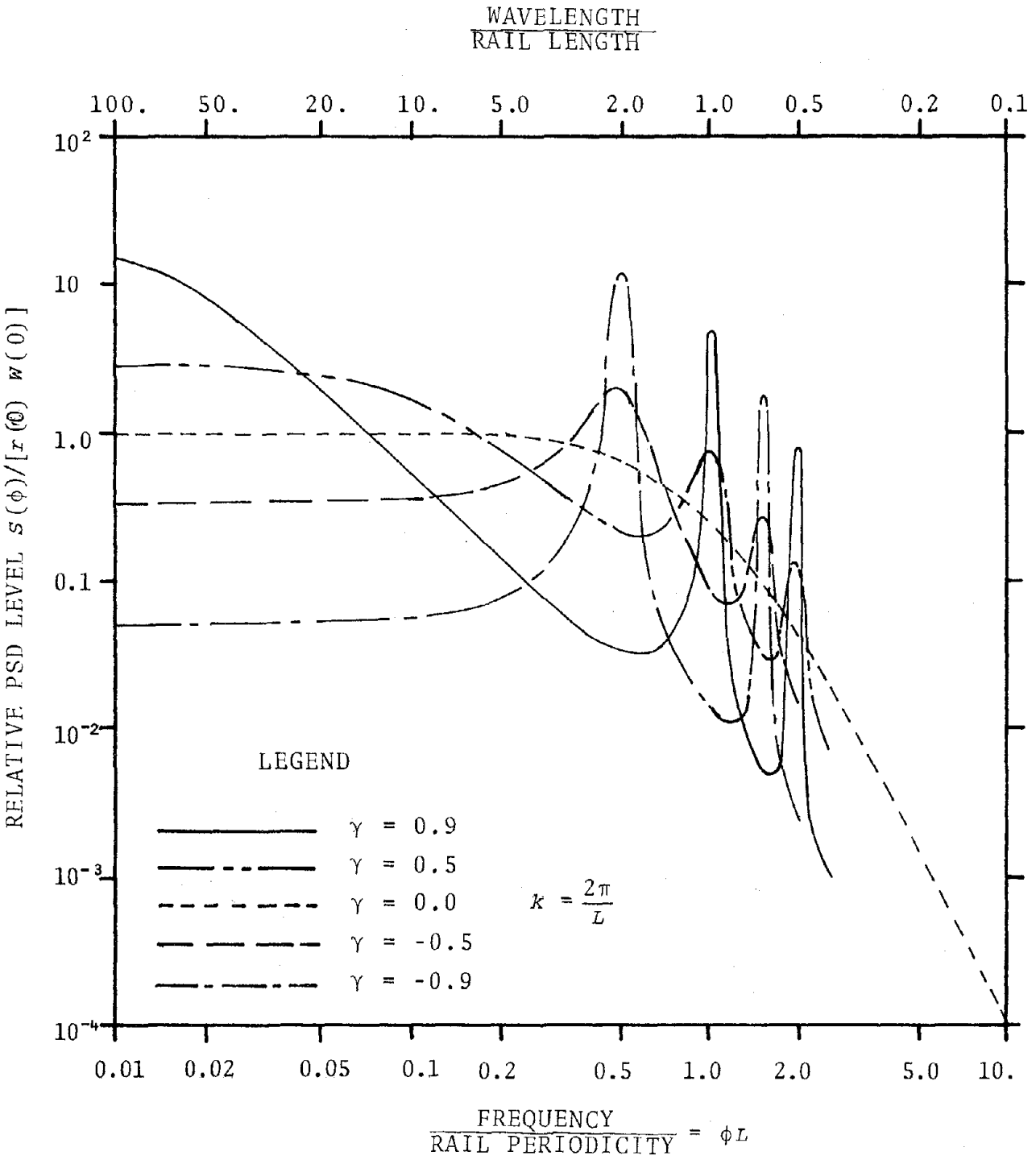

FIGURE 13. GRADUAL TRANSITION FROM HIGHLY CORRELATED (γ=0.9) TO UNCORRELATED (γ=0) TO HIGHLY ANTI-CORRELATED (γ=-0.9)

- Increasing positive correlation produces a spectral peak pattern with the fundamental corresponding to the rail length periodicity and subsequent peaks occurring at integer harmonics thereof. Higher positive correlation causes these peaks to become more pronounced.

- Decreasing negative correlation also produces spectral peaks, with the fundamental at a *two rail length periodicity* and subsequent peaks occurring at *odd* harmonics thereof. Lower negative correlation causes these peaks to become more pronounced.

- The minima and maxima of these peaks are bounded by an envelope that is proportional to $w(\phi)$, i.e.,

$$\text{Max}\{S(\phi)\} = \frac{1 + |\gamma|}{1 - |\gamma|} r(0)w(\phi),$$

and,

$$\text{Min}\{S(\phi)\} = \frac{1 - |\gamma|}{1 + |\gamma|} r(0)w(\phi).$$

These observations raise two questions relative to the use of the PSD to characterize track geometry:

- In a given situation, does the continuum describe uncorrelated random variations in the joint amplitudes or does it characterize a SRP?

- In a given situation do the spectral peaks describe highly correlated random variations of the joint amplitudes or do they characterize a PDP?

To resolve these questions the analytical PSD of a PDP is evaluated to define features that may distinguish it from the case of highly correlated random joints. Then some empirical joint amplitude data is examined.

2.3.2 PDP AS A LIMITING CASE

The PDP is represented by the following function:

$$y(x) = \overline{C} \sum_{n=-\infty}^{\infty} e^{-k|x-nL|} .$$

It is shown in Appendix B that the essential features of joint models are that they have an amplitude, a discontinuity in derivative, and a smooth return to the zero axis. Other models that share these features can be used.

The PSD's generated in this research effort have a frequency resolving bandwith, B, that is independent of ϕ. For the PDP model described above, the peaks are bounded by an envelope of the form:

$$S_e(\phi) = \frac{8}{B} \left(\frac{\overline{C}}{Lk}\right)^2 [1 + (2\pi\phi/k)^2]^{-2},$$

which has the same function form as $W(\phi)$.

This relationship suggests an immediate test to distinguish between a PDP and highly correlated random joint amplitudes. This consists of decreasing the PSD resolution bandwith. If the spectral peak continues to increase inversely with bandwidth, then it is likely that the process represented by the spectral peak is a PDP. *However, the cessation of the spectral peak growth with decreasing B is* not *necessarily an indicator of highly correlated random joint amplitudes.* A deviation from rigorously constant spacing of joints having constant amplitudes will produce the same symptom.

When converted to log-log form, $S_e(\phi)$ is characterized by two straight line asymptotes; one having a constant level as it approaches zero frequency, and the other having a ϕ^{-4} characteristic as frequency approaches infinity.

Constants that can be used to characterize the joint are prescribed by the intersection of the two asymptotes. This intersection defines a frequency on the abscissa, ϕ_0, that is related to the decay rate by:

$$k = 2\pi\phi_0 .$$

The PSD ordinate at zero frequency, $S_e(0)$, gives the average joint amplitude:

$$\bar{C} = \pm LK\left(\frac{BS_e(0)}{8}\right)^{\frac{1}{2}} = \pm\pi L\phi_0\left(\frac{BS_e(0)}{2}\right)^{\frac{1}{2}} .$$

The sign uncertainity is a consequence of the loss in phase information in PSD processing.

Figure 14 shows the application of this procedure to calculate $\bar{C}$ from the spectral peaks of an empirical profile PSD. There it is seen that,

$$\phi_0 = 0.028 \text{ cy/ft}$$
$$S_e(0) = 14.1 \text{ in}^2/\text{cy/ft},$$

so that,

$$k = 0.18 \text{ ft}^{-1},$$
$$\text{Duration} = k^{-1} = 5.6 \text{ ft}.$$

The rail length is $L = 39$ ft and the PSD bandwith is $B = 10^{-3}$ cy/ft. From this,

$$\bar{C} = \pm 0.29 \text{ in}.$$

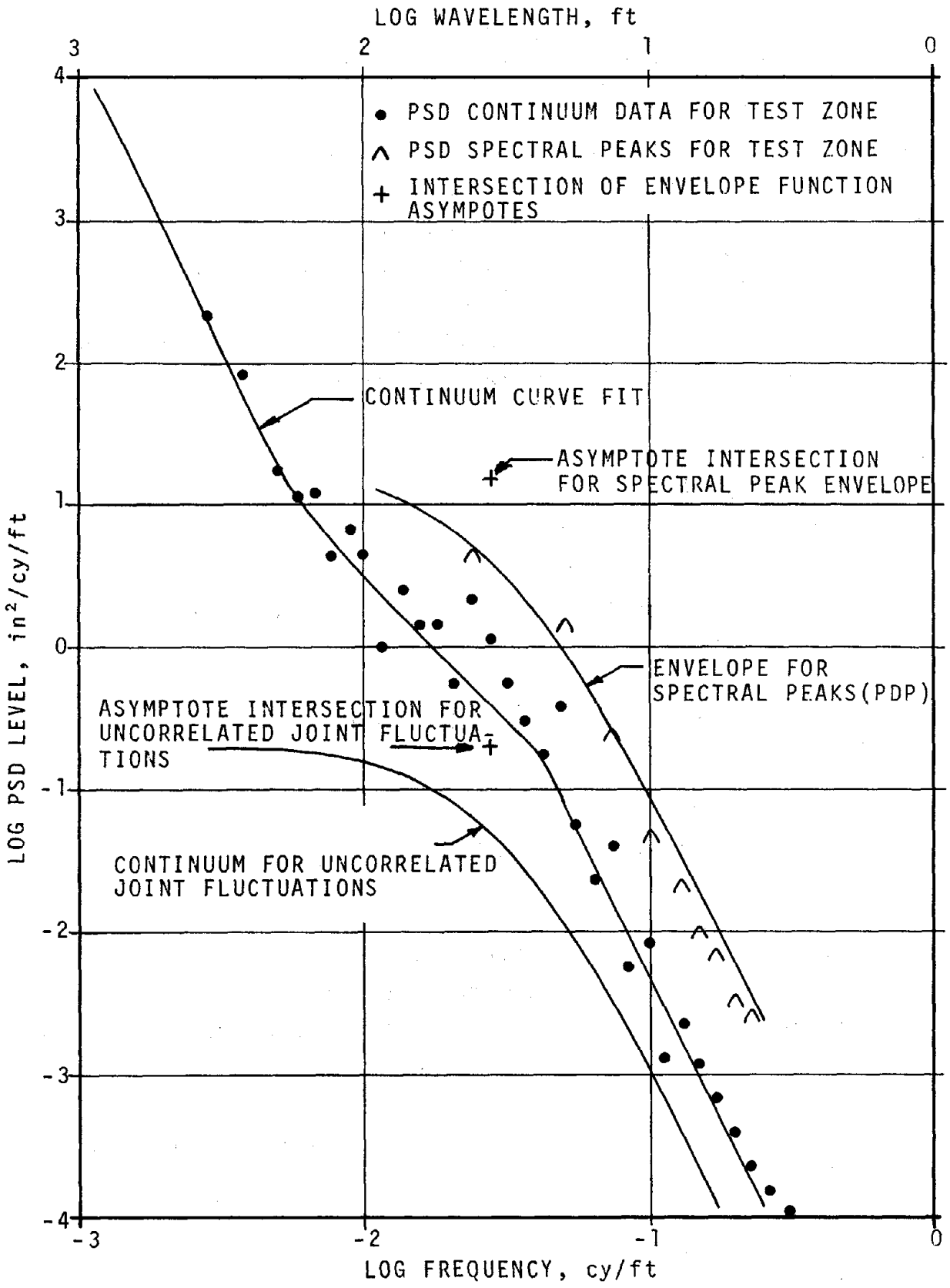

FIGURE 14. CONTRIBUTION OF PMRP CONTINUUM COMPARED WITH OBSERVED CONTINUUM

2.3.3 EMPIRICAL DISTRIBUTION OF JOINT AMPLITUDES

Both space curve and chord data is available for the zone whose PSD is shown in Figure 14. In order to investigate joint amplitude, the joints were located by their characteristic cusp signature in the space curve. Then, using a 16 ft MCO, the amplitudes of the joints were determined and measured.

Raw MCO values at joints were plotted in the histogram shown in Figure 15. The results display a skewed distribution having the following statistics:

$$\langle c_n \rangle = \bar{c} = 0.284 \text{ in},$$
$$\langle (c_n - \bar{c})^2 \rangle = r(0) = 0.0311 \text{ in}^2.$$

Note the good agreement with $\bar{c}$ as derived from the $S_e(\phi)$ parameters in the previous section.

Additionally, the statistic, $r(1)$, was computed. It was found that

$$\frac{r(1)}{r(0)} = \frac{\langle (c_n - \bar{c})(c_{n+1} - \bar{c}) \rangle}{r(0)} < 0.1.$$

Hence, it is concluded that the random component of joint amplitudes in this zone is uncorrelated ($\gamma=0$) and that the spectral peaks are associated with a PDP caused by a negative, non zero mean in the joint amplitudes.

Next, the continuum due to uncorrelated joint fluctuations was evaluated:

$$S_p(\phi) = \frac{8r(0)}{Lk^2} [1 + (2\pi\phi/k)^2]^{-2},$$

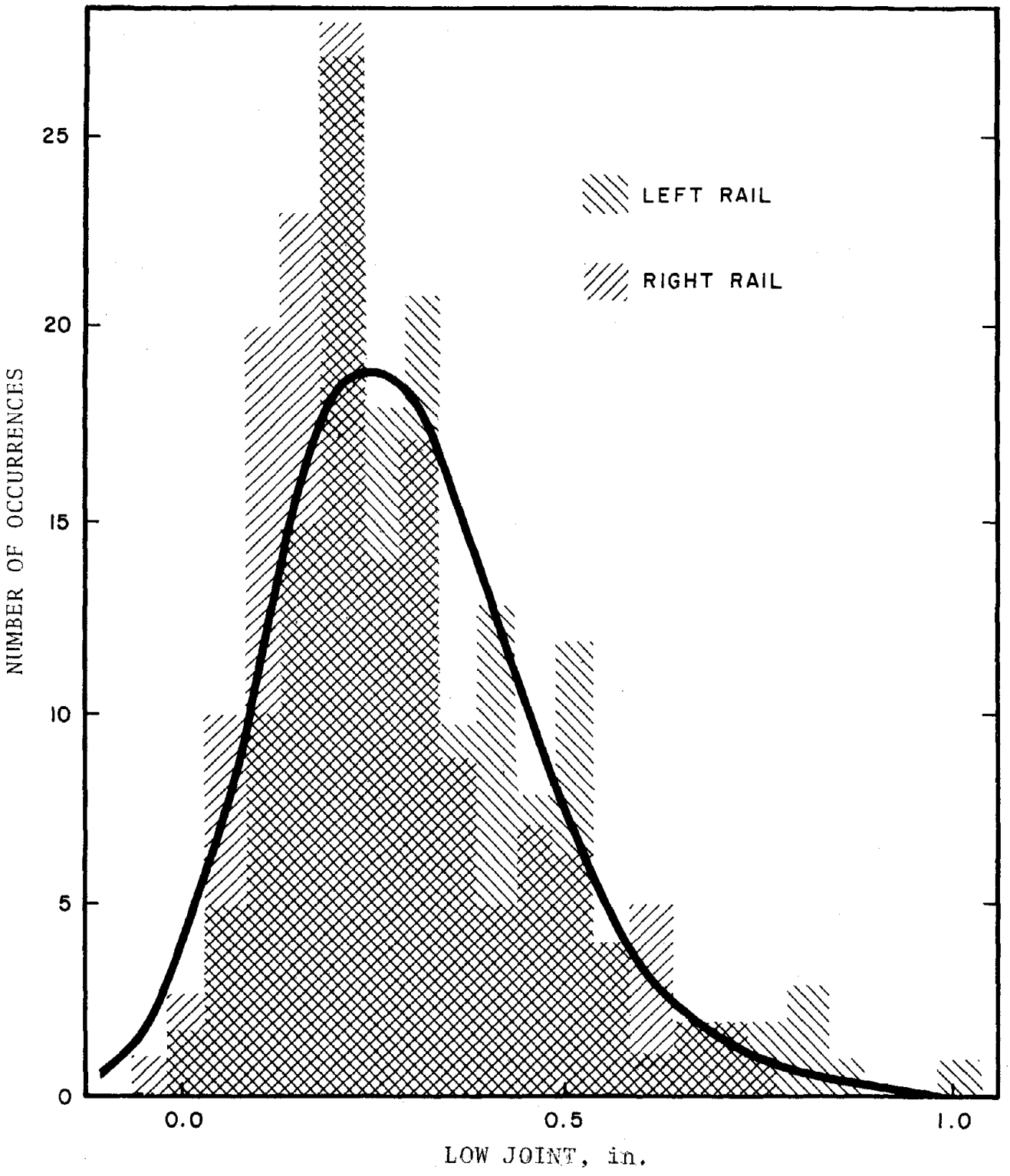

FIGURE 15. HISTOGRAM FOR 156 LEFT RAIL AND 156 RIGHT RAIL BOLTED JOINTS

which has the same asymptotic behavior as the spectral peak envelope function, $S_e(\phi)$. The intersection of the asymptotes is at frequency, ϕ_0, and spectral level, $S_p(0)$. The latter is given by:

$$S_p(0) = \frac{8r(0)}{Lk^2} = \frac{2r(0)}{\pi^2 L\phi_0^2}.$$

The function $S_p(\phi)$ is plotted in Figure 14. It is instructive to compare $S_p(\phi)$ with the PSD continuum model, $S_1(\phi)$, for the data in Figure 14. The PSD continuum model has the following parameters:

$A_1 = 3.16 \times 10^{-4}$ in^2- cy/ft,
$\phi_{13} = 0.040$ cy/ft, and
$\phi_{14} = 5.0 \times 10^{-3}$ cy/ft.

Comparison of $S_1(\phi)$ with $S_p(\phi)$ reveals that *the SRP continuum exceeds the uncorrelated joint fluctuation continuum at all frequencies by a factor of at least 4 to 1.* Therefore, *it is concluded that the PSD continuum describes the SRP rather than random variations of the joint amplitudes. Further, information concerning variance and moderate correlations in the the random variations of joint amplitudes is not given by the PSD.*

This is a severe restriction in estimating peak values or percentiles of track performance indices. It is not a deficiency in estimating the PSD's of performance indices, or in using the PSD's to estimate the variances of performance indices.

2.3.4 DISTRIBUTION MODEL FOR JOINT AMPLITUDES

The empirical joint amplitude data shown in Figure 15 is actually the result of *two* processes happening concurrently. In addition to random variations in the joint amplitudes,

there is also a contribution due to the SRP which is always present in field data. It is desired to estimate the parent distribution of the joint amplitudes.

To this end, let $p_1(c)$ be the probability distribution of the SRP contribution to the 16-ft MCO measured at joints; $p_2(c)$ be the probability distribution of the uncorrelated random component of joints; and $p_3(c)$ be the probability distribution resulting from the combination of $p_1(c)$ and $p_2(c)$. If the random processes associated with $p_1(c)$ and $p_2(c)$ are statistically independent then,

$$p_3(c) = \int_{-\infty}^{\infty} p_1(c)\ p_2(c - c)dc.$$

In other words, $p_3(c)$ is the convolution of $p_1(c)$ with $p_2(c)$.

It has already been asserted that long wavelength SRP behavior as seen by long MCO's is a normally distributed random variable with zero mean. Therefore, $p_1(c)$ is assumed to have that form. $p_3(c)$ can be estimated by a functional form fit to the empirical data of Figure 15. Then, $p_2(c)$ is given by deconvolution of the above.

Since a generalized deconvolution is a difficult procedure, an alternative approach is used. The contribution of the SRP to the MCO measurement is

$$p_1(c) = \frac{1}{\sqrt{2\pi}\ \sigma}\ e^{-\frac{1}{2}(c/\sigma)^2},$$

where $\sigma^2 = \Gamma$ = the variance of a 16 ft MCO as computed by the formula given in Paragraph 2.2.5. Using the values of A, ϕ_{13}, and ϕ_{14} given above, the standard deviation is:

$$\sigma = 0.10 \text{ in.}$$

The skewed distribution of values in Figure 15 is highly suggestive of a Γ-distribution also known as a Pearson Type III distribution.[8] Because $p_1(C)$ is a symmetric distribution, $p_2(C)$ is assumed to provide the skewed characteristic via a Γ-distribution.

$$p_2(C) = \left(\frac{n+1}{\bar{C}}\right)^{n+1} \frac{C^n e^{-[(n+1)C/\bar{C}]}}{n!} .$$

The cumulants of the empirical $p_3(C)$ distribution were evaluated from Figure 15. From these cumulants and the of $p_1(C)$, the empirical cumulants of $p_2(C)$ were calculated. Using a $\bar{C}$ equal to the first empirical $p_2(C)$ cumulant, the higher cumulants of the analytical $p_2(C)$ distribution were computed for several different values of n. The results for n=3 gave the best agreement between empirical and analytical models through the fourth cumulant calculation, as indicated in Table 8. *The fact that this agreement carries through to the 4th cumulant is a good validation of the hypothsis that:*

$$p_2(C) = \left(\frac{4}{\bar{C}}\right)^4 \frac{C^3 e^{-4C/\bar{C}}}{6} .$$

Using this form for $p_2(C)$, the analytical form for $p_3(C)$ becomes

$$p_3(C) = Ke^{-\frac{1}{2}(C/\sigma)^2}\left\{(1+\ell^2) + \frac{\sqrt{\pi}}{2}(3\ell + 2\ell^3)[1 + \mathrm{erf}(\ell)]e^{\ell^2}\right\}$$

where,

$$K = \frac{1}{3\sigma\sqrt{2\pi}} \left(\frac{4\sigma}{\bar{C}}\right)^4 ,$$

and

$$\ell = \frac{1}{\sqrt{2}} \left(\frac{C}{\sigma} - \frac{4\sigma}{\bar{C}}\right) .$$

[8] M. G. Kendall and A. Stuart, *The Advanced Theory of Statistics*, Vol. I, Ch. 6, "Standard Distributions (2)," Charles Griffin, London, 1968, p. 152-154.

TABLE 8. COMPARISON OF EMPIRICAL AND ANALYTICAL EVALUATION OF $p_2(c)$ CUMULANTS WITH $n=3$

STATISTIC	EMPIRICAL		ANALYTICAL
1st Cumulant	0.2840 in	≡	0.2840 in
2nd Cumulant	0.0210 in^2		0.0200 in^2
3rd Cumulant	0.0055 in^3		0.0029 in^3
4th Cumulant	0.0003 in^4		0.0006 in^4

Using the values for $\bar{c}$ and σ derived above, $p_3(c)$ was computed and, after rescaling, plotted on Figure 15.

The preceeding analysis, coupled with the more general observation that bolted joint amplitudes are preponderantly negative, prompts the following conclusion: *the harmonically related line components of the PSD are produced by a non-zero mean in the joint amplitude rather than by highly correlated random variations in the joint.*

2.4 ANOMALIES

An anomaly is defined as an obvious physical interruption in the track structure. Examples of anomalies are listed in Table 5. On the basis of this definition and the cited examples, there is good prima facie evidence that the causal agents for geometric variations at an anomaly site are different from those causal agents in anomaly-free track.

Experience with geometry records reveals that the greatest levels of peak deviations coincide with anomalies. Further the PMRP attributed to anomaly-free track cannot account for the frequency of occurrence of the anomaly wave shapes and the associated high amplitudes. Therefore, proper analytical description of anomalies requires that the PMRP roughness parameters vary (spot maintenance), that the PMRP be augmented by additional processes (grade crossings and short bridges) or that the PMRP be suspended and supplemented by an altogether different process (turnouts).

2.4.1 CLASSIFICATION OF ANOMALIES

The signal analysis classification diagrams of Figures 6 and 7 show anomalies falling in two places. The fixed or average component of anomalies is listed under Transients in Figure 6. The random or fluctuational component of anomalies is found under Special Classifications of Nonstationary Processes in Figure 7. In these respects, anomalies resemble joint amplitudes; they represent random fluctuations about a non-zero mean.

The principal differences between joints and anomalies are:

- Anomaly signatures are both physically and analytically more complex than a simple joint cusp;
- Anomalies appear at irregular intervals while joints usually occur with rigorous periodicity.

Otherwise, a joint is the archtypical anomaly, and the methodologies used to characterize joints can be applied to anomalies. Indeed, examination of anomaly space curves such as those shown in Appendix C reveals that they are well represented by a superposition of joint like cusps and depressions.

Proper characterization of anomalies consists of locating and then classifying the anomaly. The classification procedure must, in many cases, go to greater depths than implied by Table 5. For example, turnouts must be further identified as follows:

- Track Class
- Application (Yard, Interlocking, Siding)
- Turnout Number (up to #20)
- Frog Type (Fixed, Manganese Insert, Spring, Self-guarded)
- Right, Left, Equilateral, Curved;
- Point length and type; and
- Predominant Direction of Traffic (Facing Point, trailing point).

While this classification appears to produce an unmanageable proliferation of variables, most railroad properties limit the variety of turnouts and other track structures so that unmanageable parts inventories are not needed. For example, one local system uses #20 turnouts with manganese steel insert frogs for high speed interlockings and #10 turnouts with spring frogs for sidings.

2.4.2 ANALYTICAL PROCEDURES FOR ANOMALIES

Once it is ascertained that the anomalies are properly grouped and classified, *the proper analytical procedures are those that are appropriate to a Deterministically Modulated Random Process (DMRP). Ths is one in which means, covariances, and higher order statistics vary deterministically over the duration of the anomaly.*

The most detailed (assumption-free) approach to DMRP statistics consists of ensemble averaging across the track geometry records obtained from many examples of a particular anomaly classification. This procedure is illustrated in Figure 16 and is outlined as follows:

- Position the anomaly space curves so that the corresponding parts (points and frogs in turnouts) line up. For turnouts, this may mean reversing the direction of data flow and transposing left and right rails so that all turnouts in the classification look like, say, left hand trailing point turnouts. This collection is called the ensemble.
- Ensemble average across the above traces to obtain the mean shape or deterministic transient component of the anomaly.
- Subtract the transient from the ensemble of anomaly space curves to produce a new ensemble of fluctuation components. The covariance properties of the anomaly space curves are now determined by ensemble averaging the *products* of geometry at position 1 and geometry at position 2.
- In similar fashion, higher order statistics of the turnout DMRP are computed.

A simplified approach results if it is assumed that anomalies are a consistent system of cusps and depression shapes. The procedure is illustrated for the case of the turnout.

- Using standard trackwork plans[9], identify the expected location of joints, transition points (stock rail to switch point, frog transitions).
- Determine by least squares fitting the associated amplitude and duration of cusps and depressions as illustrated in Figure 5.

[9]The American Railway Engineering Association, Committee 5-Track, "Portfolio of Trackwork Plans," *Am. Rwy. Engr. Assoc.*, Chicago, IL. 1973.

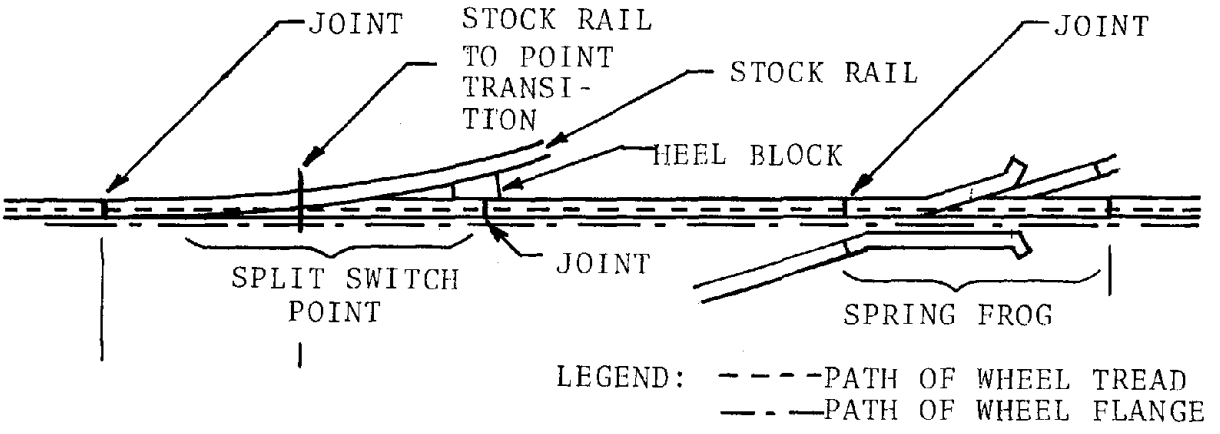

a. LAYOUT OF A TYPICAL TURNOUT OF A GIVEN TYPE

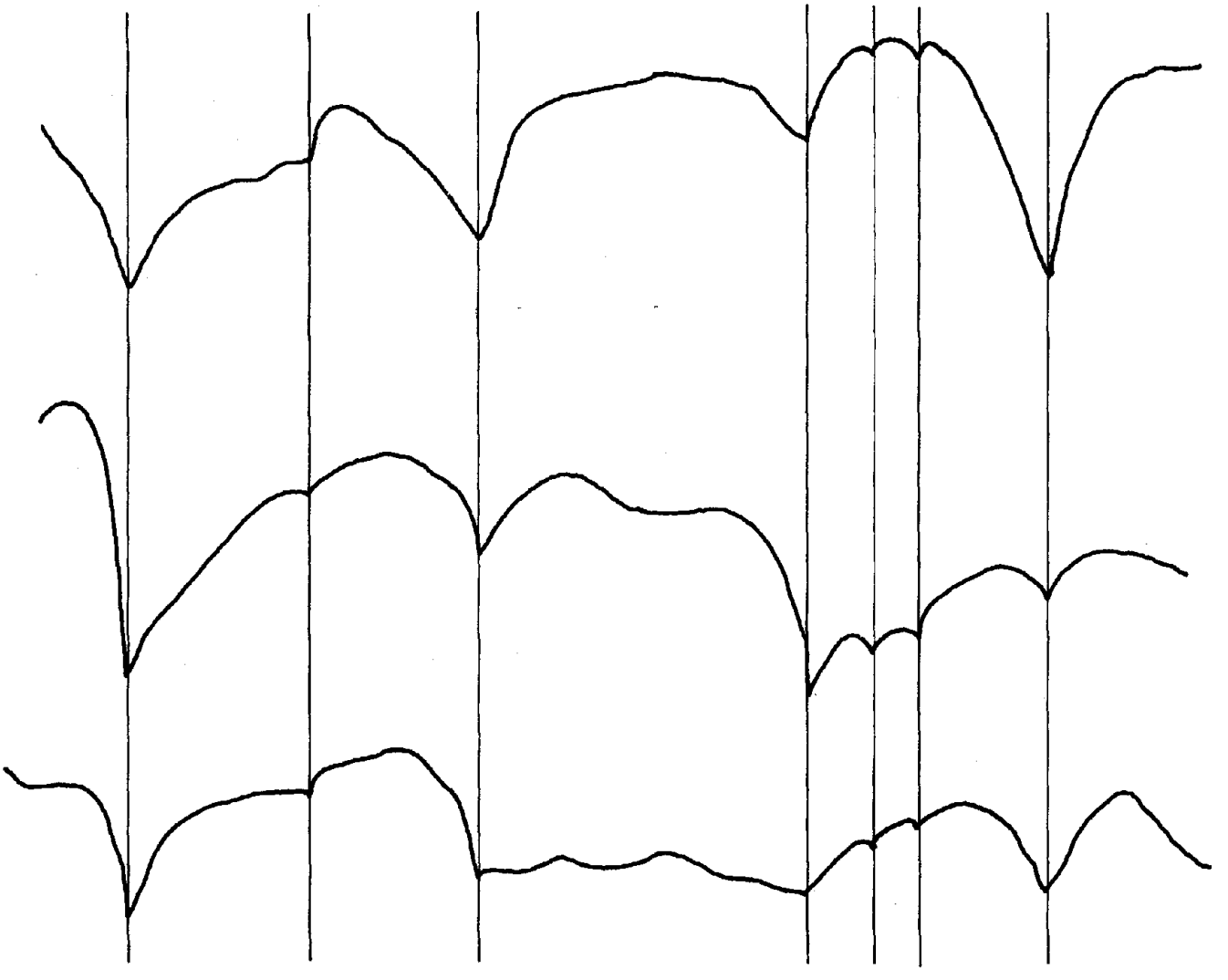

b. TRACINGS OF PROFILE GEOMETRY THROUGH 3 TURNOUTS

FIGURE 16. PROCEDURE FOR TREATING GEOMETRY DATA FOR ANOMALIES

- Locate corresponding depressions on the other rail. Determine, by least squares fitting the depression duration and amplitude.

The amplitudes and durations are tabulated. Means, variances, correlations and distributional properties are estimated from the data in much the same manner that joints were characterized in Section 2.3.

It must be emphasized that since anomalies represent isolated events, they are not properly characterized by PSD's due to the averaging and phase suppression properties of the PSD. Figure 17 shows data from a relatively short zone of 1500 feet, processed first to exclude and subsequently to include a fairly severe anomaly. As can be seen, there is very little change in the PSD by including the anomaly. At the same time, the PSD that includes the anomaly has no distinguishing features that would indicate the presence of that anomaly.

2.5 PSD DATA PROCESSING

The rationale for the PSD processing effort of the present project were:

- Establish a high degree of confidence that the scope of current track geometry PSD's is indeed correct. This covers wavelengths of 1 to 1000 feet and a dynamic range of 10^{-4} to 10^{4} $in^2/cy/ft$ which is 10,000 times the dynamic range of older PSD's.
- Use the best PSD processing tools available within the cost and time limitations of the project.
- Expand upon the knowledge learned in previous analytical work on PSD's, including reliability, wavelength range, and dynamic range.

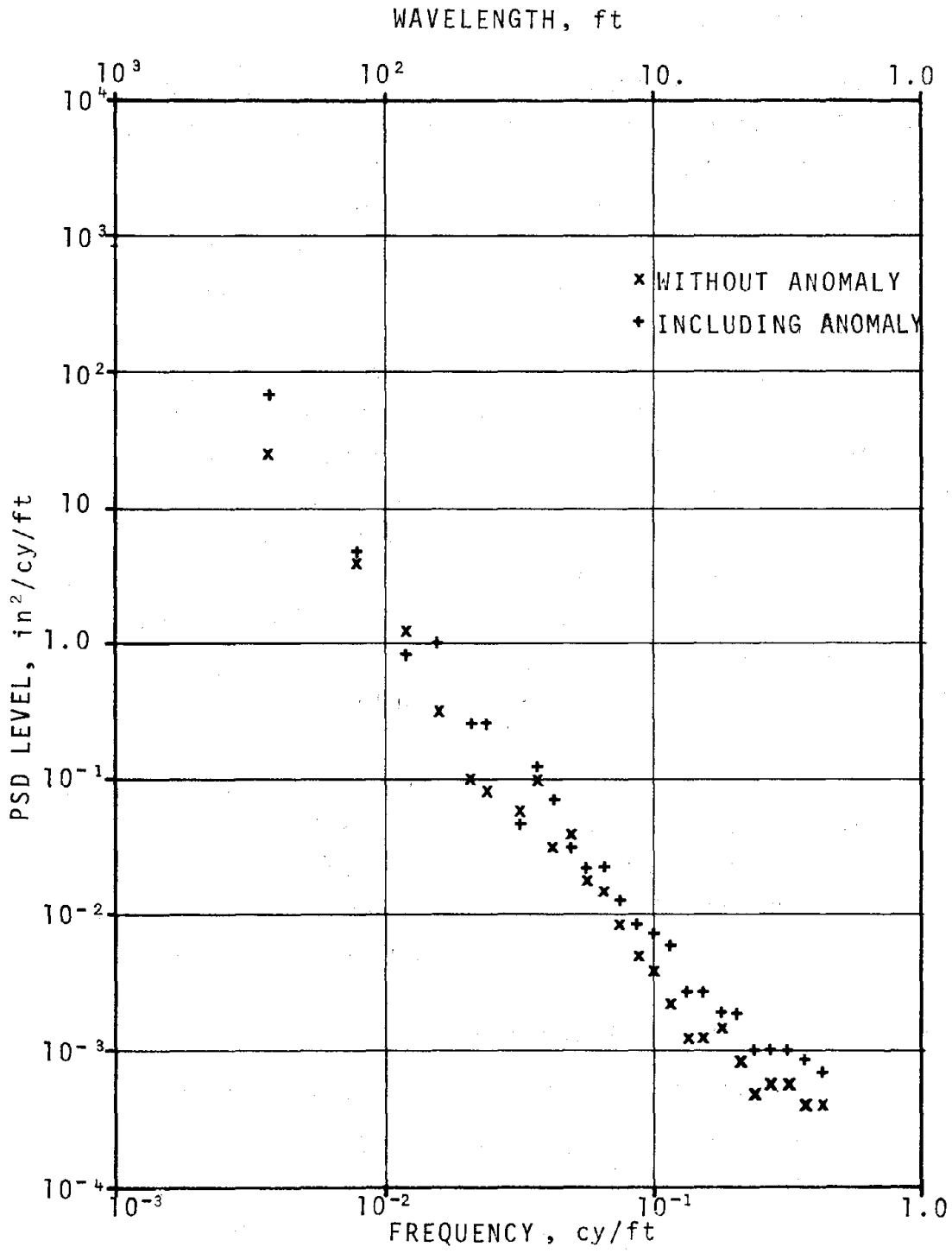

FIGURE 17. PSD OF 1500 FEET OF PROFILE GEOMETRY WITH BROAD-BAND ANOMALY BOTH INCLUDED AND EXCLUDED

2.5.1 EXTREMELY LONG AND SHORT WAVELENGTHS

Processing-induced errors, instrumentation noise, and dynamic range limitations can all give erroneous PSD's. Therefore, any independent evidence that substantiates the correctness of PSD processing is welcome. One method of doing this is to verify that trends established within the boundaries of routine PSD processing continue beyond those boundaries.

The determination of extremely long wavelength (ELW) behavior of railway track requires the use of data other than the usual track geometry measurements. It is planned to use the output of the profilometer and alignometer for routine PSD processing so these instruments do not qualify as independent sources. The track survey device, the one instrument that has a demonstrated performance capability for ELW, is too slow and cumbersome to perform measurements over the many contiguous miles of track data that are needed for ELW-PSD's.

Accordingly, survey data from railroad track charts has been used to get a first estimate of the ELW behavior of profile and alignment. An example of such a chart provided by the Atchison, Topeka and Santa Fe Railway Company is shown in Figure 18. Typical information listed in these charts is:

- Location by milepost of grade changes;
- Percent of grade between these locations;
- Altitude to the nearest 0.1 ft at the grade change locations;
- Location by milepost of curvature; and
- Degree of curvature, included angle, and length of spiral.

In the theoretical analysis of ELW profile, let y_n be the height in inches at the distance location, x_n, measured in

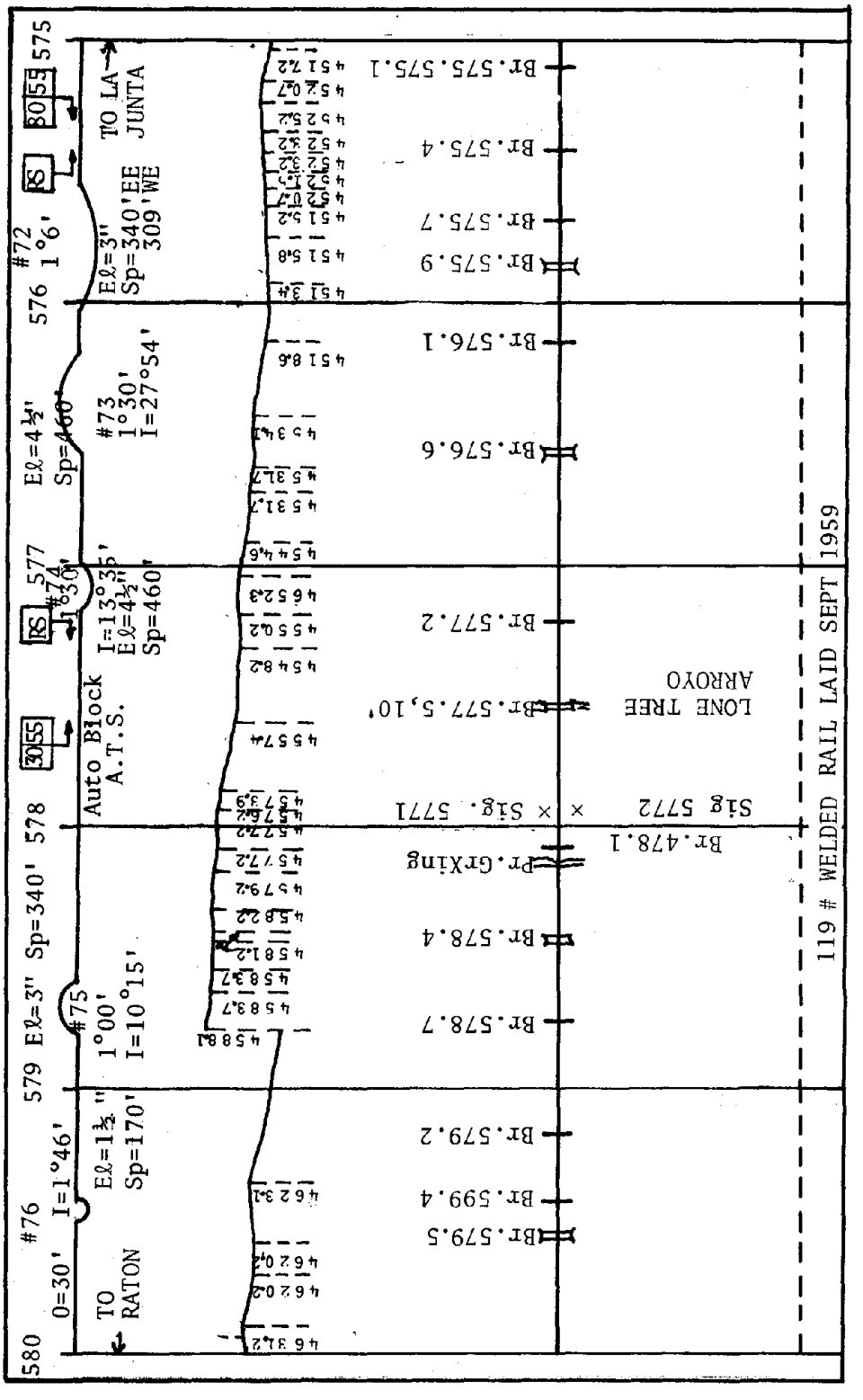

(COURTESY: AT&SF Railway Co.)

FIGURE 18. EXAMPLE OF TYPICAL TRACK CHART

feet. If the slope is uniform between x_n and x_{n+1}, then the contribution to the Fourier transform of slope (slope spectrum) between x_n and x_{n+1} is given by:

$$U_n(\phi) = M_n e^{-i2\pi\phi X_n} \left[\frac{\sin(\pi\phi L_n)}{\pi\phi}\right],$$

where

$U_n(\phi)$ = complex spectrum due to slope segment, n.

X_n = mean location of segment, (ft),

$= \frac{1}{2}(x_{n+1} + x_n)$

L_n = length of segment, (ft), $= x_{n+1} - x_n$

M_n = slope of segment, (in/ft).

$= (y_{n+1} - y_n)/L_n$.

Note that the term in the brackets is the Fourier transform of a rectangular pulse of duration L_n and amplitude A_n centered symmetrically about the origin. The exponential premultiplier is a phase shifter that moves the pulse away from the origin.

A length of track, L, is a linear combination of such track segments. The total spectrum due to N such segments is given by:

$$U(\phi) = \sum_{n=1}^{N+1} U_n(\phi),$$

where $U_{N+1}(\phi)$ is a spectrum detrending term. It is generated as above with:

$$X_{N+1} = \tfrac{1}{2}(x_{N+1} + x_1),$$

$$L_{N+1} = x_{N+1} - x_1 \equiv L,$$

$$M_{N+1} = -(h_{N+1} - h_1)/L .$$

The ELW profile PSD, $S_3(\phi)$, is then obtained by computing:

$$S_3(\phi) = \frac{1}{4\pi^2\phi^2 L} \; U(\phi)U^*(\phi),$$

where the frequency correction for slope integration is introduced. Results for ELW profile for actual track are given in Appendix D, Section D.1.

In the theoretical analysis of ELW curvature, let Ω_n be the curvature of the n^{th} segment, expressed in (degrees/100 ft). Let x_n be the location of the curve mid-point and I_n be the included angle of the curve. Then the Fourier transform of a curvature segment is given by:

$$V_n(\phi) = \ell e^{-i\pi\phi X_n} \left[\Omega_n \frac{\sin(\phi\pi L_n)}{\pi\phi}\right],$$

where

$V_n(\phi)$ = complex spectrum due to n^{th} segment

L_n = length of segment = $100(I_n/\Omega_n)$, feet

ℓ = conversion constant

$$= \frac{\pi}{1500}\left(\frac{\text{in/ft}}{\text{Degrees/100 ft}}\right).$$

The total curvature spectrum due to N segments is given by:

$$V(\phi) = \sum_{n=1}^{N+1} V_n(\phi),$$

where $V_{N+1}(\phi)$ is a spectrum detrending term. It is generated as above with:

$$C_{N+1} = -\sum_{n=1}^{N} I_n/L, \quad \text{and}$$

$$X_{N+1} = \tfrac{1}{2}L.$$

The ELW alignment PSD, $S_y(\phi)$, is obtained by computing:

$$S_y(\phi) = \frac{1}{16\pi^4\phi^4 L} V(\phi)V^*(\phi),$$

where the frequency correction for double integration is included. Results for ELW alignment are described in Appendix D, Section D.1.

To characterize extremely short wavelength behavior, some data already exists in the literature in the form of 1/3 octave RMS levels.[10] These were converted to PSD's and the results are contained in Appendix D, Section D.1.

2.5.2 PROGRAM RAINBO

In order to efficiently carry out the large volume of PSD processing required in the project, a PSD package (RAINBO) was developed which had the capability to:

---

[10] P. J. Remington, M. J. Rudd and I. L. Ver, "Wheel/Rail Noise and Vibration," Final Report (2 Vols), UMTA-MA-06-0025-75-10 and UMTA-MA-06-0025-75-11, May 1975.

- Incorporate prewhitening options in the "time" domain.
- Generate cross-PSD's and coherence functions.
- Correct for known instrument frequency responses.
- Postcolor in the frequency domain to compensate for the prewhitening introduced in the time domain.
- Expand the ordinate dynamic range to realize the long wavelength capabilities of the inertial profilometer and to process data sampled at arbitrary intervals.
- Produce graphs with linear frequency and log frequency abscissas.

A flow chart for program RAINBO is shown in Figure 19.

Two graphical display formats are provided for PSD's and X-PSD's. The first, a log amplitude, linear frequency graph is normally 2 inches high and 10 inches wide. The ordinate covers PSD levels from 10^{-4} to 10^{4} in /cy/ft. The abscissa covers PSD frequencies from 0 to folding. Figure 20 shows examples of this format for individual rail profile and mean profile. It is most useful for studying harmonically related spectral components.

The second format provides a log amplitude, log frequency display of the PSD data. This is particularly useful for studying power law relationships. An example, corresponding to the PSD in Figure 20a is provided in Figures 21. Some of the features of Figure 21 are:

- The logarithmic ordinate is scaled at twice the rate of the logarithmic abscissa. The ordinate covers a dynamic range of 10^{-4} to 10^{4} $in^2/cy/ft$, and the abscissa covers a frequency range of 10^{-3} to 1.0 cy/ft.

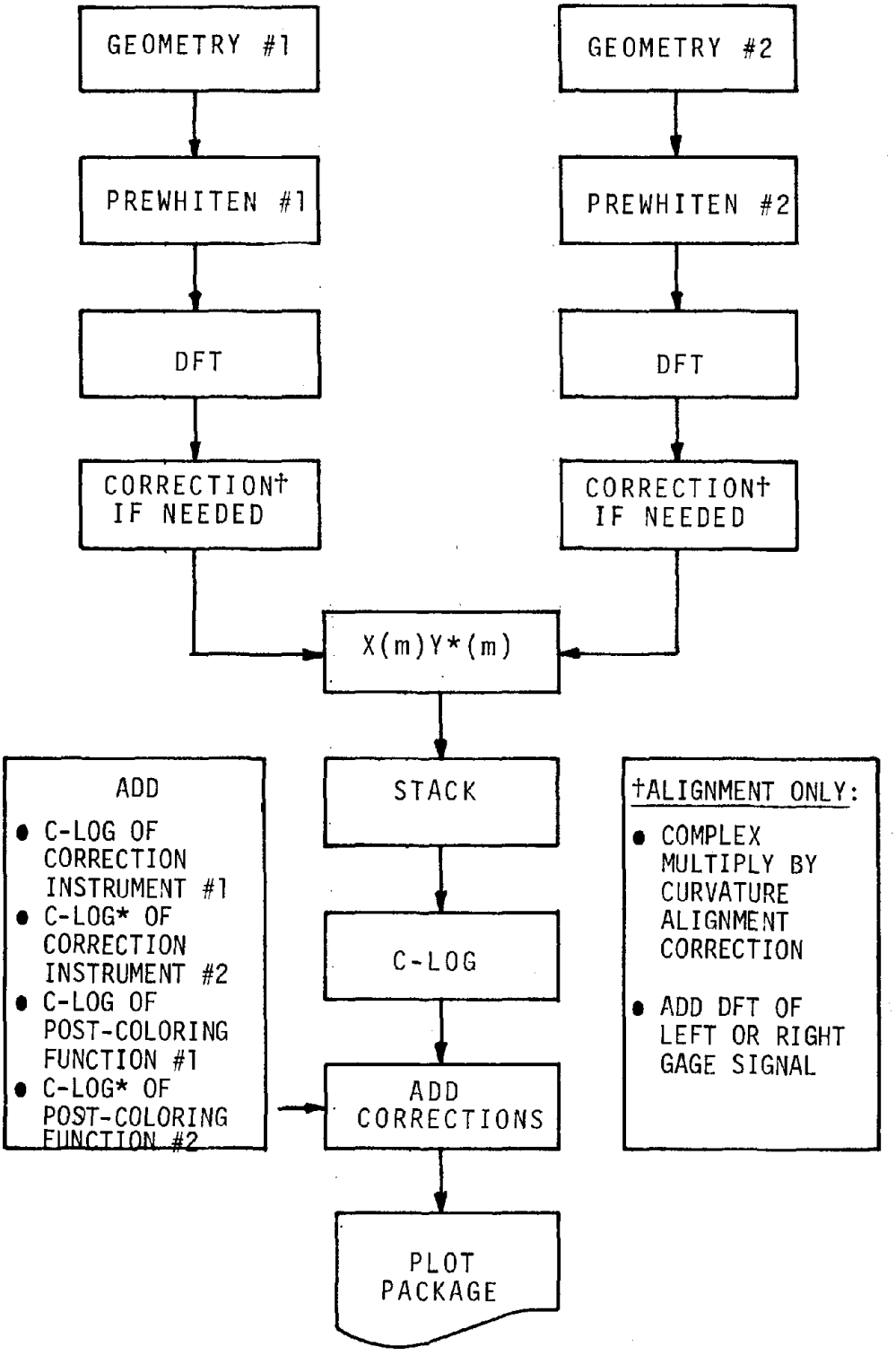

FIGURE 19. PSD PROCESSING (PROGRAM RAINBO)

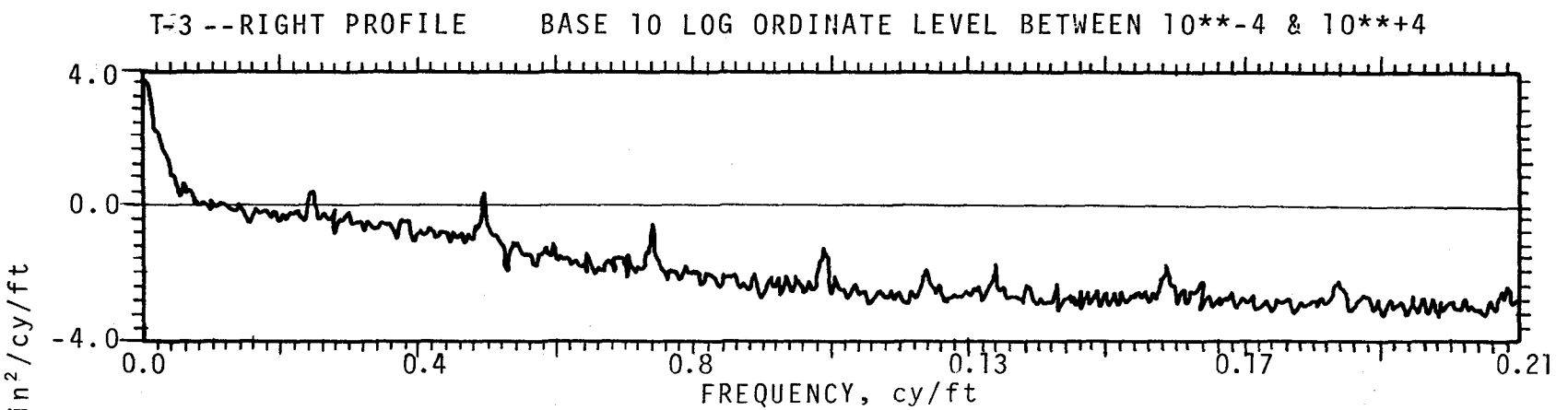

a. RIGHT PROFILE

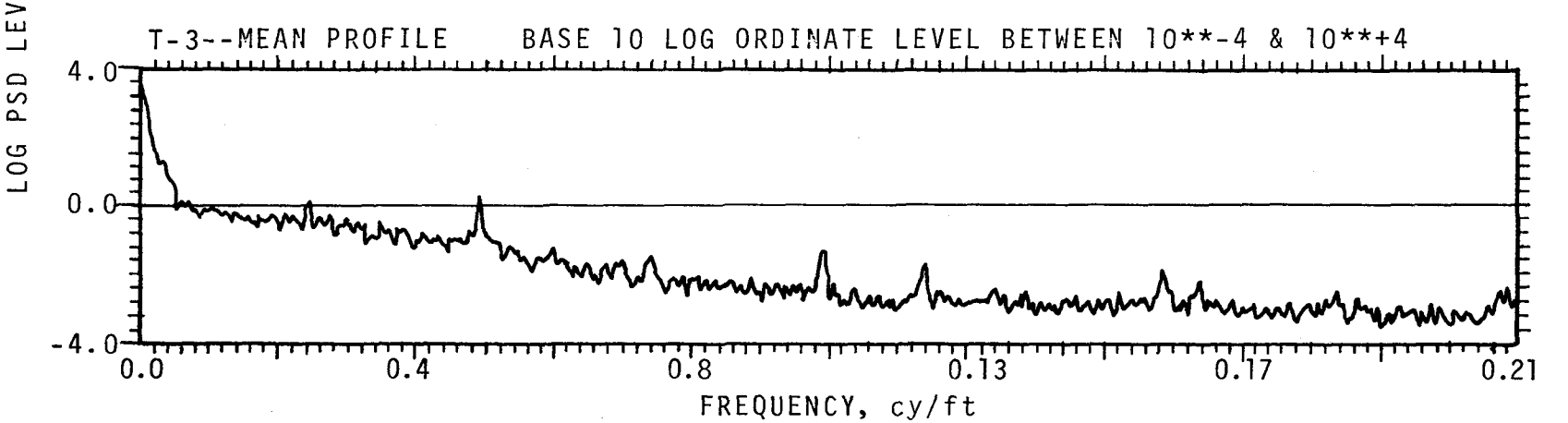

b. MEAN PROFILE

FIGURE 20. EXAMPLE OF LOG-LINEAR PSD AND X-PSD FORMAT

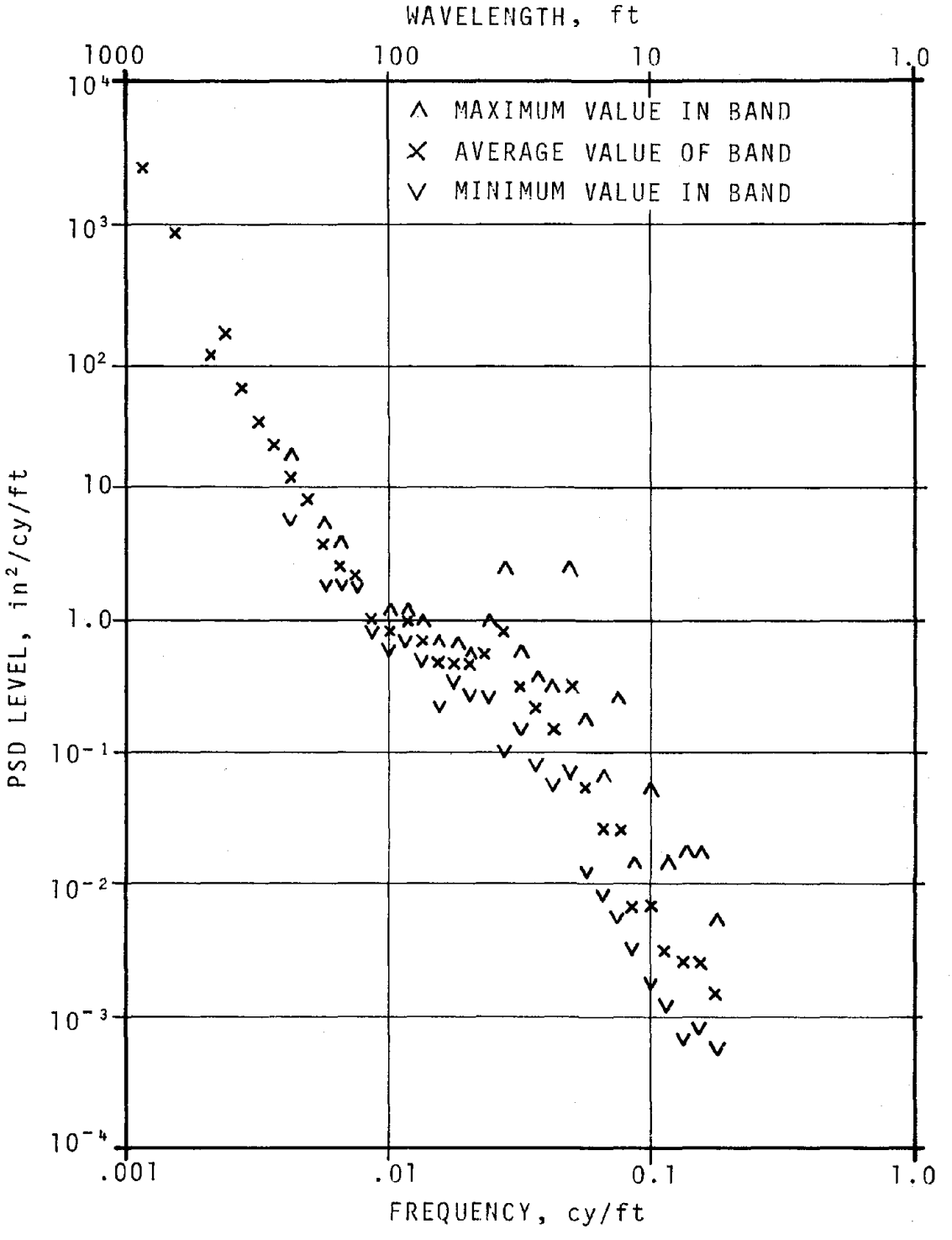

FIGURE 21. EXAMPLE LOG-LOG FORMAT, RIGHT PROFILE
(Corresponds to Figure 20a)

- A symbol, ×, indicates the PSD level at a particular frequency. Where more than one linear PSD value falls in a logarithmic frequency band, they are stacked and the max/min levels are indicated by a ^/ˇ, respectively. In this way, spectral variations and distinct peak/null frequencies can be noted.

- A symbol, ⊔, occurring in the lowermost row indicates that an × falls below the level of 10^{-4} $in^2/cy/ft$.

- A symbol, ⊓, occurring in the uppermost row indicates that an × exceeds the level of 10^4 $in^2/cy/ft$. (None of these occurred in the example shown.)

Examples of coherence function output corresponding to the PSD's in Figures 20 and 21 are shown in Figure 22.

2.5.3 DETERMINATION OF PSD PARAMETERS

PSD's generated by RAINBO are an intermediate step to the parameters needed to describe the component statistical processes. Presently this is done by manual manipulation of the PSD data. This approach was preferred since an automated procedure may not be general enough to identify an unusual rail length, to flag significant deviations from the model spectra, and to choose good starting values for the corner frequencies.

The first step of the manual procedure consists of eliminating superfluous data from the log-log PSD generated by RAINBO. Thus an × is retained if it corresponds to a good continuum value, and a ^ is retained at frequencies corresponding to the rail length periodicity and its harmonics. Prior to discarding, the markings are checked for significant deviations. If these are found, they are cross checked with the linear frequency PSD output. Application of this procedure results in a PSD graph such as shown in Figure 23 where the raw data of Figure 21 has been used.

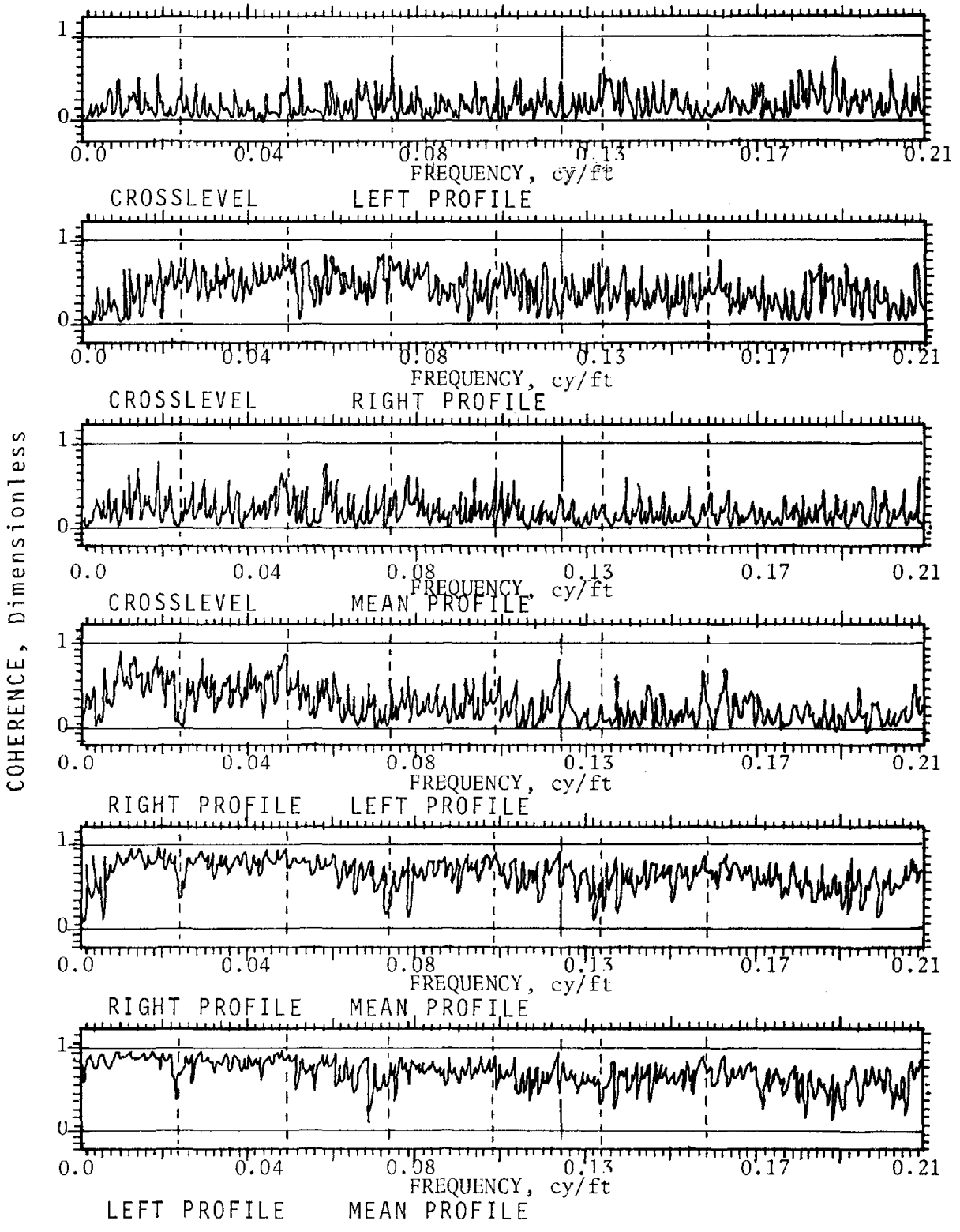

FIGURE 22. COHERENCE FUNCTION OUTPUT FOR ALL SURFACE PARAMETERS

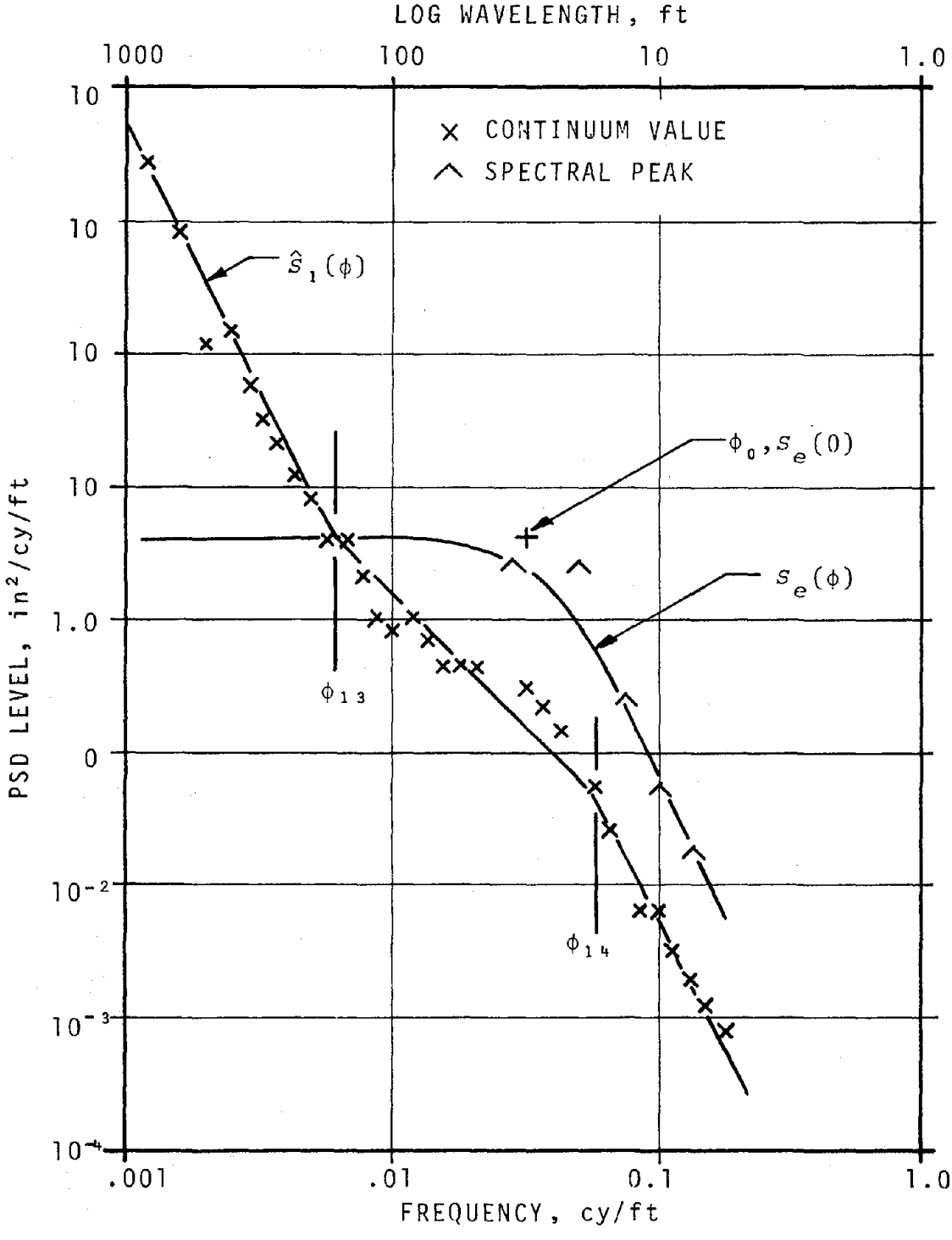

FIGURE 23. PROCEDURE FOR PARAMETER DETERMINATION FROM PSD DATA

Next, the continuum is fit using the profile -4,-2,-4,-2 power law. This procedure is shown in Figure 23. Also shown is the fitting of the envelope function, $S_e(\phi)$, to the spectral peaks.

Pertinent parameters are then extracted as follows:

$$A_1 = 1.6 \times 10^{-4} \text{ in}^2\text{-cy/ft},$$
$$\phi_{13} = 6.3 \times 10^{-3} \text{ cy/ft}, \lambda_{14} = 160 \text{ ft},$$
$$\phi_{14} = 5.6 \times 10^{-2} \text{ cy/ft}, \lambda_{14} = 18 \text{ ft},$$
$$\phi_{15} = \text{N/A},$$
$$L = 39 \text{ ft},$$
$$\phi_0 = 3.2 \times 10^{-2} \text{ cy/ft},$$
$$S_e(0) = 4.0 \text{ in}^2/\text{cy/ft}.$$

From these, the formulae developed in Paragraph 2.2.5 and 2.3.1.1 are used to compute:

$$\Lambda_1(31) = 0.066 \text{ in}^2,$$
$$\sigma(62 \text{ ft-MCO}) = 0.260 \text{ in},$$
$$k = 0.20 \text{ ft}^{-1},$$
$$\overline{C} = 0.11 \text{ in},$$

where B, the bandwidth of the PSD processor, is 4.1×10^{-4} cy/ft.

2.6 COMPUTER SIMULATION OF TRACK GEOMETRY

2.6.1 ASSUMPTIONS

Early in the project, a simulator of track geometry was developed and programmed, and its output evaluated both in space curve and in spectral form. This simulator was designed on the basis that track geometry data consists of the two additive component processes discussed in Paragraphs 2.2 and 2.3.

Features incorporated in this early simulator are:

- The SRP of mean profile, crosslevel, mean alignment and gage are all independent of one another and they are generated from four independent white noise sources operated on by linear filters having appropriate power responses.

- Crosslevel and gage are produced by the power response:

$$\left|H_n(\phi)\right|^2 \cong \frac{A_n \phi_{n4}^2}{(\phi^2 + \phi_{n3}^2)(\phi^2 + \phi_{n4}^2)}$$

  with n=4 and 8, respectively.

- High passed versions of profile and alignment space curve are produced by the same filter form with n=3 and 7, respectively. The power response of the high pass is given by $|G(\phi)|^2$ as follows:

$$\left|G_n(\phi)\right|^2 = \frac{\phi^4}{(\phi^2 + \phi_{n3}^2)^2} .$$

- The joint-related process is generated by using periodic impulses of random amplitude having non-zero mean gated at fixed rail length intervals and subsequently convolved with a joint shape filter.

- The joint amplitude is assumed to be independent from one joint to the next and between profile and alignment components. No tests have been performed to dispute this supposition although its validity is questionable.

- Allowance is made for joint geometry cross-fed from one rail to another. Recent investigation of degraded half-stagger bolted rail reveals that a low joint on one rail is accompanied by a depression on the other.

On the basis of these assumptions, the simulator can be represented by the block diagram of Figure 24. Details of its working elements are described below.

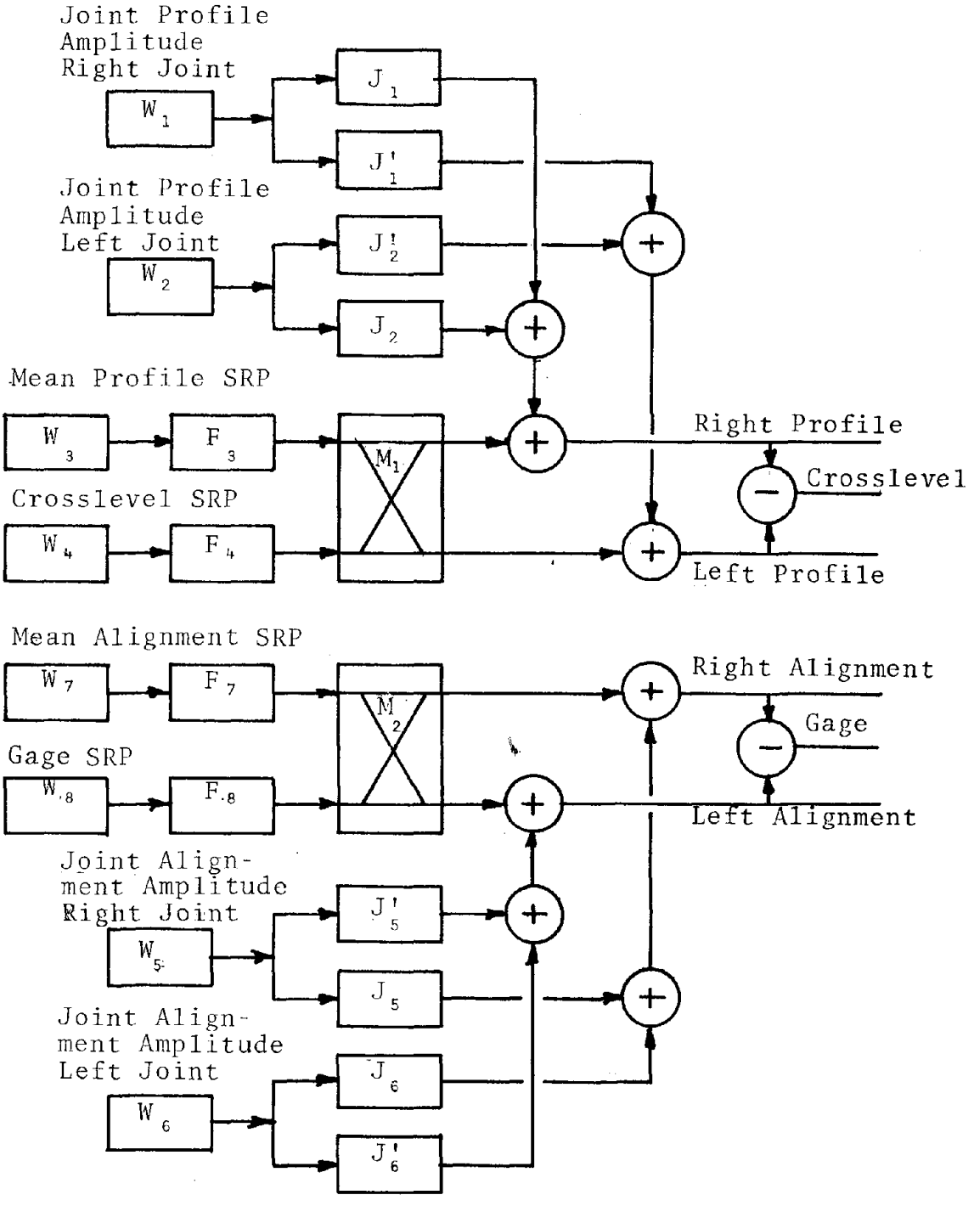

FIGURE 24. TRACK GEOMETRY SIMULATOR

2.6.2 RANDOM VARIABLE GENERATORS

Random variable generators indicated in blocks W_1 through W_8 in Figure 24 produce strings of random numbers, ξ, that are uniformly distributed between 0 and 1, and which have 0.5 mean and a $1/\sqrt{12}$ standard deviation. The variable ξ is then converted to a random variable w, that has mean, μ, and standard deviation, σ. For a pseudo normally distributed random variable with maximum values of $\pm 3\sigma$, the following transformation is used:

$$w = \mu + \sigma \times \begin{cases} 2\sqrt[3]{6\xi} - 3, \text{ for } 0 < \xi \leq 1/6; \\ 2\sqrt{3} \sin \theta/3, \text{ for } 1/6 < \xi < 5/6; \text{ and} \\ 3 - 2\sqrt[3]{6(1 - \xi)}, \text{ for } 5/6 \leq \xi \leq 1. \end{cases}$$

In the above,

$$\theta = \sin^{-1}\left[\frac{2}{\sqrt{3}}(2\xi - 1)\right] .$$

For a uniformly distributed random variable the transformation is given by:

$$w = \mu + \sigma[\sqrt{3}(2\xi - 1)].$$

Both forms of random variable transformation have been programmed and are used in the simulator.

Since the random variable generator produces white noise, its PSD should be constant over the entire frequency range of 0 to ½L where L is the sampling interval in feet. This was verified to be the case for at least 8000 samples.

2.6.3 SRP FILTERS

Simulation of the SRP in mean profile, crosslevel, mean alignment and gage is accomplished by the set of independent random

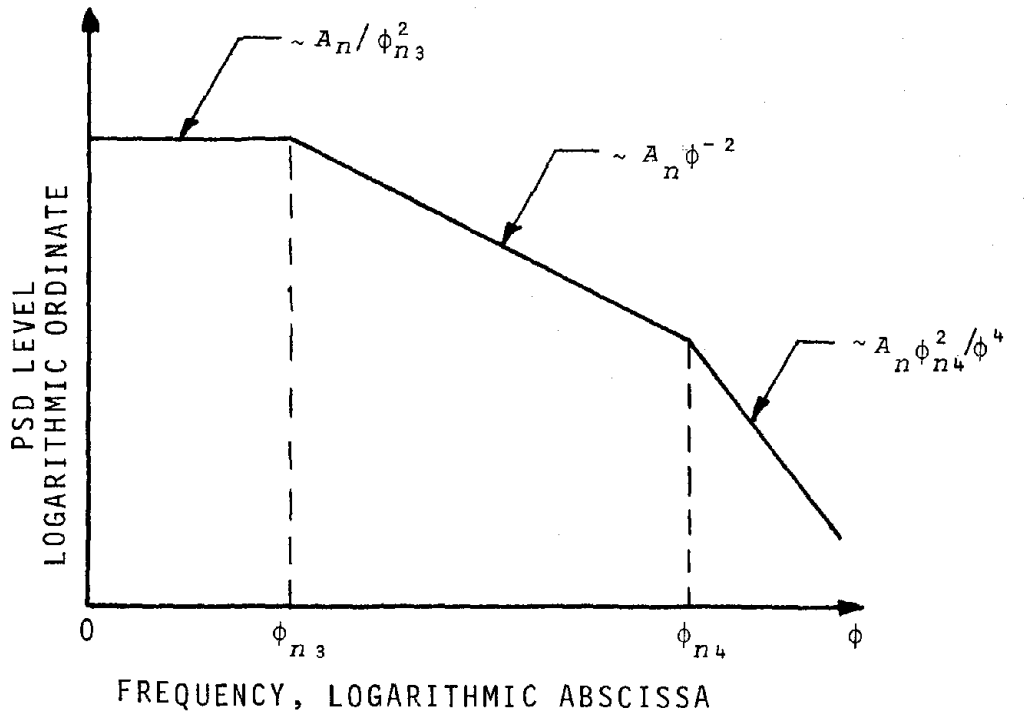

FIGURE 25. DESIRED PSD CHARACTERISTIC FOR SRP SIMULATOR

variable generators, W_3, W_4, W_7 and W_8. These feed four filters, F_3, F_4, F_7 and F_8 whose function is to act on the input random variable and generate an output random walk that has the PSD characteristic shown in Figure 25. The recursive digital filter that produces the desired random walk is given as follows:

$$y_m = [2 - (\alpha_4 + \alpha_3)]y_{m-1} - (1 - \alpha_3)(1 - \alpha_4)y_{m-2} + \alpha_3\alpha_4 h_0 w_m ,$$

where,

$\alpha_3 = 2\pi\phi_{n3}X$, radians,
$\alpha_4 = 2\pi\phi_{n4}X$, radians, and
X = sampling interval, feet.

TABLE 9. VALUES OF CORNER FREQUENCIES

Track Parameter	n	ϕ_{n_3}	ϕ_{n_4}
Profile	3	0.001	0.05
Crosslevel	4	0.01	0.05
Alignment	7	0.001	0.05
Gage	8	0.01	0.05

The standard deviation of the white noise input is given by,

$$\sigma_n = h_0 = \frac{2\pi}{\alpha_3} \sqrt{\tfrac{1}{2} A_n X} ,$$

and the values of corner frequencies are given in Table 9.

An illustration of the action of the filter, w_n, operating on white noise is given in Figure 26. A typical PSD for this random walk when adjusted for Class 6 SRP profile is shown in Figure 27. To derive this SRP, the value of σ was gradually reduced until no exceptions to Class 6 safety standards resulted.

Prior to adding in the joint-related process it is necessary to matrix mean profile and crosslevel into the individual rail profiles. This is done at block M_1 in Figure 24. A similar operation, M_2, converts mean alignment and gage into individual rail alignment.

2.6.4 SIMULATION OF THE JOINT-RELATED PROCESS

Joint-related activity is introduced by convolving gated impulses with a linear filter whose impulse response represents the joint shape. The amplitude of the impulse determines the amplitude of the joint. This is illustrated in Figure 28a which shows a single impulse generating a single joint.

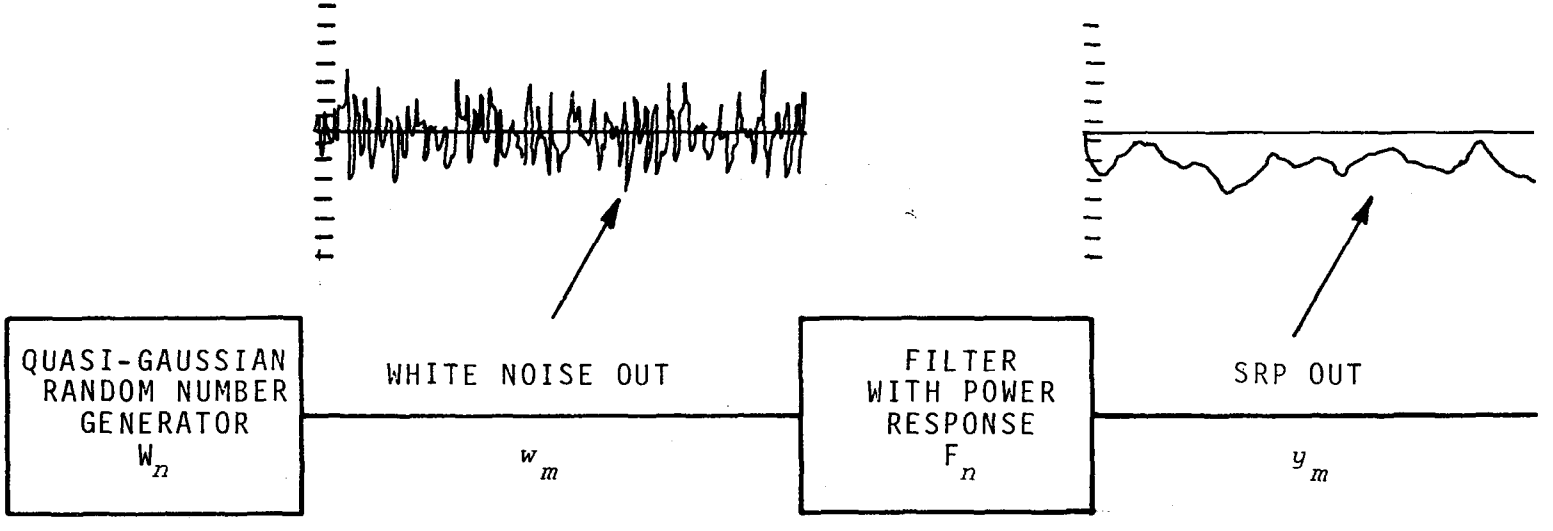

FIGURE 26. GENERATION OF SRP BY FILTERING WHITE NOISE

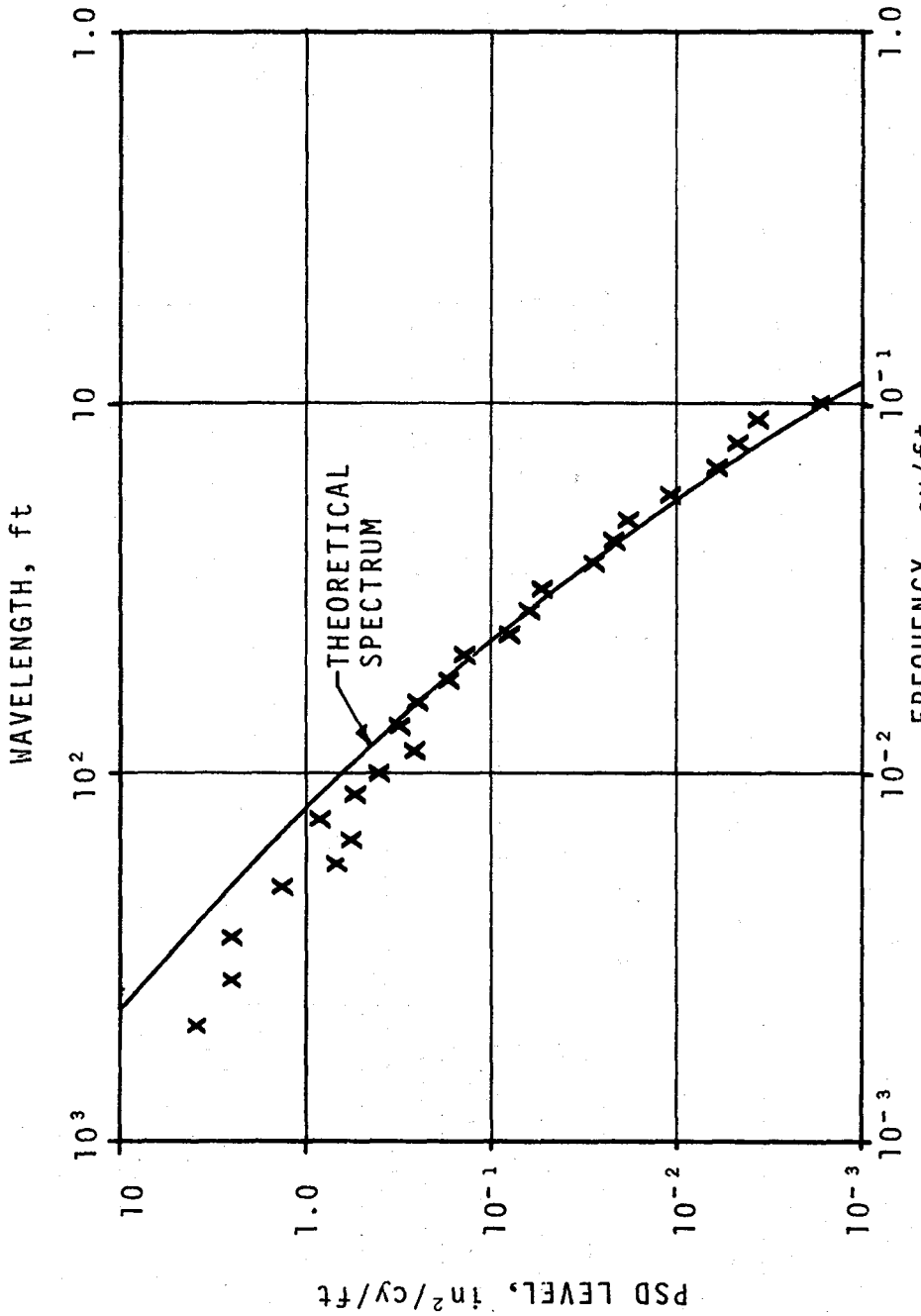

FIGURE 27. PSD OF SIMULATED CLASS 6 TRACK PROFILE, SRP ONLY

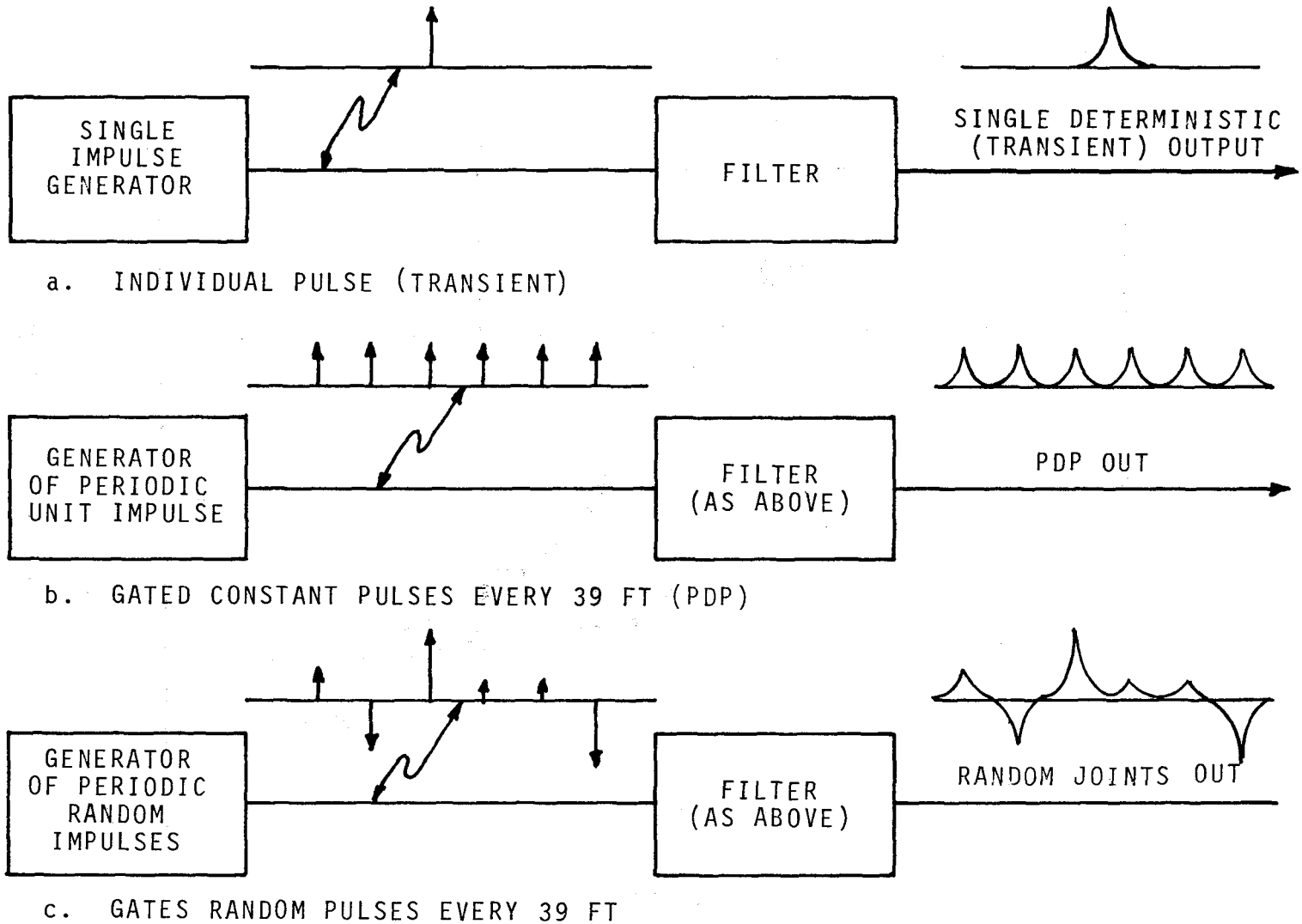

FIGURE 28. GENERATION OF JOINT AMPLITUDES AND JOINT SHAPES

A system of joints such as found on railway track is generated by periodically gating the impulses. If the impulses have a constant mean value, they generate a PDP as shown in Figure 28b. If the impulses are random with zero means, the pattern of joints having random amplitude shown in Figure 28c results.

Returning to Figure 24, the boxes labeled W_n, $n = 1,2,5,6$, are quasi-Gaussian generators, scaled by σ_n, biased by μ_n, and gated at preselected intervals corresponding to the rail length and stagger. W_1 and W_5 are gated at the same time but are otherwise independent. This is true with W_2 and W_6. The joint shapes are implemented via the filters J_n, $n = 1$, 2,3,4, using the truncated convolution sequence,

$$F_n \leftrightarrow f_m = e^{-|m|kX}, |m| \leq 50.$$

By choosing appropriate μ and σ, the simulator gives a PDP or uncorrelated joint amplitude output which can be analyzed by PSD. The PSD for a simulated PDP that just satisfies the class 6 FRA Safety Standards is shown in Figure 29. The PSD for a random joint amplitudes that just satisfies the class 6 FRA Safety Standards is shown in Figure 30.

The joint-related activity is readily combined with the SRP to produce a composite track simulation. A summary of the control constants for the simulator components is given in Table 10. By specifying all of these constants simultaneously, a PMRP is output that simulates track geometry variations. The effect of adding these components and their associated PSD's to produce a space curve is summarized in Figure 31.

Overall effectiveness of the program can be seen in a comparison between field data and simulator data for Class 2 track,as

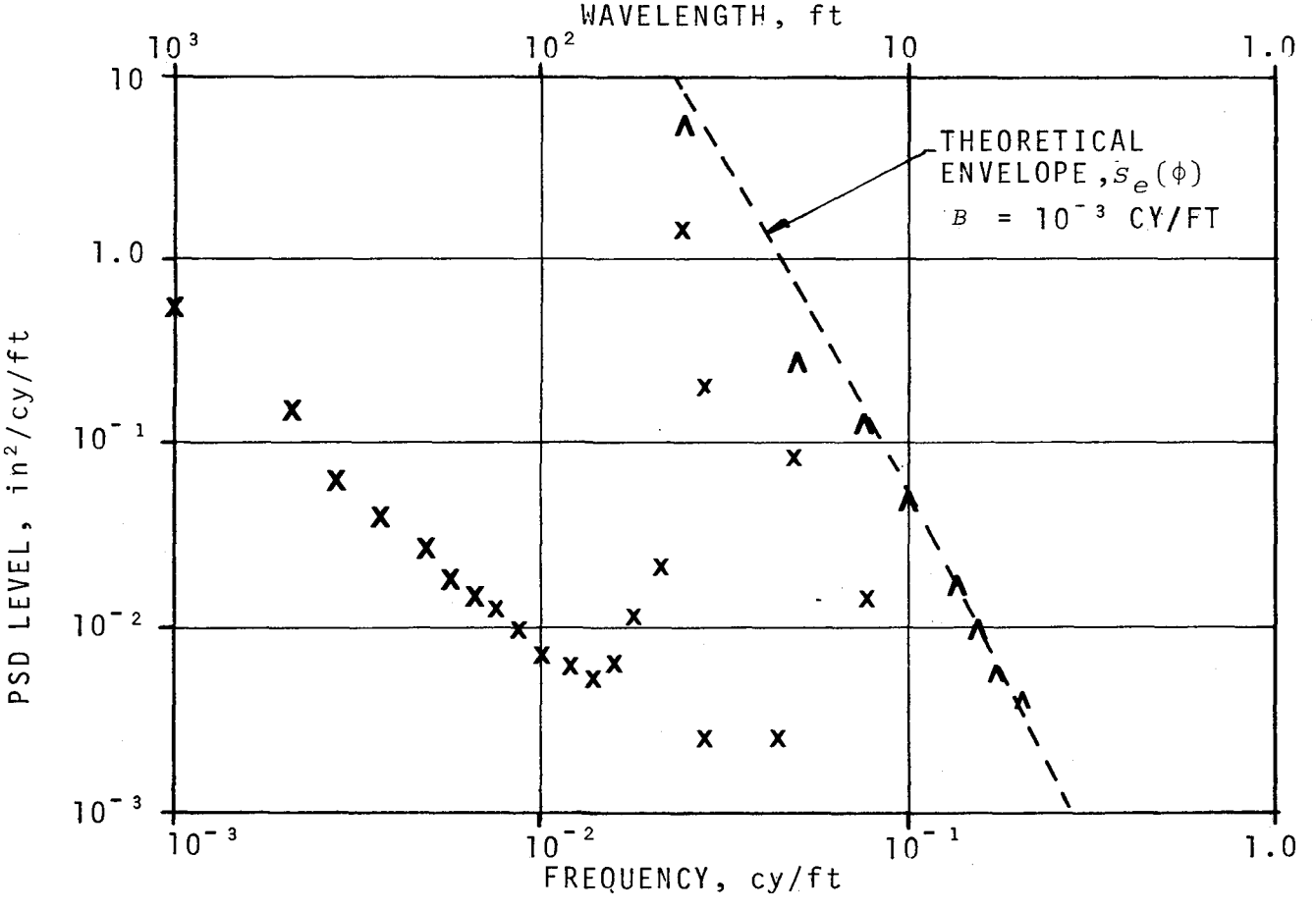

FIGURE 29. PSD OF PERIODIC DETERMINISTIC PROCESS, CLASS 6 TRACK

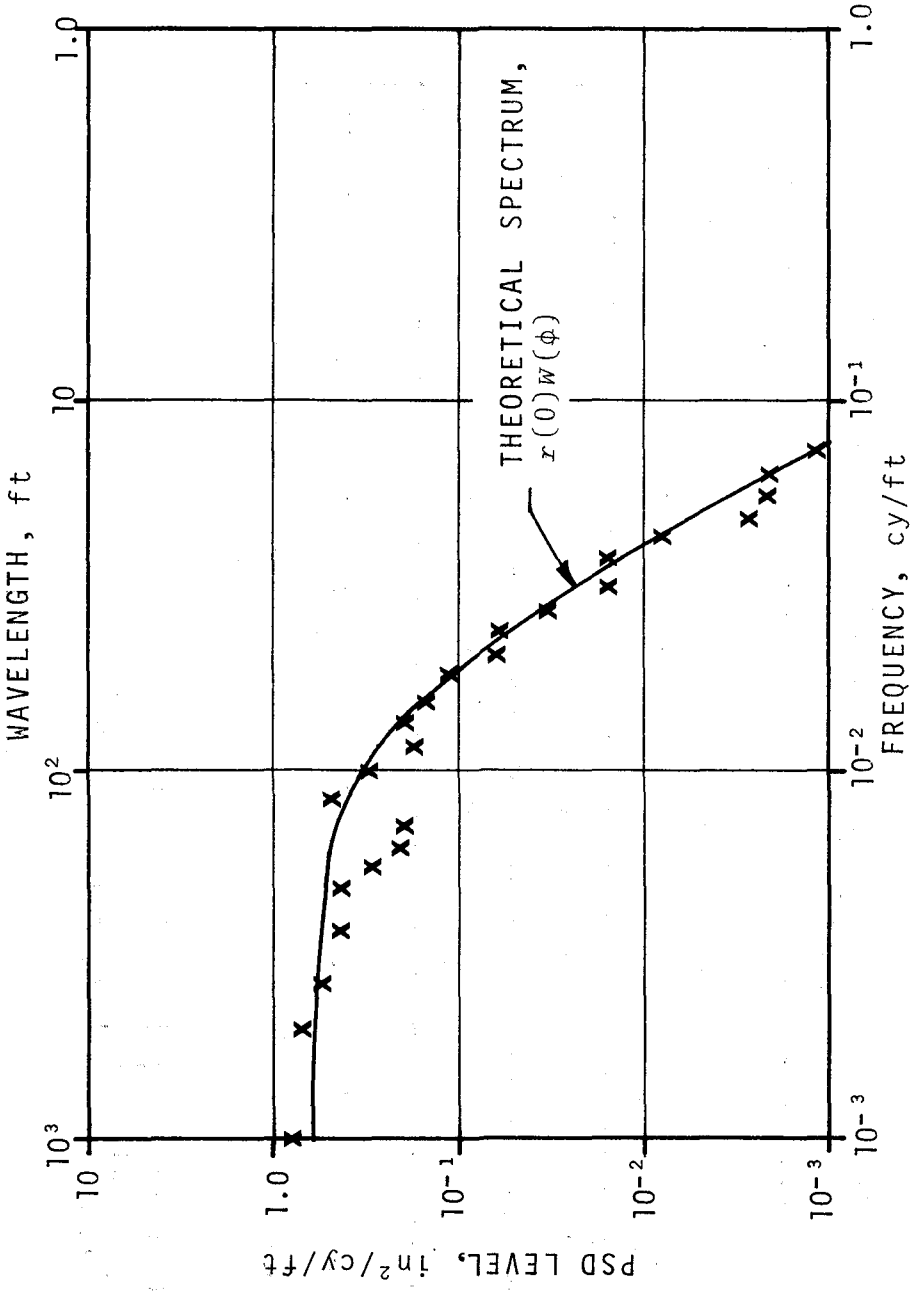

FIGURE 30. PSD OF RANDOM JOINTS, CLASS 6 TRACK

TABLE 10. MATRIX FOR SELECTING VALUES FOR SIMULATOR COMPONENTS

	W_3	W_4	W_7	W_8	W_1	W_2	W_5	W_6
SRP	σ_3	σ_4	σ_7	σ_8	0	0	0	0
PDP	0	0	0	0	μ_1	μ_2	μ_5	μ_6
RANDOM JOINTS	0	0	0	0	σ_1	σ_2	σ_5	σ_6
PMRP	σ_3'	σ_4'	σ_7'	σ_8'	μ_1', σ_1'	μ_2', σ_2'	μ_5', σ_5'	μ_6', σ_6'

For track in which left and right rail have identifical statistics

$$\left\{ \begin{array}{ll} \mu_1 = \mu_2 & \mu_5 = -\mu_6 \\ \sigma_1 = \sigma_2 & \sigma_5 = \sigma_5 \end{array} \right.$$

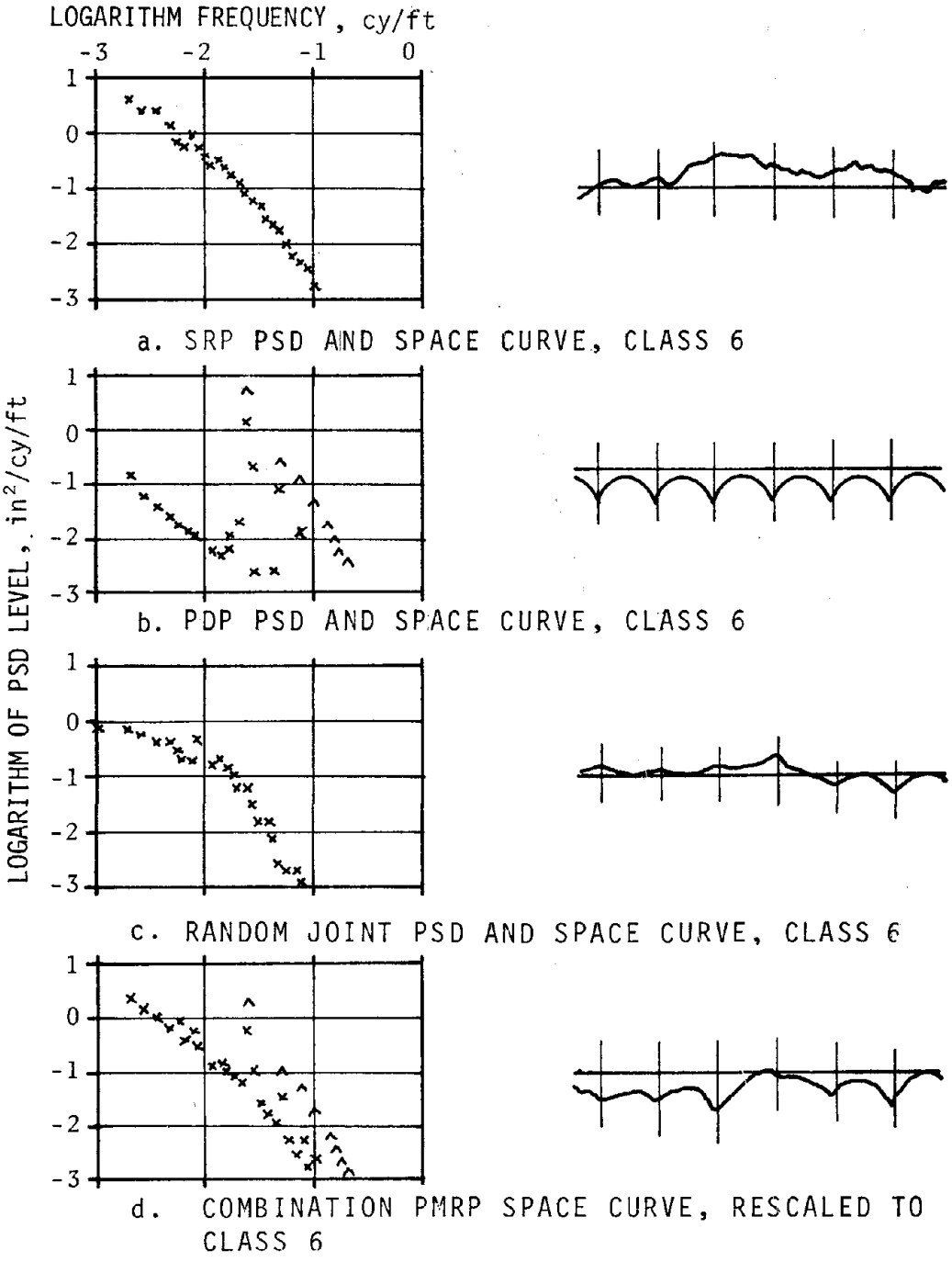

FIGURE 31. SIMULATION OF CLASS 6 TRACK BY COMBINING COMPONENT PROCESSES

shown in Figure 32. The lack of long wavelength deviations in the field data is the result of excessive high pass filtering that was characteristic of early space curves generated from field data.

2.6.5 RECOMMENDED IMPROVEMENTS TO TRACK SIMULATOR

While the track simulator was demonstrated to be capable of comprehensively representing actual railroad track, some improvements are possible. These are:

- A dip response should be incorporated in J_1' and J_2' to feed low geometry to opposite rail when a joint is encountered.
- A Γ-distribution should be used for the joint amplitude random number generators.

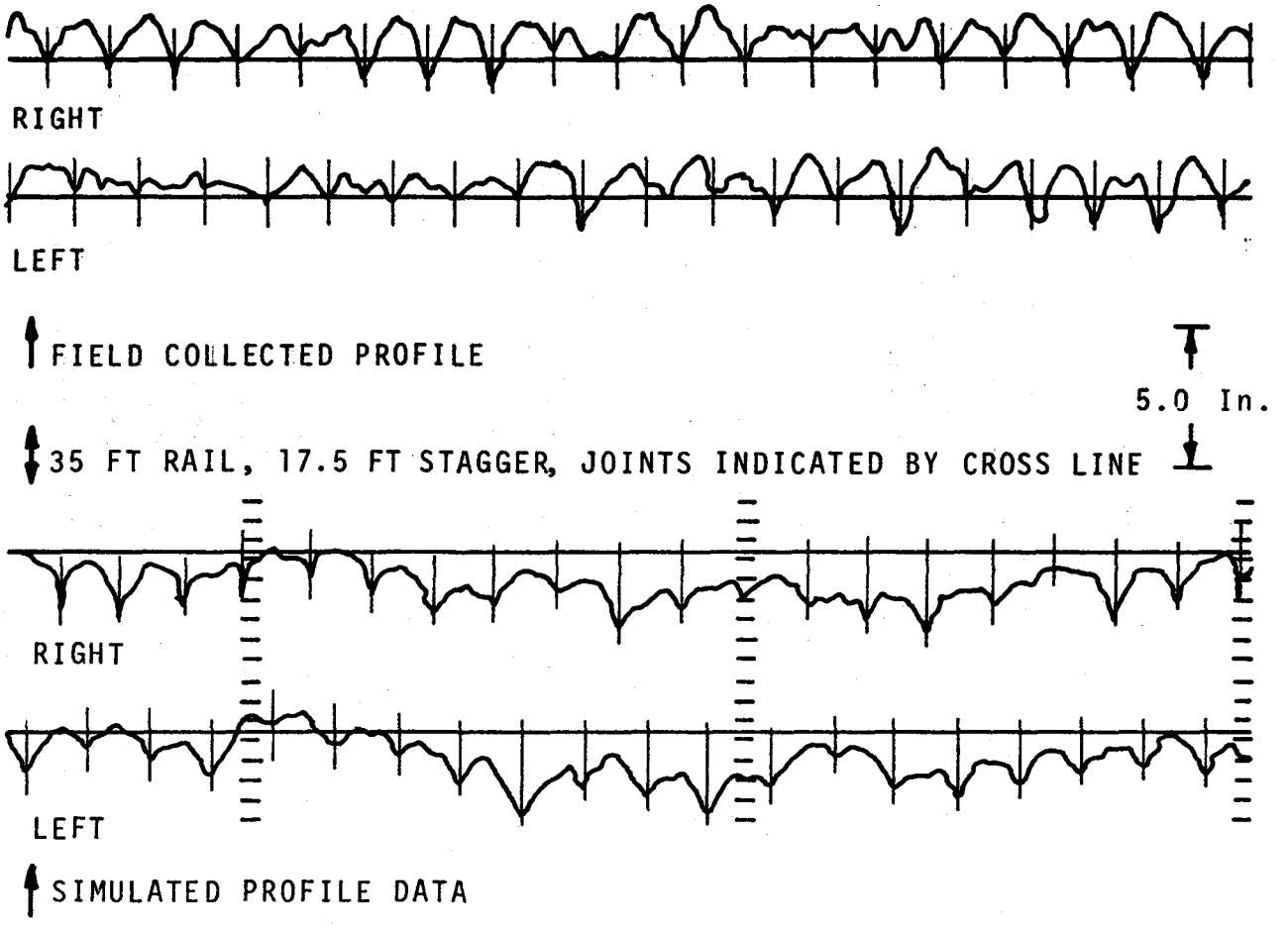

FIGURE 32. COMPARISON OF FIELD AND SIMULATOR PROFILE DATA FOR CLASS 2 TRACK

3. SPECIFIC TASKS

3.1 MEASUREMENT SYSTEM ERRORS

The track geometry measurement systems on the FRA track survey cars were analyzed to obtain estimates of the errors of these measurement systems. The analyses included consideration of the instrument system transfer functions, signal-to-noise ratios and other potential error sources. This work provided estimates of the power spectral densities of the system measurement errors.

3.1.1 GENERAL THEORETICAL CONSIDERATIONS

The statistical characterization of serial data can be a difficult process even when the data is not contaminated by errors and noise. Given that a validated model has been found and that error-free signals are provided, the associated statistical representations are subject to the uncertainty of sampling statistical data. Add noise contaminants, and the statistical details are quickly clouded.

Only signal averaging of serial data and ensemble averaging over parallel data streams are able to improve signal-to-noise ratios of statistical estimators. Other standard statistical procedures for serial data, such as analysis of covariance, PSD's, and higher order moments, and evaluating histograms, process noise as signals and are not able to distinguish between the two. For example, PSD's have a considerable dynamic range, and it is important to know instrumentation noise floors so that invalid wavelengths can be ignored.

In attempting to quantify a spectral noise floor, three major and real sources of error were identified. These are listed as follows:

- The noise floor of individual and combined system components;
- System responses to unintended or uncompensated inputs;
- Quantization noise where the A-D dynamic range is less than needed for the input data.

Experience with data from a wide variety of measuring systems assists in developing a good ability to recognize faulty data. This is particularly true in the case of the PSD. Some specific examples where questionable data was identified and subsequently associated with a flaw or fault in the instrumentation are described in Paragraph 3.1.5.

3.1.2 INSTRUMENTATION NOISE FLOORS

The full complement of FRA track measurement techniques employed over the years is quite varied.[11] The ultimate test of each system has been its utility in enforcing the FRA track safety standards.[3] Acceptance or rejection of measurement equipment has been based on its ability to ascertain compliance with these standards.

Since the measurement data to be analyzed for errors was from diverse sources, the types of measurements were identified in the orderly relation shown in Figure 33. The primary distinction is between single-plane and multi-plane measurements. A plane is defined as being perpendicular to the

[11] W. W. Gunn, "DOT Test Train Program System Instrumentation Manual - Seventh Edition," Annual Report, FRA-OR&D-76-254, June 1976.

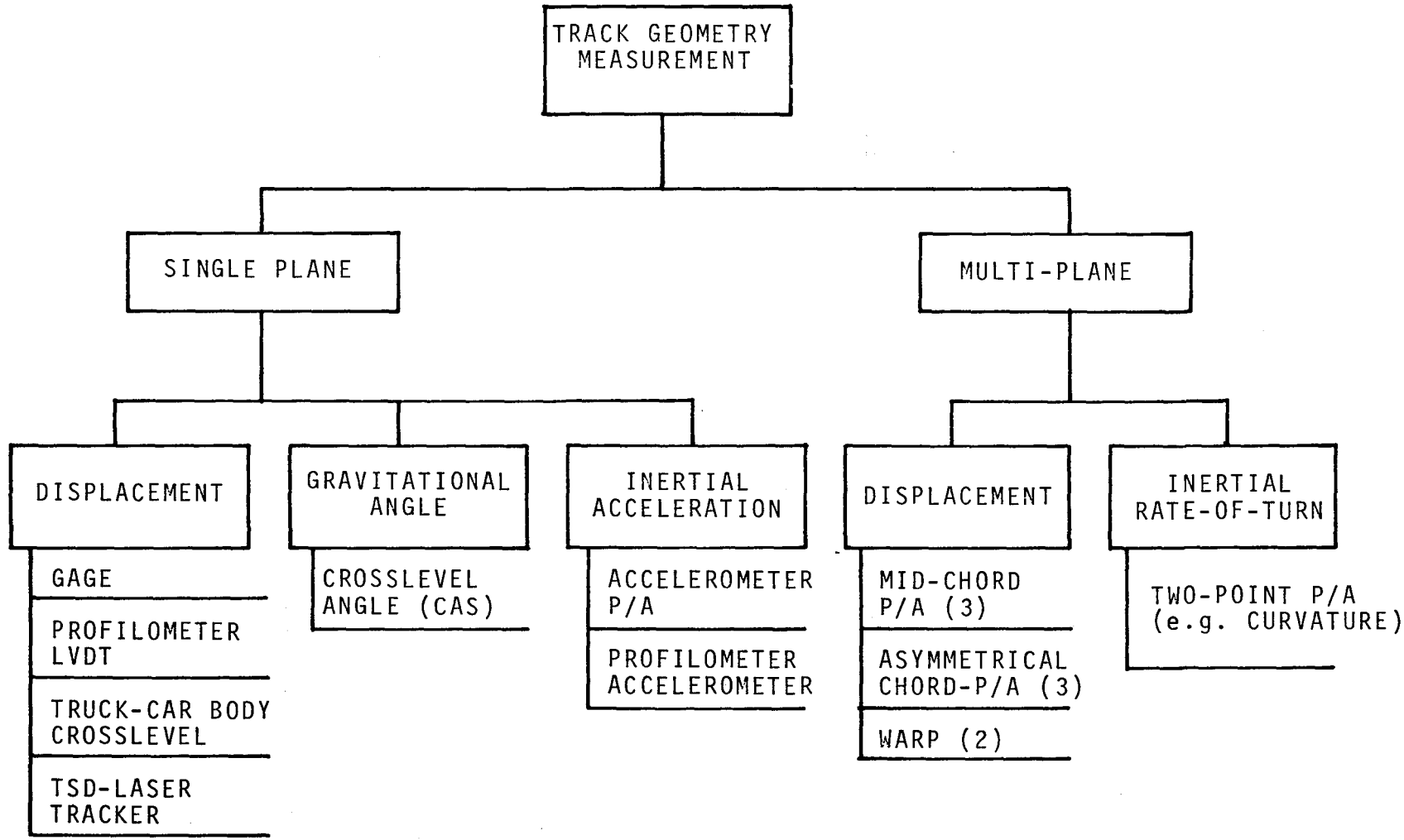

FIGURE 33. TRACK GEOMETRY MEASUREMENTS AND ASSOCIATED EQUIPMENT

track at the longitudinal position in the track where the measurement is performed. The essence of this distribution is that:

- Single-plane measurements give valid single-point representation of the track geometry. If the frequency response function has zeros, these are only at zero frequency and the output of the system can be an undistorted space curve.

- Multi-plane measurements provide distributed representations of geometry that are distorted by chordal response functions.

The multi-plane measurements characteristically emphasize some wavelengths and attenuate others. Attempts to recover the deemphasized portions of the spectrum will elevate the noise floor at those wavelengths.

Measurement systems are further subdivided as shown in Figure 33 according to whether the instrument system involves no temporal filtering (displacement transducer), compensated temporal filtering (gravitational angle measured from moving platform), or full temporal integration (inertial instrument).

The theoretical computation of noise floors is described in Appendix E. The procedure consists of assuming that the error appears at the instrument input where it is characterized by a white noise of a given standard error and bandwidth. Results of this analysis for the various track geometry instruments along with typical ranges of spectra, are presented in Figures 34 through 37. The noise floor of the Track Survey Device (TSD) is included in Figure 38 as a standard since it provides the lowest noise floors. Unfortunately, data collection is both slow and expensive with this system.

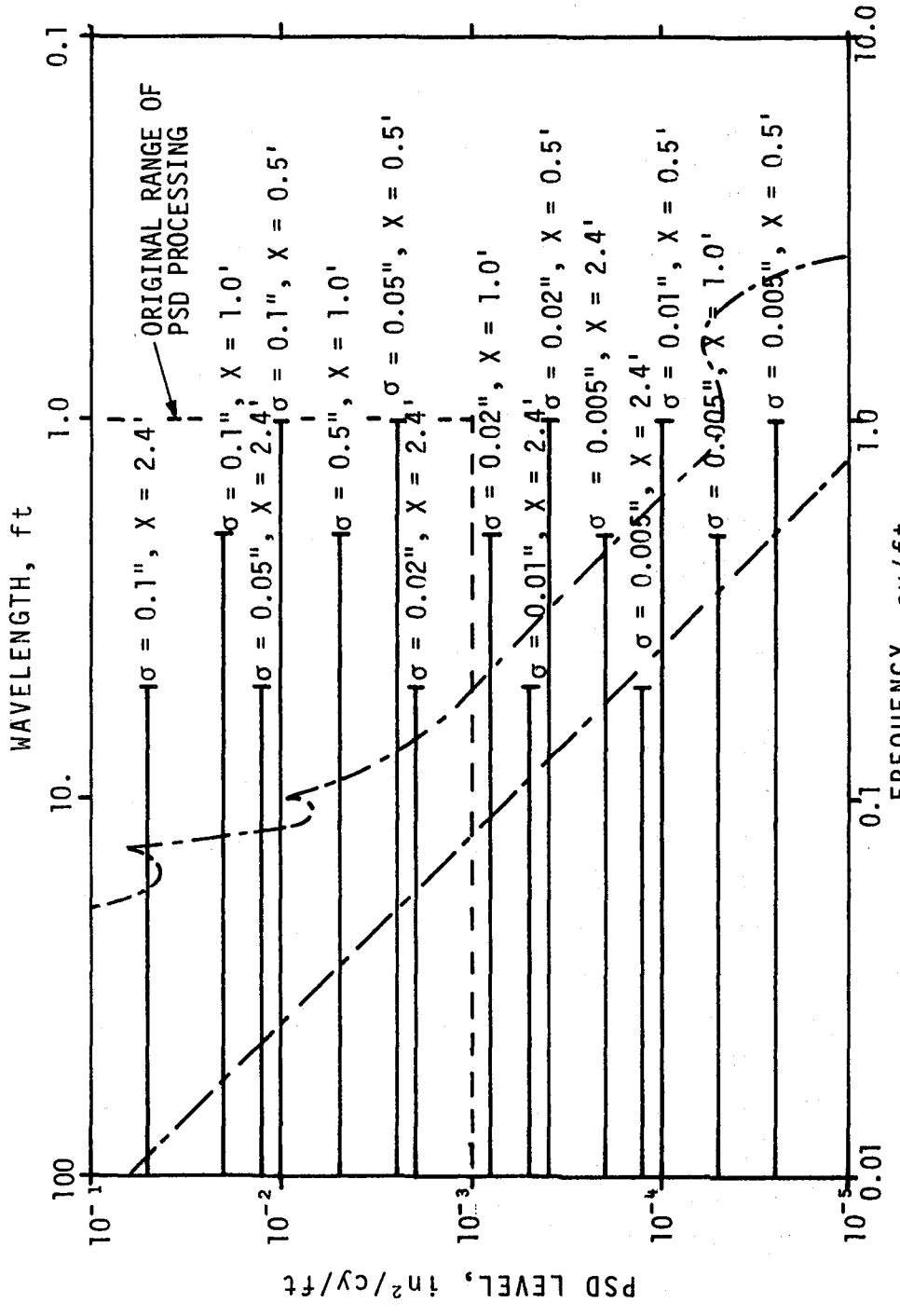

X = sample interval along the track.

σ = overall system error standard deviation.

FIGURE 34. DISPLACEMENT TRANSDUCER NOISE FLOORS

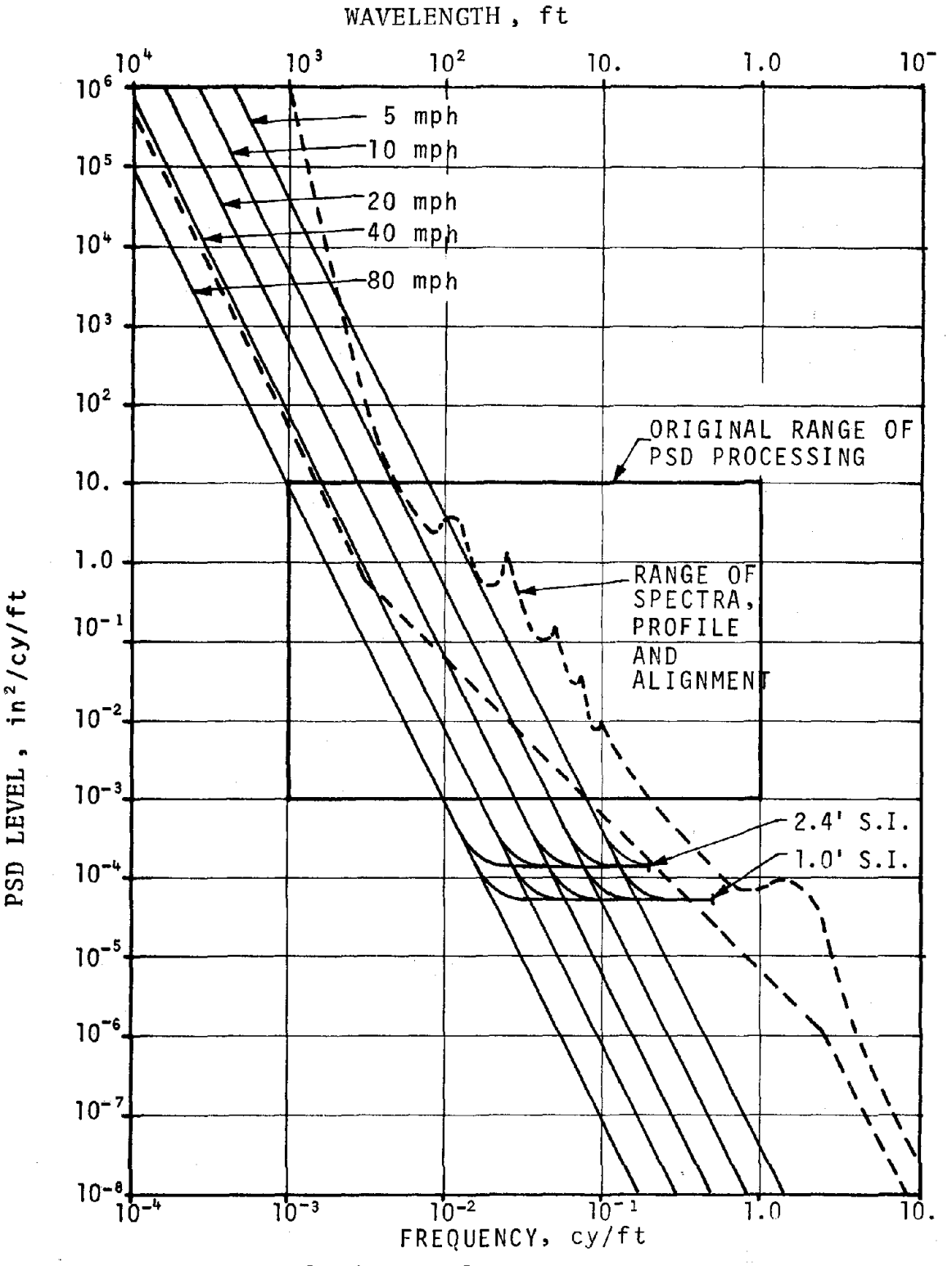

S.I. is sample interval.

FIGURE 35. ACCELEROMETER/PROFILOMETER NOISE FLOORS

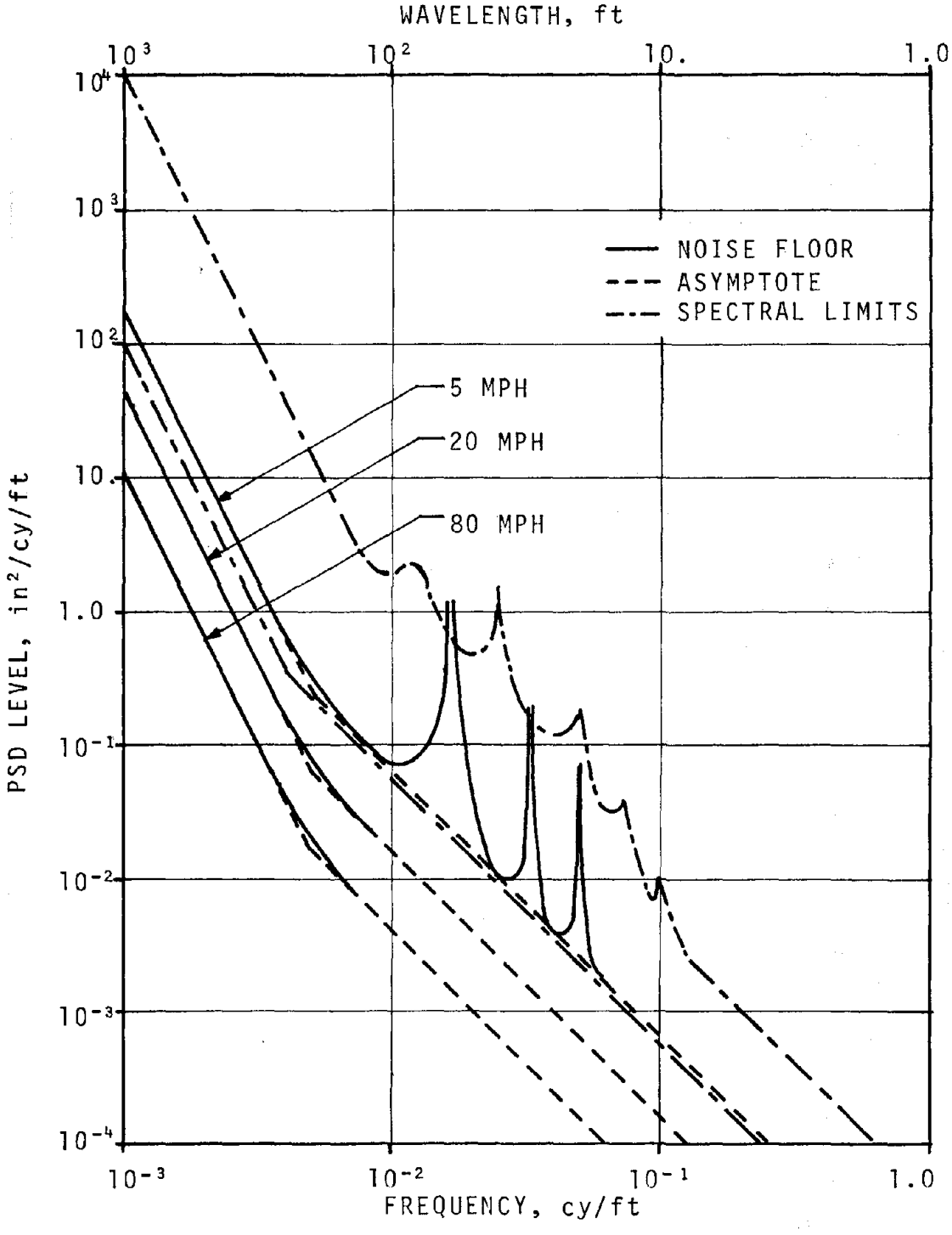

FIGURE 36. CURVATURE SYSTEM NOISE FLOOR

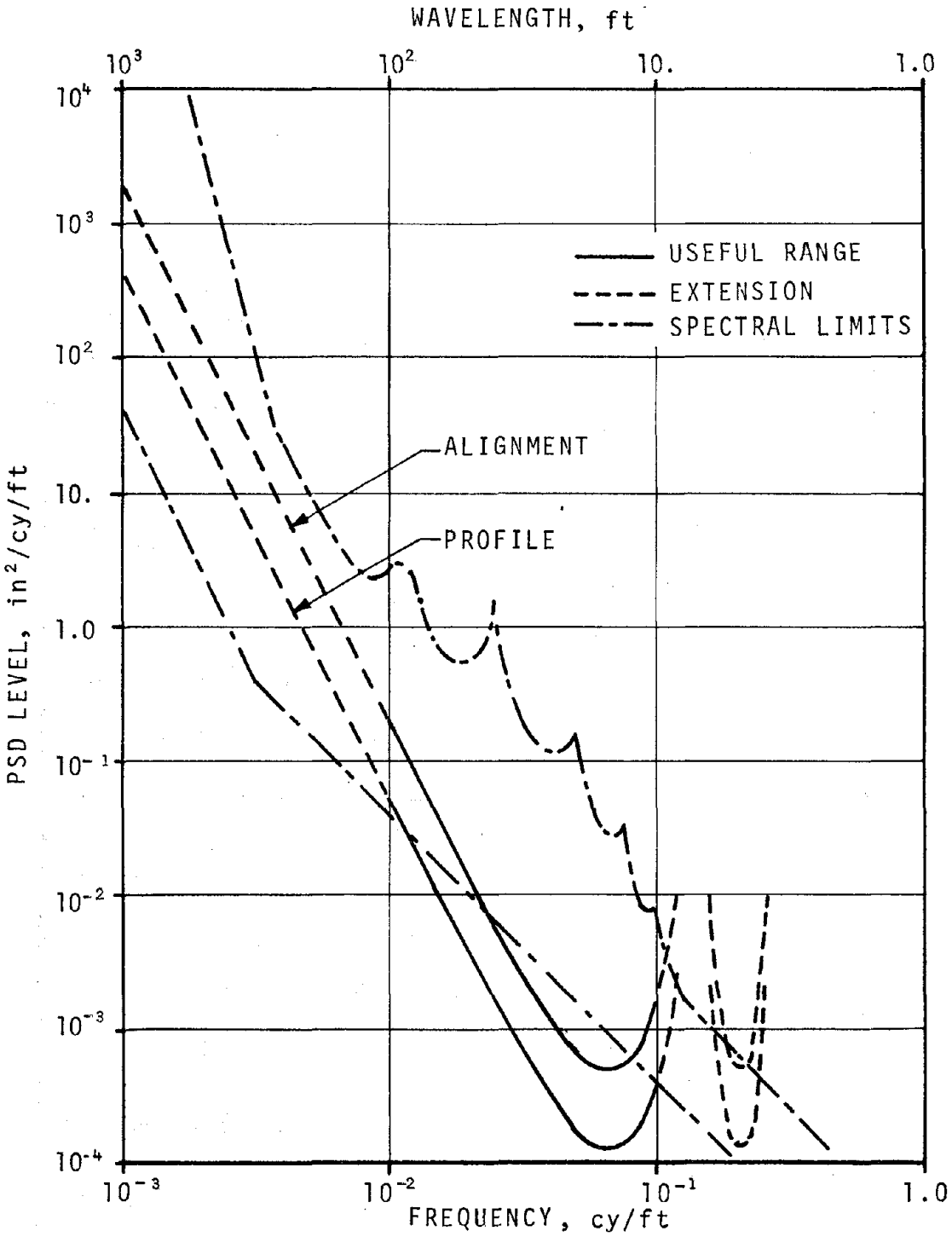

FIGURE 37. MCO NOISE FLOORS, ALIGNMENT AND PROFILE AT 14.5 FT

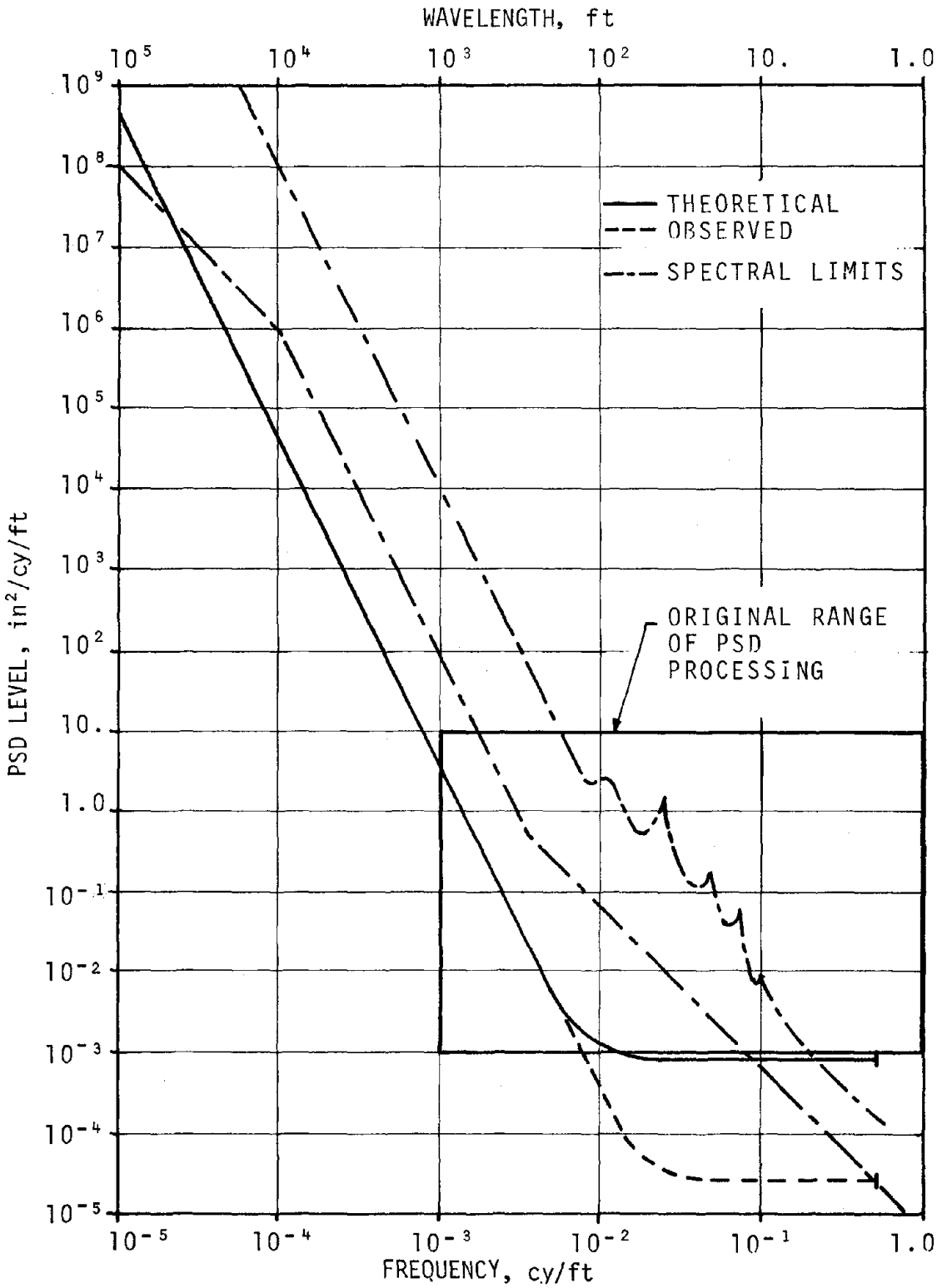

FIGURE 38. TSD NOISE FLOORS

3.1.3 ERRORS ASSOCIATED WITH INERTIAL INSTRUMENTS

The implementation of new track geometry measurement systems is replete with examples where the system responded in an unexpected way. This has been very much the case with the development of inertial measurements where many factors can wreak havoc with the desired output. Factors that may produce unexpected adverse effects include:

- Invalid analog integrator.
- Differences among platform coordinates, earth coordinates, and true inertial coordinates.
- Axial sensitivity in a nonprimary direction.
- Improper gain and phase relationships between components in systems where multiple sensors are used.

Synopses of typical errors are presented in Table 11. Included are such items as the fallacy involved, its effects on the output, and resolution of the problem.

3.1.4 NOISE CAUSED BY QUANTIZATION OF SIGNAL

The analog-to-digital (A-D) conversion of a signal is optimally accomplished by considering its dynamic range versus A-D capability. The latter is governed by the capability of digitizers available. In general, if the desired dynamic range exceeds digitizing resolution, suitable analog preprocessing can be introduced. Compensation for the analog processing is done in the digital processing where dynamic range is less restricted.

TABLE 11. SUMMARY OF INERTIAL MEASUREMENT SYSTEM CONCEPTUAL ERRORS

System	Profilometer-Alignometer Accelerometer	Crosslevel in Compensated Accelerometer System (CAS)	Profilometer-Alignometer Accelerometer
Design Fallacy	...let's see. All we need to do is integrate this signal and we have...	...and since ε is small, its ability to produce system errors is negligible...	...so keep the system bias down to the equivalent of 10^{-100}g at the input...
Technical Problems Involved	Signals cannot be integrated indefinitely so some phase shift results	The combination of high grade angle sharp turns, cross axis sensitivities, & long integration time produces erroneous crosslevel.	Conversion of the accelerometer output to short chord involves an analog filter whose d-c gain is quite high.
Effect on Signal	Representations of P/A are both speed and direction dependent.	Extended transients on entering or leaving one of the above types of curve.	The original digital processing scheme allows d-c offset & time-between-samples (TBS) to multiply. Control of bias is impractical. Therefore, large errors result when TBS changes.
Correction	Convert to good digital short chord and use digital filtering to achieve desired output.	Reduce integration time, increase filter roll-off rate, compensate for car body yaw	Use modified digital processing algorithm that keeps bias away from multiplication.
Effectiveness of Correction	Applied with good results.	A multiple input system that gives good results when properly calibrated.	Applied with good results.

At the inception of the FRA track measurement program, eight-bit analog to digital converters were used. This was quite adequate for the capacitive sensors whose peak range was ± 2.5 inches giving a resolution of 0.02 in/bit. Crosslevel, whose range was ± 10 inches, had the poorest resolution at 0.08 in/bit.

With the development of the profilometer and its all-weather capability, the capacitive measurement of profile and alignment was discontinued. However, the attempt to minimize profilometer phase shift problems required long integration time constants which increased the peak range up to ±20.0 inches, given a resolution of only 0.16 in/bit!

The prediction of noise floor due to the digitizing process is difficult because it involves nonlinear processes. Deutsch[12] gives a prescription whereby the correlation function of the quantization error can be generated from the correlation function of the signal. By Fourier transformation, the correlation functions can be converted into PSD expressions. The application of this technique to PSD models of crosslevel and profile is shown in Appendix F, and the results are outlined in Figure 39. As can be seen an eight fold improvement in resolution produces a dramatic improvement in noise floor.

A more insidious form of quantization error appears in the alignment-crosslevel coherence functions of TSD data. In collecting data, the TSD laser tracker is shifted horizontally by crosslevel because of its height above the rails.[13] In processing this data, correction is made for this motion. However the resolution of the horizontal laser tracker is twice that of the crosslevel inclinometer. On the smoother

---

[12] R. Deutsch, *Non-linear Transformations of Random Processes*, Prentice Hall, Englewood Cliffs, NJ, 1962, p. 79-81.

[13] H. Medicki and S. Panuzio, "Track Geometry Survey Device for LIM Research Vehicle Test Track," Final Report, FRA-ORD&D-74-36, October 1973.

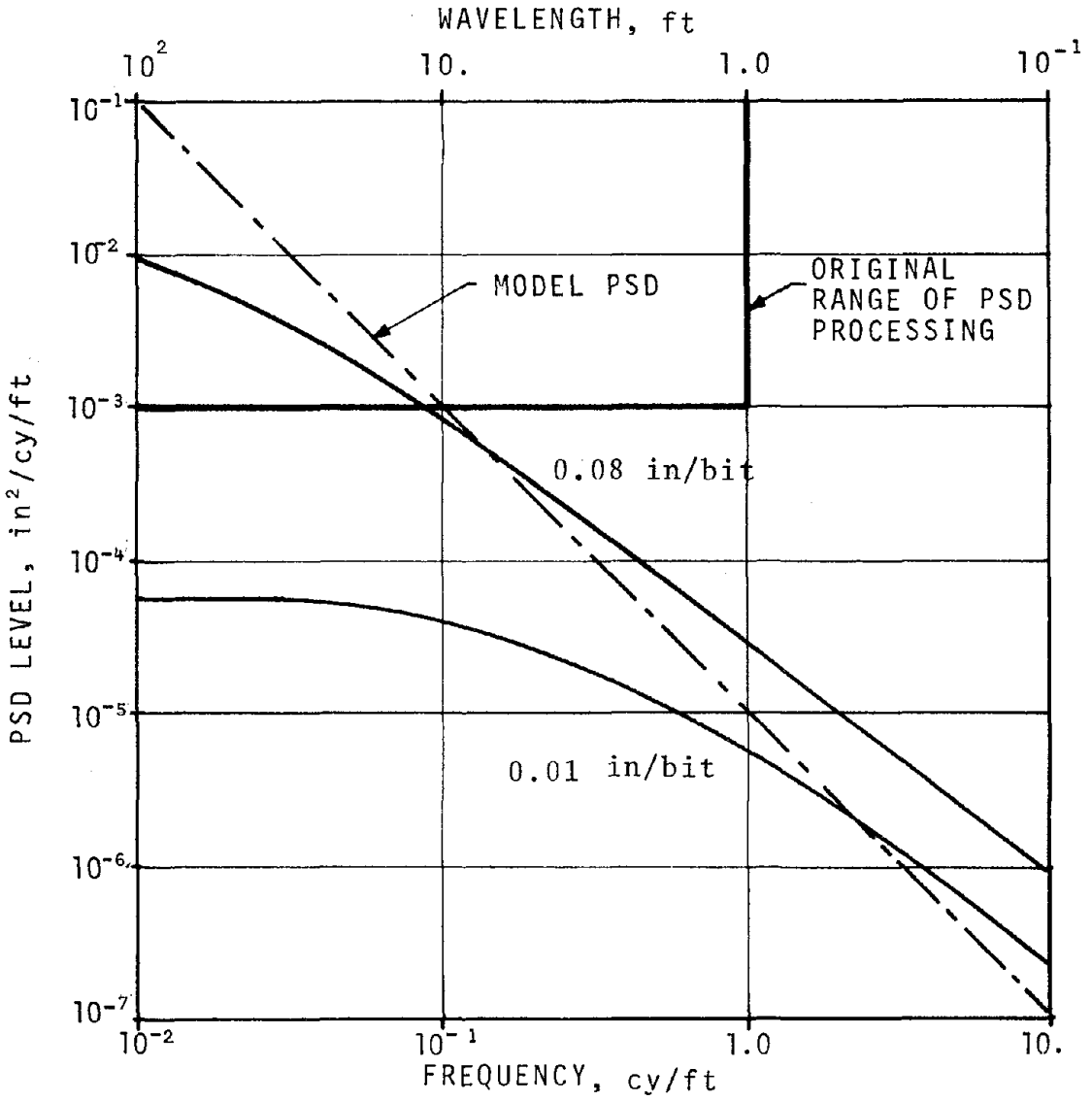

FIGURE 39. NOISE FLOOR FOR QUANTIZATION

sections of track, this produces a strong coherence as shown in Figure 40a. Figures 40b and 40c show lower coherences corresponding to progressively rougher track.

3.1.5 NOISE FLOOR IDENTIFICATION FROM PSD PROCESSING

It was suggested that characterization of geometry by its PSD might prove to be such a highly uncertain procedure that noise could interfere with spectral estimates. However, track

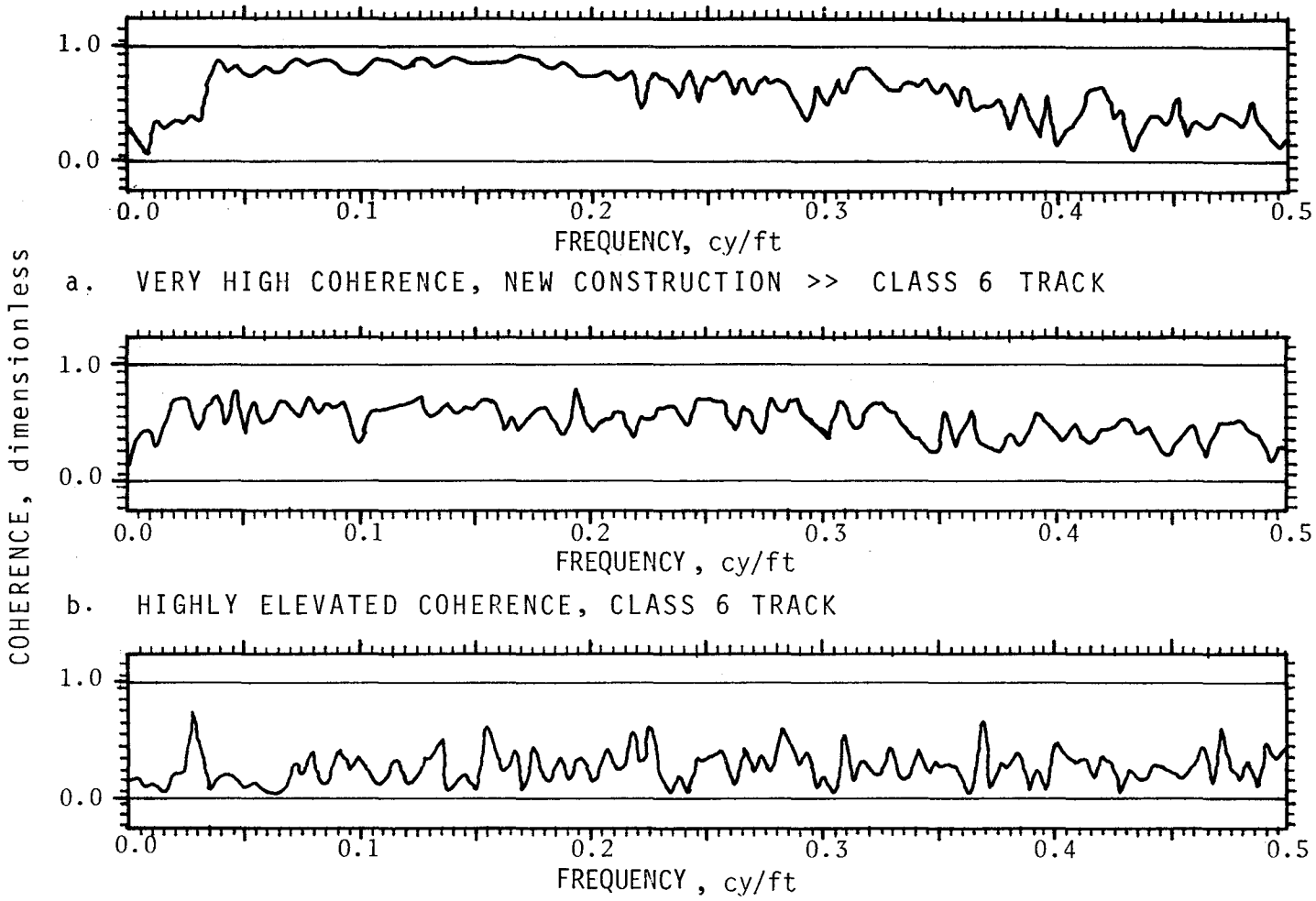

Figure 40. ANOMALOUS COHERENCES IN MEAN ALIGNMENT - CROSSLEVEL FOR TSD DATA

geometry PSD's were found to follow such predictable and definite patterns that measurement system defects have been successfully identified from the patterns. Some examples where this has occurred are described in the following paragraphs.

Figure 41 shows the range of some crosslevel PSD's collected by the self-erecting gyro system used on T-3 in 1971. In the long wavelength range, they behave as expected. Toward the middle wavelengths, they exhibit a consistently rapid roll-off starting at 40 feet and an excessive rise in the neighborhood of 10 feet. The difference between these curves was ascertained and the results plotted as the dotted line in Figure 42.

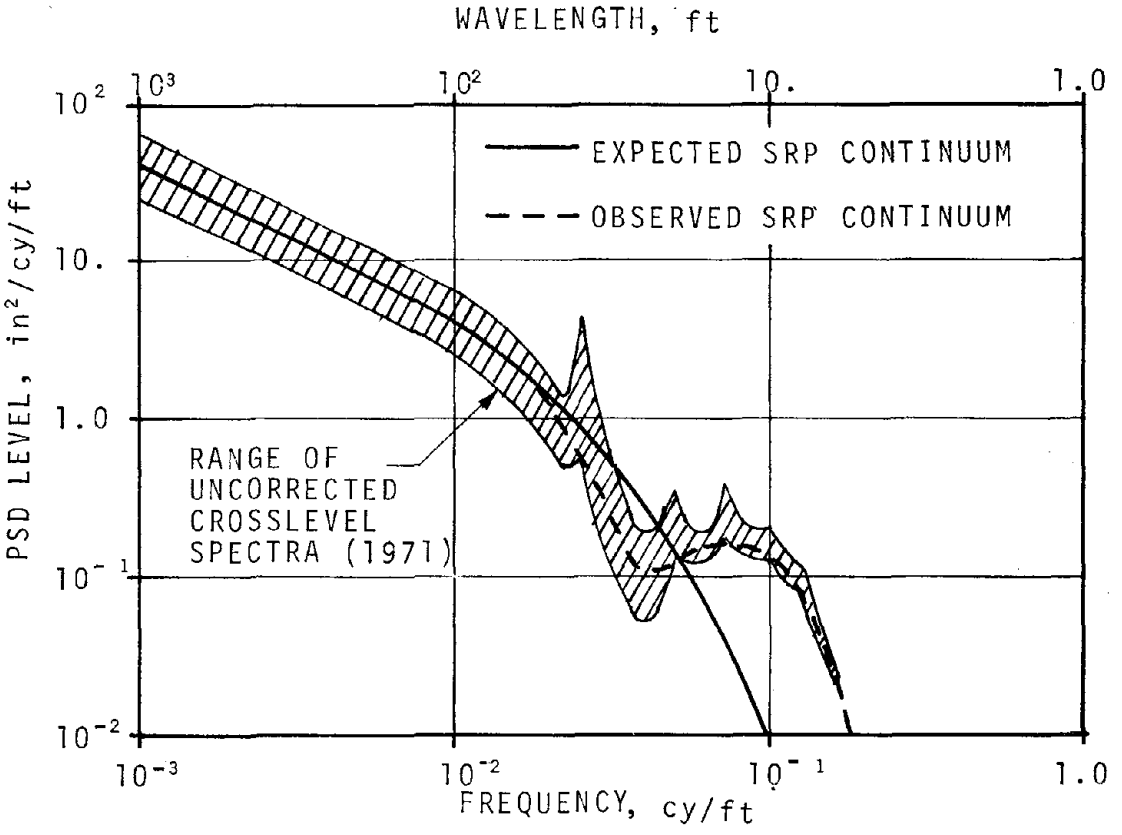

FIGURE 41. DISCREPANCY BETWEEN OBSERVED AND EXPECTED CROSSLEVEL

This first estimate of the discrepancy from empirical data resembles a chordal response function. The crosslevel system was configured so that many individual sensors contributed to the final measurement and sign inversion on one or more of these sensors was suspected.

The theoretical effects of inverting sensor outputs was examined, and the most likely incorrect combination produced the solid curve of Figure 42. Adding in the system noise floor produces the dashed line which is in good agreement with the empirical results. It is interesting to note that the same incorrect combination of sensors was discovered during the T-3 validation effort.[14]

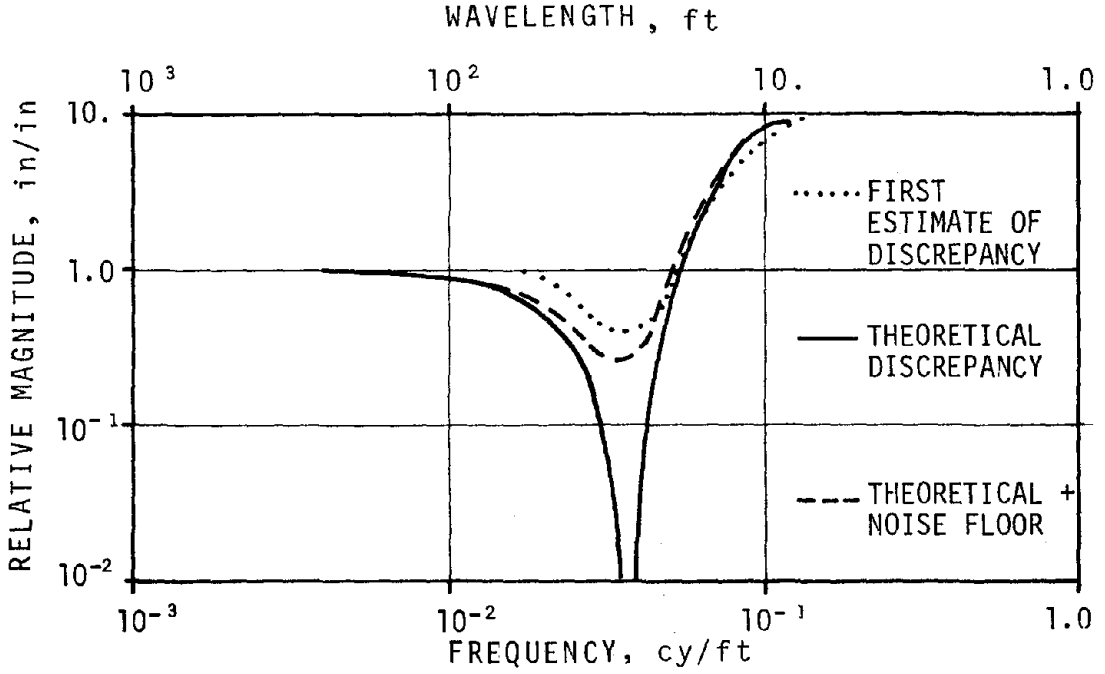

FIGURE 42. FIRST ESTIMATE AND THEORETICAL PREDICTION OF DISCREPANCY

[14] T-L. Yang, "FRA Track Geometry Measurement System Validation Report," Final Report FRA-ORD&D-73-08, June 1974.

PSD's of the profile measurements from T-2 and gage measurements from T-3 are shown in Figure 43. Both reveal problems. The T-2 PSD is highly elevated in the short wavelength limit. It displays interactions between profile measurement and wheel irregularities. Distinct peaks correspond to the wheel circumference wavelength of 8.5 feet, and its harmonics. Evidence of modulation of this periodic process appears as sidebands on either side of the peak. The T-3 gage PSD reveals a form of random noise that appears at speeds over 50 mph. This was caused by relative vibratory motion between the independent gage sensor support beams.

Towards the long wavelength limit, track surface is characterized by large amplitudes that are similar for both the left and right rail. A good diagnostic check for profile performance at these wavelengths is that:

- Left and right profile PSD's should be nearly identical, and
- Coherences between left and right profile should approach unity at wavelengths greater than 20 feet.

Figure 44 displays a comparison of T-2 PSD's for left and right profile on the same section of track. They are dramatically different for virtually all wavelengths. A comparison of T-3 PSD's for left and right profiles, collected in the 35-70 mph speed range, is shown in Figure 45. There is considerable improvement, but a consistent difference is observed in the neighborhood of 250 feet. Finally, T-2 and T-3 coherence functions are shown in Figure 46. In the T-2 plot, coherence is observed only at the wheel irregularity wavelengths. It decreases only at the wheel irregularity wavelengths. In the T-3 plots, the coherence starts to increase with increasing wavelength at about 16 feet (0.06 cy/ft). This trend continues to a

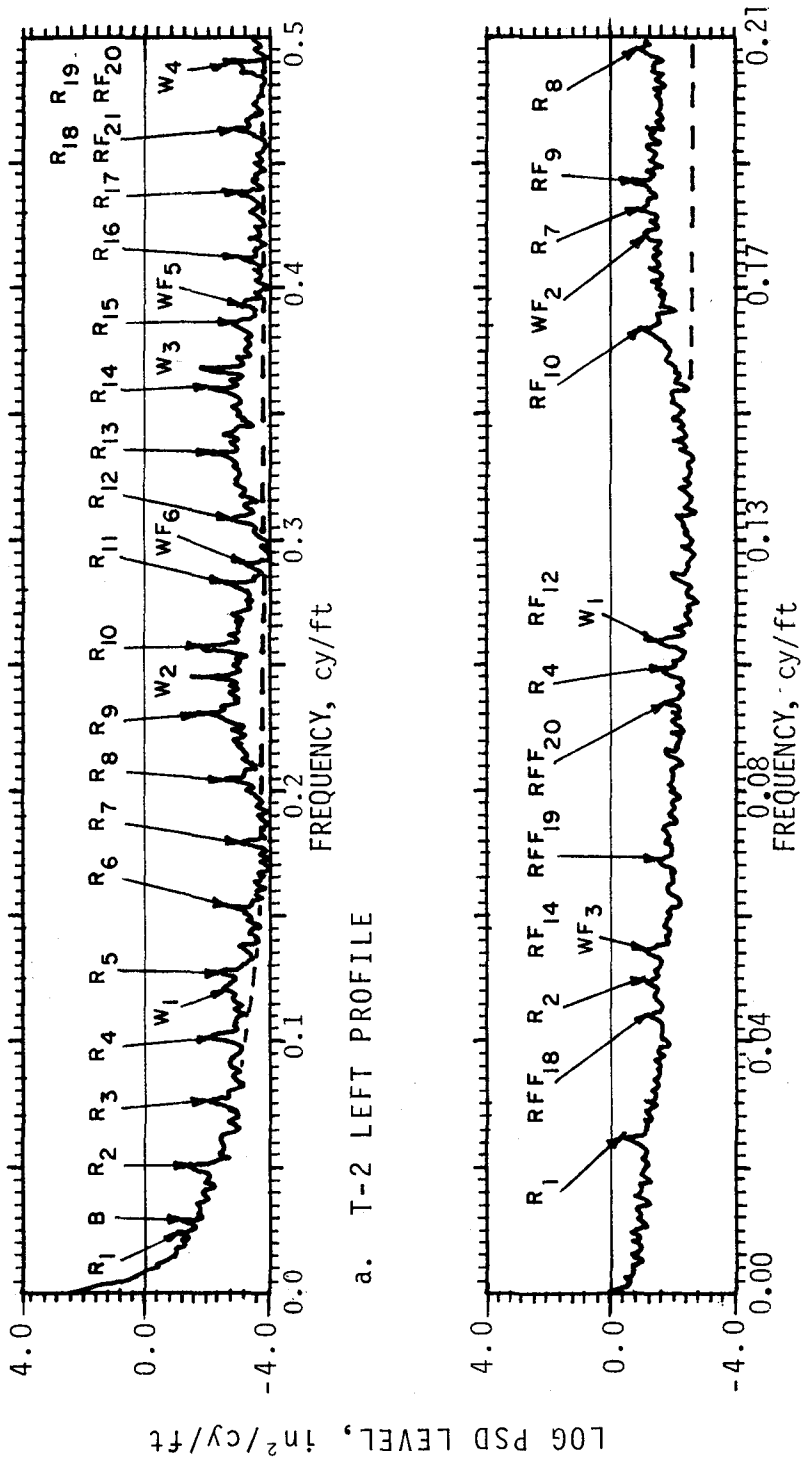

LEGEND: R→RAIL LENGTH; B→BALLAST MEMORY; W→WHEEL CIRCUMFERENCE;
F→FOLDED COMPONENT; ---- EXPECTED CONTINUUM

FIGURE 43. NOISE IN PROFILE AND GAGE

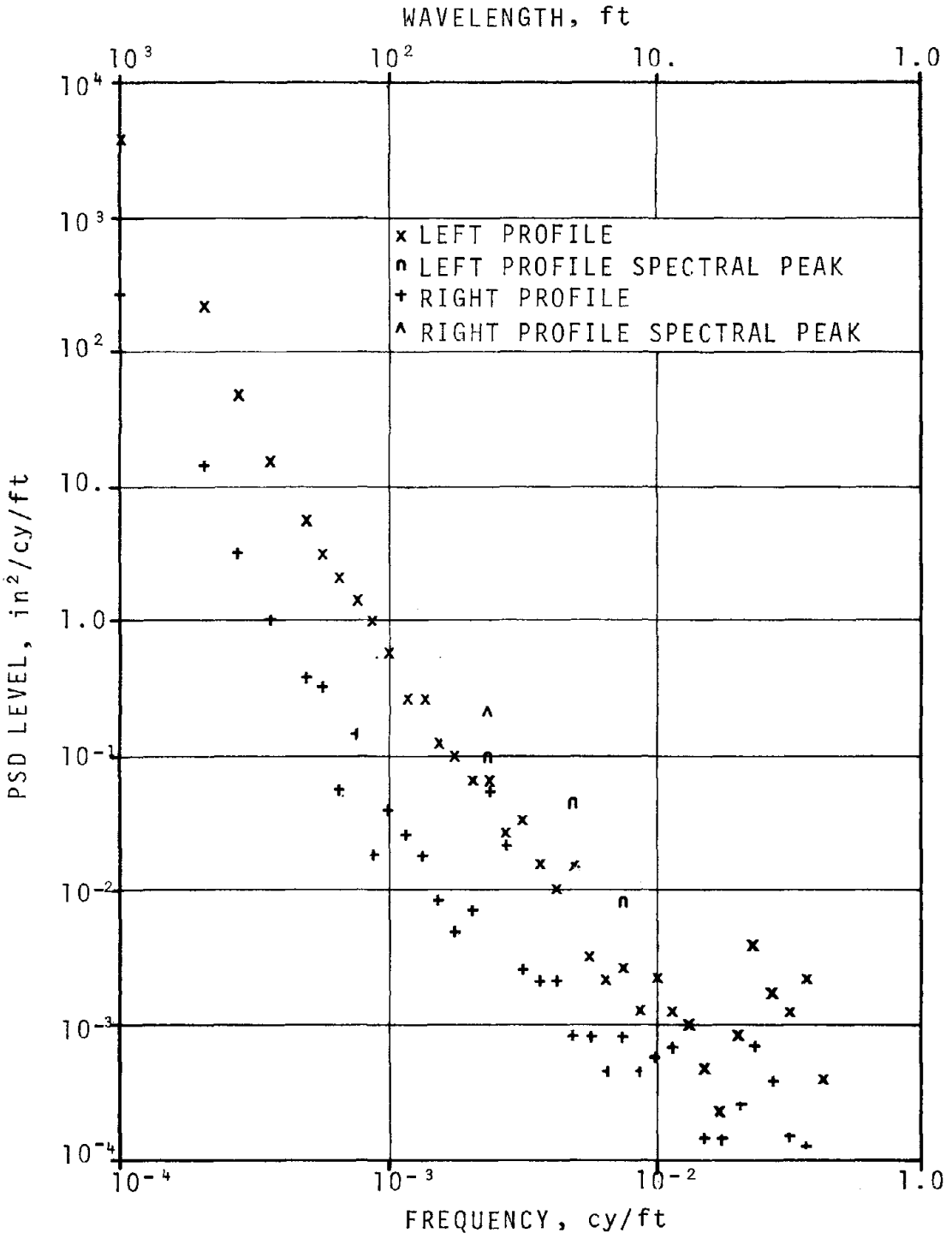

FIGURE 44. T-2 PSD's FOR RIGHT AND LEFT PROFILE

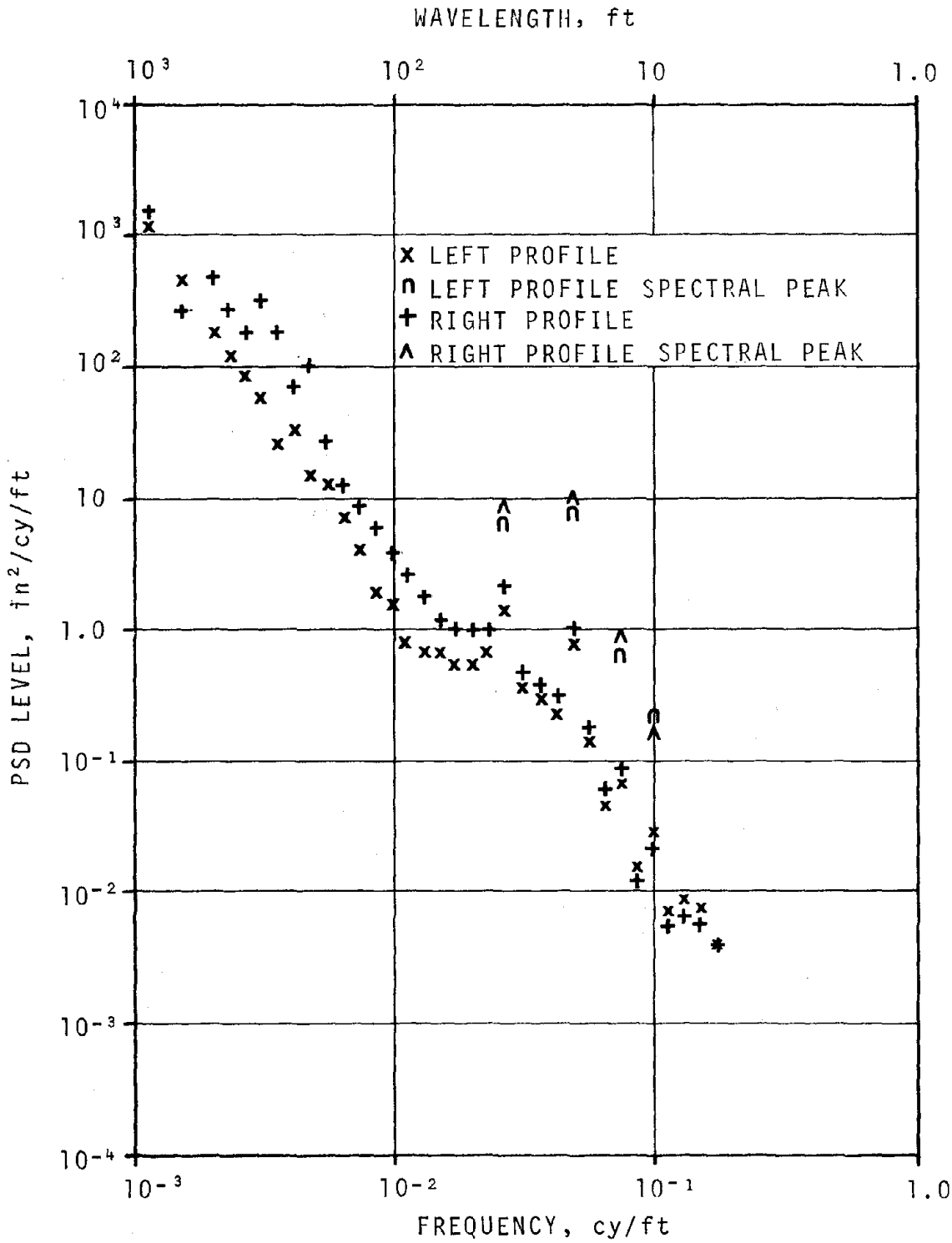

FIGURE 45. T-3 PSD's FOR RIGHT AND LEFT PROFILE

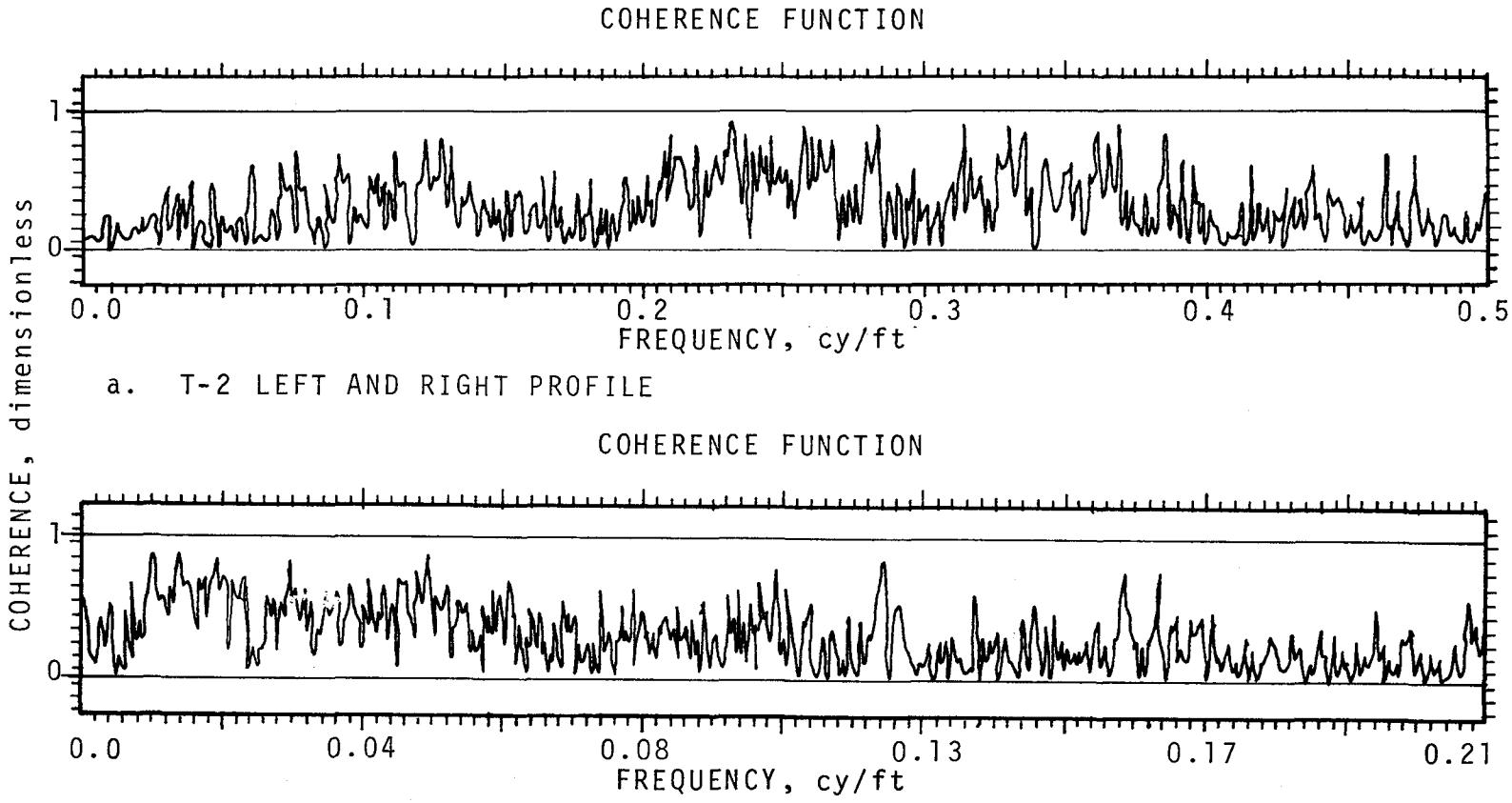

FIGURE 46. COHERENCES BETWEEN LEFT AND RIGHT PROFILOMETERS

wavelength of 120 feet (0.008 cy/ft) where it drops off sharply.

3.1.6 PSD PROCESSING AND INTERPRETATION ERRORS

The crux of PSD processing packages is an efficient (fast) realization of the Discrete Fourier Transform (DFT). Therefore it is critical that the user be aware of the theory of the DFT so that processing and interpretation errors do not abound. One characteristic of the DFT is discreteness in both the time domain *and* the frequency domain. The DFT takes *sampled temporal data* and converts it into *sampled frequency data*. Consequently:

- Frequency components fold over. If X is the distance between samples in feet, there exists a folding frequency, ϕ_c (cy/ft) given by $\phi_c = (2X)^{-1}$. A frequency component, ϕ, in the original data is reinterpreted as ϕ' as follows:

$$\phi' = |\text{Mod}[\phi + \phi_c, 2\phi_c] - \phi_c|.$$

- The DFT operates on N consecutive samples of the data at any one time. It treats those samples as though they repeat themselves every N samples.

A number of precautionary measures and data interpretation techniques have been developed to avoid the peculiarities of sampled data and the DFT. These include:

- Anti-Alias filtering.
- Prewhitening.

- Methods of handling periodic components and PDP's that are incommensurate.*

These techniques are described in the paragraphs that follow.

3.1.6.1 Anti-Alias Filtering

As a result of the folding of frequency components by the DFT, frequencies are reinterpreted according to the following scheme:

$$\phi' = |\text{Mod}[\phi + \phi_c, 2\phi_c] - \phi_c|.$$

Only frequencies in the range ($0 \leq \phi \leq \phi_c$) are not assigned new values. All others are aliased into the range ($0 \leq \phi \leq \phi_c$)'. Examples of folded periodic components are shown in Figure 43.

This error can be corrected by anti-alias filtering of the data while it is still in analog form, using low-pass filtering to suppress all frequencies over ϕ_c. Adequate anti-alias filtering is considered to take place if the signal PSD rolls off at ϕ^{-2} or better at folding. Track geometry PSD's naturally roll off at this rate without filtering provided they are not contaminated by noise or by strong PDP's. Accordingly, anti-alias filtering of track geometry data is an absolute necessity only when instrumentation noise problems are severe.

3.1.6.2 Prewhitening

Prewhitening requires an advance guess of the form of the PSD. It consists of processing the data through a time domain digital filter whose power response approximates the inverse of the

*An incommensurate periodic component is one which *does not* repeat itself an integer number of times in N samples.

PSD. The outputs of the filtering are data whose spectrum is relatively flat. Compensation for the prewhitening is accomplished by frequency domain post-coloring.

The advantages of prewhitening are:

- It removes long wavelength trends from the data.
- It provides spectral estimators that are not biased by frequency spectrum trends.
- It makes better use of the computational dynamic range of the DFT.
- For Gaussian or near-Gaussian random input, each PSD ordinate is distributed as χ^2 with two (2) degrees of freedom and is independent of every other ordinate.

Certain kinds of data must be detrended, either directly or through proper prewhitening operations. Otherwise long wavelength trends are truncated and treated as part of a repetitive noise with period, NX. The PSD of this superimposed signal easily swamps the PSD of the real fluctuations. Examples are profile and alignment space curves. Failure to remove the long wavelength trends has the consequences shown in the PSD of Figure 47.

On the other hand, some caution must be exercised in using prewhitening and an example of applying inappropriate prewhitening is shown in Figure 48. Here effective utilization of the DFT dynamic range has not been achieved, and the computation noise floor can be seen in the plots.

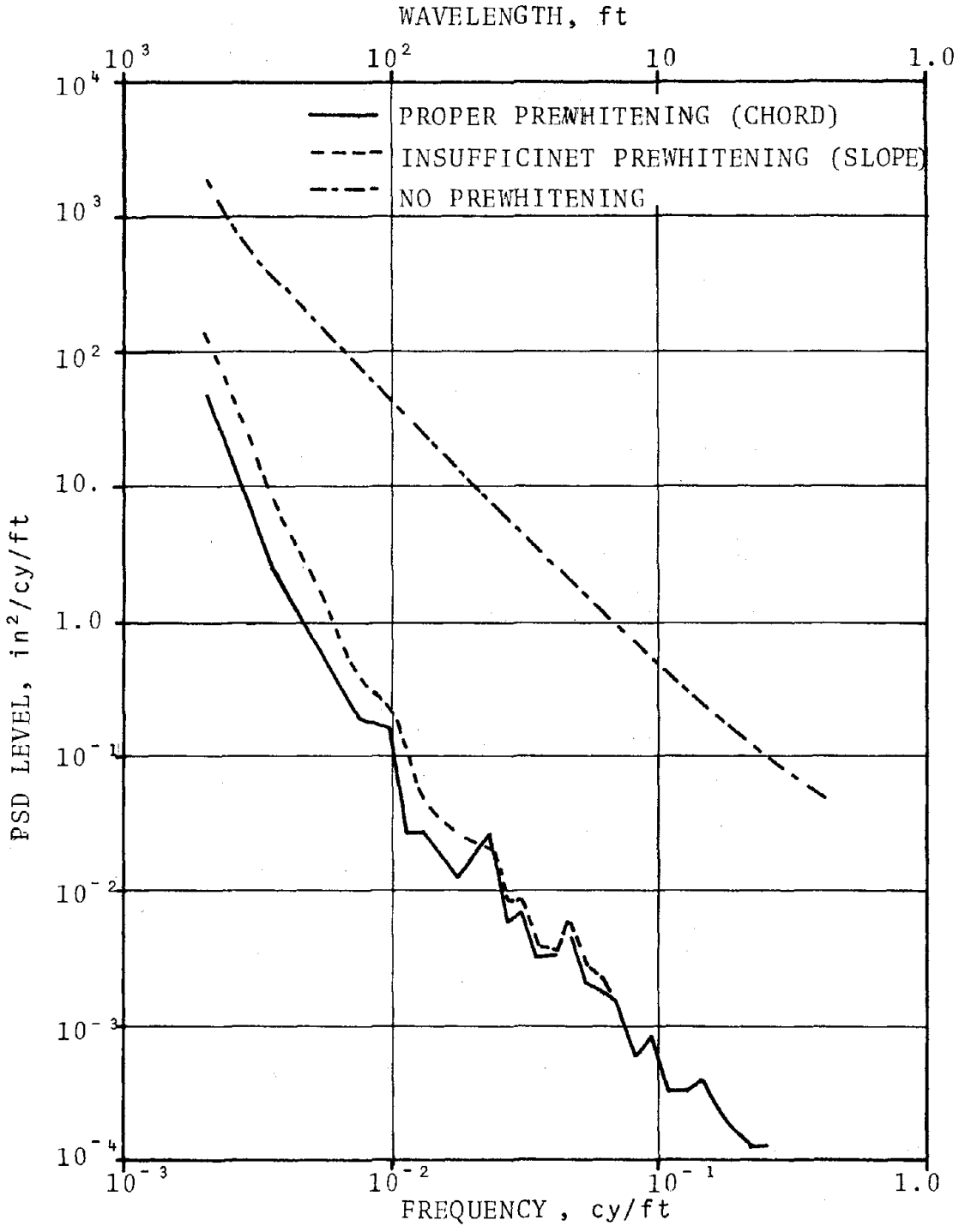

FIGURE 47. PSD OF PROFILE/ALIGNMENT TYPE SPECTRA SHOWING EFFECTS OF INSUFFICIENT AND PROPER PREWHITENING

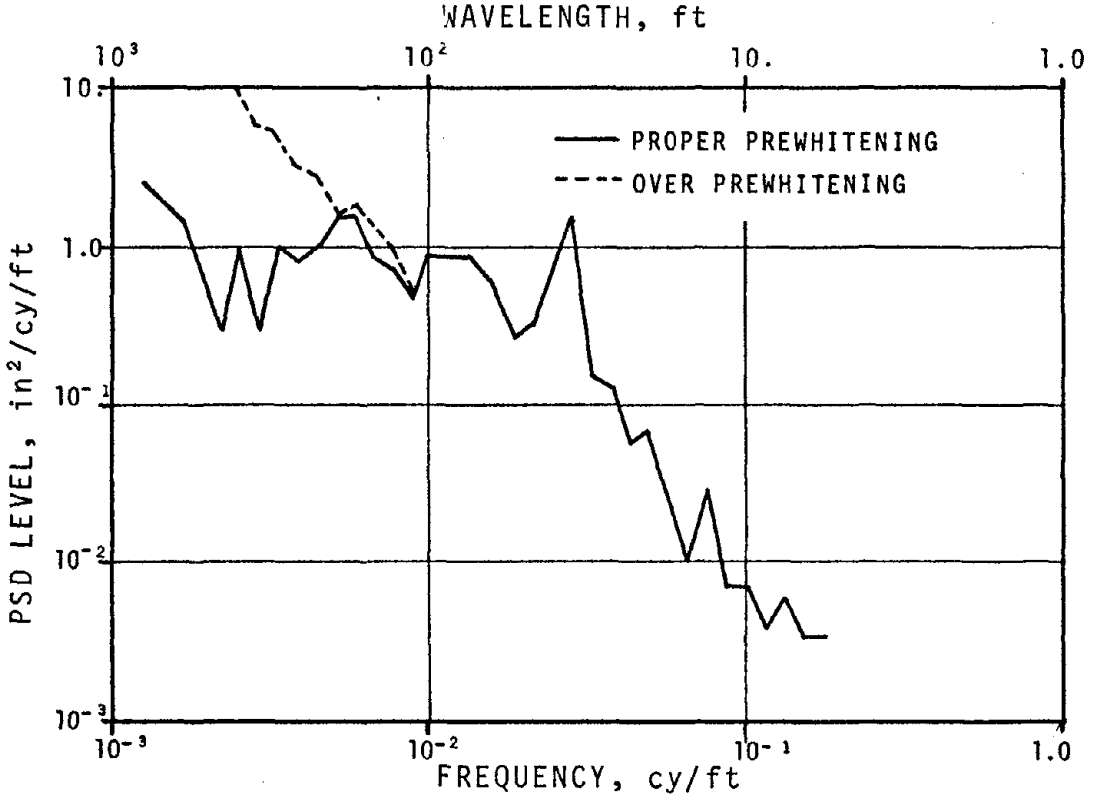

FIGURE 48. CROSSLEVEL/GAGE TYPE SPECTRA SHOWING THE EFFECTS OF PROPER AND OVER PREWHITENING

3.1.6.3 Incommensurate Periodicities

An incommensurate periodicity is one that does not repeat itself an integer number of times in the N samples windowed by the DFT. The DFT treats the sequence of N data points as though it repeats itself cyclically every N samples. Commensurate periodic components join perfectly in this cyclic operation, while incommensurate components experience a jump discontinuity or kink where end points are joined. As a result, the expected line component is smeared out and its peak value may be attenuated by a factor up to $(2/\pi)^2 \cong 0.405$.

The phenomenon itself is illustrated in Figure 49. This figure shows two PDP's whose wavelengths are 32 samples and 39

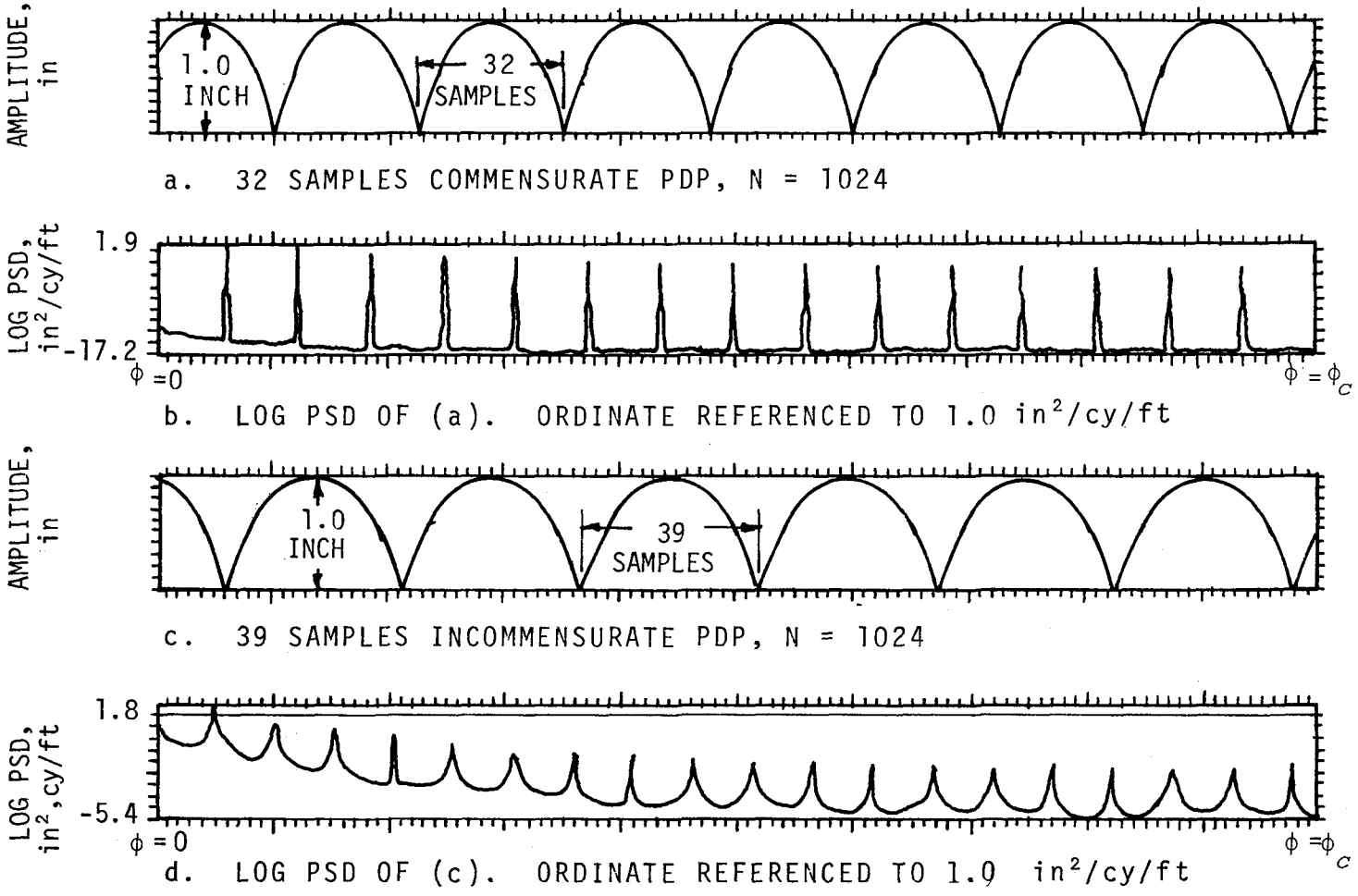

FIGURE 49. COMPARISON OF PSD'S FOR COMMENSURATE AND INCOMMENSURATE PSD's

samples, respectively. Using a DFT with N = 1024, the 32-sample waveform is commensurate, and the 39-sample waveform is not. The PSD associated with the former shows well-defined peaks, while the PSD associated with the latter exhibits considerable broadening of the spectral line and a high computational noise floor.

The usual procedure for eliminating this error is to apply a Hamming window to the time series data.[7] This works well provided the periodic processes are rigorously periodic. In track geometry, the PDP cadence is frequently interrupted by rails of unusual length. Therefore window shaping will not be a totally effective solution.

Window shaping operations also have deleterious effects on the distribution properties of SRP spectral ordinates. After window shaping, they are approximately χ^2 distributed, with fewer than two degrees of freedom. They are no longer statistically independent of one another.[15]

3.1.7 CONCLUSIONS ON MEASUREMENT SYSTEM ERRORS

The following conclusions were reached relative to the track geometry instruments on the FRA track survey cars:

- The best noise floor for gage is found on T-6 which uses a common beam system to support both gage sensors. T-2 and T-3 use independent mounts and relative motion of these is possible. This introduces substantial system noise at wavelengths less than 20 feet and at speeds greater than 50 mph.

---

[15] M. G. Kendall and J. Stuart, *The Advanced Theory of Statistics*, Vol. III, Ch. 49, "Spectrum Theory," Charles Griffin, London, 1968, p. 454, 469.

- The crosslevel systems on T-2, T-3 and T-6 are nearly identical. But performance at wavelengths less than 10 feet is best on that system which has the least wheel roughness and the least wheelset conicity.

- Inertial measurement of profile has a better noise floor than the obsolete 14.5-foot MCO even in the range of wavelengths from 10 to 100 feet.

- Valid inertial profile data at wavelengths less than 10 feet depends on wheel roughness. Valid inertial profile data at wavelengths greater than 100 feet depends on integrator noise floor.

- The T-6 profilometer provides the best performance. Unlike T-2 and T-3 profilometers, it does not electronically high-pass the accelerometer signal, and after digital filtering, it gives a correctly phased output signal. It is also corrected for gravitational effects induced by crosslevel variations.

- An inertial alignment system was not available to support this effort. The only available alignment data was produced by the 14.5-foot MCO, which has a high noise floor and restricted wavelength range.

A quantitative evaluation of the overall capabilities of the FRA track survey vehicles is given in Table 4.

3.2 ANALYTICAL REPRESENTATIONS OF PSD's

3.2.1 OLDER MODELS

The status of PSD models at the start of this research effort is described in Appendix G. They were derived from data that, in many cases, lacked both dynamic range and broad frequency coverage.

Only a scattering of cross power spectral densities (X-PSD's) or coherence functions were reported in the literature. The common belief that mean profile and crosslevel SRP's are uncorrelated

was promoted by Gilchrist.[16] The current research has strengthened and broadened this conclusion by demonstrating the general statistical independent of the SRP's associated with the main dynamic inputs (mean profile, mean alignment and cross level).

Over the years, a small but select number of PSD's have been generated from geometry data collected by the FRA track survey cars. These were assembled and graphically summarized in order to establish a base with which current PSD processing could be compared. These PSD's are discussed and shown in Appendix D, Section D.2. A brief summary of this PSD data including the methods used to measure the track geometry, general geographical location of the surveys, track classes involved, and other pertinent information is provided in Table 12.

As mentioned above, the earlier PSD's are rather restricted with respect to frequency and dynamic range. Furthermore, some trends present in them may have resulted from processing errors. To verify the validity of these earlier PSD's, the initial efforts of the current study were concentrated on expanding the frequency range.

The procedure to obtain extremely long wavelength information was described earlier in Paragraph 2.5.1. In addition, some data on extremely short wavelengths was available in the form of 1/3-octave rms representations of accelerometer output.[10] The short wavelength data were converted to PSD levels, and the results are presented in Appendix D, Section D.1. Both the extremely long and the extremely short representations display

---

[16] A. O. Gilchrist, "A Report on Some Power Spectral Measurements of Vertical Rail Irregularities," Technical Note DYN/8, August 1965, British Railways Research Department, Derby, England.

TABLE 12. SYNOPSIS OF OLDER PSD DATA SELECTED FOR PROCESSING

	British Rail	ENSCO 1971	ENSCO 1973	SNCF
Mean Profile	Manual Survey	-	-	Mauzin Chord
Individual Rail Profile	-	14.5' MCO	14.5' MCO	-
Mean Alignment	Manual Survey	-	-	Mauzin Chord
Individual Rail Alignment	-	14.5' MCO	-	-
Crosslevel	Manual Survey	Self-Erecting Gyro	-	-
Gage	-	Capacitive	Capacitive	-
Broken Down by Track Class	Class 4 & Better Main Line CWR	Class 5,4,3,	Class Super 6,5,4,3,2	See Titles
Territory Covered	Great Britian	Northeast (NE) Area	New Construction NE Area, Chicago Pittsburgh,Florida	France
Number of PSD Diagrams	3 (D-1 thru D-3)	12 (D-4 thru D-15)	10 (D-16 thru D-25)	2 (D-26 and D-27)
Number of PSD's per Range Diagram	12	3 (average)	3 (average)	
Typical Length of Data/PSD	Unknown	3 mi. (average)	3 mi. (average)	1-2 km
Resolution of Peaks	Unknown	0.05 Decade	0.05 Decade	Unknown

continuity and overlap the trends established by the older intermediate wavelength PSD's. This is shown in Figure 50.

3.2.2 NEW ANALYTICAL MODELS FOR PSD's

Initially PSD models that had been developed during earlier research were used. However, the range of wavelengths in the PSD's generated in the current research was much greater than in the older PSD's, and it became evident that many additional corner frequencies were needed. Accordingly, a second model was developed that incorporated observed long wavelength behavior and a third model was developed later to accommodate the short wavelengths. The evolution of profile SRP-PSD models is outlined in Table 13.

The first model had been developed using profile data from the 14.5-foot MCO. Because of its chordal response, the bandpass of this data was limited to wavelengths in the 10-foot to 100-foot range. Salient features of the model are:

- A single break frequency, ϕ_{14} , corresponding to a wavelength of 20 feet.
- λ^4 , or Type 3 random walk for wavelengths shorter than λ_{14} ;
- λ^2 , or Type 2 random walk for wavelengths longer than λ_{14}.

Note that the long wavelength behavior is unbounded. In order to simulate bounded SRP space curves, it is necessary to limit long wavelength deviations. Hence a fictitious break frequency, ϕ_{11}, was introduced.

In developing the second and third continuum models, it was observed that the two break frequencies, ϕ_{11} and ϕ_{12}, are well outside of the range of dynamic interest and reliable observation.

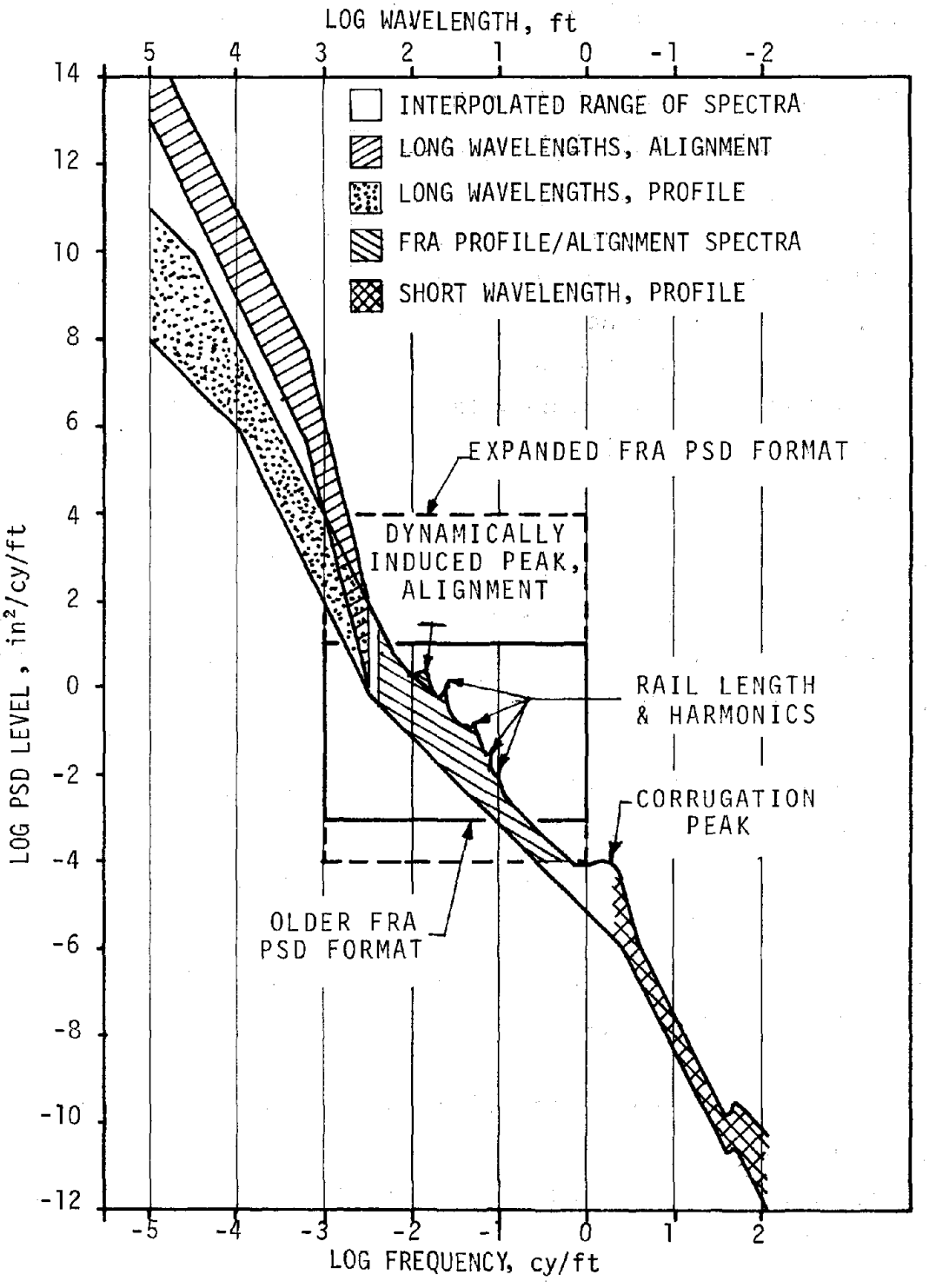

FIGURE 50. COMPOSITE OF PROFILE AND ALIGNMENT SPECTRA DRAWN FROM A VARIETY OF SOURCES

TABLE 13. PSD MODELS FOR INDIVIDUAL RAIL PROFILE SRP

First SRP Profile Model

$$S_1(\phi) = \frac{A_1 \phi_{14}^2}{(\phi^2 + \phi_{11}^2)(\phi^2 + \phi_{14}^2)} \cong \frac{A_1 \phi_{14}^2}{\phi^2(\phi^2 + \phi_{14}^2)}$$

$\phi_{11} << 10^{-3}$ cy/ft (used to limit dynamic range)

$\phi_{14} = \lambda_{14}^{-1}$, $\lambda_{14} \cong 25$ ft.

Second SRP Profile PSD Model, expanded to include extremely long wavelength behavior

$$S_1(\phi) = \frac{A_1(\phi^2 + \phi_{13}^2)\phi_{14}^2}{(\phi^2 + \phi_{11}^2)(\phi^2 + \phi_{12}^2)(\phi^2 + \phi_{14}^2)} \cong \frac{A_1(\phi^2 + \phi_{13}^2)\phi_{14}^2}{\phi^4(\phi^2 + \phi_{14}^2)}$$

ϕ_{11} , ϕ_{12} are outside of range of interest ($<<10^{-3}$ cy/ft).

$\phi_{13} = \lambda_{13}^{-1}$, $\lambda_{13} = 140$ ft.

Final SRP Profile PSD Model expanded to include short wavelength behavior

$$S_1(\phi) = \frac{A_1(\phi^2 + \phi_{13}^2)(\phi^2 + \phi_{15}^2)\phi_{14}^2}{(\phi^2 + \phi_{11}^2)(\phi^2 + \phi_{12}^2)(\phi^2 + \phi_{14}^2)(\phi^2 + \phi_{16}^2)}$$

$$\cong \frac{A_1(\phi^2 + \phi_{13}^2)(\phi^2 + \phi_{15}^2)\phi_{14}^2}{\phi^4(\phi^2 + \phi_{14}^2)(\phi^2 + \phi_{16}^2)}$$

$\phi_{15} = \lambda_{15}^{-1}$ $\quad$ $\lambda_{15} \sim 5 - 10$ ft.

$\phi_{16} = \lambda_{16}^{-1}$ $\quad$ $\lambda_{16} \cong 1$ ft.

Usually they are ignored, or they are allowed to approach zero in the course of analysis.

3.2.3 ANALYTICAL REPRESENTATIONS OF X-PSD'S AND COHERENCES

Modeling efforts for X-PSD's and coherence functions proceeded on the basis of the following information obtained from anomaly-free tangent track data:

- In the SRP for tangent track, the four track geometry variables, mean profile, mean alignment, gage and crosslevel, appear to be completely uncorrelated. With a sufficiently large number of stackings, all X-PSD's and coherences tend toward zero.
- Any coherence that may exist between mean profile and crosslevel is attributable to a non-zero mean and/or random joint amplitude.

On the basis of this information, models for X-PSD's, and coherence functions for all combinations of mean profile, individual rail profile, and crosslevel were derived. These are given in Table 14, together with the individual rail profile PSD's.

3.2.4 STATISTICAL DISTRIBUTION OF SPECTRAL ESTIMATORS

The spectral models listed in Tables 1 and 2 define an explicit list of parameters that apply to the SRP. These include:

- An overall roughness amplitude, A_m, where m = 1, 2, 3,...8 corresponding to the track geometry variable being examined.
- A number of transition frequencies, ϕ_{mn}

The A_m values in Tables 1 and 2 define the ordinates where the asymptotic -2 slope between ϕ_{m_3} and ϕ_{m_4} intersects the

TABLE 14. SUMMARY OF PSD'S, CROSS PSD'S AND COHERENCE FUNCTIONS FOR STATIONARY RANDOM PROCESS IN SURFACE PARAMETERS

	y_1	y_2	y_3	y_4
y_1	$\cong \dfrac{A_1\phi_{14}^2(\phi^2+\phi_{13}^2)}{\phi^4(\phi^2+\phi_{14}^2)}$	$\dfrac{A_9\phi_{94}^2(\phi^2+\phi_{93}^2)}{\phi^4(\phi^2+\phi_{94}^2)}$	$\dfrac{A_3\phi_{34}^2(\phi^2+\phi_{33}^2)}{\phi^4(\phi^2+\phi_{34}^2)}$	$= \dfrac{\frac{1}{2}A_4\phi_{44}^2}{(\phi^2+\hat{\phi}_{43}^2)(\phi^2+\phi_{44}^2)}$
y_2	$\dfrac{\phi_{13}^2\phi_{94}^2(\phi^2+\phi_{14}^2)(\phi^2+\phi_{93}^2)}{\phi_{14}^2\phi_{93}^2(\phi^2+\phi_{13}^2)(\phi^2+\phi_{94}^2)}$	$\dfrac{A_1\phi_{14}^2(\phi^2+\phi_{13}^2)}{\phi^4(\phi^2+\phi_{14}^2)}$	$\dfrac{A_3\phi_{34}^2(\phi^2+\phi_{33}^2)}{\phi^4(\phi^2+\phi_{34}^2)}$	$= \dfrac{-\frac{1}{2}A_4\phi_{44}^2}{(\phi^2+\hat{\phi}_{43}^2)(\phi^2+\phi_{44}^2)}$
y_3	$\left[\dfrac{\phi_{13}^2\phi_{34}^2(\phi^2+\phi_{14}^2)(\phi^2+\phi_{33}^2)}{\phi_{14}^2\phi_{33}^2(\phi^2+\phi_{13}^2)(\phi^2+\phi_{34}^2)}\right]^{\frac{1}{2}}$		$\equiv \dfrac{A_3\phi_{34}^2(\phi^2+\phi_{33}^2)}{\phi^4(\phi^2+\phi_{34}^2)}$	0
y_4	$\left[\dfrac{\lvert\phi_{14}^2\phi_{93}^2-\phi_{13}^2\phi_{14}^2\rvert(\phi^2+\phi_{14}^2)\phi^4}{\phi_{14}^2\phi_{93}^2(\phi^2+\phi_{13}^2)(\phi^2+\hat{\phi}_{43}^2)(\phi^2+\phi_{44}^2)}\right]^{\frac{1}{2}}$	0		$= \dfrac{A_4\phi_{44}^2}{(\phi^2+\hat{\phi}_{43}^2)(\phi^2+\phi_{44}^2)}$

Parameters defined as follows:

$A_1 \equiv A_2 = A_3 + \frac{1}{4}A_4$; $\phi_{14}^2 = [A_3\phi_{34}^2 + \frac{1}{4}A_4\phi_{44}^2]/A_1$; $\phi_{13}^2 = A_3\phi_{33}^2/A_1$

$A_9 = A_3 - \frac{1}{4}A_4$: $\phi_{94}^2 = [A_3\phi_{34}^2 - \frac{1}{4}A_4\phi_{44}^2]/A_9$: $\phi_{93}^2 = A_3\phi_{33}^2/A_9$

For Alignment on Tangent Track: $A_1 \rightarrow A_5 \equiv A_6$; $A_3 \rightarrow A_7$; $A_4 \rightarrow A_9$

ϕ = 1.0 cy/ft abscissa. Other roughnesses, $A_m(n)$, are now defined such that $A_m(n)$ is the roughness ordinate where the straight line segment between frequencies ϕ_{mn} and $\phi_{m,n+1}$ intersects the ϕ = 1 cy/ft abscissa. The roughnesses of a given continuum are interrelated by

$$A_m(n-1) = A_m(n)\ \phi_{mn}^{\pm 2},$$

where the $\pm$ applies to an increase/decrease in power law across ϕ_{mn}.

In practice, the $A_m(n)$ and the ϕ_{mn} are estimated from the continuum portion of a PSD. This means they are themselves distributed random variables. If the SRP geometry data is passed through the appropriate prewhitener and converted to a PSD, each spectral ordinate will be χ^2 distributed with 2 degrees of freedom. As such, each ordinate will have a standard error that is equal to its expected value.

This disturbing condition can be remedied in two ways:

- Stacking spectra from consecutive segments of track having stationary statistics;
- Using spectral smoothing or fitting techniques to average over adjacent spectral bands.

The $A_m(n)$ are effectively averages of the independent spectral ordinates lying between ϕ_{mn} and $\phi_{m,n+1}$. Therefore, they are χ^2 distributed with $N_m(n)$ degrees of freedom where:

$$N(n) = 2\ (\phi_{mn} - \phi_{m,n-1})L,$$

and where L is the duration of the spectral stacking.

Assuming that data is sampled every foot, that 10^3 feet of data are used per PSD, and that five stackings (~1 mile) are used, the resultant degrees of freedom, $N(n)$, and the ratio of standard error to expected value for the $A(n)$ are given in Table 15. For the χ^2 distribution, this ratio is given by:

$$\frac{\{\mathrm{Var}[A_m(n)]\}^{\frac{1}{2}}}{E[A_m(n)]} = \frac{1}{\sqrt{\frac{1}{2}N(n)}} \quad .$$

Rearranging the formulation given above, it is seen that:

$$\phi^2_{mn} = \left(\frac{A_m(n-1)}{A_m(n)}\right) \pm 1$$

In other words, ϕ^2_{mn} is the ratio of two χ^2 distributed random variables of $N_m(n)$ degrees of freedom, respectively. The distribution associated with ϕ^2_{mn} is known as a Fisher Type 1, or F-distribution.[17] The ratio of standard error of ϕ^2_{mn} to expected value of ϕ^2_{mn} is given by:

$$\frac{\{\mathrm{Var}[\phi^2_{mn}]\}^{\frac{1}{2}}}{E[\phi^2_{mn}]} = \left\{\frac{2(N_1 + N_2 - 2)}{N_1(N_2 - 4)}\right\}^{\frac{1}{2}} ,$$

with

N_1 = Degrees of freedom of numerator
N_2 = Degrees of freedom of denominator

Note that N_2 must be greater than 4 for this ratio to exist. In Table 15, all values of $N(n)$ are sufficiently greater than

---

[17] M. G. Kendall and J. Stuart, The Advanced Theory of Statistics, Vol. I, Ch. 16, "Distributions Associated with the Normal," Charles Griffin, London, 1968.

TABLE 15. DEGREES OF FREEDOM AND UNCERTAINTY RATIOS FOR SRP ROUGHNESS PARAMETERS (ASSUMED: 1 MILE OF 1 FT SAMPLED DATA)

		Longest Wavelength of Range, n	Shortest Wavelength of Range, n	Power Law for Continuum	$N(n)$ Degrees of Feedom of $A_m(n)$	Standard Error $A_m(n)$ / Expected Value $A_m(n)$
P	0	∞	λ_{11}	0	-	-
R	1	λ_{11}	~10,000 ft	-2	-	-
O	2	~10,000 ft	140 ft	-4	60[b]	0.18
F	3	140 ft	25 ft	-2	280[a]	0.08
I	4	25 ft	10 ft	-4	500[a]	0.06
L	5	5 ft	1 ft	-2	-	-
E	6	1 ft	0.02 ft	-4	-	-
A	0		~5,000 ft	-4	-	-
L'	1	~5,000 ft	400 ft	-6	-	-
G	2	400 ft	100 ft	-4	50	0.20
N	3	100 ft	18 fy	-2	400[a,c]	0.07
M'	4	18 ft	10 ft	-4	300[a,c]	0.08
N	5	5 ft	1 ft	-2	-	-
T	6	1 ft	0.02 ft	-4	-	-
	0-2	∞	140 ft	0	60[b,d]	0.18
X	3	140 ft	18 ft	-2	400[b]	0.07
L	4	18 ft	10 ft	-4	360[a]	0.07
E	5	5 ft	1 ft	-2	-	-
V	6	1 ft	0.02 ft	-4	-	-
	0-2	∞	110 ft	0	70[b,c,d]	0.17
G	3	110 ft	14 ft	-2	500[a,c]	0.06
A	4	14 ft	10 ft	-4	225	0.09
G	5	5 ft	0.5 ft	-2	-	-
E	6	0.5 ft	0.02 ft	-4	-	-

[a] Computed for deleting PDP lines (40 degrees of freedom per PDP spectral line)
[b] Wavelengths over 1000 ft ignored.
[c] Wavelengths between 80 and 125 ft ignored.
[d] Effective corner frequency ϕ_{43} and ϕ_{83}, used.

unity that the above expression simplifies to an expression that is symmetrical in N_1 and N_2. Hence:

$$\frac{\{\mathrm{Var}[\phi^2_{mn}]\}^{\frac{1}{2}}}{E[\phi^2_{mn}]} \cong \left\{\frac{2}{N(n)} + \frac{2}{N(n-1)}\right\}^{\frac{1}{2}},$$

or,

$$\frac{\{\mathrm{Var}[\phi_{mn}]\}^{\frac{1}{2}}}{E[\phi_{mn}]} \cong \left\{\frac{1}{2N(n)} + \frac{1}{2N(n-1)}\right\}^{\frac{1}{2}}.$$

Using values from Table 15, uncertainty ratios were generated for the ϕ_{mn}, and these are displayed in Table 16.

3.2.5 ANALYTICAL HISTOGRAMS

In the course of the work under this task, analytical histograms were derived for the three component processes. Assuming a space curve format and a 50% joint stagger, the histograms shown in Figure 51 were obtained. The exponential joint model described in Paragraph 2.3 was used for the PDP and for random joint amplitudes. A normal distribution of the amplitudes was assumed for the latter.

TABLE 16. UNCERTAINTY RATIOS FOR SRP CORNER FREQUENCIES, ϕ_{mn}

n ↓	Parameter→ m →	Profile 1	Crosslevel 4	Alignment 5	Gage 8
3	$N_m(2)$	60	60	50	70
	$N_m(3)$	280	400	400	500
	Uncertainty	0.10	0.10	0.11	0.09
4	$N_m(3)$	280	400	400	500
	$N_m(4)$	500	360	300	225
	Uncertainty	0.05	0.05	0.05	0.05

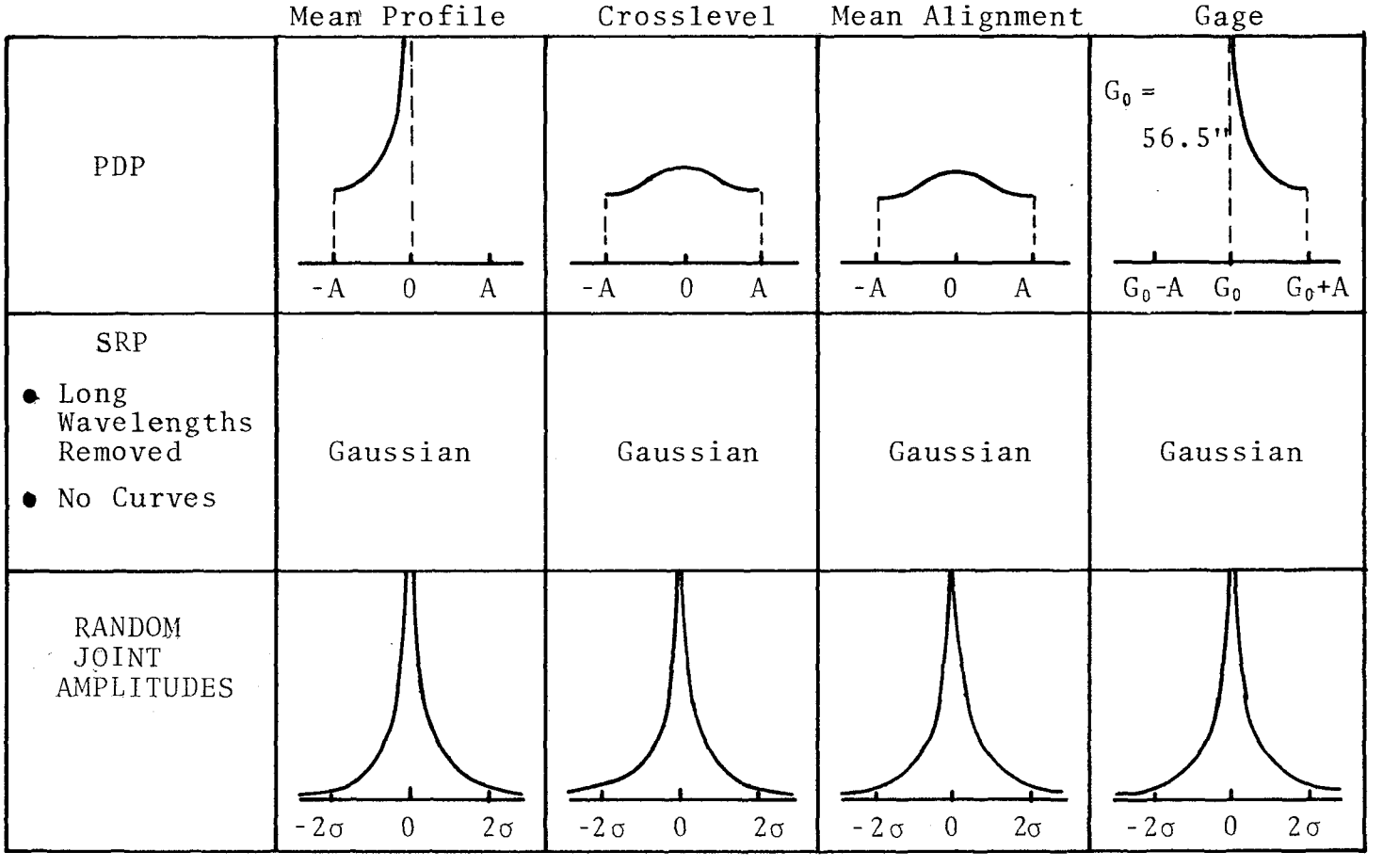

FIGURE 51. SPACE CURVE HISTOGRAMS FOR THE COMPONENT PROCESSES

3.3 FORMULATION AND TESTING OF HYPOTHESES

Five formal hypotheses were identified as pertinent to this effort. Formal statements of these and their proofs are provided in the following paragraphs.

3.3.1 FIRST HYPOTHESIS: NECESSARY PROCESSES

The first hypothesis is stated as follows:

> There are at least three component processes in anomaly-free railway track. These are: (1) a Stationary Random Process (SRP); (2) a Periodic Deterministic Process (PDP) that results from periodically spaced joints having a non-zero mean amplitude, and (3) random fluctuations in the amplitudes of the periodically spaced joints. These are encompassed in an all inclusive, Periodically Modulated Random Process,(PMRP), one whose means, covariances and higher order moments vary periodically at the same rate as the rail periodicity.

The existence of processes (1) and (2) are generally acknowledged as discussed in Appendix G and in previous work leading to the current research.[18,19] Less understood is the third process which was discovered by time series analysis techniques[20] and whose general existence can be demonstrated by application of the following procedure:

---

[18] J. C. Corbin and T-L. Yang, "Application of Guideway Roughness Power Spectral Density as a Management Tool," American Society of Mechanical Engineers Report 73-1CT-144, June 1973.

[19] J. C. Corbin and W. M. Kaufman, "Classifying Track by Power Spectral Density," in "Mechanics of Transportation Suspension Systems," Winter Annual Meeting, ASME, Houston, December 1975.

[20] J. C. Corbin, "Statistical Characerization of Railway Track Behavior," ASME/IEEE, Joint Railroad Conference, Pittsburgh, IEEE Paper No. C74903-31A, April 1974.

1) Prewhiten a rail geometry signal, such as profile.

2) Determine its PSD and look for all PDP peaks.

3) Determine the PDP by stacking at all PDP fundamental intervals indicated by step 2. Divide by the number of stackings to obtain the mean shape in the prewhitened form.

4) Subtract the result of step 3 from the result of step 1. This gives a new prewhitened signal devoid of PDP's.

5) Square the results of step 4 and take the PSD.

6) Examine the PSD for statistically significant peaks at the PDP frequencies.

In exercising this procedure, significant peaks are consistently found at rail length related frequencies proving the existence of a periodically varying second moment. That this is associated with process (3) is amply demonstrated by the procedures outlined in Paragraph 2.3.

3.3.2 SECOND HYPOTHESIS: SUFFICIENT PROCESSES

The second hypothesis is stated as follows:

> The three component processes described in the first hypothesis are sufficient to encompass all anomaly-free geometry behavior found in railway track.

Assuming that the signal classification presented in Paragraph 2.1 is complete, then the only additional process that could exist and which could escape notice is a non-stationary process whose statistics vary indeterministically over the processing intervals that are customarily used for analysis. These are:[21]

---

[21] K. Bradley, et al., "Acquisition and Use of Track Geometry Data in Maintenance-of-Way Planning," Technical Report No. FRA-ORD&D-75-27, March 1975.

- 1000-25,000 feet for PSD's and histograms, and
- at least 5,000 feet for track maintenance indices.

When systematic changes in moment statistics are detected, they are universally attributable to one of the anomalous causes listed in Table 5. Since anomalies are excluded by stipulation, the only process left over is a modulation of an SRP in which the sampled moments of the distribution very randomly and in excess of the levels implied by sampling theory. Unless these random variations can be linked to events in the surroundings making them deterministic (anomalies) such variations require more detailed models than those already considered.

The problem of identifying statistical processes in anomaly-free track is analogous to determining that the output of a random number generator is truly random. The two most powerful tests for randomness are histograms of long versus short sequences, and spectral tests. It has already been shown that spectral tests are quite instrumental in detecting periodic modulations of the SRP. This has been appropriately identified as a separate component process that is associated with the rail length. Once removed, systematic variations are no longer observed.

3.3.3 THIRD HYPOTHESIS: THE SRP IS A MARKOV PROCESS

The third hypothesis is stated as follows:

> The SRP in railway track geometry is a stationary Markov process.

A Markov process is defined as an evolutionary process, one in which a new state vector is completely defined by *one* state vector at a previous time interval, an additive random

vector (white noise) and a transition matrix between the previous state and the present state. The statistics of the Markoff process are completely embodied in the transition matrix which defines the joint probability between any two vectors by a fixed separated time interval. The reader who wishes a further mathematical treatment is referred to Caughey who has authored one of the landmark papers on this subject.[22]

The definition of the Markov process is very reminiscent of the discussions on random walks, linear digital filters, and differo-integral operators given in Section 2. Indeed, the Type 2 random walk fits the definition exactly. This walk is given by

$$y_n = y_{n-1} + h_0 w_n ,$$

so that the placement of a new step is the sum of one old step and a scaled random number.

The type 3 random walk would not appear to fit the definition since a new step is generated from two previous steps:

$$y_n = 2y_{n-1} - y_{n-2} + h_0 w_n .$$

However, by defining an intermediate variable, e_n, given by,

$$e_n = y_{n-1} + h_0 w_n ,$$

this random walk can be rewritten in the vector form:

---

[22]T. K. Caughey, "Derivation and Application of the Fokker-Planck Equation to Discrete Nonlinear Dynamic Systems Subjected to White Random Excitations," *J. Acoust. Soc. Am.* 35, p. 1683-1692, November 1963.

$$\begin{bmatrix} e_n \\ y_n \end{bmatrix} = \begin{bmatrix} 1 & 0 \\ 1 & 1 \end{bmatrix} \times \begin{bmatrix} e_{n-1} \\ y_{n-1} \end{bmatrix} + \begin{bmatrix} h_0 w_n \\ 0 \end{bmatrix}$$

This is true of any digital filter that can be rationalized as described in Paragraph 2.2.2.

3.3.4 FOURTH HYPOTHESIS: THE SRP IS A NORMALLY DISTRIBUTED RANDOM VARIABLE

The fourth hypothesis is stated as follows:

> The SRP in railway track geometry is completely represented by a bivariate normal probability density function.

By virtue of the Markov property of SRP's, track measures such as high-pass space curve, MCO, warp, gage, and crosslevel variations are given as the weighted sum of many consecutive values of w_n. Unless these random numbers are members of an ill-formed distribution (for example, a Cauchy distribution) the central limit theorem states that these measures will be normally distributed. A demonstration of this fact is given in Figure 52 where a simulated SRP space curve is first generated from normally distributed w_n, and then from the same sequence of w_n rectangularly distributed.

3.3.5 FIFTH HYPOTHESIS: PSD FORM OF THE SRP

> Over the dynamically important range of frequencies the PSD of the SRP is analytically represented by the polynomial form given in Tables 1 and 2.

PSD's of railway track geometry are typically generated from more than a mile of data that is assumed to be stationary. For a frequency resolution of 10^{-3} cy/ft, each spectral ordinate will be χ^2 distributed with 15 degrees of freedom. This means that the ratio of standard error to expected value will be 35%.

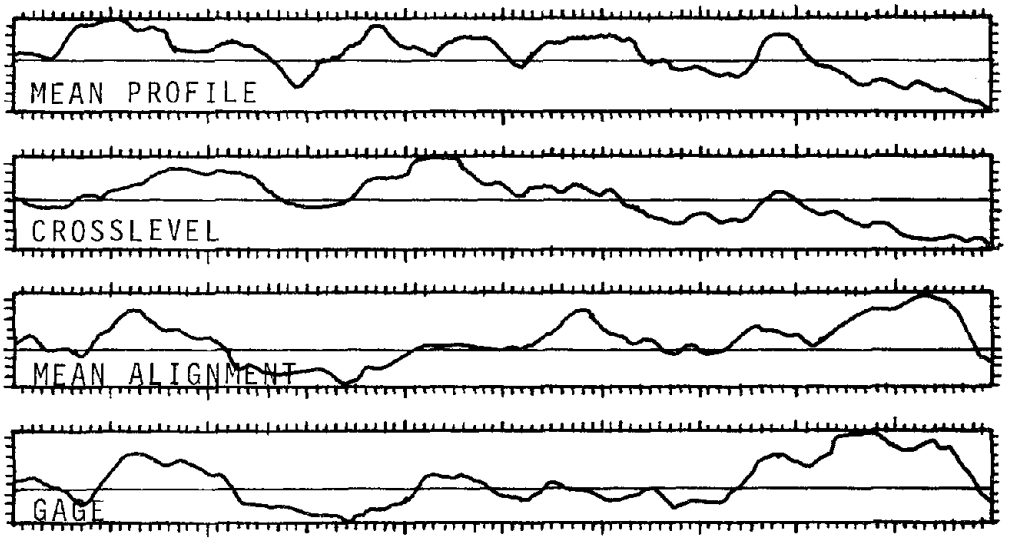

a. GENERATED BY QUASI-NORMAL RANDOM NUMBER GENERATOR

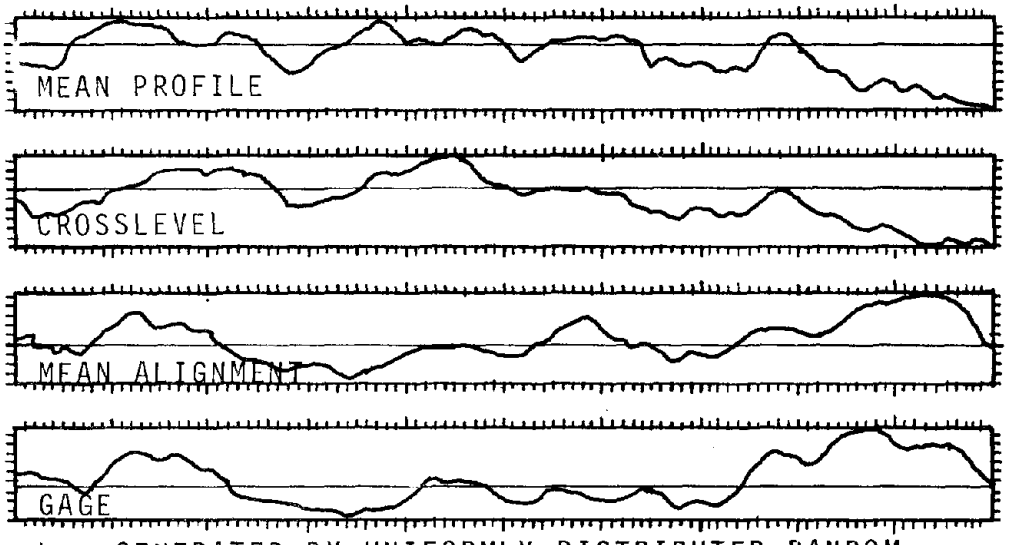

b. GENERATED BY UNIFORMLY DISTRIBUTED RANDOM NUMBER GENERATOR

FIGURE 52. COMPARISON OF SRP GENERATED FROM NORMALLY AND UNIFORMLY DISTRIBUTED RANDOM NUMBER SOURCES

The uncertainty for $A(n)$ estimates given in Table 15 are also computed for 1 mile samples. It is seen that in most frequency bands the best that can be expected for the $A(n)$ is an accuracy in the 5-10% range. When actual curve fits are performed on PSD's using the Table 1 forms, a 70% (2σ) error is rarely observed between individual spectral ordinates and the PSD model. In view of the theoretical uncertainty associated with ordinate fluctuations and the agreement with empirical observation, it appears that the Table 1 and 2 models represent the best estimates of SRP behavior currently available to dynamicists, and that little is gained by developing more detailed models.

3.4 PROCESSING OF DATA

The models developed in Section 3.2 and the methodologies discussed in Section 2 were applied to sections of empirical track geometry records. These data were collected from 29 sections of track representing a broad cross section of U.S. practice, and were processed into PSD's, parametric representations of the component statistical processes, and standard deviations of all measurements prescribed by the current Track Safety Standards.

Of these 29 zones, 10 represent historical data as outlined in Table 12; 14 were processed under this research effort and are described in Table 17; and 5 were processed under a companion effort that was also concerned with the physical details of specific zones.[23] An overview of these data sources is provided in Table 18. The rationale for selecting these segments from the extensive library of available data is summarized in Table 19. Regressions of these data are used to generate Table 3 and Figure 2.

---

[23] J. Corbin, "Correlation of Statistical Representations of Track Geometry with Physical Appearance," Final Report, FRA-ORD-79-35, June 1975.

TABLE 17. SYNOPSIS OF PSD DATA GENERATED UNDER THIS PROGRAM

	NEC and ENVIRONS 1977	Track Survey Device, Data from TG-69 (1973)
Mean Profile	Avg. T-3 Profilometers	Laser Tracker + Corrections
Individual Rail Profile	T-3 Profilometer	Laser Tracker + Crosslevel + Measurement Frame Dimensions
Mean Alignment	N/A	Laser Tracker + Corrections
Individual Rail Alignment	N/A	Laser Tracker + Gage + Crosslevel + Measurement Frame Dimensions
Crosslevel	CAS	Electronic Pendulum (Low Speed)
Gage	N/A	Hydraulically Loaded Wheels
Broken Down by Track Class	Class 6 thru Class 3	Class 6 thru Class 1
Territory Covered	Washington, DC, New Haven, Harrisburgh, Philadelphia	Area of Pueblo, Colorado
Resolution of Peaks	8.0×10^{-4} cy/ft	1.0×10^{-3} cy/ft
No. of Diagrams	2	8
Number of PSD's Per Range Diagram	4	5
Typical Length of Data/PSD	5 mi. to 25 mi.	700 ft. to 7000 ft.

TABLE 18. OVERVIEW OF DATA SOURCES

Letter Symbol on Graphs	Source Measurement vehicle	Data Vintage	Number of Zones	Available Geometry Variables	Profile-Alignment Source	Further Discussion
A	T-3	1971	3	A11	14.5 ft MCO	Table 12, Appendix D
B	T-3	1973	7	P,G	14.5 ft MCO	Section D.2
C	T-2	1977	4	P,X	Inertial	Table 17, Appendix D
D	TSD	1973	10	A11	Absolute	Sections D.3 & D.4
E	T-6 / T-2	1978	4 / 1	A11 / P,X	Inertial	Reference 24

P = Profile
X = Crosslevel
A = Alignment
G = Gage

TABLE 19. RATIONALE FOR DATA SELECTION

	Debits	Credits	Decision
TSD Old Processing Test #(TG-69)	• Data is dated. • High crosslevel/alignment attributed to quantization (see Para 3.1.4).	• Data has a high pedigree since detailed records were taken. • Data has an exceptionally good noise floor.	PSD's generated and provided in Appendix D, Section D.3.
TSD New Processing Test #(TG-128)	• New processing algorithm is unvalidated (some anomalous output noted).	• Data is recent. • Data has a high pedigree since detailed records were taken. • Data has an exceptionally good noise floor.	Not used.
T-2/T-3 Capacitive Beam System (Obsolete)	• Data is dated and diffiult to relate to Speed Class. • Profile/Alignment via 14.5 ft beam limited to 10-100 ft. • Erroneous Crosslevel due to gyro response. • Erroneous Crosslevel due to incorrect sensor connection prior to 1972. • Erroneous long wavelength gage on curves with bolted rail.	• Existing PSD's do have a high pedigree. • X-level sensor problem is correctable. • There is a lot of data collected with this system. • Alignment data is available.	Existing PSD's used as a base line in Appendix D, Section D.2.
T-3 Inertial + Capacitive System	• Profile/Alignment via 14.5 ft. beam limited to 10-100 ft. • Profilometer has high quantization error (see Para. 3.1.4). • Slow CAS error in curves (see Para. 3.1.3).	• Some data is recent and can be linked to Speed Class.	Not Used.
T-3 Current Inertial System	• Spurious profilometer responses in the 100-500 ft. range on lower speed settings (see Para's 3.1.3 & 3.1.5). • No alignment system, Curvature valid for mean alignment at wavelengths of 250 ft. and longer. • Both capacitive and magnetic gage develop excessively high noise floors at speeds over 50 mph (see Para. 3.1.5). • Generally high noise floor in at least one profilometer (see Para. 3.1.5).	• Very recent data from a wide range of territory • Good profile and crosslevel at high speed (CAS problem corrected).	Profile and Crosslevel PSD's generated and provided in Appendix D, Section D.3.
T-2 Current Inertial System	• Gage system is identical to T-3 so that the same problem is suspected. • No alignment system. • Data supply is limited	• Data avaiable is recent.	Not Used.
T-6	• Supply of data limited.	• Data is recent. • Data is of excellent quality. • System incorporates low speed capability for characterizing very rough track profiles. • Alignometer working & available. • Phase shiftless space curve from profilometer/alignometer available.	Used to characterize joints and anomaly profiles (see Section 3.5, Appendix B, & Appendix C).

3.4.1 REGRESSIONS ON CONTINUUM - SRP PARAMETERS

Values of the roughnesses, A_3, A_4, A_7, and A_8, corresponding to mean profile, crosslevel, mean alignment, and gage, were tabulated and then plotted against one another for all six possible pair combinations as shown in Figures 53 through 58. *In these graphs and those which follow, letter symbols identify data sources as defined in Table 18. An overbar, ($\overline{D}$), indicates tangent CWR, a carat, ($\hat{D}$), indicates tangent bolted and a tilde, ($\tilde{D}$), indicates curved CWR.*

Figures 53-58 display a linear pattern of data values. After discarding some questionable or extremal data points, the following least squares relationships are found to exist among the A_n:

$$A_3 = 200A_4^{\frac{3}{2}} = \sqrt{2}\,A_7 = \sqrt{2}\,A_8 .$$

Of all of these regressions, mean profile versus mean alignment (Figure 54) gives the tightest fit. However, alignment roughness exhibits a lower bound of $A_7 = 2.5 \times 10^{-5}$ in^2- cy/ft. All data points on this ordinate are derived from the TSD which must combine several independent measurements* in order to obtain alignment. This suggests the possible contamination of this data by noise.

Values of profile corner frequency were tabulated and plotted against profile roughness, A_3, in Figure 59. ϕ_{34} was found to be invariant with respect to roughness over a wide range of A_3-values. ϕ_{33}, on the other hand, exhibited two significant branches if data points were further identified as follows:

---

*Horizontal laser tracker, gage, and crosslevel.

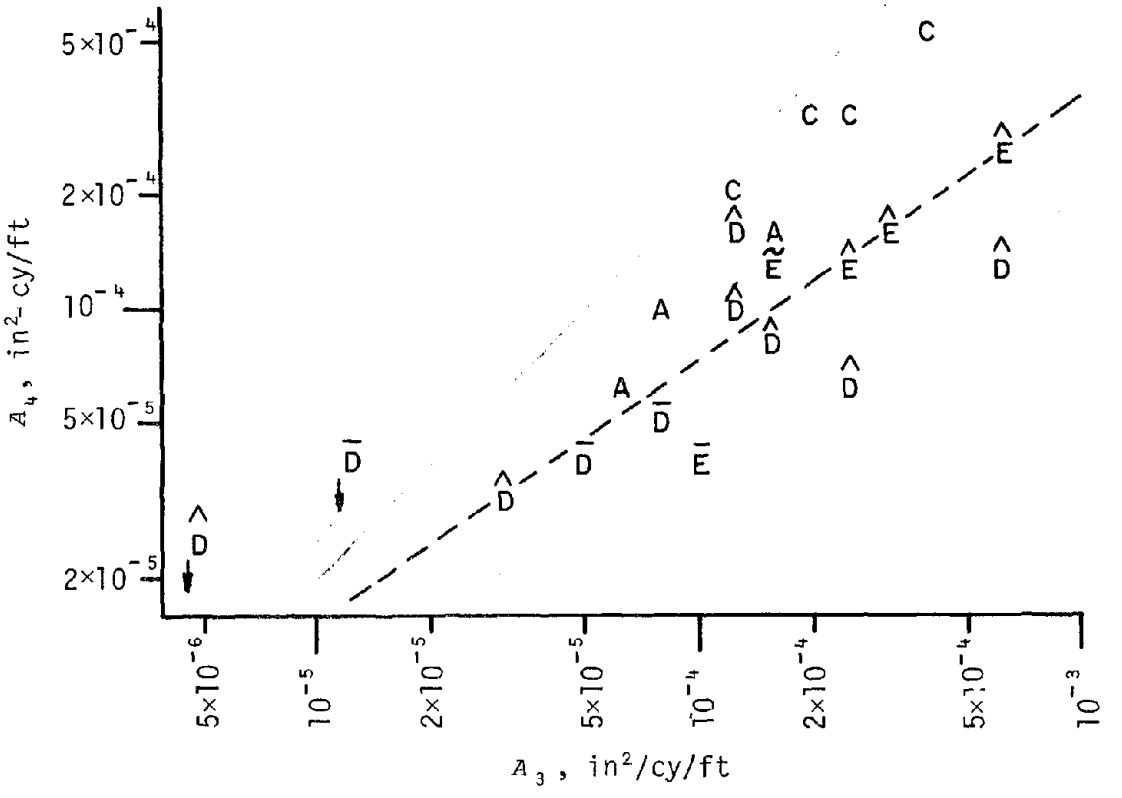

FIGURE 53. VARIATION OF PROFILE VERSUS CROSSLEVEL ROUGHNESSES

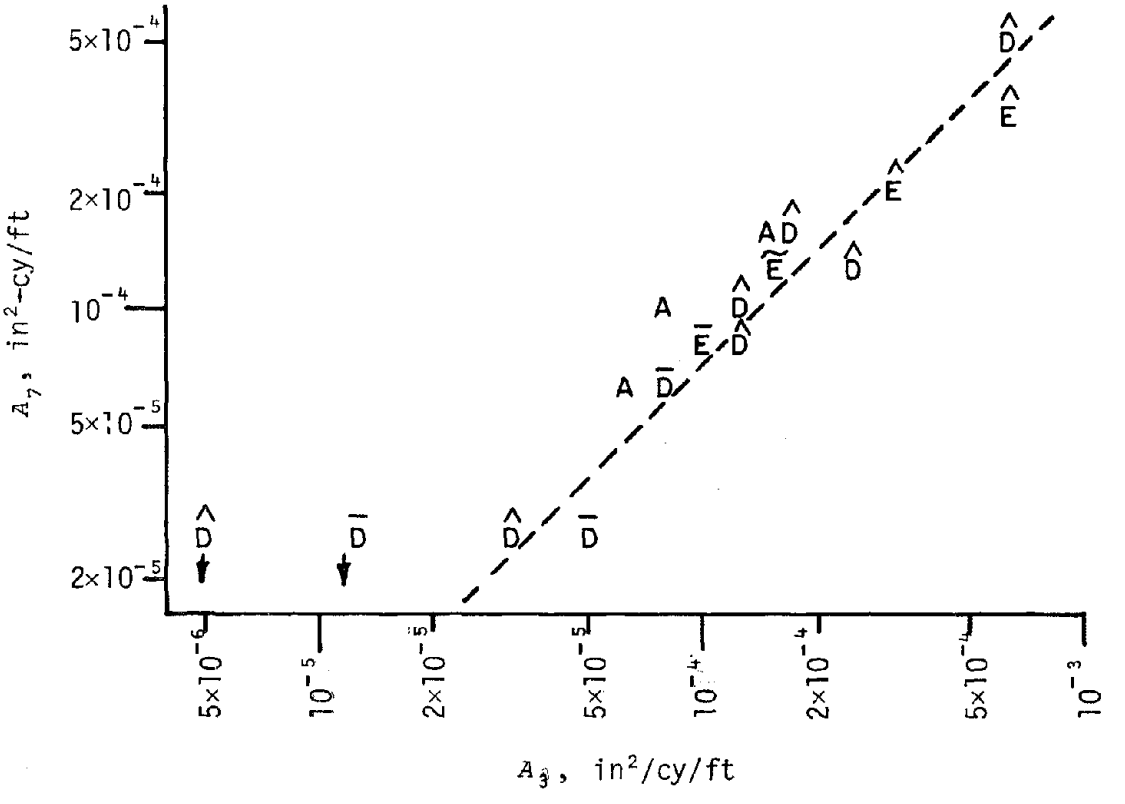

FIGURE 54. VARIATION OF PROFILE VERSUS ALIGNMENT ROUGHNESSES

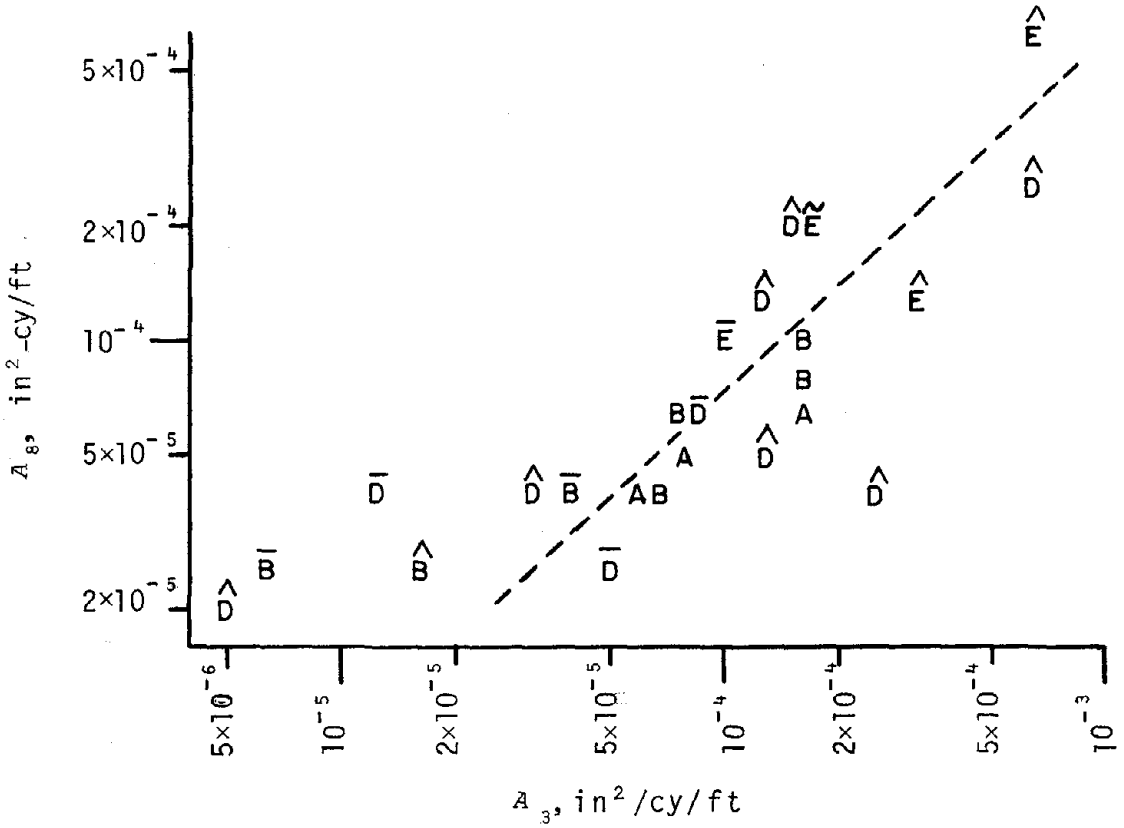

FIGURE 55. VARIATION OF PROFILE VERSUS GAGE ROUGHNESSES

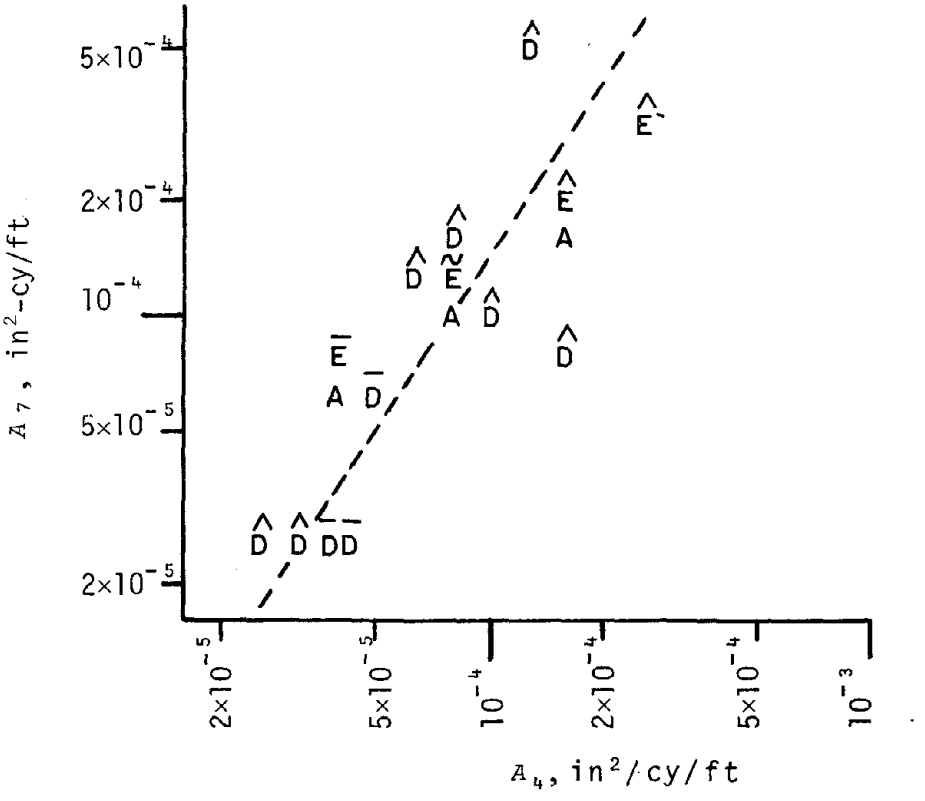

FIGURE 56. VARIATION OF CROSSLEVEL VERSUS ALIGNMENT ROUGHNESSES

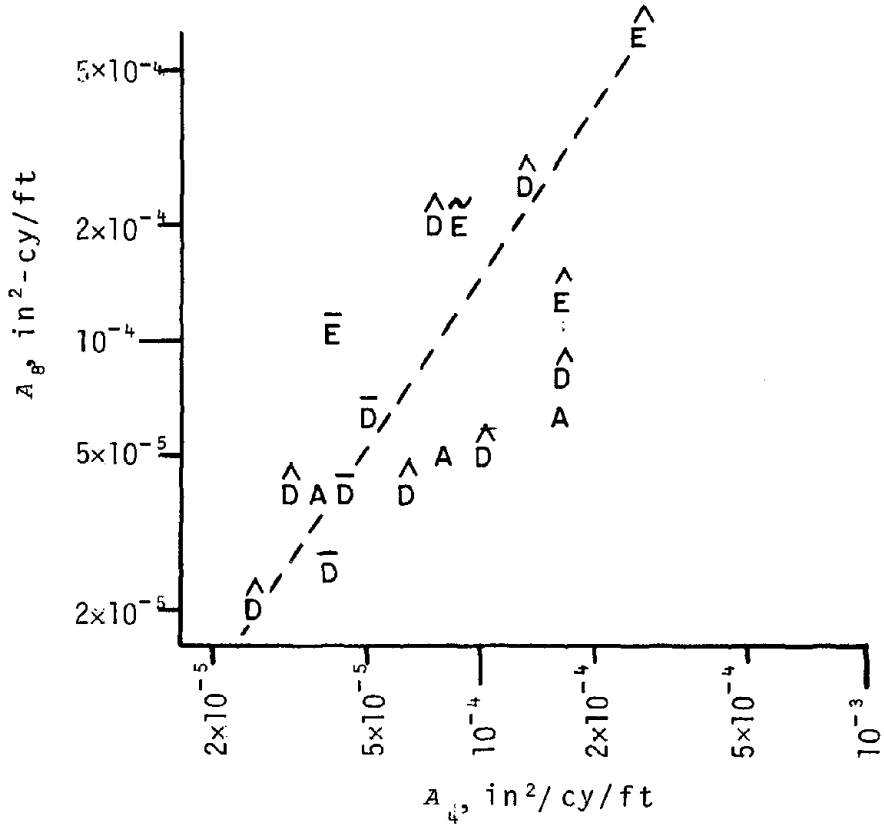

FIGURE 57. VARIATION OF CROSSLEVEL VERSUS GAGE ROUGHNESSES

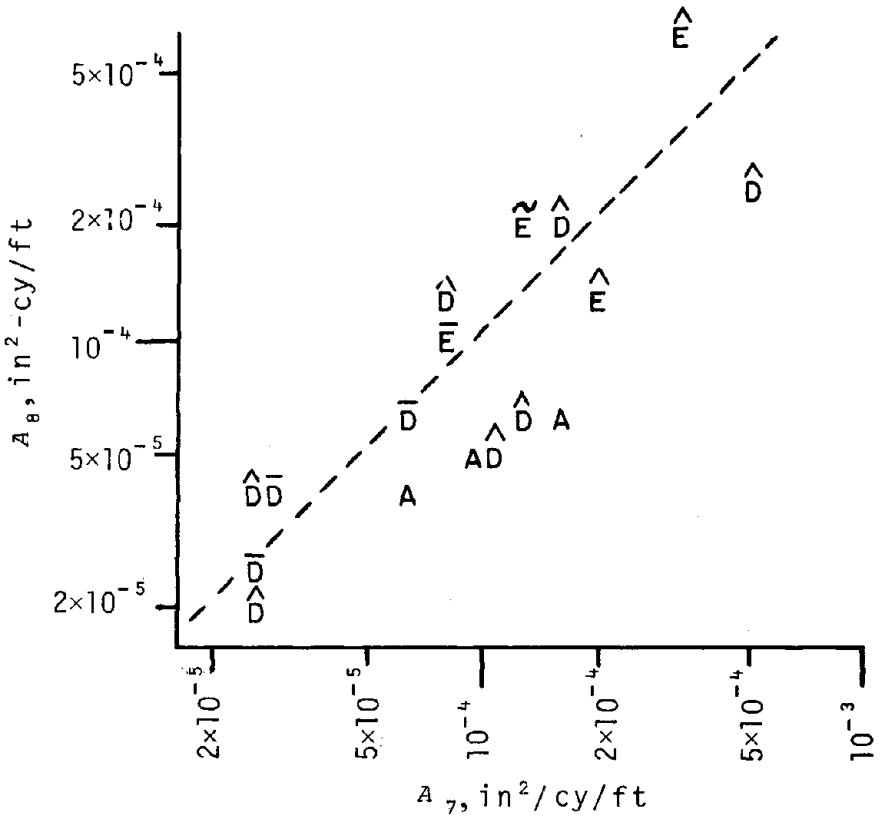

FIGURE 58. VARIATION OF ALIGNMENT VERSUS GAGE ROUGHNESSES

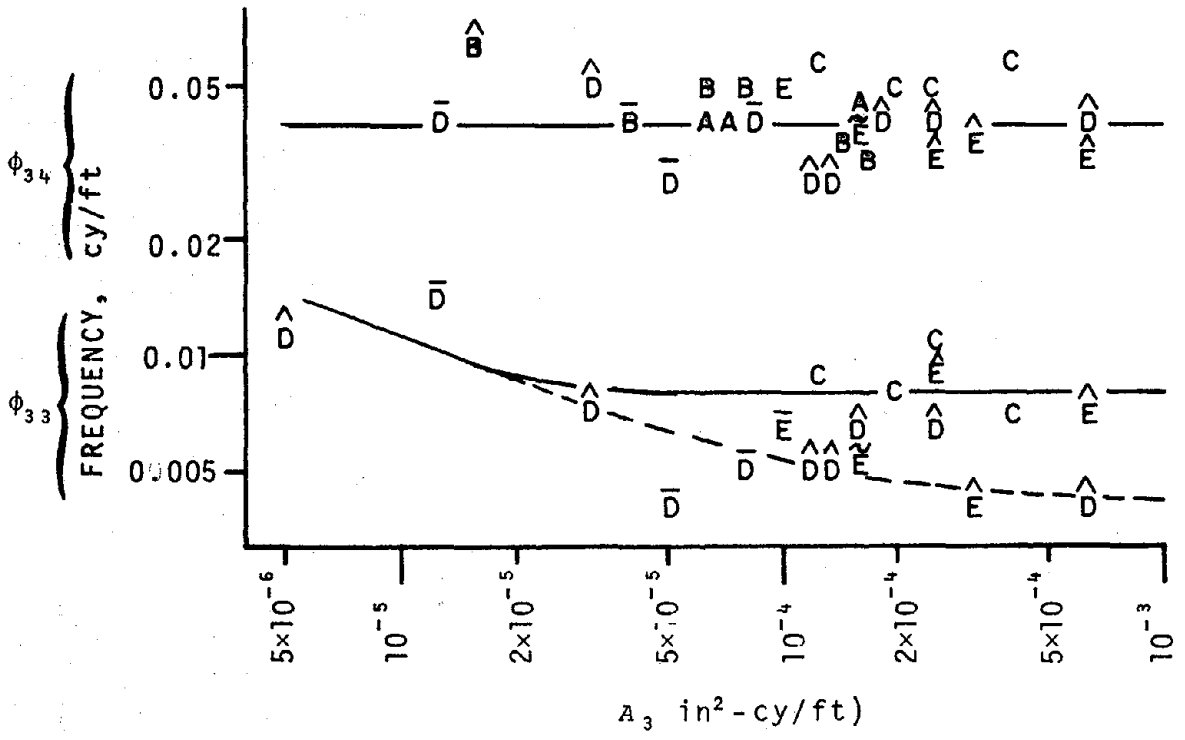

FIGURE 59. PROFILE ROUGHNESS VERSUS PROFILE CORNER FREQUENCIES

- High roughness lines representing either low speed track paralleling high speed main lines or highly degraded states of former high speed lines cluster about the constant solid line.
- Branch lines, which are not as well graded to remove terrain effects, cluster about the dotted line which exhibits a slight but significant decrease with increasing roughness.

A survey of other corner frequencies, ϕ_{n_3} and ϕ_{n_4}, revealed no significant variations with respect to the corresponding roughness, A_n. Values for these corner frequencies are tabulated in Table 3.

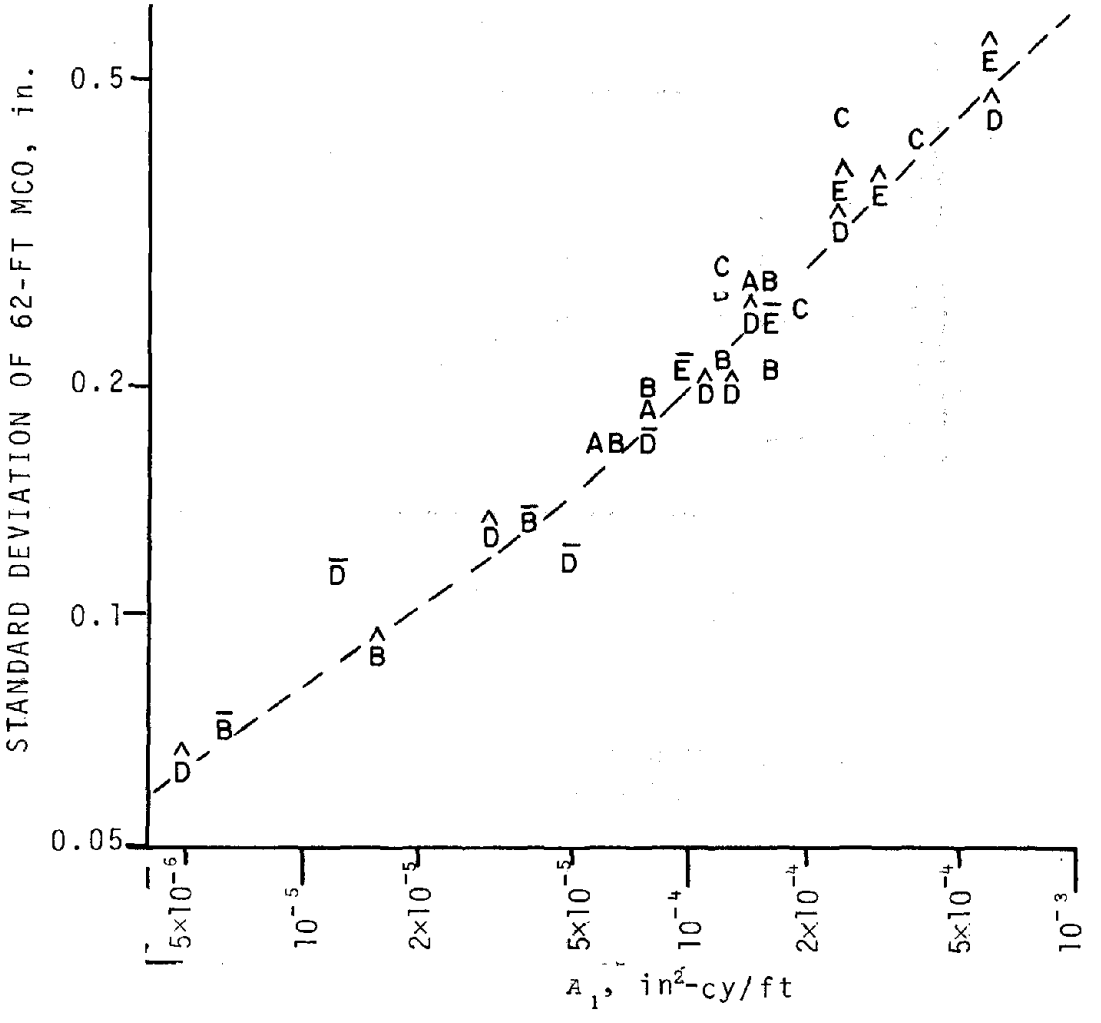

FIGURE 60. PROFILE ROUGHNESS VERSUS STANDARD DEVIATION OF 62-FT PROFILE MCO

3.4.2 REGRESSIONS OF SRP STANDARD DEVIATIONS AGAINST TRACK CLASS AND EXCEPTION LEVELS

First, it was desired to establish that the SRP roughness parameters are tightly linked to the standard deviations of measures specified in the Track Safety Standards. Figure 60 illustrates that this is indeed the case for profile roughness versus the standard deviation of a 62-ft MCO.

The regression fit is relatively tight despite the fact that the MCO computation described in Paragraph 2.2.5 includes

the profile roughness and two corner frequencies. While the latter are constant *in the mean*, they are still subject to fluctuation uncertainty, and the good regression fit actually observed is *not* guaranteed. The upper linear portion of the curve indicates the relationship:

$$\sigma \cong 21 \sqrt{A_1} .$$

Next, the standard deviations of a 62 ft MCO responding to SRP profile were plotted against the exception levels for the corresponding zone track class. The disappointing results are shown in Figure 61. A review of the graph does reveal that most of the data points *and* all of the lower track classes are bunched at the top of the graph.

In order to obtain a more even distribution of points, Figure 61 data was replotted in Figure 62 with track class on a linear ordinate. This graph presents one of the most interesting regressions of this entire exercise: *In spite of the fact that the spacing of profile exception thresholds is highly nonlinear on virtually any ordinate, the logarithms of the standard deviations of the 62 ft MCO as derived from the empirical data are directly proportional to track class*! The linear relationship is indicated by the dotted line which is given by:

$$\sigma = 10^{-(0.6+\nu)/8},$$

where ν = track class. Note that most data points are within 1.5 track class of this line.

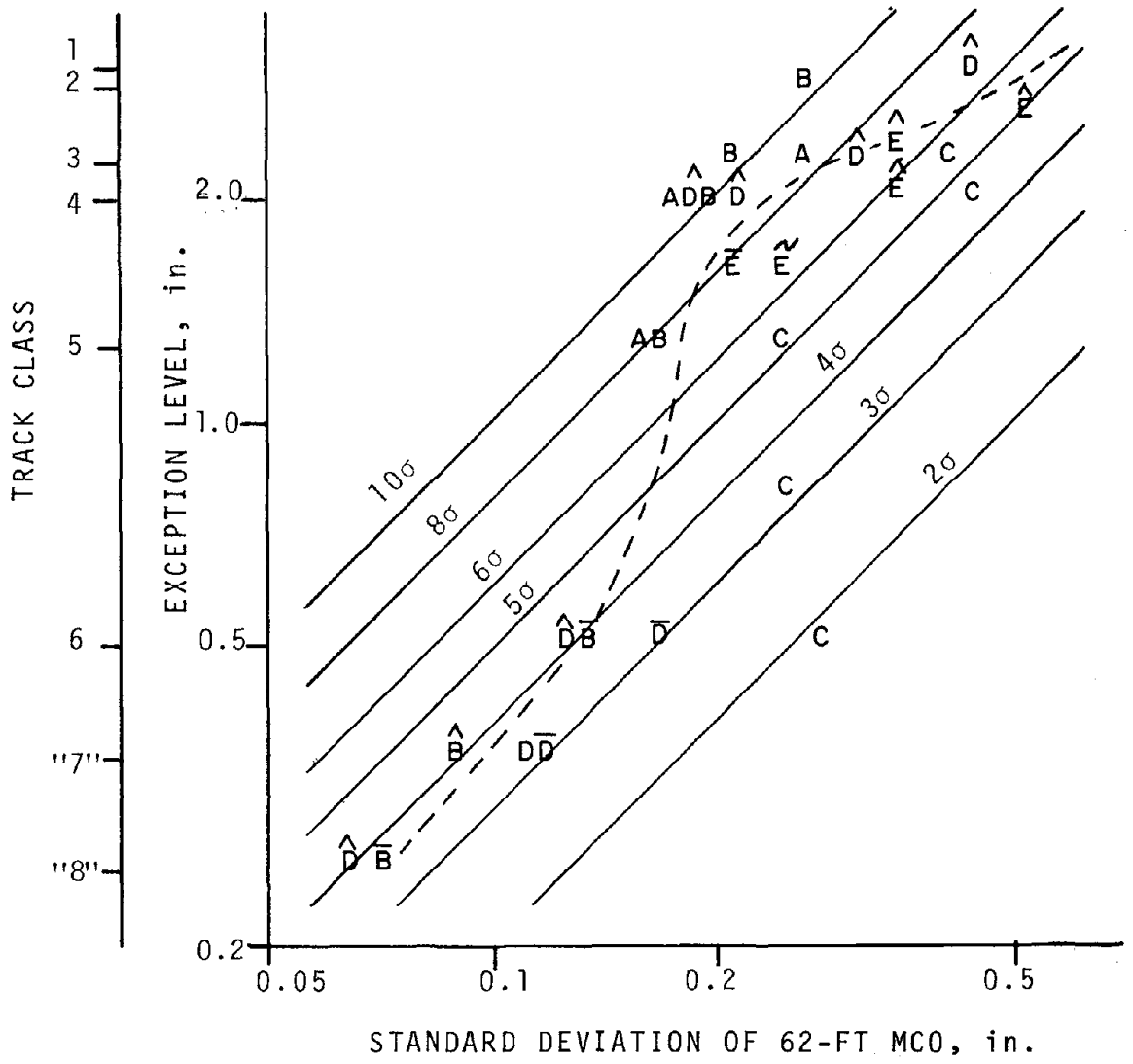

FIGURE 61. STANDARD DEVIATION OF 62 FT PROFILE MCO VERSUS TRACK CLASS AND EXCEPTION THRESHOLDS

This regression line has been transposed back onto Figure 61 where it is represented by the meandering dotted line. Also displayed on Figure 61 are diagonal lines which define the multiplicative factors of σ needed to exceed an exception threshold. On the basis of the dotted regression line, the following σ-factors are needed to produce an exception:

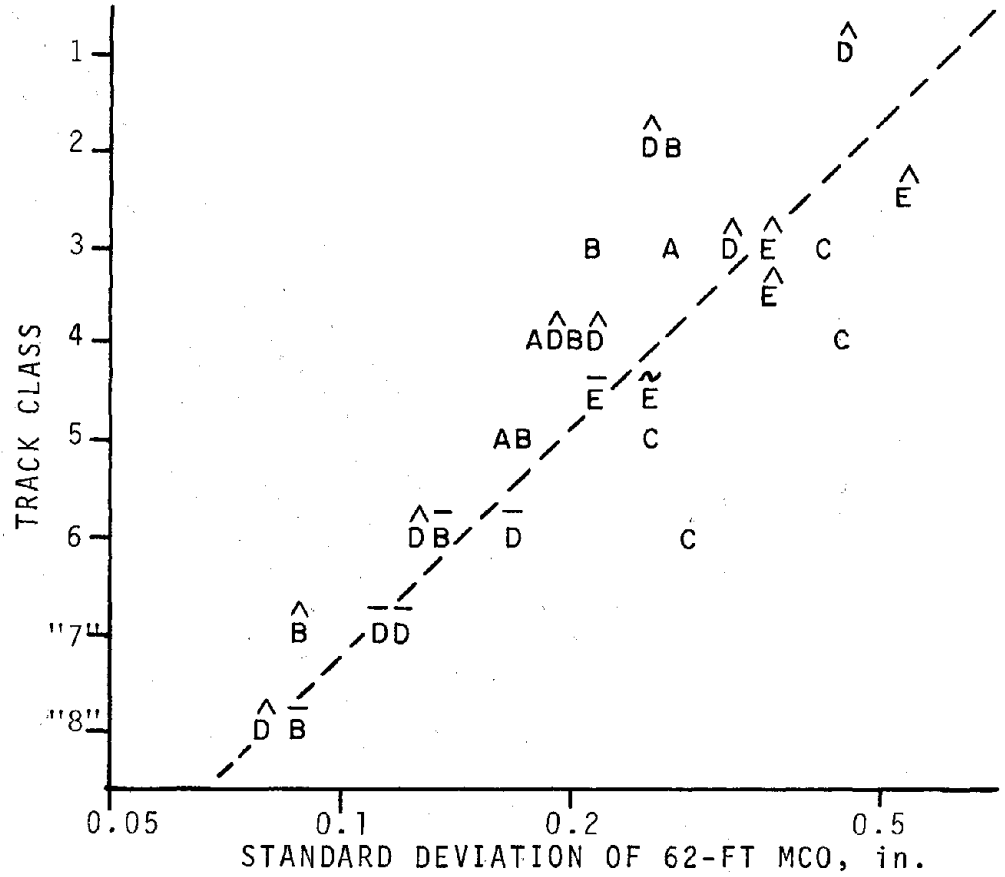

FIGURE 62. STANDARD DEVIATION OF 62 FT PROFILE MCO VERSUS TRACK CLASS ON LINEAR ORDINATE

- Class 6 and higher, a 3.5σ event;
- Classes 5-3: a 6σ event or higher; and
- Classes 2 & 1: a 5.5σ event.

A similar treatment was given to the standard deviation of crosslevel, 31-ft warp, 62-ft alignment MCO, and gage. These results are tabulated in Figures 63 through 66. Generally the pattern of data values is more linear than those found in Figure 61. It is also noted that the exception thresholds

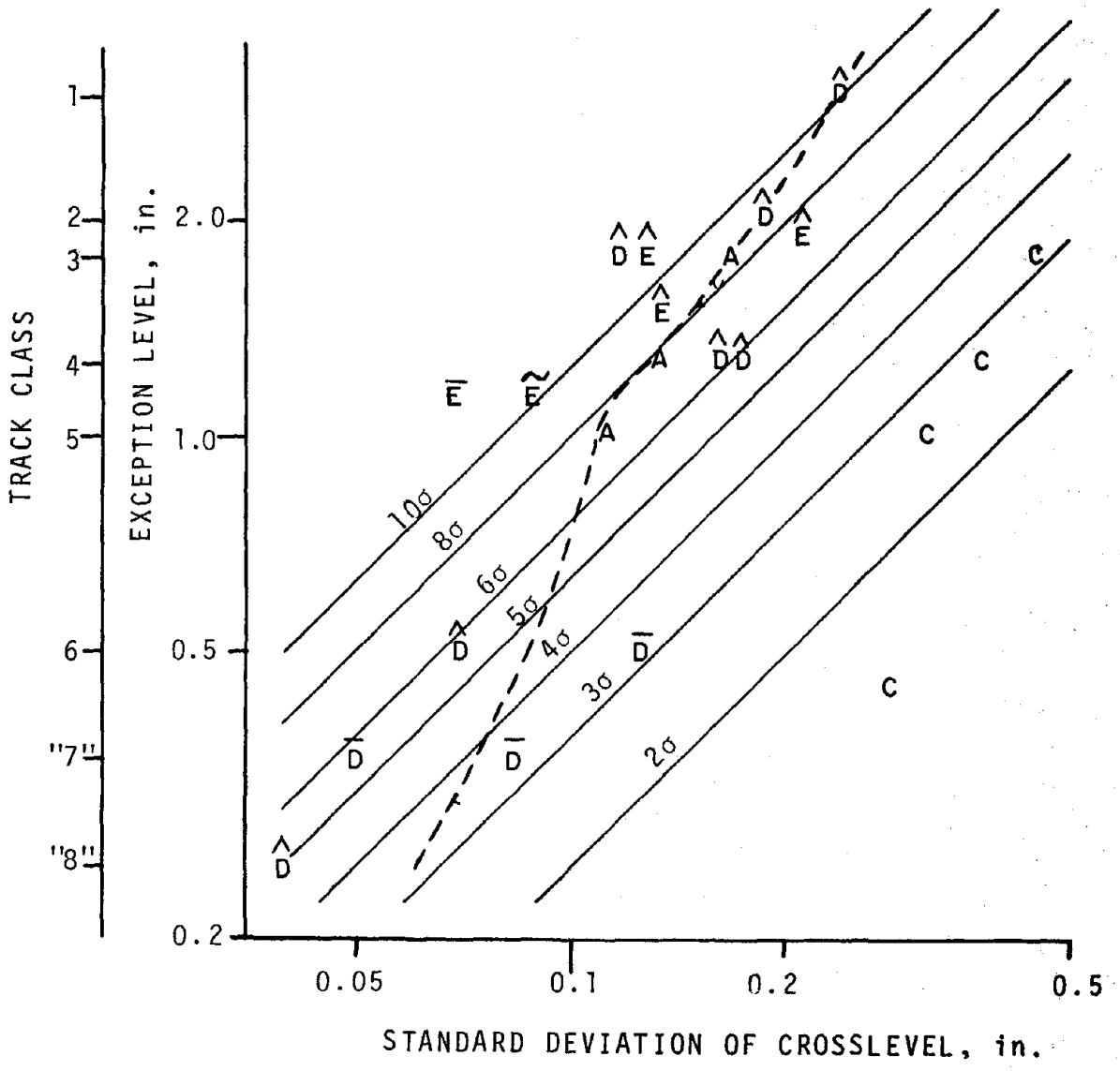

FIGURE 63. STANDARD DEVIATION OF CROSSLEVEL VERSUS TRACK CLASS AND EXCEPTION THRESHOLD

for these variables are more uniformly spaced along the ordinate than was the case for profile, reinforcing and perhaps explaining the observed linearization of profile data when replotted in Figure 62.

In this series of graphs, dotted lines show expected values of the data points based on the linear relationships developed in Paragraph 3.4.1 and the log roughness versus linear track class characteristic developed in Figure 62.

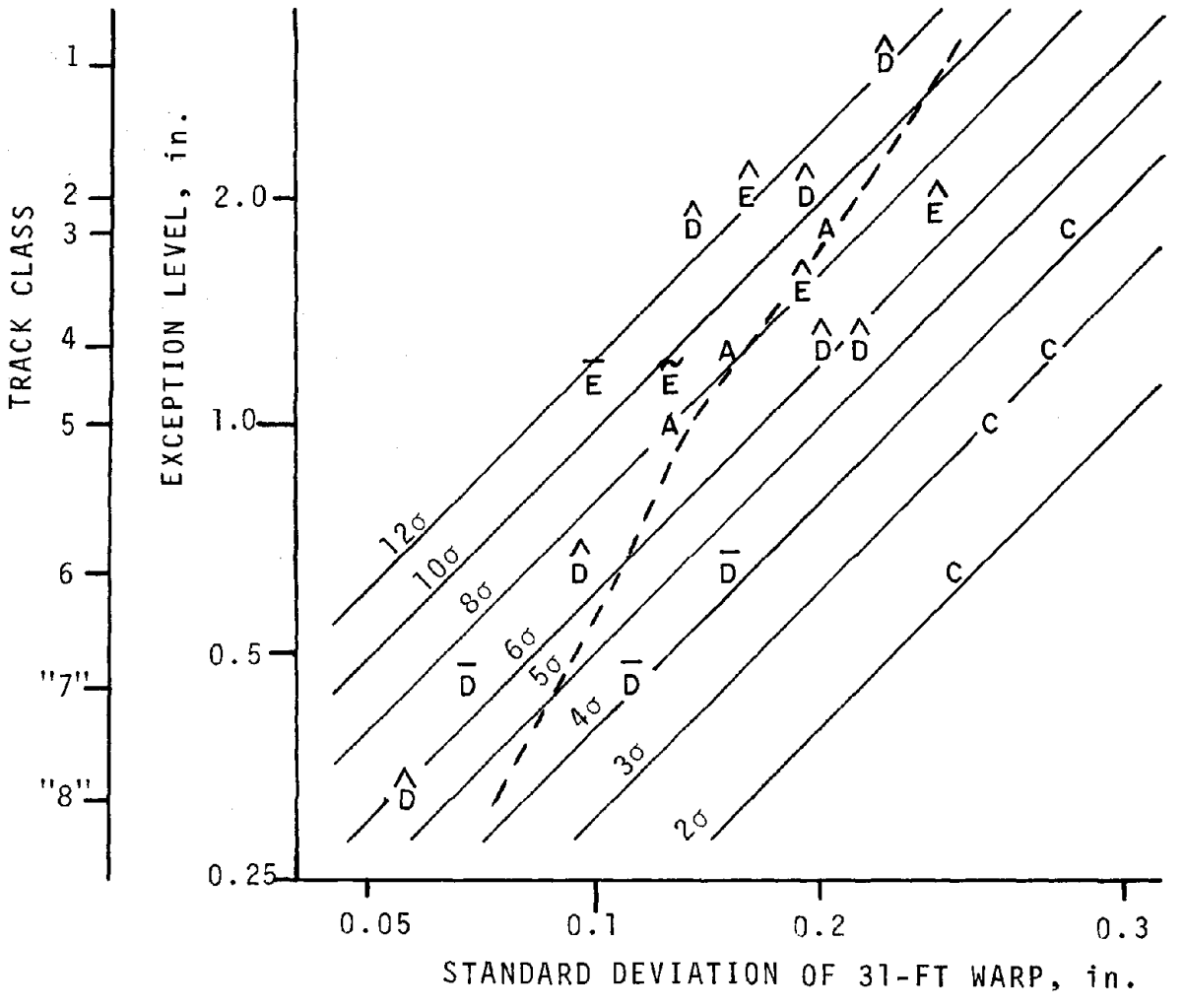

FIGURE 64. STANDARD DEVIATION OF 31-FT WARP VERSUS TRACK CLASS AND EXCEPTION THRESHOLD

Figure 65 is worthy of special attention. While the exception level exhibits a very wide dynamic range, the abscissa is relatively constricted. Note that as track class increases, the data values deviate farther from the dotted line, and the ratio of exception threshold to σ becomes significantly lower. Again, this is attributed to the intrusion of measurement system noise floors as was previously noted relative to Figure 54.

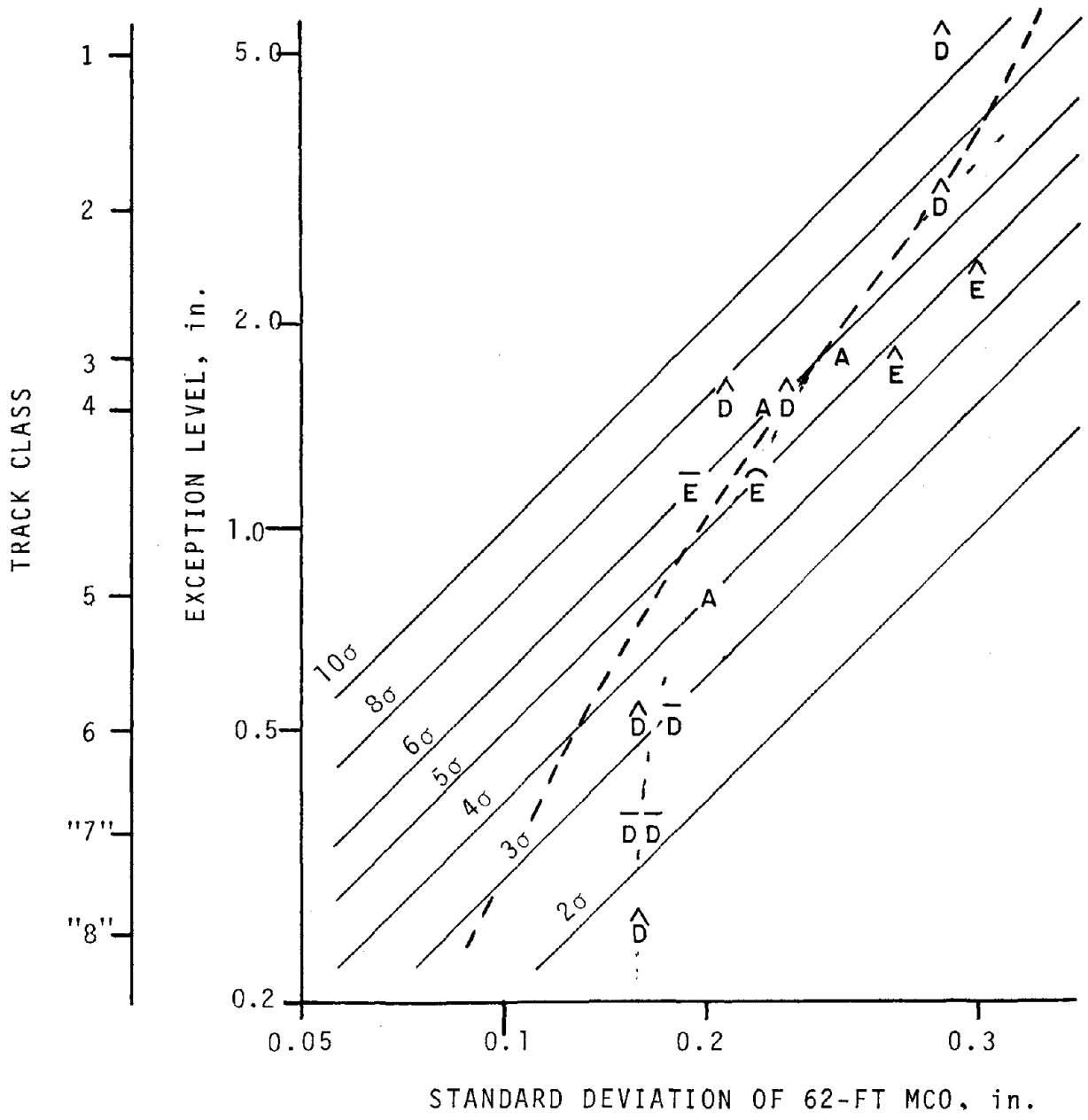

FIGURE 65. STANDARD DEVIATION OF 62-FT ALIGNMENT MCO VERSUS TRACK CLASS AND EXCEPTION THRESHOLD

Lines of constant multiples of σ versus threshold are also shown. A survey of Figures 61 and Figures 63 to 66 reveals that the gage SRP is most likely to produce an exception. As seen in Figure 66, a gage exception requires a 5σ event for classes 4-6 and a 4σ event for classes 2 and 3.

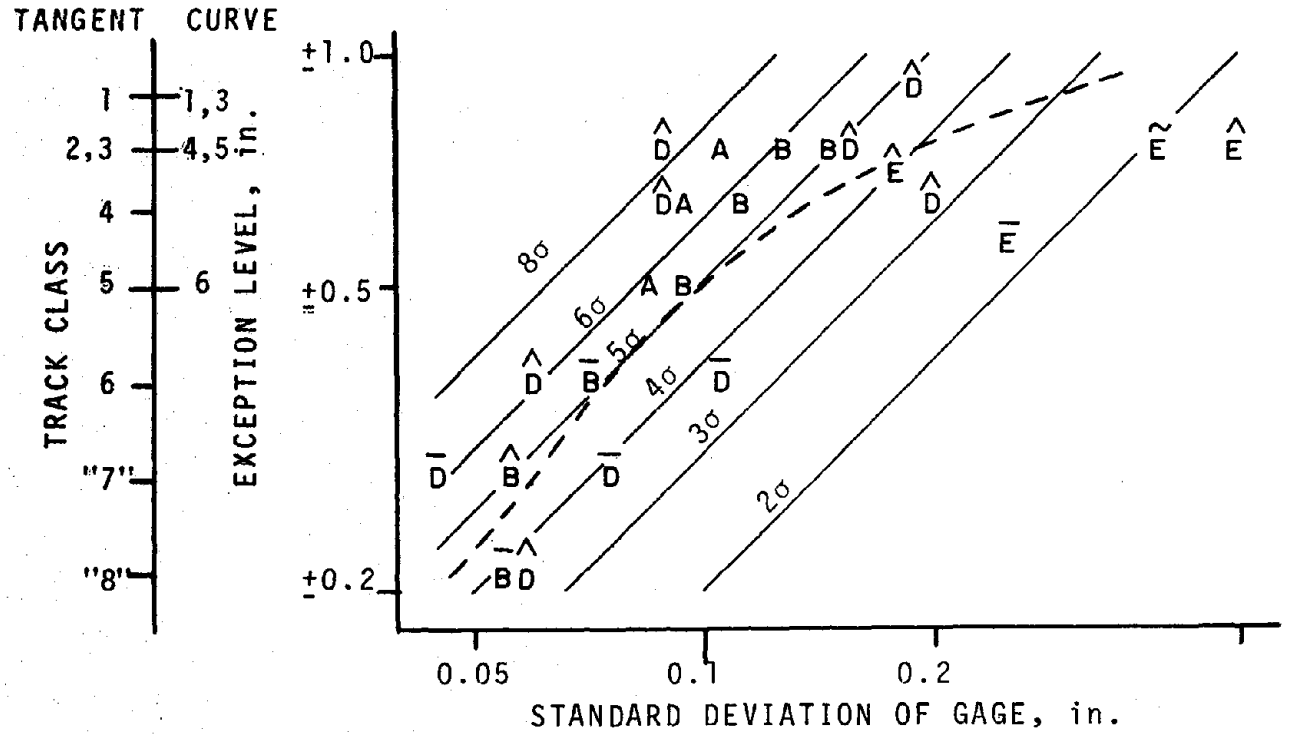

FIGURE 66. STANDARD DEVIATION OF GAGE VERSUS TRACK CLASS AND EXCEPTION THRESHOLD

3.4.3 REGRESSIONS ON PDP PARAMETERS

Regressions were performed to determine how $\overline{c}_1$ for profile and $\overline{c}_5$ for alignment varied with the corresponding roughness parameters, A_1 and A_5, and with decay rates, k_1 for profile and k_5 for alignment. Results are shown in Figures 67 through 70.

Figure 67 shows profile data values for A_1 versus $\overline{c}_1$. The bulk of the data values fall in a linear pattern where

$$\overline{c}_1^2 \cong 200A_1.$$

Some data values fall sufficiently far from the bulk of the values to require further explanation. The hypothesis was

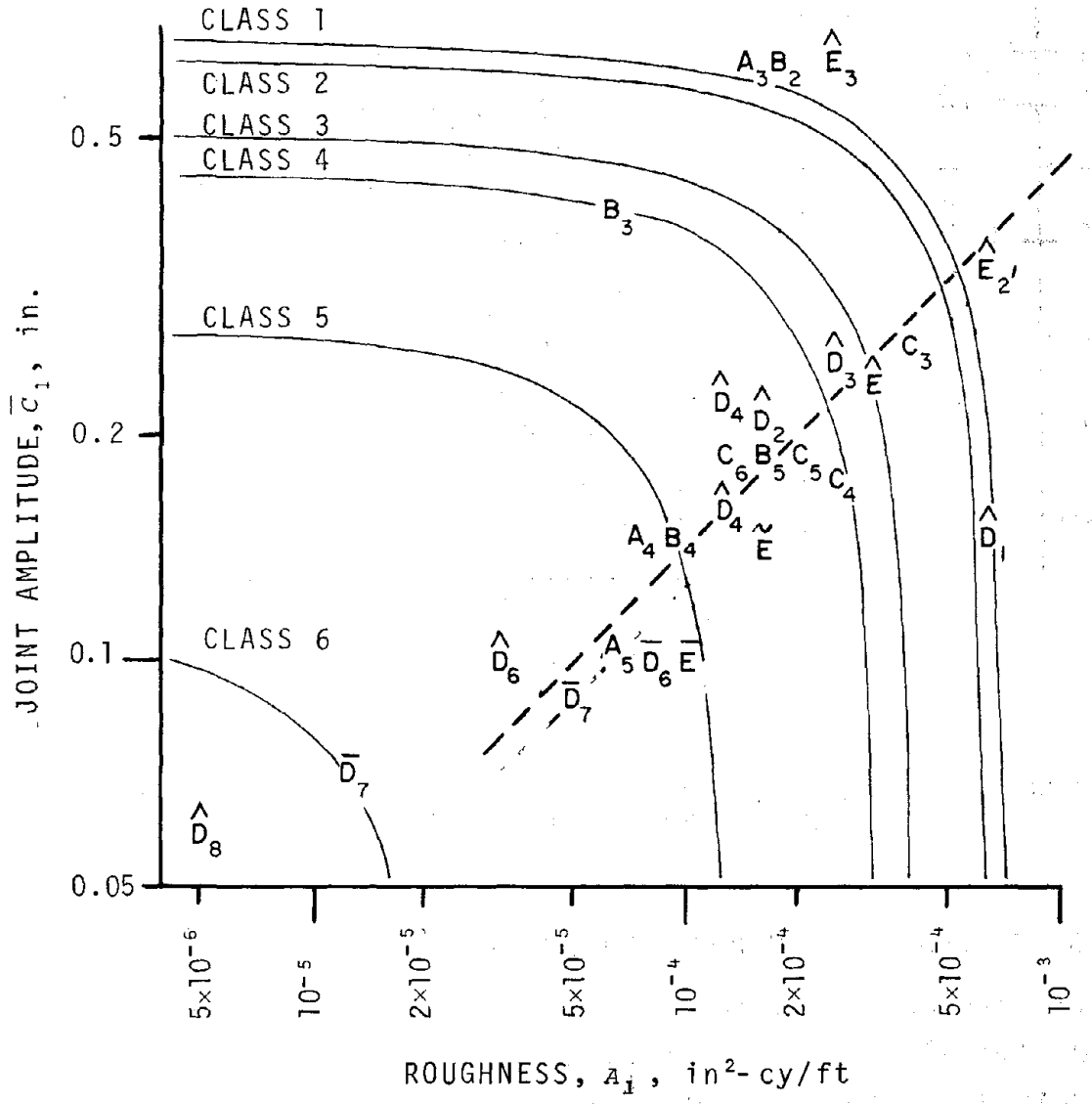

FIGURE 67. PROFILE ROUGHNESS VERSUS PROFILE JOINT AMPLITUDE

advanced that some linear combination of A_1 and $\bar{c}_1^2$ created a given track class:

$$\alpha_1 A_1\Big|_\nu + \beta_1 \bar{c}_1^2\Big|_\nu = t_1^2\Big|_\nu \quad ,$$

where

α_1, β_1 = constants for profile, and
$t_1|_\nu$ = 62 ft MCO profile exception level for track class, ν.

To test this hypothesis, data values were tagged with subscripts representing track class. Then a family of six curves satisfying the above relationship for each track class was adjusted to minimize classification error as shown in Figure 67. This was achieved for:

$$\alpha_1 \cong 1.25 \times 10^4 \text{ ft},$$
$$\beta_1 \cong 20 \text{ (dimensionless)}.$$

In this fit only a few zones fail to be classified within one track class. Comparing this result with the findings of Figure 62 prompts the following conclusions. *For most sections of track, joint amplitude increases linearly with roughness. However, a more universal description provides for track of a given class to be a linear mix of SRP and PDP, with the proportion of each component being broadly distributed about a mean mix.*

Figure 68 shows alignment data values for A_5 versus $\bar{C}_5$. A linear pattern is displayed with,

$$\bar{C}_5^2 = 250A_5.$$

The scatter of data values about the regression line was not sufficient to determine whether class ν alignment was adequately represented by simply letting $\bar{C}_5^2$ be proportional to A_5 as implied above, or by imposing a linear constraint on these values as was determined for profile.

Figures 69 and 70 display regressions of $\bar{C}_1$ against profile decay rate, k_1, and $\bar{C}_5$ versus alignment decay rate, k_5. The graphs are similar to each other and reveal an inverse relationship between mean joint amplitude and decay rate.

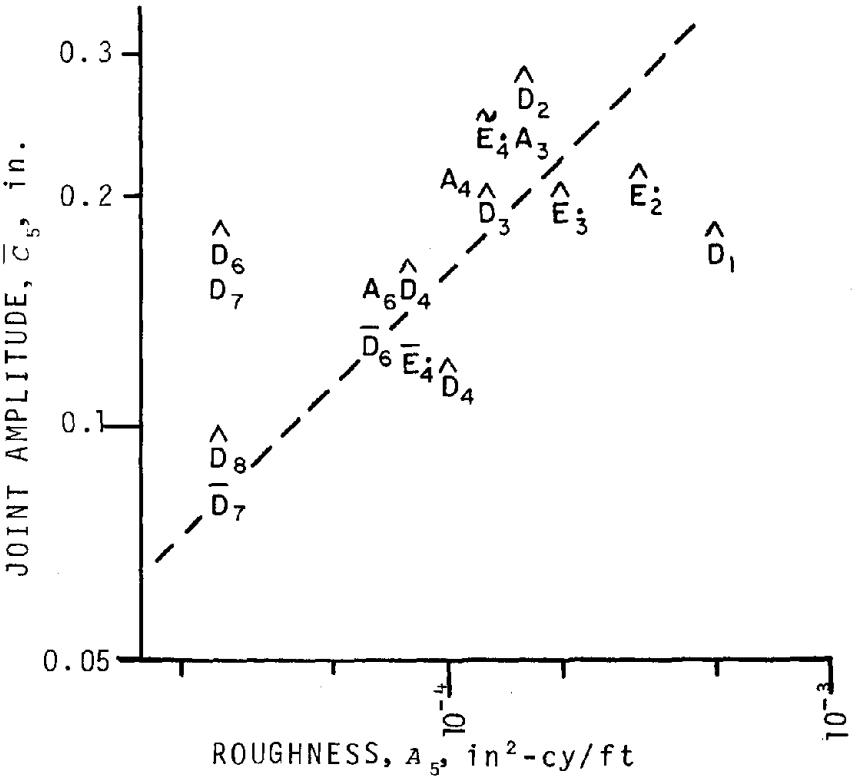

FIGURE 68. ALIGNMENT ROUGHNESS VERSUS ALIGNMENT JOINT AMPLITUDE

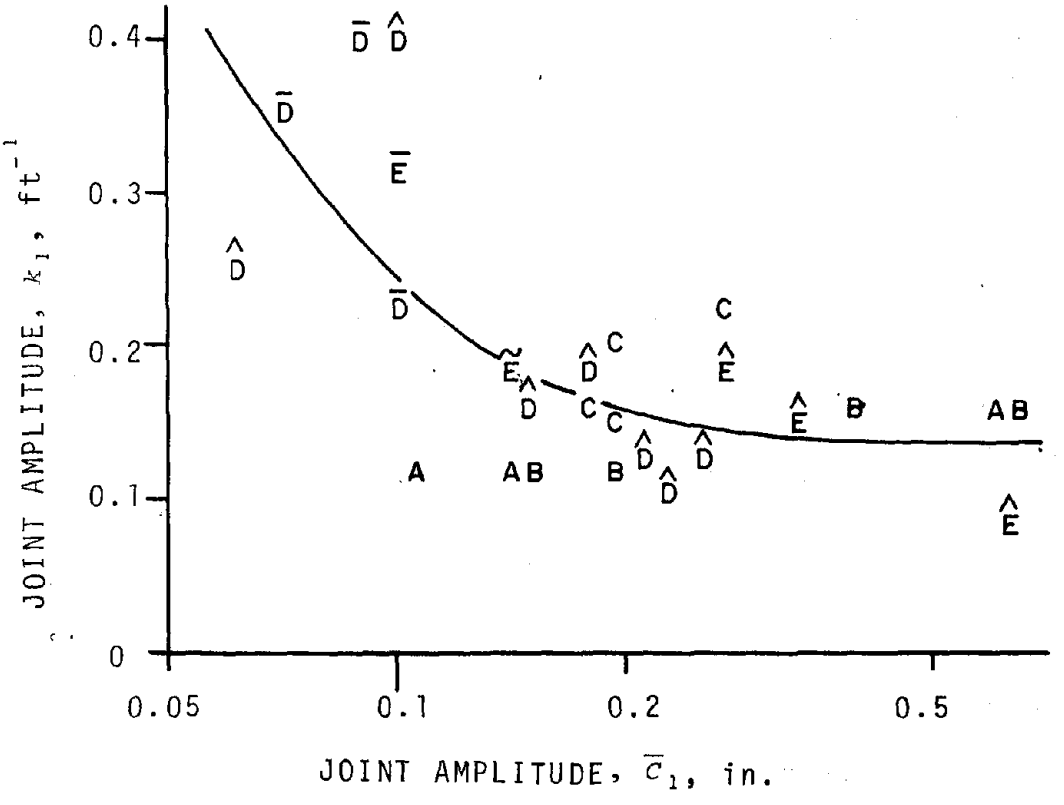

FIGURE 69. PROFILE JOINT AMPLITUDE VERSUS PROFILE DECAY RATE

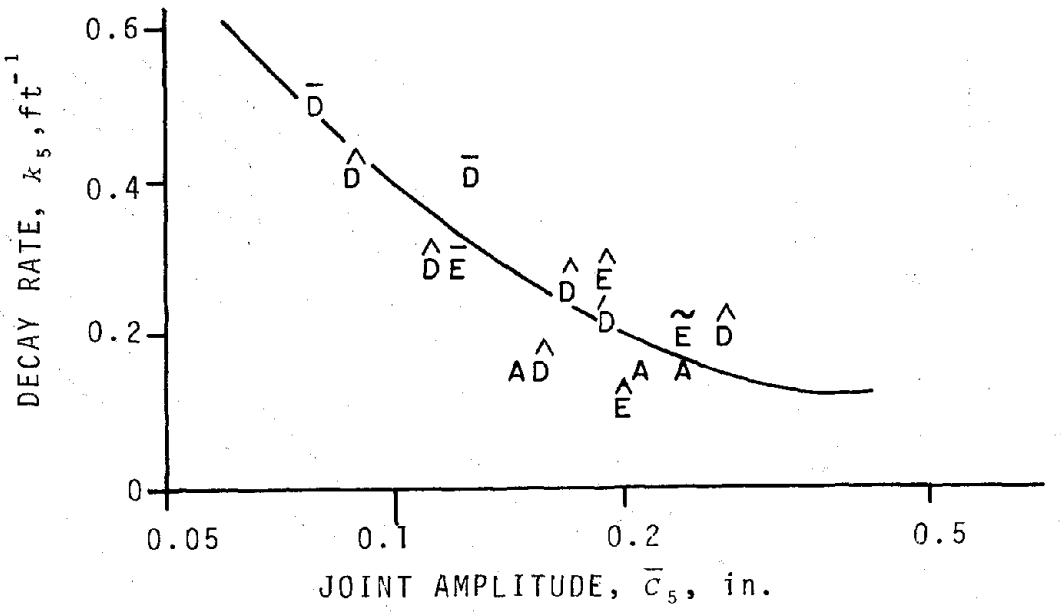

FIGURE 70. ALIGNMENT JOINT AMPLITUDE VERSUS ALIGNMENT DECAY RATE

In the case of profile, the decay rate starts at relatively high values for undegraded track, and as track degrades, it eventually settles to a value of 0.14/ft. Alignment decay rates approach the same value but not so quickly.

One of the more surprising results is that there does not appear to be a significant difference between the patterns developed by bolted rail and by CWR.

3.4.4 REGRESSIONS OF PDP MEAN AMPLITUDE AGAINST TRACK CLASS AND EXCEPTION LEVELS

Regressions were performed to determine how the mean joint amplitude varied with the exception thresholds for surface variables as prescribed in the Track Safety Standards. Here, it is assumed that joints are staggered, and that:

- 62 ft MCO for profile and alignment have a mean offset of $\bar{c}_1$ when the chord is centered at a joint;

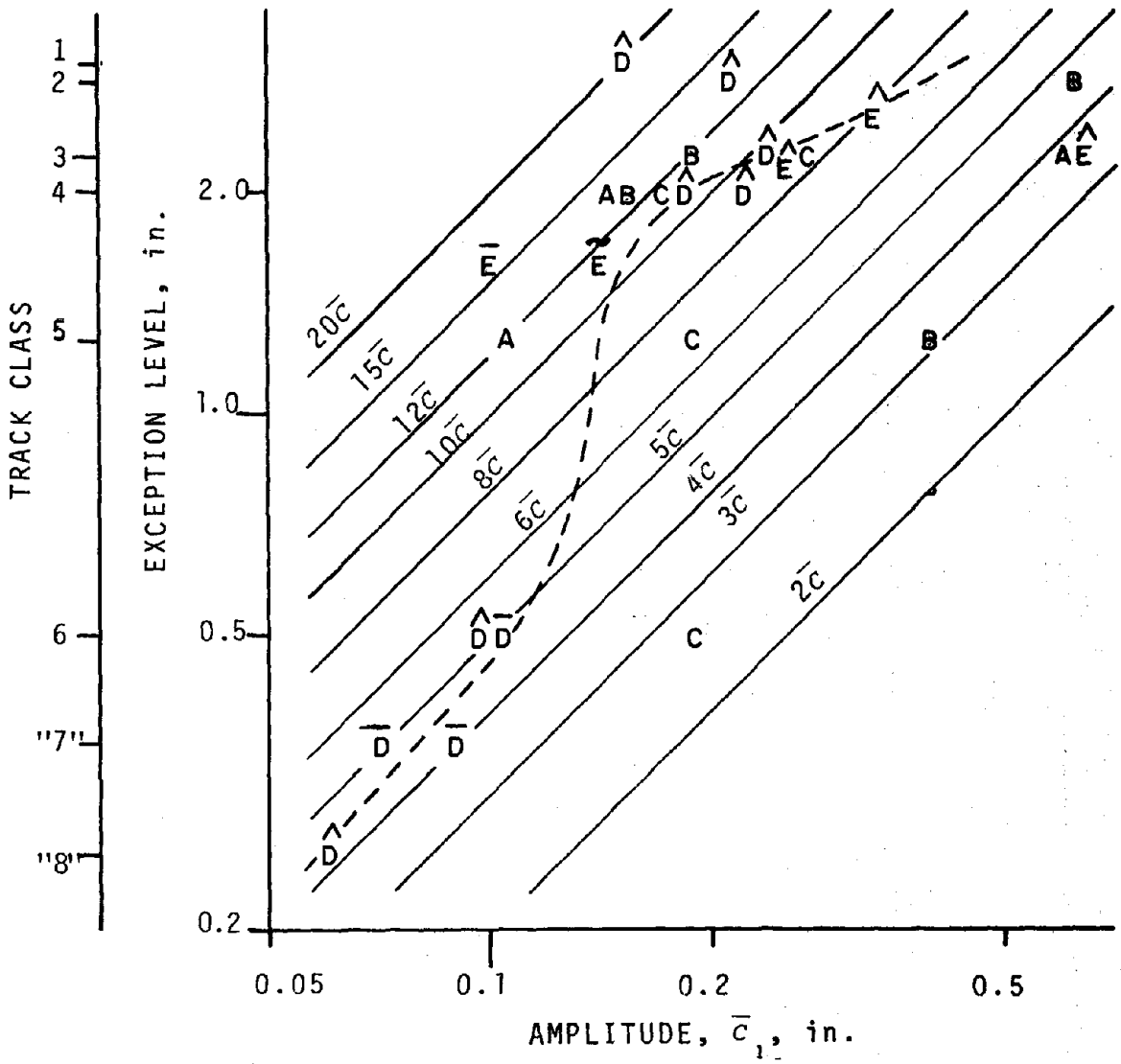

FIGURE 71. PROFILE MEAN JOINT AMPLITUDE VERSUS TRACK CLASS AND EXCEPTION THRESHOLD

- Crosslevel and gage have a mean value of $\bar{c}$ when the measurement location is at a joint; and,
- Warp has a mean value of $2\bar{c}$ when one measurement point is on a left rail joint and the other is on a right rail joint.

Figure 71 presents mean amplitude data versus track class and exception threshold. The scatter of data shows a trend similar

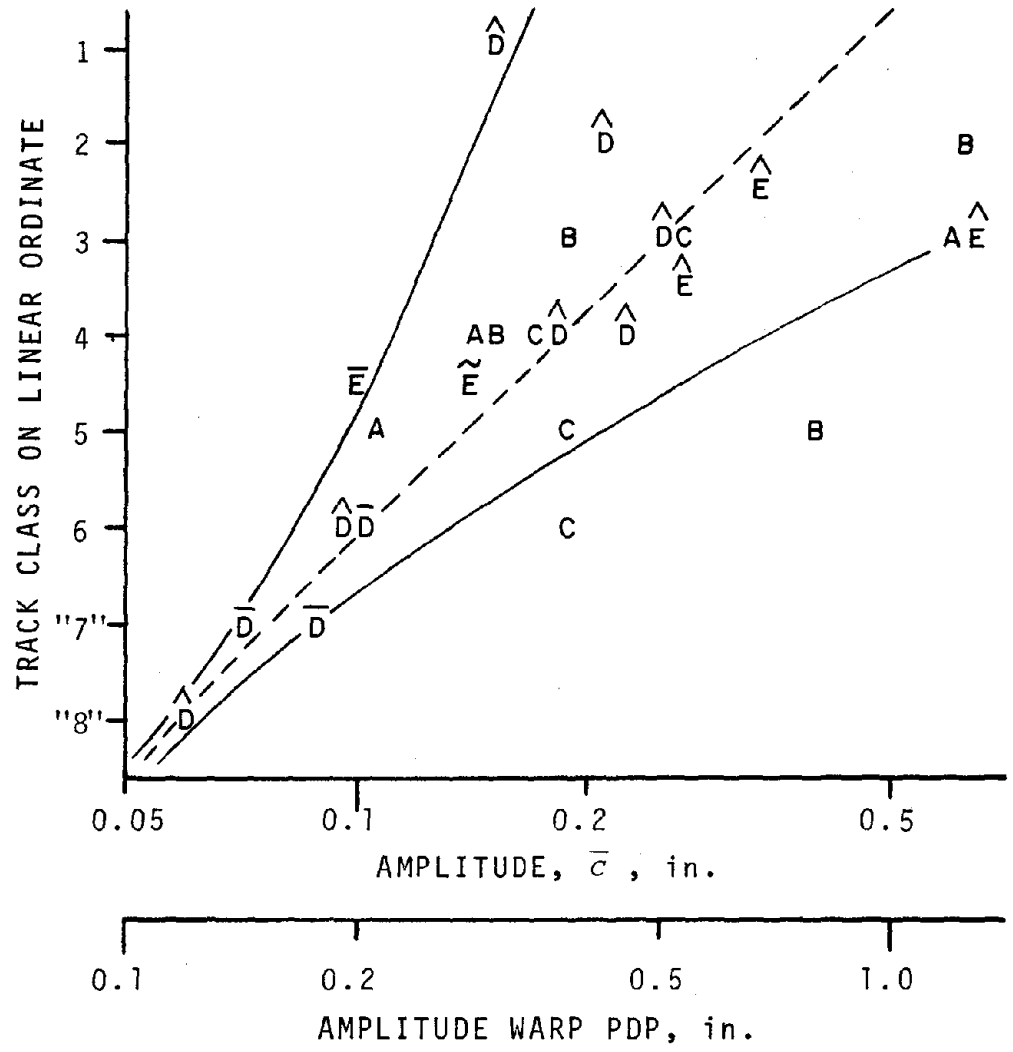

FIGURE 72. DETERMINISTIC PEAK VALUES VERSUS TRACK CLASS ON LINEAR ORDINATE

to that found in Figure 61. Accordingly, it was replotted with track class on a linear ordinate as shown in Figure 72. Again, this format produces a linear pattern with,

$$\bar{c}_1 = 10^{-(2.0+\nu)/8}$$

However, there is an increase of scatter with decreasing track class. By contrast the SRP component shown in Figure 61

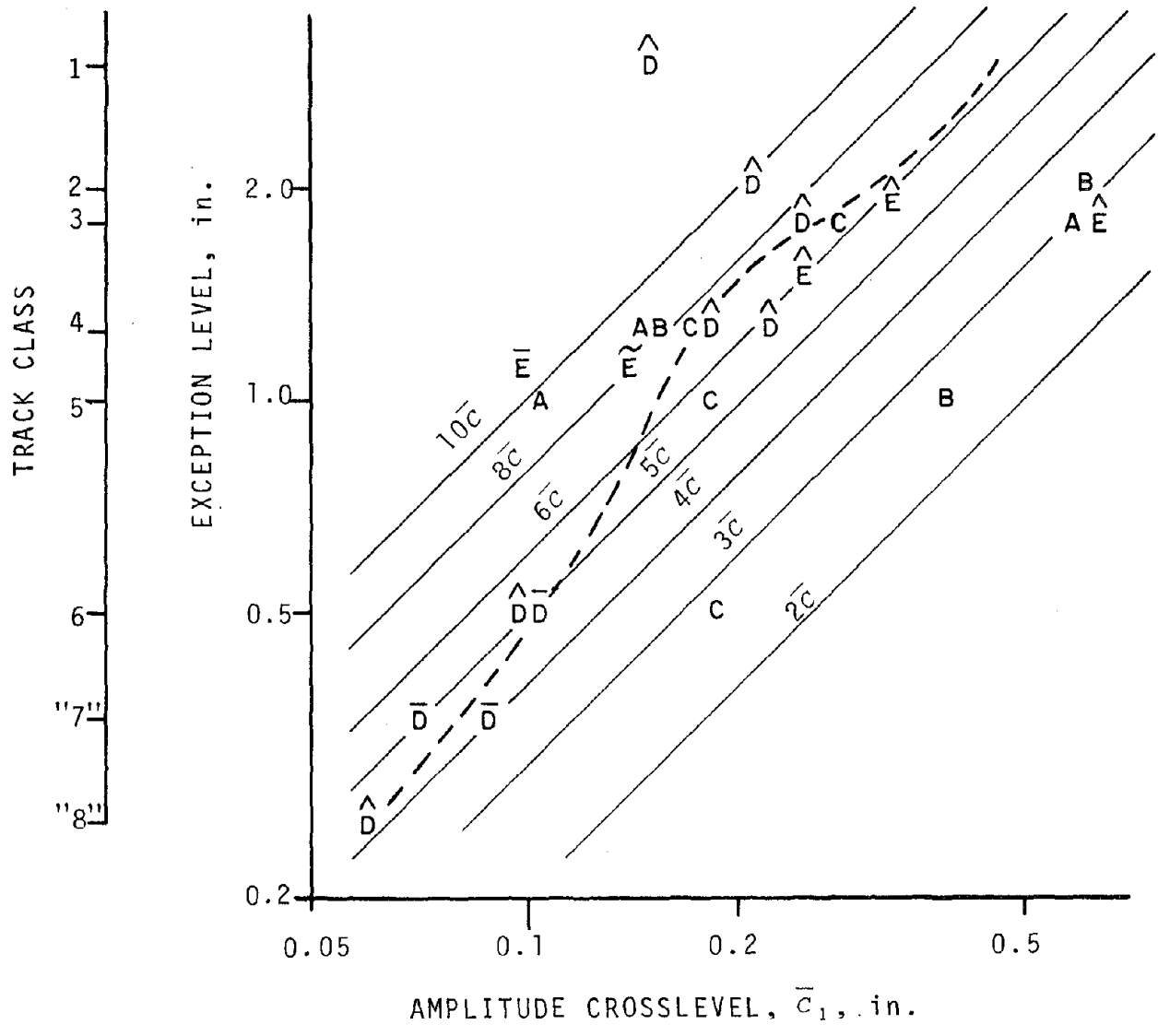

FIGURE 73. CROSSLEVEL MEAN JOINT AMPLITUDE VERSUS TRACK CLASS AND EXCEPTION THRESHOLD

exhibits no significant variations in scatter with respect to track class.

Figure 73 through 76 show the crosslevel, warp, alignment, and gage PDP peak values versus track class and exception thresholds. Figures 71 and 73 through 76 have diagonal lines that define the ratio of $\bar{c}$ to the exception threshold.

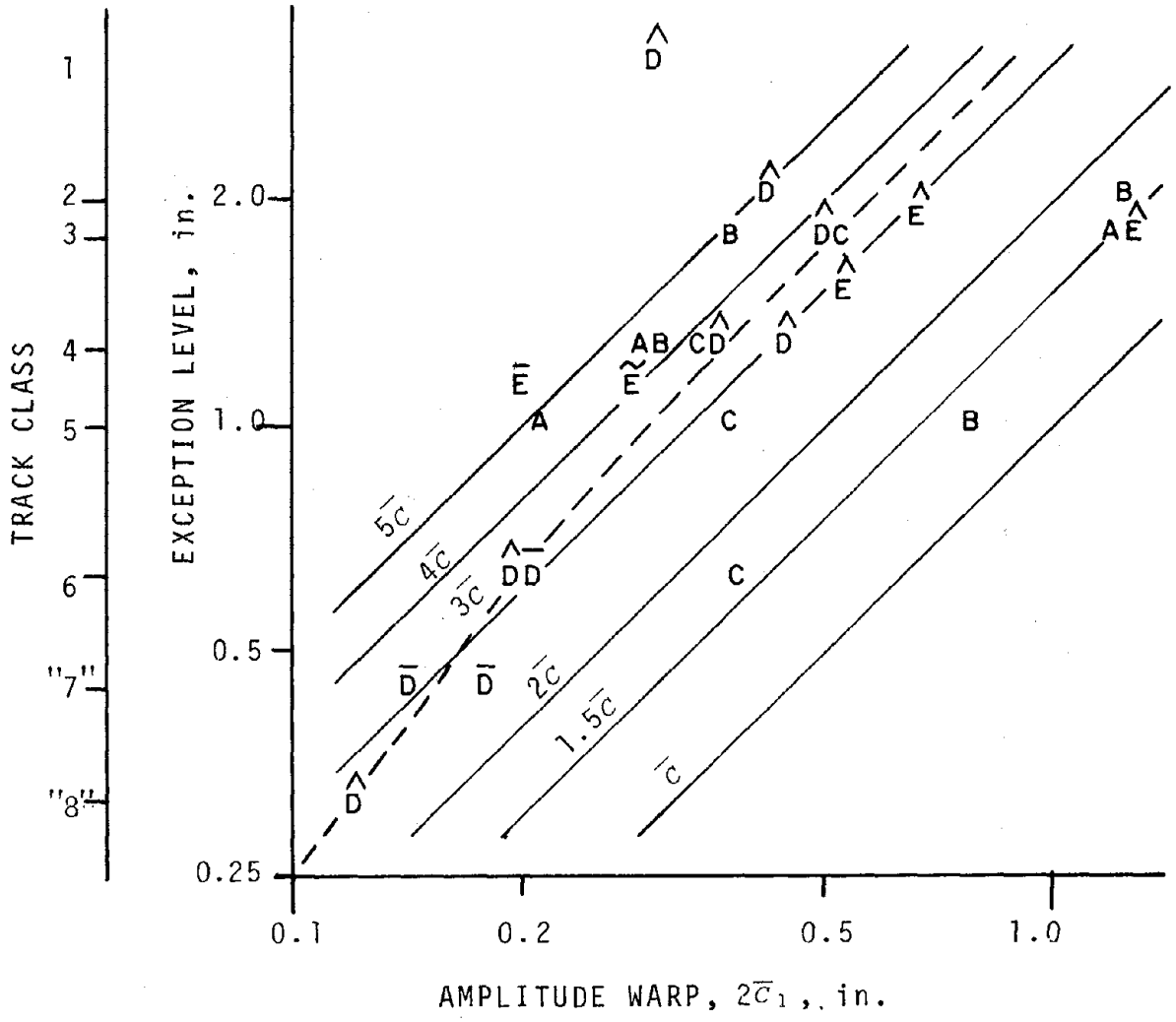

FIGURE 74. WARP DETERMINISTIC PEAK VALUE VERSUS TRACK CLASS AND EXCEPTION THRESHOLD

On the basis of this analysis, warp is the most likely to produce an exception requiring only a *pair* of random joint amplitudes on opposite rails that exceed $3.5\,\overline{C}$.

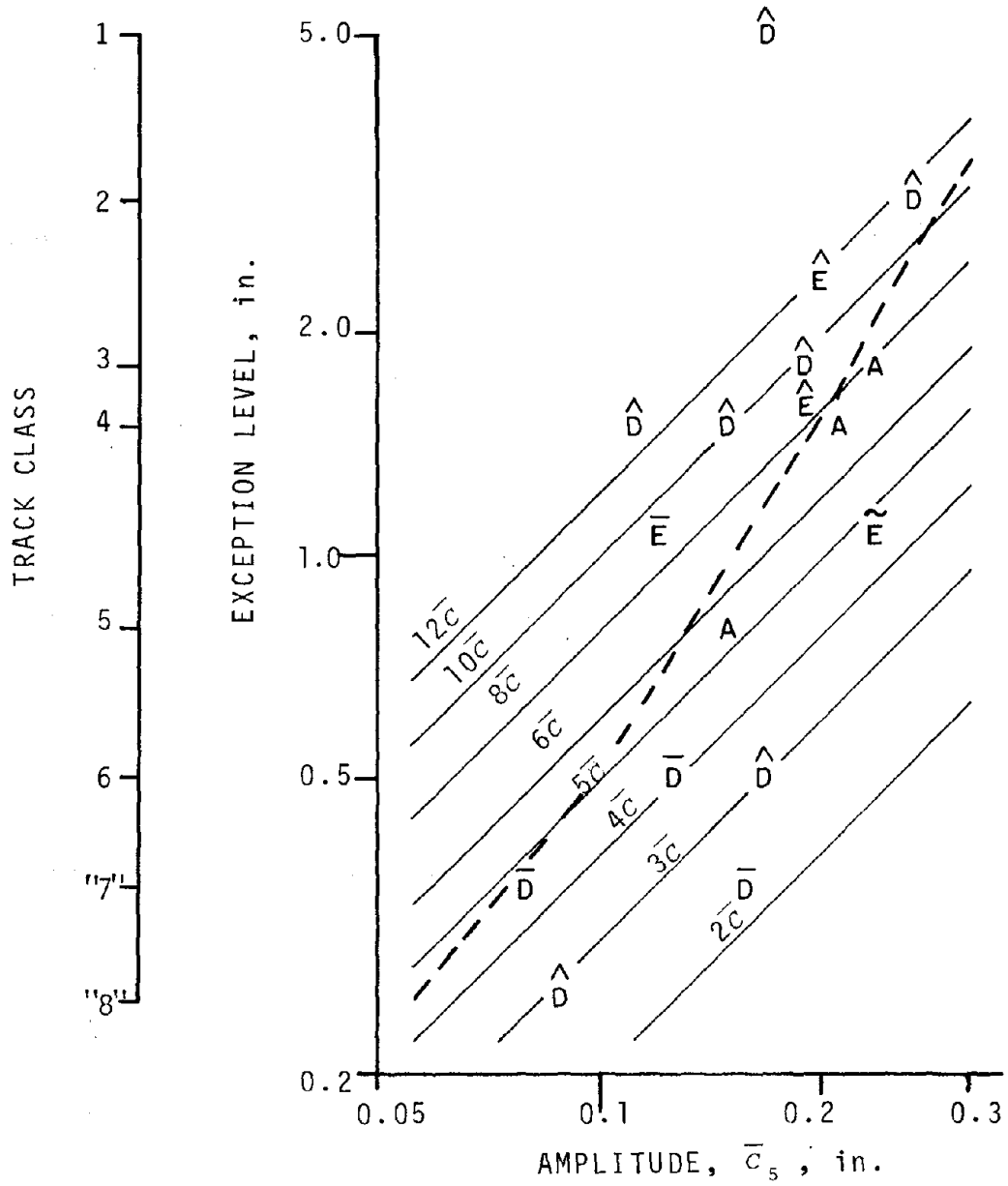

FIGURE 75. ALIGNMENT MEAN JOINT AMPLITUDE VERSUS TRACK CLASS AND EXCEPTION THRESHOLD

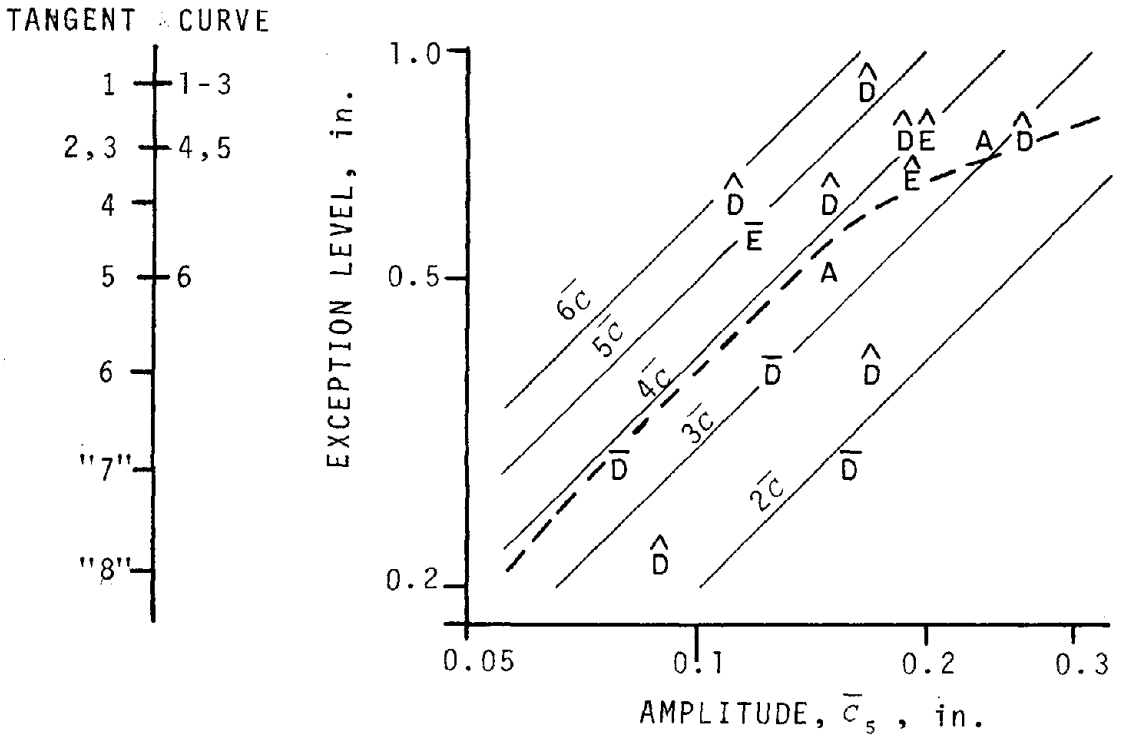

FIGURE 76. GAGE MEAN JOINT AMPLITUDE VERSUS TRACK CLASS AND EXCEPTION THRESHOLD

3.4.5 SUMMARY OF REGRESSION ANALYSIS - RESULTS

The following is a summary of the principal observations and results of the data analysis described in this section:

- Based on log-log regressions, parameters directly related to roughness, such as the SRP roughness parameter, log A_n, the logarithm of standard deviations of track geometry measures, and the mean amplitudes of joints, log $\bar{c}_n$, vary linearly with respect to each other and with respect to track class.
- Parameters, such as the corner frequencies ϕ_{n3} and ϕ_{n4}, are insensitive to variations and roughness.

- Decay rate decreases with increasing but small values of $\bar{c}_n$ and levels off to a constant level with larger values of $\bar{c}_n$.

- All of these regressions describe how parameters vary with respect to one another *in an average sense*. In each case, there is more or less scatter about the regression line. The scatter is within the range of fluctuations expected for statistical estimation from samples data. However parameters for a specific section of track can deviate from the mean or expected behavior, and in some cases this can be considerable.

- The SRP is most likely to produce gage exceptions. Random variation of joint amplitudes is most likely to produce warp exceptions.

3.5 CHARACTERIZATION OF ANOMALIES

The effort to characterize anomalies has as its objective the typification of events described in Table 3. Because anomalies represent isolated short duration events (transients), they do not register a strong or distinguishing impact on long duration averaging procedures such as employed by the PSD. This property of anomalous events was demonstrated by the experiment described in Paragraph 2.4.2 and illustrated in Figure 17.

It was noted that anomalies fall in two places on the signal classification diagrams of Figures 6 and 7. The deterministic or mean component of an anomaly is listed under Transients. The random component is found under Special Classifications of Non-Stationary Processes. Neither of these classifications is amenable to standard statistical procedures. Hence, it was determined that the examination of geometry time records offered the most promising approach to the mathematical characterization of anomalies.

At first, crosslevel and chordal profile data were used. This included the older 14.5 foot MCO data and the more recent 62 foot MCO profiles. Because crosslevel is the *difference* in the absolute profile of *two* rails, and because of the wavelength response characteristics chords, anomaly details were hopelessly obscured by all of these geometry measures.

It was determined that a phase distortionless space-curve of individual rail profile would circumvent these problems. A computer program was completed to obtain such representations of profile using signals from the T-6 profilometers. While the track data processed through this program was measured over limited territory, the results provided clear insights into anomalous geometry that had previously required tedious manual surveys or data from the Track Survey Device.

As described in Appendix C, T-6 generated profile space curves were examined, and the location of known anomalies was established. In addition, other excursions in the geometry that appeared abnormal to the eye were flagged for further investigation. Subsequent field trips revealed that there existed discernible changes or interruptions in the track structure at the site of these anomalous geometry variations.

These space curves were then catalogued by anomaly type, and the salient features of the anomaly were summarized. The principal findings of this investigation were:

- The largest deviations in track geometry to be found are associable with obvious physical interruptions in the track structure. On track containing anomalies, they are the limiting factor with respect to track speed and safety considerations.
- The abnormally large and highly structured geometry excursions generated by anomalies occur with greater frequency than inferred

by the PMRP. Given that the PMRP produces a rare large excursion comparable to those found in anomalies, this excursion is not likely to have the highly structured waveform generated by an anomaly.

- Anomalies in profile can be represented by a series of appropriately positioned cusp and depression shapes as shown in Figure 5. Each of these is quantifiable by an amplitude and a duration.

Two approaches to the further analysis, modeling, and quantification of anomalies were developed and they are outlined in Section 2.4. These procedures have not yet been applied to geometry time records of anomalies.

3.6 IDENTIFICATION OF THE TRACK STATISTICAL PARAMETERS FROM FIELD DATA

Track geometry field data can be drawn from two sources. Most permanent records of geometry are collected by automated track survey cars such as those operated by the FRA. It is also conceivable that a major source of data could be track inspections on foot using manual methods of track measurement such as the Track Analyzer^{TM}, Roll-Ordinator^{TM}, or Trak Chek^{TM}.* Methods for developing the various track parameters from these sources of data were developed in this effort and they are described below.

3.6.1 DATA FROM TRACK SURVEY CARS

In track geometry data collected by the FRA track survey cars some statistical and parametric characterizations are already performed in down-stream processing. All current statistical processing packages use homogeneous techniques such as PSD's, X-PSD's and histograms. When zones are to be analyzed, sufficiently detailed records are available so that anomalous locations can be deleted prior to analysis of the zones.

---

* Trade Mark names of the American Railroad Curveliner Corporation.

It was shown in Section 2 that the SRP and the PDP are adequately characterized directly by the PSD. On the other hand, PSD's of the random variation of joint amplitudes produce a continuum that is similar to the SRP continuum and as a result, complete characterization of anomaly free track requires a number of assumptions about the distribution, location, and statistical independence of low joints.

A more complete PMRP identification procedure is outlined in Appendix H. First, a mathematical model of railway track embodying periodic modulation of first and second order statistics is formulated. Then system identification procedures based on the mathematical model are developed. Finally the analysis is translated into a computer program for automatically identifying a PMRP from raw geometry data. This computer program is called a Track Parameter Extractor (TPE). It is a time-domain processor that performs the operations outlined in Figure 77.

The TPE was partially programmed to the extent that it can completely identify periodic modulation of the mean as represented by the PDP. Characterization of periodic modulation of second order statistics proved to be too involved to be completed within the present project and additional effort is required to complete this part of the TPE.

3.6.2 DATA COLLECTED MANUALLY

The method described in Appendix A for extracting track statistical parameters is amenable to data collected with hand tools or equipment such as the Track Analyzer described above. The procedure will develop the following output:

- Determine the mean shape of the PDP based on four points per rail length. The two quarter points can be used to quantify directional asymmetry and the joint point can be compared to the other positions to quantify the average depth of joints.

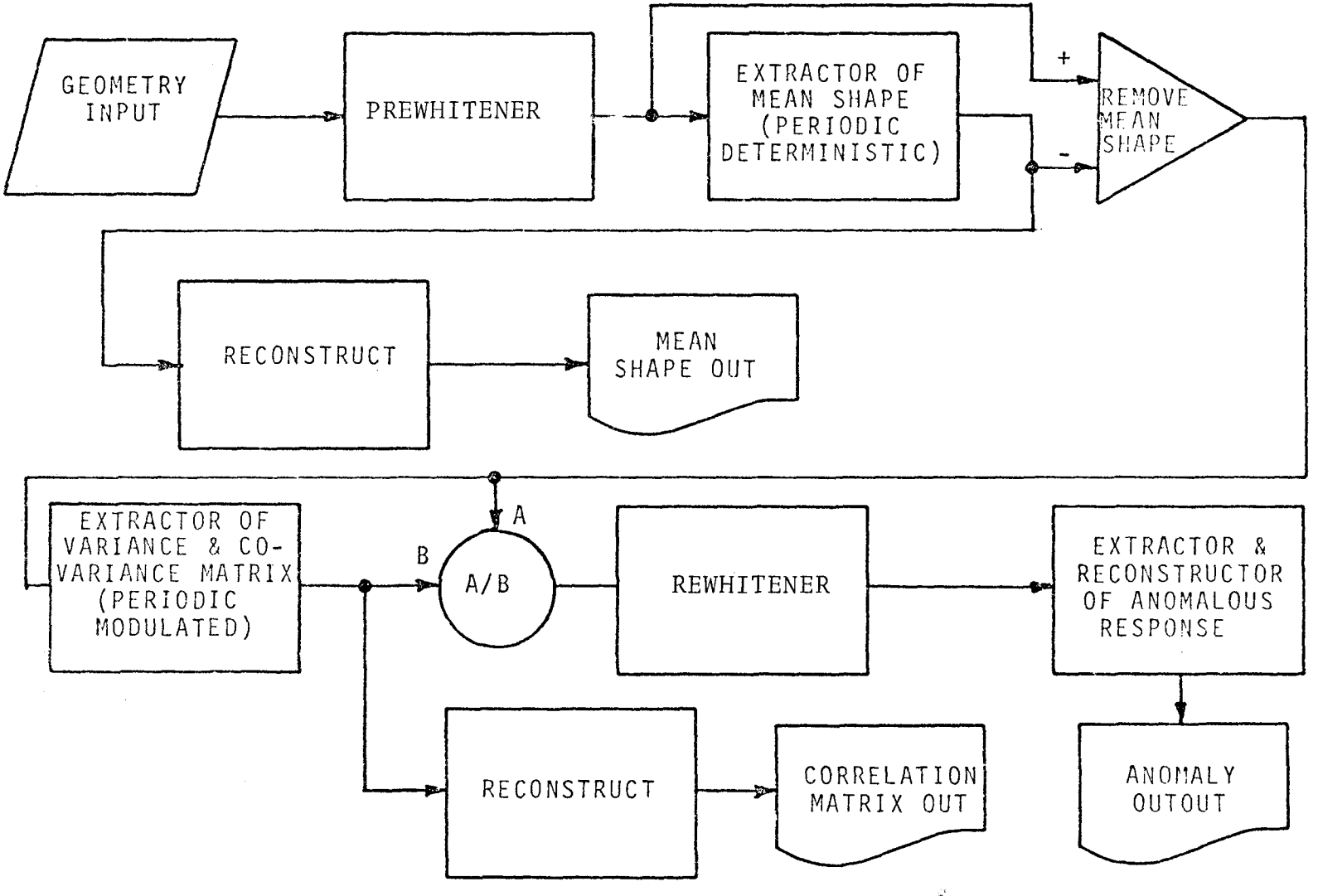

FIGURE 77. TRACK PARAMETER EXTRACTOR COMPUTER PROGRAM

- Determine the three parameters associated with the PSD of the SRP for both profile and alignment as follows:

  -- The amplitude of the roughness parameters, A_1 for profile and A_5 for alignment.

  -- The break frequencies ϕ_{13} and ϕ_{14} for profile and ϕ_{53} and ϕ_{54} for alignment.

- Quantify the statistical distribution but not the correlation properties of joint amplitudes.

- Provide confidence intervals for all the above.

The procedure outlined above was not implemented using actual data during the present project.

3.7 CHARACTERISTICS OF RAILHEAD WEAR

Existing data on rail cross section was reviewed and an attempt was made to develop a statistical characterization of the rail cross section as a function of wear condition. In addition railhead wear was measured in and near a four-degree curve in mainline track of a cooperating railroad. Wear of the 132-pound AREA rail was measured with a special tool similar to tools used on other railroads. It gives one measurement of wear on the gage side of the head and one on the surface.

The railhead wear tool is illustrated in Figure 78. It is made from an aluminum shape machined to fit snugly against the flange, web, and underside of the railhead. This tool has spring-loaded plungers of stainless steel, set in stainless steel sleeves as shown. The plungers are calibrated to give direct readings of railhead wear in increments of 1/16 inch. Gage wear is measured above the lower corner of the railhead, depending on the wear pattern, and the surface measurement is made approximately 1/2 inch on the gage side of the centerline

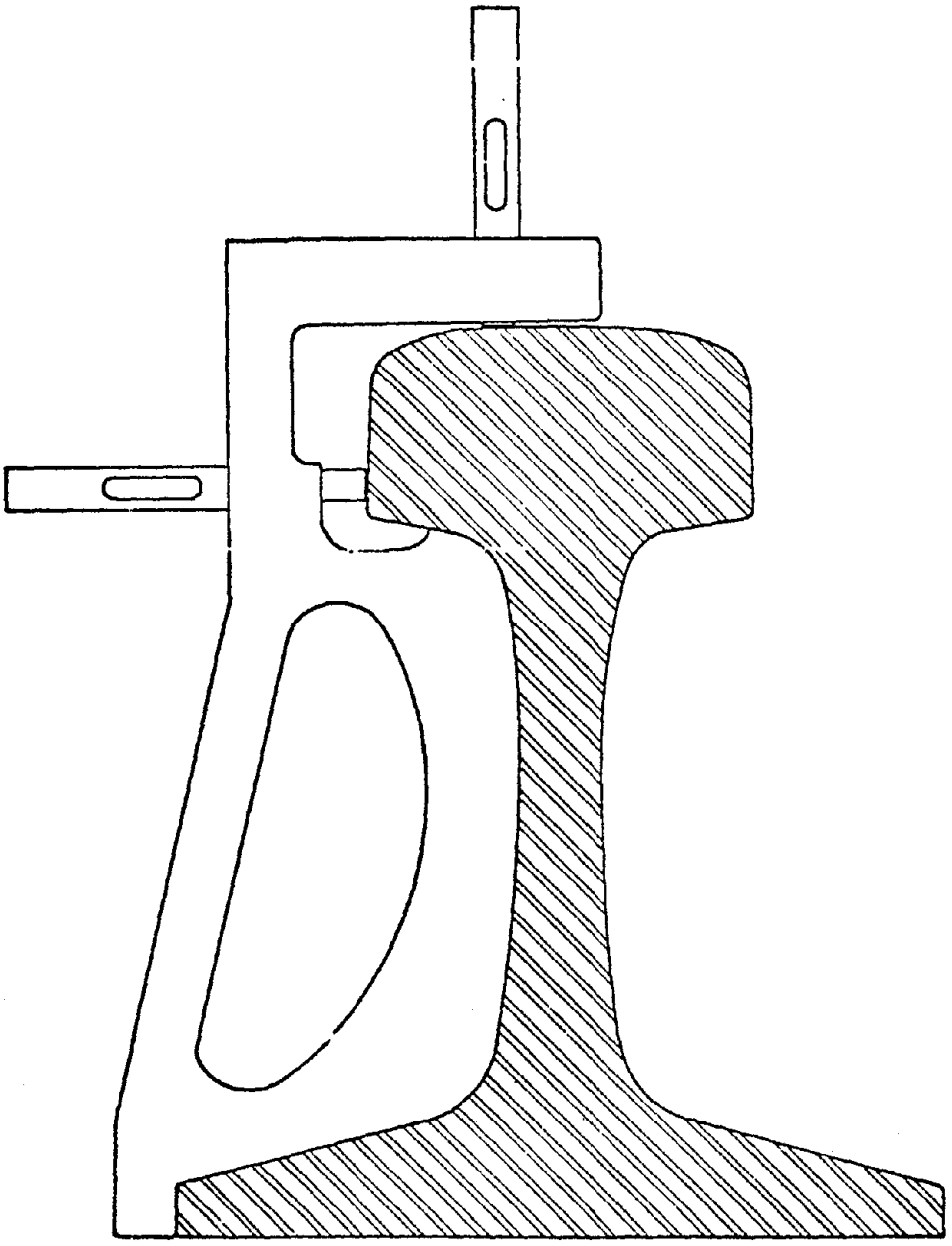

FIGURE 78. RAILHEAD WEAR TOOL ON 132-POUND RAIL

of the rail. Small errors may occur in the measurements made with gages of this type because of local deformations in any of the rail surfaces that are contacted by the tool or because of warping of the railhead in relation to the web.

Transverse profiles of the railhead shape were also plotted with a contour tool fitted with thin parallel rods. This device shows approximate contours when the tool is pressed against curved surfaces.

An examination of both of these instruments revealed that in general errors of at least 0.03 inch exist in the collected data. This is sufficient accuracy for purposes of determining when to replace or change over worn rail. Bearing in mind its 0.03-inch accuracy limitations, measurements were performed in a test zone that encompassed curve body, transition spiral, and tangent track. Evaluation of the data revealed:

- No cyclic variations in rail head wear associated with positions in the rail.
- No cyclic variations were found at hunting wavelengths such as 90 feet.
- A gradual transition in wear pattern occurred from curve to tangent.

A detailed discussion of the railhead wear characterization effort is contained in Appendix I.

3.8 CHARACTERIZATION OF VERTICAL TRACK STIFFNESS

Under contract DOT-FR-64113, ENSCO developed a prototype stiffness system for the FRA. Data were collected from a local cooperating railroad and were processed to yield the actual deformations that would be measured by the vehicle. Using a Winkler foundation model, the results were equated to the static stiffness or compliance that would be observed in a conventional point load wayside measurement.

A review of this data reveals the following stiffness characteristics for anomaly-free track[4]:

- There are slow, long wavelength variations in compliance that vary from 2.0 to 6.0 μin/lb with the more compliant track resting on an embankment (fill) or a swampy area, and less compliant track resting in a cut.
- There are sinusoidal variations of 39 ft wavelength whose peak-to-peak variations are 0.8 μin/lb on stretches of track in which welds are not staggered.
- There are sinusoidal variations of 19.5 ft wavelength whose peak-to-peak variations are 0.4 μin/lb on stretches of track where welds are staggered.

Anomalies cannot be property characterized by this measurement technique without performing a detailed analysis of the compliance measurement system as related to the specific track structure.[5]

4. REFERENCES

1. R. Cousty and G. Tro, "A Theoretical Study of the Development of Progressive Permanent Deformation in Longitudinal Profile of Railway Track under the Influence of Repeated Rollings Loads, *Revue Generale des Chemins de Fer 91*, p. 205-216, March 1972.

2. K. W. Schoenenberg, "Rail Research--Problem Definition," Report No. R-120, AAR Research Center, Chicago IL, March 1973.

3. Title 49, Code of Federal Regulations, Part 213.

4. G. Gunn, "Test Results Report, Track Stiffness Evaluation Program," Report No. FRA-ORD-77-45, December 1977.

5. G. Hayes, P. Joshi, and J. Sullivan, "Track Stiffness Measurement System Evaluation Program," Final Report, FRA/ORD-79/30, May 1979.

6. J. S. Bendat and A. G. Piersol, *Random Data: Analysis and Measurement Procedures*, Wiley, NY, 1971, p. 2-14.

7. L. R. Rabiner and B. Gold, *Theory and Application of Digital Signal Processing*, Prentice Hall, Englewood Cliffs, NJ, 1975, p. 205-292.

8. M. G. Kendall and A. Stuart, *The Advanced Theory of Statistics*, Vol. I, Ch. 6, "Standard Distributions (2)," Charles Griffin, London, 1968, p. 152-154.

9. The American Railway Engineering Association, Committee 5-Track, "Portfolio of Trackwork Plans," *Am. Rwy. Engr. Assoc.*, Chicago, IL. 1973.

10. P. J. Remington, M. J. Rudd, and I. L. Ver, "Wheel/Rail Noise and Vibration," Final Report (2 Vols.), UMTA-MA-06-0025-75-10 and UMTA-MA-06-0025-75-11, May 1975.

11. W. W. Gunn, "DOT Test Train Program System Instrumentation Manual - Seventh Edition," Annual Report, FRA-OR&D-76-254, June 1976.

12. R. Deutsch, *Non-linear Transformations of Random Processes*, Prentice Hall, Englewood Cliffs NJ, 1962, p. 79-81.

13. H. Medicki and S. Panuzio, "Track Geometry Survey Device for LIM Research Vehicle Test Track," Final Report, FRA-ORD&D-74-36, October 1973.

14. T-L. Yang, "FRA Track Geometry Measurement System Validation Report," Final Report FRA-ORD&D-73-08, June 1974.

15. M. G. Kendall and J. Stuart, *The Advanced Theory of Statistics*, Vol. III, Ch. 49, "Spectrum Theory," Charles Griffin & Co., London, 1968, p. 454,469.

16. A. O. Gilchrist, "A Report on Some Power Spectral Measurements of Vertical Rail Irregularities," Technical Note DYN/8, August 1965, British Railways Research Department, Derby, England.

17. M. G. Kendall and J. Stuart, *The Advanced Theory of Statistics*, Vol. I, Ch. 16, "Distributions Associated with the Normal," Charles Griffin, London, 1968, p.369-393.

18. J. C. Corbin and T-L. Yang, "Application of Guideway Roughness Power Spectral Density as a Management Tool," American Society of Mechanical Engineers Report 73-1CT-144, June 1973.

19. J. C. Corbin and W. M. Kaufman, "Classifying Track by Power Spectral Density," in "Mechanics of Transportation Suspension Systems," Winter Annual Meeting, ASME, Houston, December 1975.

20. J. C. Corbin, "Statistical Characterization of Railway Track Behavior," ASME/IEEE, Joint Railroad Conference, Pittsburgh, IEEE Paper No. C74903-31A, April 1974.

21. K. Bradley, et al.,"Acquisition and Use of Track Geometry Data in Maintenance-of-Way Planning," Technical Report No. FRA-ORD&D-75-27, March 1975.

22. T. K. Caughey, "Derivation and Application of the Fokker-Planck Equation to Discrete Nonlinear Dynamic Systems Subjected to White Random Excitations," *J. Acoust, Soc. Am.* 35, p. 1683-1692, November 1963.

23. J. Corbin, "Correlation of Statistical Representations of Track Geometry with Physical Appearance," Final Report, FRA-ORD-79-35, June 1975.

*U.S. GOVERNMENT PRINTING OFFICE : 1980 0-624-029/1561

110 copies